1169

A UNITED STATES DEPARTMENT OF COMMERCE PUBLICATION

SECTION A

JOURNAL OF RESEARCH

of the NATIONAL BUREAU OF STANDARDS

Volume 74A, Number 3, May–June 1970

Physics and Chemistry

U.S. DEPARTMENT OF COMMERCE
National Bureau of Standards

Journal of Research

of the

National Bureau of Standards

A. Physics and Chemistry

May–June • 1970

VOLUME • 74A

NUMBER • 3

Editor: C. W. Beckett

Associate Editor: D. D. Wagman

Publication dates:
Feb. 1, Apr. 1, June 1, Aug. 1, Oct. 1, Dec. 1, 1970

J. Res. Nat. Bur. Stand. (U.S.), A
CODEN: JNBAA 74A (3) 309–459 (1970)

JOURNAL OF RESEARCH

The National Bureau of Standards Journal of Research reports research and development in the fields of activity shown at right. Also included from time to time are survey articles on topics closely related to the Bureau's scientific and technical program.

The Journal is published in three separate sections as follows:

A. Physics and Chemistry

Contains papers of interest primarily to scientists working in these fields. Issued six times a year. Annual subscription: domestic, $9.50; foreign $11.75. Single copy, varies.

B. Mathematical Sciences

Presents studies and compilations designed mainly for the mathematician and the theoretical physicist. Issued quarterly. Annual subscription: domestic, $5.00; foreign, $6.25. Single copy, $1.25.

C. Engineering and Instrumentation

Reports research and development results of interest chiefly to the engineer and the applied scientist. Issued quarterly. Annual subscription: domestic, $5.00; foreign, $6.25. Single copy, $1.25.

The National Bureau of Standards [1] was established by an act of Congress March 3, 1901. Today, in addition to serving as the Nation's central measurement laboratory, the Bureau is a principal focal point in the Federal Government for assuring maximum application of the physical and engineering sciences to the advancement of technology in industry and commerce. To this end the Bureau conducts research and provides central national services in four broad program areas. These are: (1) basic measurements and standards, (2) materials measurements and standards, (3) technological measurements and standards, and (4) transfer of technology.

The Bureau comprises the Institute for Basic Standards, the Institute for Materials Research, the Institute for Applied Technology, the Center for Radiation Research, the Center for Computer Sciences and Technology, and the Office for Information Programs.

THE INSTITUTE FOR BASIC STANDARDS provides the central basis within the United States of a complete and consistent system of physical measurement; coordinates that system with measurement systems of other nations; and furnishes essential services leading to accurate and uniform physical measurements throughout the Nation's scientific community, industry, and commerce. The Institute consists of an Office of Measurement Services and the following technical divisions:

Applied Mathematics — Electricity — Metrology — Mechanics — Heat — Atomic and Molecular Physics—Radio Physics [2]—Radio Engineering [2]—Time and Frequency [2]—Astrophysics [2]—Cryogenics.[2]

THE INSTITUTE FOR MATERIALS RESEARCH conducts materials research leading to improved methods of measurement standards, and data on the properties of well-characterized materials needed by industry, commerce, educational institutions, and Government; develops, produces, and distributes standard reference materials; relates the physical and chemical properties of materials to their behavior and their interaction with their environments; and provides advisory and research services to other Government agencies. The Institute consists of an Office of Standard Reference Materials and the following divisions:

Analytical Chemistry—Polymers—Metallurgy—Inorganic Materials—Physical Chemistry.

THE INSTITUTE FOR APPLIED TECHNOLOGY provides technical services to promote the use of available technology and to facilitate technological innovation in industry and Government; cooperates with public and private organizations in the development of technological standards, and test methodologies; and provides advisory and research services for Federal, state, and local government agencies. The Institute consists of the following technical divisions and offices:

Engineering Standards—Weights and Measures—Invention and Innovation — Vehicle Systems Research — Product Evaluation — Building Research — Instrument Shops — Measurement Engineering — Electronic Technology—Technical Analysis.

THE CENTER FOR RADIATION RESEARCH engages in research, measurement, and application of radiation to the solution of Bureau mission problems and the problems of other agencies and institutions. The Center consists of the following divisions:

Reactor Radiation—Linac Radiation—Nuclear Radiation—Applied Radiation.

THE CENTER FOR COMPUTER SCIENCES AND TECHNOLOGY conducts research and provides technical services designed to aid Government agencies in the selection, acquisition, and effective use of automatic data processing equipment; and serves as the principal focus for the development of Federal standards for automatic data processing equipment, techniques, and computer languages. The Center consists of the following offices and divisions:

Information Processing Standards—Computer Information—Computer Services—Systems Development—Information Processing Technology.

THE OFFICE FOR INFORMATION PROGRAMS promotes optimum dissemination and accessibility of scientific information generated within NBS and other agencies of the Federal Government; promotes the development of the National Standard Reference Data System and a system of information analysis centers dealing with the broader aspects of the National Measurement System, and provides appropriate services to ensure that the NBS staff has optimum accessibility to the scientific information of the world. The Office consists of the following organizational units:

Office of Standard Reference Data—Clearinghouse for Federal Scientific and Technical Information [3]—Office of Technical Information and Publications—Library—Office of Public Information—Office of International Relations.

[1] Headquarters and Laboratories at Gaithersburg, Maryland, unless otherwise noted; mailing address Washington, D.C. 20234.
[2] Located at Boulder, Colorado 80302.
[3] Located at 5285 Port Royal Road, Springfield, Virginia 22151.

U.S. DEPARTMENT OF COMMERCE
Maurice H. Stans, Secretary
NATIONAL BUREAU OF STANDARDS
Lewis M. Branscomb, Director

Order all publications from the Superintendent of Documents
U.S. Government Printing Office, Washington, D.C. 20402

Use of funds for printing this publication approved by the Director of the Bureau of the Budget (June 22, 1966).

JOURNAL OF RESEARCH of the National Bureau of Standards—A. Physics and Chemistry
Vol. 74A, No. 3, May–June 1970

The Crystal Structure of Hydrazinium Trinitromethide, $(N_2H_5^+[C(NO_2)_3]^-$ at ~ -160 °C)

Brian Dickens

**Institute for Materials Research, National Bureau of Standards
Washington, D.C. 20234**

(January 27, 1970)

The crystal structure of hydrazinium trinitromethide ($N_2H_5^+[C(NO_2)_3]^-$) has been determined using 1914 x-ray data collected photographically from a single crystal held at ~ -160 °C. The unit cell at ~ -160 °C is $a=7.91(2)$, $b=11.77(2)$, $c=13.98(2)$ Å, $\beta=104.9(3)°$, and contains eight formula weights in space group $P2_1/n$. The calculated density is 1.93 g·cm^{-3}. The structure has been refined isotropically to $R=0.10$ by full-matrix least-squares procedures. The two crystallographically independent trinitromethide anions are propeller shaped, with angles of 41°, 7°, 8°, and 74°, 5°, 4°, respectively, between the NO_2 and CN_3 plane normals. The central CN_3 part of each anion is almost planar. In one anion, the C atom is 0.008 Å out of the N_3 plane; in the other, the C atom is 0.033 Å out of the N_3 plane. Hydrogen atoms have been located approximately in an electron density difference synthesis. Their positions agree with those obtained from independent calculations involving the minimization of a function which is a first approximation to the electrostatic hydrogen bonding energy. These analyses provide evidence that one hydrazinium ion is eclipsed and the other is staggered.

Key words: Crystal structure; hydrazinium; hydrazinium trinitromethide; hydrogen bonding; trinitromethide; x-ray diffraction.

1. Introduction

The Hammett *para*-substituent constants [1][1], the acid strengths [2], the ionization behavior [3], the equilibrium constants [4], and the strengths of the electron-withdrawing power in, but lack of resonance with, aromatic systems [5] have all provided evidence for the stability of the trinitromethide $[C(NO_2)_3]^-$ and tricyanomethide $[C(CN)_3]^-$ anions and their derivatives. Such stability has been attributed to charge delocalization (i.e., resonance). The greater charge delocalization indicated in the tricyanomethide anion has suggested that while the tricyano anion is probably planar, the trinitromethide anion may not be so. To provide structural details on the trinitromethide anion, the structure of hydrazinium trinitromethide, $N_2H_5^+[C(NO_2)_3]^-$, has been determined. A preliminary report of the structure has been published [6].

[1] Figures in brackets indicate the literature references at the end of this paper.

*The digits in parentheses are estimates of the uncertainties in the least significant digit of the cell dimensions and are based on the standard errors of the measurements. They are compatible with experience with the technique. In the author's opinion, they may be considered to give an estimate of the standard deviations.

2. Experimental Procedure

Needle-shaped crystals of $N_2H_5^+[C(NO_2)_3]^-$ were grown from an ethanol solution at about 2 °C. Since the crystals decomposed within a few hours in the x-ray beam at room temperature, a single crystal 0.2 mm in diameter ($\mu_{Mo}=3.2$ cm^{-1}) was sealed in a borate glass capillary and cooled to ~ -160 °C on a Weissenberg camera modified [7] to allow the routine collection of data at low temperatures. The unit cell was determined from Weissenberg and oscillation photographs to be* $a=7.91(2)$, $b=11.77(2)$, $c=13.98(2)$ Å, $\beta=104.9(3)°$ (at ~ -160 °C) with space-group $P2_1/n$ and eight formula weights per cell. The equivalent positions are x, y, z; $\bar{x}, \bar{y}, \bar{z}$; $\frac{1}{2}+x, \frac{1}{2}-y, \frac{1}{2}+z$; $\frac{1}{2}-x, \frac{1}{2}+y, \frac{1}{2}-z$. The reciprocal lattice extinctions are $h0l$, $h+l=2n+1$; $0k0$, $k=2n+1$. The density was not determined directly but is calculated from the x-ray data to be 1.93 g·cm^{-3}. X-ray data from 1914 reflections were collected photographically by the equi-inclination method for the levels $0 \rightarrow 7$, k, l, using molybdenum radiation, an 0.001 inch Nb filter and multiple films interleaved with .0015 inch brass sheets. The intensities of observed reflections

were estimated visually and corrected for the combined Lp and reflection size effects but not for absorption. The calculation of the quasi-normalized structure factors confirmed the centrosymmetry of the unit cell and gave initial values for the equi-inclination level scale factors. The equi-inclination levels were not sclaed experimentally but the initial estimates agree with the final values from the full-matrix least-squares refinements within 5 percent on the average.

2.1. Determination of the Structure

One-hundred and six (106) phases were determined using a program by Chastain and Stewart [9, 10] which is an extension of the symbolic addition procedure [11, 12]. The structure was found from an E map calculated with these phases and from subsequent F_o Fourier syntheses. The structure was refined isotropically to $R = \Sigma \| F_o | - | F_c \| / \Sigma | F_o | = 0.12$ using full-matrix least-squares procedures. The quantity minimized in the least-squares refinements is $\Sigma (w \| F_o | - | F_c \|)^2$. The weighting scheme used was 1 for reflections with $F_o \leq 6$ and $6/F_o$ for reflections with $F_o > 6$. The atomic scattering factors used are those of the neutral atoms. Those for C, N and O were taken from reference 13 and those for H from reference 14.

A difference electron density synthesis with coefficients weighted by the least-squares weights showed indications of the 10 hydrogen atoms of the hydrazinium ions. When the rest of the difference synthesis was examined, it was found that 8 of the peaks assigned to hydrogen were among the 12 highest peaks in the map. The peaks assigned to H(6) and H(7) were the 16th and 22nd highest peaks in the map but seemed to be relatively clearly defined in the map and in chemically reasonable positions. Of the 23 highest peaks, those not assigned to be hydrogen atoms were 0.36 to 0.75 Å away from the oxygens of the trinitromethide ions.

Hydrogen atoms were introduced at the positions suggested from the examination of the difference synthesis and the structure including the hydrogen positional parameters was refined isotropically to $R = 0.10$. Hydrogen thermal parameters were kept fixed at 2.0 Å^2. The effect of all reflections calculating over 60 was ignored in these least-squares refinements because these reflections probably contained extinction and/or film scaling errors. No anisotropic refinement was attempted because of the correlation between the β_{11} thermal parameters and the level scale factors. Since the data were collected at ~ -160 °C, the thermal motion is expected to be relatively small, however.

The largest correlation coefficients are 0.3 between the scale factors, 0.3 between the scale factors and the atomic temperature factors and 0.4 between the temperature factors themselves. All other correlation coefficients are much less than 0.1.

The observed and calculated structure factors are compared in table 1 and the parameters of atoms other than hydrogen are given in table 2. The positions of the hydrogens from the weighted difference synthesis, the least-squares refinements, and from calculation (see later) are compared in table 3. The refinement changed the hydrogen positions obtained from the difference synthesis by an average of 0.17 Å. The average N–H distance thus changed from 0.86 Å to 0.89 Å. The location of covalently bonded hydrogen atoms by x-ray methods is known to be accompanied by a systematic error which makes the observed bond distance 0.1 to 0.2 Å shorter than the internuclear distance. The N–H distances observed here are therefore reasonable.

3. Description of the Structure

The crystal structure is shown in figure 1. There are two trinitromethide ions and two hydrazinium ions in the asymmetric unit. Each trinitromethide ion is propeller shaped with the plane of its N(1) nitrogroup twisted much more from the central CN_3 plane than are the planes of the other two nitrogroups. The central CN_3 part of each trinitromethide ion is essentially planar. One hydrazinium ion appears to be eclipsed (see figure 4); the other appears to be staggered (see figure 5).

The packing in the structure shows the following features. Anions of type 1 form a zigzag along the two-fold screw axis. The planes of neighboring anions are about 100° to one another. The zigzag results because adjacent anions are hydrogen bonded to the same hydrazinium ions. The O(15) . . . O(15) close approach of

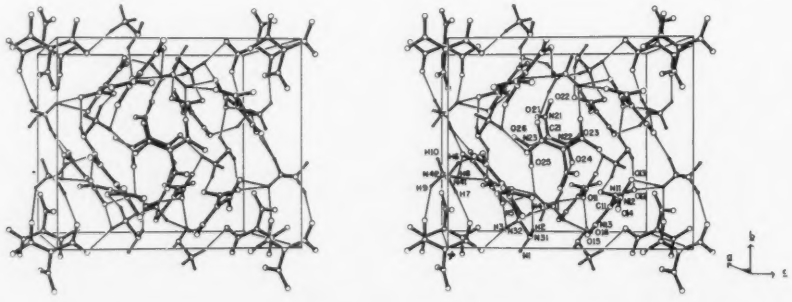

FIGURE 1. *A stereoscopic view of the* $N_2H_5^+[C(NO_2)_3]^-$ *structure.*
The origin of the unit cell is denoted by °.

2.93 Å occurs when the zigzags come into close approach along the *c* axis.

The anions of type 2 are roughly equally spaced along the *a* axis with their centers almost on a straight line and with all atoms but O(21) and O(22) in a plane approximately parallel to the *bc* plane for a given anion.

The hydrazinium ions hold the anion 1 zigzags (along *a*) and anion 2 lines (along *b*) together in a three dimensional network. O(21) and O(22) in anion 2 are twisted almost perpendicular to the plane of the rest of the anion in order to squeeze between two anions of type 1.

4. Discussion

4.1. The Trinitromethide Ions

The bond distances and angles in the two propeller-shaped trinitromethide anions are given in table 4. The anions and their environments are shown in figures 1, 2, and 3. The central part $C(N)_3$ of anion 1 is essentially planar; C(11) is only 0.008(5) Å out of the $(N)_3$ plane. The central part of anion 2 is more distorted with C(21) 0.033(5) Å out of the $(N)_3$ plane. All but one of the N—O distances in the nitrogroups are within two standard deviations (~ 0.01 Å) of the average N—O distance, 1.232 Å. N(21)—O(22), the shortest at 1.214(4) Å, lies out of this range. This may be related to weak or non-existent hydrogen bonding to O(22) (see sec. 4.2).

The dihedral angles between the normals to the planes of the nitrogroups and the normal to the best plane through the central CN_3 region of the anion are:

N(11) O(11) O(12):CN_3	41°
N(12) O(13) O(14):CN_3	7°
N(13) O(15) O(16):CN_3	8°
N(21) O(21) O(22):CN_3	74°
N(22) O(23) O(24):CN_3	5°
N(23) O(25) O(26):CN_3	4°

The intra-ionic O(21) . . . O(26) and O(22) . . . O(23) distances of 2.89 Å and 2.95 Å are much greater both than the corresponding intra-ionic distances in anion 1 (2.62, 2.57 Å) and than the other intramolecular O—O distances of 2.59, 2.65, 2.59, and 2.65 Å in both anions. These long distances allow the N(21) nitrogroup to be sandwiched between, and in approximate contact with, two anions of type 1 (figs. 1 and 3). The distances of closest approach between the N(21) nitro-

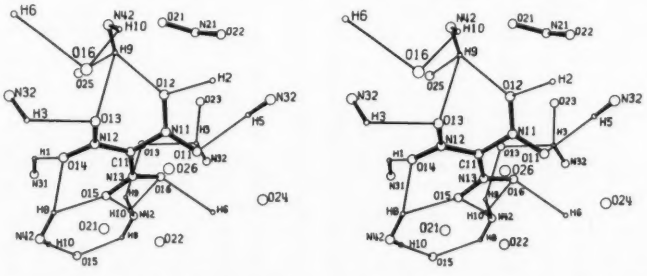

FIGURE 2. *The environment of trinitromethide anion 1 (viewed perpendicular to the* ab *plane) showing the probable hydrogen bonding.*

O . . . H distances ≤ 2.4 Å, other inter-atomic distances ≤ 3.1 Å are included.

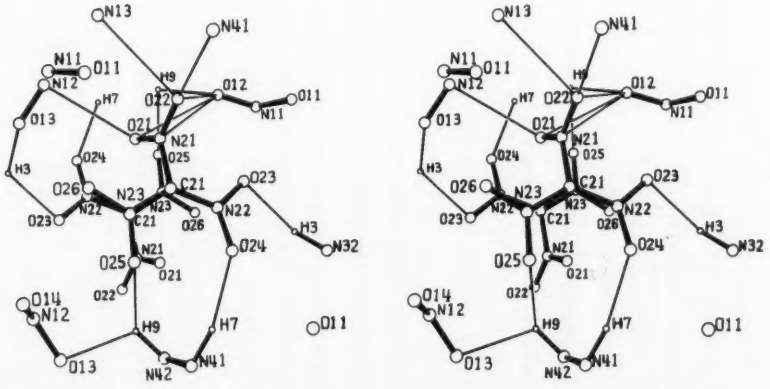

FIGURE 3. *The environment of trinitromethide anion 2 (viewed perpendicular to the* bc *plane) showing the probable hydrogen bonding and possible van der Waals bonding to atoms 2.7–3.0 Å away from atoms in anion 2.*

Otherwise as for figure 2.

TABLE 1. Observed and calculated structure factors [a] for $N_2H_5^+$ $[C(NO_2)_3]^-$ (Columns are l, $10F_o$, $10F_c$)

0,0,L		10 137 -146		1,5,L		-1 223 212		-1 801E -739		2,7,L		7 325 298		-12 117 -127		5 256 262							
		11 185 176				0 95 -90		0 1043E-1314				8 55 -75		-11 108 109		6 81 -70							
4 72 77		13 85 108		-16 58 41		1 56 47		1 272 -289		-15 57 69				-10 88 104		8 150 137							
6 810E 720				-15 37 42		2 243 256		2 1168E 1223		-14 36 54		2,13,L		-9 258 -220		9 51 44							
8 461 431		1,0,L		-13 291 244		3 56 -60		3 275 245		-13 79 -87				-8 63 53		10 53 -50							
10 506 480				-11 38 -39		4 164 129		5 180 163		-12 247 -233		-7 62 80		-7 264 -240		11 63 -79							
12 561 448		-15 86 -87		-9 411 404		5 213 -218		6 168 -172		-10 142 143		-6 124 139		-6 70 -57									
14 197 194		-9 130 121		-8 376 -343		6 279 281		7 292 -249		-8 94 109		-4 54 -50		-5 117 83		3,9,L							
16 188 -144		-5 525E -602		-7 740E 724		8 120 -97		8 417 394		-7 238 192		-3 102 96		-4 136 119									
		-3 94 125		-6 739E 706		11 56 -55		9 86 -77		-6 439 -407		-2 77 -66		-3 243 -230		-13 29 -26							
0,1,L		1 980E 579		-4 124 -145				10 112 117		-5 426 374		0 28 -14		-2 33 -52		-12 54 59							
		3 192 -213		-3 270 -268		1,11,L		11 72 -76		-4 77 -77		2 475 478		-1 247 -273		-10 52 -63							
2 350 -264		5 180 186		-2 235 -239				12 214 -190		-3 46 68		4 29 -31		0 445 -379		-9 202 -182							
3 640 606		7 187 -186		-1 1246E 1384		-11 32 -29		13 337 305		-2 325 301		5 22 -30		1 371 405		-8 38 22							
4 120 128		7 339 -386		1 121 -143		-9 60 -64				-1 74 91				2 263 265		-7 271 -241							
5 341 -298		9 585 543		3 74 -77		-7 260 200		2,9,L		0 93 -107		2,14,L		3 278 -310		-6 304 282							
6 580 -441		11 160 159		5 353 361		-6 87 93				1 152 158				4 169 -193		-5 138 125							
8 242 259				7 71 65		-5 539 441		-17 171 146		2 186 -203		-4 53 -62		5 91 -112		-4 134 -118							
10 123 -124		1,1,L		8 103 -105		-4 131 127		-15 73 72		3 69 56		-2 62 64		6 27 39		-3 87 -79							
11 937 412				9 145 -121		-3 112 -122		-14 144 149		4 231 -240		-1 48 48		7 260 -286		-2 292 -205							
12 127 -114		-16 50 45		11 44 19		0 69 76		-13 203 -212		5 164 162		0 62 73		8 248 246		-1 58 43							
14 218 227		-15 138 130		12 90 -51		1 87 112		-12 373 -387		6 258 254		1 58 47		9 243 247		0 194 -180							
15 381 -281		-14 41 -50		13 207 204		2 105 -112		-11 34 -45		7 75 -86		2 89 -87		10 299 -341		1 29 -41							
16 148 -148		-12 68 -65		14 84 -70		3 270 -291		-10 279 -229		8 180 -217				11 211 -189		2 291 265							
		-11 256 -248				4 55 58		-9 92 98		10 93 88		3,0,L		12 186 175		3 146 -118							
0,2,L		-10 385 363		1,6,L		7 287 250		-8 148 141		12 76 -82				13 83 -76		4 149 157							
		-9 57 86				8 85 73		-7 23 16								5 44 43							
0 156 -140		-8 373 -372		-15 115 -111		9 124 -131		-6 177 161		2,8,L		-17 95 82		3,9,L		6 79 -81							
1 204 183		-7 199 226		-13 142 127		10 116 -90		-5 300 -237				-15 176 142				7 38 -40							
2 927E 708		-6 605E -650		-12 297 253				-4 363 341		-14 91 74		-13 83 -86				8 208 -196							
3 129 122		-4 246 -263		-11 283 -249		1,12,L		-2 586 -523		-12 326 -289		-11 40 30		-16 131 -103		9 189 173							
4 2211E-1878		-3 304 -330		-9 82 85				-1 839E -802		-11 207 157		-9 65 -76		-14 64 38		10 49 -44							
5 436 -390		-2 287 296		-8 180 -194		-10 99 -126		0 975 -959		-9 209 -244		-7 770E 711		-13 248 -240		11 159 -204							
6 183 -185		-1 199 173		-7 90 -99		-9 50 -67		1 21 -21		-8 204 185		-5 89 -95		-12 251 218									
7 379 -348		1 234 190		-6 645E 595		-8 100 100		2 352 -342		-7 92 -88		1 285 320		-10 247 214		3,10,L							
8 33 -31		2 209 -185		-5 290 -237		-7 134 -128		3 161 -160		-6 216 228		3 666E 663		-9 77 -45									
9 229 -245		4 617E -630		-2 124 97		-5 175 173		4 304 296		-5 204 204		5 345 340		-8 103 81		-12 48 -51							
10 110 -135		5 747E 749		0 204 196		-3 158 153		5 288 290		-4 349 -365		7 321 -322		-7 506 -477		-11 219 -203							
11 111 -116		6 203 -218		2 200 -217		-2 109 -102		6 362 361		-3 192 -198		9 114 131		-6 560 -484		-9 36 24							
12 220 196		8 36 -32		3 113 -128		-1 102 -93		7 146 141		-2 37 -28		11 335 -382		-5 130 86		-8 364 -309							
13 206 -187		9 186 -182		4 61 -66		0 201 -250		8 273 -276		0 71 27				-4 80 -54		-7 101 111							
14 47 -33		10 148 146		5 89 73		1 50 65		10 63 50		1 26 -26		3,1,L		-3 281 -254		-6 115 -125							
16 104 -103		11 134 126		6 71 62		2 307 -264		11 71 -77		2 429 -407				-2 95 92		-4 198 -200							
		12 283 264		7 200 222		4 180 174		12 211 -156		4 461 468		-14 108 104		-1 232 -205		-5 198 -200							
0,3,L				8 35 -29		5 48 30		13 127 124		5 154 -154		-13 135 -138		0 28 25		-4 109 -96							
		1,2,L		10 56 71		6 230 -200				6 75 -88		-12 195 -205		1 80 90		-3 131 133							
1 425 420				11 194 181		8 164 -152		2,6,L		7 64 64		-11 146 -136		2 102 -92		-2 74 71							
2 274 -262		-15 37 -50		12 95 82						8 158 -186		-10 168 -167		3 168 -192		-1 85 80							
3 720E -575		-14 99 85		13 424 349		1,13,L		-13 176 -137		9 108 121		-8 87 71		4 64 -62		0 260 -272							
4 665 -590		-13 61 -72		14 198 -193				-12 265 -263		10 285 -240		-7 232 -238		5 485 -542		1 369 -394							
5 1125E 814		-12 75 85				-7 67 70		-11 150 163		11 120 106		-6 245 287		6 26 16		2 69 83							
6 477 457		-11 112 -117		1,7,L		-5 79 72		-10 72 53				-5 496 -433		7 246 -252		3 86 101							
7 255 -253		-10 203 -197				-4 78 -86		-9 237 -216		2,9,L		-4 104 108		9 254 283		4 435 -451							
8 346 -316		-9 113 -116		-14 80 -83		-2 37 44		-8 383 -340				-3 79 66		10 82 -90		5 42 55							
11 263 256		-8 44 -49		-13 45 -58		-1 143 -143		-7 46 -47		-13 115 108		-2 522 -424		11 120 -115		6 42 50							
13 180 147		-7 73 69		-11 52 -47		0 143 -121		-6 193 191		-11 156 -125		-1 153 -153		12 97 110		7 24 37							
14 168 -158		-6 752E 765		-10 134 -145		1 210 -196		-5 144 -147		-10 35 36		0 320 -349		13 53 46		8 51 -41							
16 40 -50		-5 169 194		-9 140 130		2 144 -151		-4 65 -64		-9 243 -203		1 645E -658				9 175 -176							
		-4 758E 771		-8 126 -116		3 135 -133		-3 34 -24		-8 28 -28		2 250 -259		3,8,L									
0,4,L		-3 676E -748		-5 398 -390		4 84 -74		-2 940E -918		-7 26 19		3 548 570				3,11,L							
		-2 639E 804		-4 140 -144		5 40 42		-1 86 -81		-6 27 25		4 383 408		-15 43 41									
0 538 495		-1 599E 662		-3 174 142		7 30 -28		0 143 128		-5 53 74		5 530 -525		-14 202 -178		-10 57 63							
1 61 -55		0 247 -255		-2 556 -573				1 41 -47		-4 382 -362		6 397 415		-13 192 186		-9 36 -29							
2 1026E -856		1 253 -305		-1 64 -92		1,14,L		2 363 -349		-3 102 -79		7 75 -55		-11 92 103		-8 88 -79							
3 612 554		2 517 565		0 227 -236				3 338 330		-2 52 -45		8 28 -40		-10 134 127		-7 62 -47							
4 203 -214		3 45 -50		1 347 372		-4 133 133		4 97 -84		-1 360 -332		10 140 -156		-9 65 -59		-6 66 46							
8 62 -40		4 1482E 1649		2 95 85		-3 84 -81		5 24 -21		0 973 -946		11 128 -144		-8 306 -269		-4 236 203							
9 301 306		5 102 -103		3 458 -480		-2 105 75		7 71 -65		1 30 -34		12 72 68		-7 316 314		-3 76 55							
11 129 -112		6 542 491		4 140 -160		-1 63 -57		8 239 217		2 244 -236				-6 150 -131		-2 351 -334							
12 128 109		7 261 272		5 51 56		0 91 49		9 236 -201		3 178 -188		3,2,L		-5 171 -146		0 102 76							
14 123 136		8 376 349		6 146 -160		1 165 -145		10 112 -106		4 54 -46				-4 81 -73		2 151 141							
15 196 174		9 258 -222		7 86 88		2 144 182		11 163 178		5 76 -75		-14 162 155		-3 57 43		3 123 -111							
16 52 -50		10 150 167		8 110 117		3 30 29		12 72 56		6 87 83		-13 166 163		-2 160 -145		5 65 -60							
		11 65 63		9 206 -212		4 66 78		13 119 -119		8 54 57		-12 157 -156		-1 193 173		6 136 -127							
0,5,L		12 150 156		11 65 44						9 127 -107		0 197 -182		8 50 -69									
		13 57 50		14 51 54		2,0,L		2,5,L		10 366 -283		-11 295 -254		1 211 -176		3,12,L							
2 156 -164		14 66 57								11 37 23		-9 254 250		2 248 -240									
3 165 174				1,8,L		-14 111 -135		-16 165 204				-8 216 -175		3 214 207									
4 94 102		1,3,L				-12 173 -173		-15 76 -85		2,10,L		-7 220 206		4 229 -224		9 53 -78							
5 216 -208				-13 188 -168		-10 161 -207		-14 106 -97				-6 60 67		5 115 127		-7 86 -72							
6 70 -78		-15 45 48		-12 111 86		-8 525 -516		-13 96 -87		-11 110 -100		-5 263 242		6 29 37		-6 58 -67							
7 304 324		-13 68 -55		-11 161 301		-6 60 54		-11 180 -182		-10 42 -40		-4 311 236		7 140 156		-5 55 -48							
8 568 519		-12 93 99		-10 103 -117		-4 868E 732		-9 51 43		-9 77 74		-3 672E -563		8 143 -159		-4 59 63							
9 251 -238		-11 135 -157		-9 147 -155		-2 1028E -1266		-7 121 -144		-8 194 195		-2 705E -627		9 35 -42		-3 92 57							
11 87 99		-10 192 -197		-8 110 102		2 432 -390		-6 229 210		-7 60 54		-1 55 -53		10 36 40		-2 115 -91							
13 100 107		-9 305 -300		-7 241 -251		6 744E -703		-5 132 -122		-6 43 -45		0 189 210		11 49 40		-1 82 63							
		-8 244 227		-6 231 221		8 281 -301		-4 172 144		-5 155 134		1 59 -59		12 101 -108		0 392 342							
0,6,L		-7 540 487		-5 70 -59		10 256 -263		-3 50 45		-4 132 -147		2 120 -103		13 65 -105		2 153 -147							
		-6 171 -154		-4 78 71				-2 241 238		-3 137 136		3 426 465				3 130 -129							
1 504 485		-5 804E 833		-3 124 -123		2,1,L		-1 183 -179		-2 137 136		4 82 -108		3,7,L		5 114 105							
2 528 545		-4 908E -952		-2 96 -74				0 380 361		-1 329 -350		5 132 -140				6 88 -106							
4 555 472		-3 326 335		-1 180 189		-17 70 73		1 631E -593		0 210 -208		6 236 244		3,13,L									
5 139 160		0 449 510		0 424 419		-16 213 218		2 58 79		3 236 -189		-15 55 -53											
6 109 137		1 493 511		3 143 -151		-15 58 48		3 298 331		4 167 193		7 143 146		-14 43 -45									
7 91 128		2 329 400		4 326 333		-14 171 -178		4 348 341		5 96 105		8 103 -111		-13 60 56									
10 264 233		3 624E -703		5 153 -163		-13 384 -421		6 241 245		6 357 328		9 382 -415		-11 145 111		-7 40 -40							
11 169 151		4 217 251		6 246 255		-12 208 240		7 87 -100		8 57 -49		10 145 -153		-10 105 115		-6 94 -95							
13 108 102		5 457 462		7 157 -171		-11 233 -233		8 450 478		9 87 -97		11 49 44		-9 243 -231		-4 132 -153							
		6 101 97		8 85 106		-10 220 -224		9 31 42		10 52 49		12 177 -165		-8 194 149		-3 59 68							
0,7,L		7 392 393		9 124 129		-9 271 282		10 142 -148						-7 290 -260		-2 64 73							
		8 92 88		10 121 130		-8 158 -158		11 95 -90		2,11,L		3,9,L		-6 28 -20		0 46 -50							
1 414 414		9 477 -466		11 166 167		-7 64 77		12 138 124		-10 51 -46		-17 43 37		-5 97 76		1 179 -177							
2 114 -135		10 143 176		12 170 155		-6 802E 944		13 61 -70		-9 138 -121		-16 83 92		-4 51 45		2 171 -158							
3 299 -302		11 164 -174		13 81 -83		-5 266 279				-8 81 68		-15 125 -118		-3 51 45		3 186 159							
4 65 76		12 44 41				-4 433 -394		2,6,L		-7 146 125		-14 54 -53		-2 171 -158									
5 203 -222		13 201 211		1,9,L		-3 486 -463				-5 227 205		-13 123 118		-1 231 -231		4,0,L							
7 263 -244						-2 344 -345		-15 91 -95		-4 118 90		-12 35 46		0 74 -77									
8 221 -215		1,4,L		-11 120 -113		-1 698E -698		-14 219 -212		-3 73 -70		-11 149 149		1 513 560		-16 81 98							
10 376 312				-10 52 48		0 615E -620		-13 124 139		-2 91 -59		-10 243 -208		2 229 223		-14 297 306							
12 223 -210		-15 315 277		-9 42 -53		1 104 -89		-12 180 194		-1 312 288		-9 319 296		3 183 -180		-12 410 -425							
		-13 276 -237		-8 126 151		2 454 -437		-11 92 -98		0 110 96		-8 327 326		4 327 326		-10 239 205							
0,8,L		-12 49 50		-7 308 301		3 181 143		-10 109 102		1 74 -63		-7 125 -126		5 566E -601		-8 96 102							
		-11 60 67		-6 56 45		4 222 -201		-9 435 366		2 280 267		-6 108 -92		7 429 472		-6 600E 544							
0 181 193		-10 309 -286		-5 102 105		5 131 -131		-8 435 366		3 202 192		-5 407 362		9 67 -81		-4 256 215							
1 238 -237		-9 187 170		-4 184 -181		6 131 -131		-7 253 -251		4 225 213		-4 24 -27		10 54 62		4 362 380							
2 149 156		-8 196 -203		-3 411 391		7 178 192		-6 27 -23		5 140 117		-3 20 26		11 36 -31		6 447 422							
3 194 197		-6 78 54		0 231 218		8 207 -173		-5 66 51		6 130 -110		-2 891E 711		12 17 27		8 166 -158							
4 37 55		-5 312 296		1 219 -215		9 419 -441		-4 138 130		9 240 221		-1 114 -107				10 135 154							
5 230 -251		-4 488 465		2 153 157		10 319 -332		-3 123 125				0 841 -852		3,8,L									
6 104 -111		-3 578E 668		3 239 244		11 438 -455		-2 235 -223		2,12,L		1 730E 720				4,1,L							
7 137 -160		-2 528 -537		4 136 -139		12 90 -89		-1 190 151				2 170 -166		-14 35 -43									
9 352 -284		-1 290 -277		5 444 429				0 332 -273		-9 43 -53		3 82 -80		-13 141 -134		-14 158 -177							
10 85 91		0 821E -923		6 125 144		2,2,L		1 497 445		-8 72 85		4 81 -80		-12 98 78		-13 187 215							
11 87 -98		1 128 117		7 73 -71				2 512 555		5 87 -82		5 87 -82		-11 147 -137		-12 110 -134							
12 143 116		2 530 -535		8 126 113		-16 92 80		3 50 76		-7 63 80		6 123 -141		-10 61 74		-11 80 -78							
14 93 -99		4 161 -166		11 72 56		-15 87 78		4 325 -316		-6 146 164		7 103 -117		-9 259 221		-10 143 -156							
		5 59 76				-14 131 -100		-5 146 164		-4 34 -42		8 110 127		-8 144 -124		-9 196 168							
0,9,L		6 116 94		1,10,L		-13 54 -52		5 26 32		10 195 -202		9 110 127		-7 167 -177		-8 194 -174							
		7 76 -75				-11 228 -202		6 236 211		-3 65 -55		11 82 98		-6 297 -297		-7 296 274							
1 610 610		8 469 -454		-12 76 -56		-9 301 301		7 150 -159		-2 153 161		12 244 -251		-5 297 252		-6 148 135							
2 210 230		9 152 -167		-11 46 52		-8 234 -208		8 179 -206		-1 35 -37		13 66 -93		-4 348 349		-5 218 -208							
3 218 233		11 147 -171		-9 103 -109		-7 140 -136		9 204 210		0 112 112				-3 55 56		-4 786E -668							
4 43 -63		12 142 -141		-8 88 69		-6 74 94		10 139 -158		1 39 -41		3,4,L		-2 110 82		-3 201 183							
5 214 -226		13 90 -93		-6 343 280		-5 255 211		11 69 76		2 249 -248				1 299 -312		-1 443 414							
6 263 -279		14 193 -189		-4 43 47		-4 949E 932		12 122 -118		3 147 147		-16 69 41		0 128 82		0 93 36							
9 454 374				-3 169 186		-2 172 -198		13 50 -44		4 102 106		-15 203 -185		1 49 59		1 106 -126							
										5 56 54		-14 118 -94		2 136 -135		2 491 -445							
										6 203 196		-13 103 -108		4 145 165		3 343 358							

TABLE 1. Observed and calculated structure factors [a] for $N_2H_5^+$ $[C(NO_2)_3]^-$ —Continued. (Columns are l, $10F_o$, $10F_c$)

| | | |

TABLE 2. *The crystallographic coordinates in* $N_2H_5^+[C(NO_2)_3]^-$

Atom	*x*	*y*	*z*	*B*
Trinitromethide anion 1				
O(11)	[a] 1.0245(4)	0.2576(2)	0.2062(2)	1.53(6)
O(12)	0.9407(4)	.2422(2)	.3406(2)	1.71(6)
O(13)	.6213(4)	.1781(2)	.2729(2)	1.54(6)
O(14)	.4573(4)	.3086(2)	.1895(2)	1.67(6)
O(15)	.6052(4)	.4415(2)	.0878(2)	1.64(6)
O(16)	.8842(4)	.4519(2)	.1374(2)	1.48(6)
N(11)	.9157(5)	.2689(3)	.2534(2)	1.33(6)
N(12)	.6019(4)	.2656(3)	.2230(2)	1.22(6)
N(13)	.7460(4)	.4063(2)	.1404(2)	1.17(6)
C(11)	.7503(5)	.3158(3)	.2044(3)	1.28(7)
Trinitromethide anion 2				
O(21)	0.9957(4)	0.6472(2)	0.4666(2)	1.86(6)
O(22)	.7380(4)	.7257(2)	.5074(2)	1.78(6)
O(23)	.8344(4)	.5462(2)	.6584(2)	1.95(6)
O(24)	.6853(4)	.3965(2)	.5992(2)	1.97(6)
O(25)	.6176(4)	.3789(2)	.4040(2)	2.00(6)
O(26)	.6695(4)	.5329(2)	.3300(2)	1.87(6)
N(21)	.8161(4)	.6430(3)	.4892(2)	1.29(6)
N(22)	.7535(5)	.4886(3)	.5871(2)	1.49(6)
N(23)	.6727(5)	.4777(3)	.4057(2)	1.41(6)
C(21)	.7398(6)	.5314(3)	.4946(3)	1.62(7)
Hydrazinium ion 3				
N(31)	0.2074(5)	0.0376(3)	0.3594(3)	1.82(7)
N(32)	.3198(5)	.1121(3)	.3221(2)	1.53(6)
Hydrazinium ion 4				
N(41)	0.0930(5)	0.3367(3)	0.0018(3)	1.53(6)
N(42)	.2647(5)	.3413(3)	−.0125(3)	1.37(6)

[a] The values quoted in parentheses are the standard errors in the last digit and were calculated from the final full-matrix least-squares refinement cycle. Average shift/error for last cycle = 0.17 for all parameters except hydrogens.

TABLE 3. *Comparison of hydrogen positions in* $N_2H_5^+[C(NO_2)_3]^-$

	Weighted difference electron density synthesis			Least squares [a] refinements			Calculation [b]		
	x	*y*	*z*	*x*	*y*	*z*	*x*	*y*	*z*
H(1)	0.189	0.000	0.324	0.187	0.007	0.308	0.180	−0.033	0.315
H(2)	.139	.084	.367	.156	.075	.385	.093	.080	.359
H(3)	.349	.076	.281	.358	.075	.281	.365	.070	.269
H(4)	.386	.140	.365	.397	.143	.368	.424	.136	.380
H(5)	.256	.160	.293	.253	.169	.289	.250	.183	.292
H(6)	.088	.392	.043	.091	.382	.069	.076	.404	.045
H(7)	.101	.269	.034	.086	.267	.033	.078	.261	.036
H(8)	.349	.330	.041	.337	.328	.044	.354	.324	.054
H(9)	.306	.290	−.054	.288	.286	−.060	.274	.282	−.065
H(10)	.285	.416	−.034	.289	.411	−.033	.287	.422	−.036

[a] Estimated random standard errors from the least squares refinement are 0.01 in *x*, 0.006 in *y* and 0.005 in *z* (i.e., about 0.13 Å total). The systematic error known to accompany the location by x-ray methods of a covalently bonded hydrogen is 0.1–0.2 Å.

[b] Assuming sp^3 hybridization of N and N—H = 1.03 Å (see text). Ends of $N_2H_5^+$ ions rotating independently of each other.

TABLE 4. *The trinitromethide anion geometries.*

Atoms	Distance, Å	Atoms	Angle, deg.
Anion 1			
C(11), N(11)	[a] 1.432(5)	N(11), C(11), N(12)	117.3(3)
N(12)	1.397(5)	N(11), C(11), N(13)	118.4(4)
N(13)	1.385(5)	N(12), C(11), N(13)	124.3(3)
N(11), O(11)	1.225(5)	O(11), N(11), O(12)	123.6(3)
O(12)	1.226(4)	O(13), N(12), O(14)	122.0(4)
N(12), O(13)	1.231(4)	O(15), N(13), O(16)	120.4(3)
O(14)	1.228(4)	O(11), N(11), C(11)	118.3(3)
N(13), O(15)	1.238(4)	O(12), N(11), C(11)	118.1(4)
O(16)	1.228(4)	O(13), N(12), C(11)	118.1(3)
O(11), O(12)	2.159(5)	O(14), N(12), C(11)	120.0(3)
O(12), O(13)	2.572(4)	O(15), N(13), C(11)	120.7(3)
O(13), O(14)	2.150(4)	O(16), N(13), C(11)	118.9(3)
O(14), O(15)	2.587(4)		
O(15), O(16)	2.140(4)		
O(16), O(11)	2.618(4)		
Anion 2			
C(21), N(21)	1.456(5)	N(21), C(21), N(22)	116.7(3)
N(22)	1.366(5)	N(21), C(21), N(23)	115.9(3)
N(23)	1.374(5)	N(22), C(21), N(23)	127.2(4)
N(21), O(21)	1.225(5)	O(21), N(21), O(22)	124.3(3)
O(22)	1.214(4)	O(23), N(22), O(24)	121.4(3)
N(22), O(23)	1.239(4)	O(25), N(23), O(26)	123.2(3)
O(24)	1.241(4)	O(21), N(21), C(21)	117.6(3)
N(23), O(25)	1.239(4)	O(22), N(21), C(21)	118.2(4)
O(26)	1.237(4)	O(23), N(22), C(21)	117.3(3)
O(21), O(22)	2.156(5)	O(24), N(22), C(21)	121.3(3)
O(22), O(23)	2.945(4)	O(25), N(23), C(21)	120.1(3)
O(23), O(24)	2.163(4)	O(26), N(23), C(21)	116.8(3)
O(24), O(25)	2.650(4)		
O(25), O(26)	2.178(4)		
O(26), O(21)	2.891(4)		

[a] The quantities quoted in parentheses are standard errors based on the standard errors of the positional parameters and the standard errors of the cell dimensions.

group and atoms in neighboring anions of type 1 are O(21) . . . O(12)= 2.92 Å, O(22) . . . O(12)= 2.89 Å, N(21) . . . O(12)= 2.97 Å on one side and O(21) . . . N(21)= 2.93 Å, O(22) . . . N(13)= 2.99 Å on the other side.

Among the differences in the two trinitromethide anions in this structure, the C(11)—N(11) and C(21)—N(21) distances of 1.43 and 1.46 Å, respectively, may reflect in part the decrease in π orbital overlap between C and N since their π orbitals are at 41° and 74° to each other in the two cases. The increased electron density in the remaining C—N π bonds on going from anion 1 to anion 2 is consistent with the shorter distances (table 3) in these bonds in anion 2. Superimposed on this result, however, would be the changes in σ bond length due to differing bond angles and hence different hydridizations of the orbitals in the σ bond skeleton [15]. Further, the N(22) . . . C(21) . . . N(23) angle of 127° may be at first considered to result from the fact that the N(22) and N(23) nitrogroups are almost coplanar (dihedral angles of 5° and 4°) with the $C(N)_3$ part of the anion 2. However, the shortest intra-ionic inter-nitrogroup oxygen-oxygen distance is 2.572 Å for O(12) . . . O(13). If the O(24) . . . O(25) oxygens were this far apart, the N(22) . . . C(21) . . . N(23) angle could decrease by about 2.5°.

Trinitromethide anions and related species have been found in a variety of conformations in crystal structures of other compounds. The following examples show that the conformations these anions assume are very strongly influenced by the environments. The trinitromethide conformations observed in hydrazinium trinitromethide are seen to be plausible when compared with the conformations in the examples.

The trinitromethide anion in $Rb^+[C(NO_2)_3]^-$ has been found in a preliminary study [16] to have an approximately planar $C(N)_3$ central region, with one NO_2 group twisted about 45° to this central plane, with the oxygens of another NO_2 group above the $C(N)_3$ plane, and with the oxygens of the third NO_2 group below this plane. In the trinitromethide anion in $Cs^+[C(NO_2)_3]^-$ [16], two of the NO_2 groups have been rotated in opposite directions, one about 75° and the other, 35°. The oxygens of the third NO_2 group are on the same side of the $(N)_3$ plane as the central C atom.

In $Na^+[C(CN)_3]^-$, the central C atom is 0.024 Å out of the central $(C)_4$ plane [17]; this is similar to the situation found in anion 2. In $K^+[C(CN)_3]^-$ the corresponding deviation is 0.015 Å. These deviations from planarity have been attributed to the effect of packing in the structure. In $K^+[p(NO_2)C_6H_4C(CN)_2]^-$ the bonding about the central carbon atom is pyramidal and there seems to be some effect of resonance on the aromatic character of the phenyl ring [18].

In $K^+[C(NO_2)_3^-]$, one nitrogroup is perpendicular to the rest of the anion [19]. In $Ca^{2+}[C(C(CN)_2)_3]^{2-}\cdot 6H_2O$, each $C(CN)_2$ group is rotated out of the plane of the four central carbon atoms by 24° [20]. In a completely planar and symmetrical trinitromethide anion (with distances and angles the averages of those in anion 1) the O . . . O distance between adjacent oxygens in different nitrogroups would be 2.42 Å. If the closest permissible approach of these adjacent oxygens is assumed (judging from anion 1) to be about 2.60 Å, the trinitromethide anion cannot be planar and would have to rotate all its nitrogroups by about 21° about the C—N bonds to achieve a regular trigonal configuration. This angle is close to the 24° reported in reference 20 for $Ca_2^{2+}[C(C(CN)_2)_3]^{2-}\cdot 6H_2O$.

4.2. The Hydrazinium Ions

The N—N distances in the hydrazinium ions are N(31)—N(32)= 1.438(6) and N(41)—N(42)= 1.424(7) Å. Possible positions for the hydrogen atoms in the hydrazinium ions were found in the weighted difference synthesis. These positions suggest that the N(31)—N(32) hydrazinium ion is approximately eclipsed and the N(41)—N(42) hydrazinium ion is approximately staggered.

As an independent check on the observed hydrogen positions and in a first-approximation attempt to gain some insight into the hydrazinium conformations found, idealized hydrazinium ions with N—N—H angles of 109.5° (sp^3 hybridization of N), N—H distances of 1.03 Å and N—N distances of 1.431 Å (the average of those quoted above) were first generated in both exactly eclipsed and exactly staggered conformations. The lone pair of electrons in each hydrazinium ion was considered to be on each nitrogen atom in turn. These idealized ions were rotated over 360° in steps of 3° about the N—N vector in an environment of all atoms other than hydrogen which are nearer than 3.5 Å to the nitrogen atoms in the hydrazinium ions. Because of uncertainty in the nature of the hydrogen bond (see for example reference 21), the shortest H_i . . . X distance, D_i, for each hydrogen at each step of the rotation was summed up as

$$\sum_i D_i \quad \text{and} \quad \sum_i 1/D_i$$

to obtain quantities predictive of the hydrazinium orientation. When maximised, $\Sigma 1/D_i$ is an approximation to the electrostatic term in the hydrogen bonding; it assumes (a) all hydrogens are equally charged, (b) all atoms in the environment are equally charged, (c) there is no electrostatic interaction between hydrogen atoms either within a given ion or in different ions, and (d) the shortest H_i . . . X distance is of overriding importance. Its use involves the reasonable assumption that the electrostatic term is dominant in hydrogen bonding at H . . . X distances of ~1.9 Å to ~ 2.4 Å. When minimised, ΣD_i places greater weight on the shortest H . . . X distances, which are known to be the strongest hydrogen bonds.

The hydrogen positions for best hydrogen bonding (according to the ΣD and $\Sigma 1/D$ criteria) for the *exactly eclipsed* N(31)—N(32) hydrazinium ion with three hydrogen atoms on N(32) were found to agree fairly closely with those observed. For this orientation, $\Sigma D = 10.437$, $\Sigma 1/D = 2.403$. The best orientation for the *exactly staggered* form of N(31)—N(32) gave $\Sigma D = 10.610$ and $\Sigma 1/D = 2.369$ and thus showed poorer hydrogen bonding to the environment. The form with three hydrogens (the configuration observed in the difference synthesis) on N(32) was able to form better hydrogen bonds than the form with three hydrogens on N(31) according to the ΣD and $\Sigma 1/D$ criteria. The best hydrogen bonding for the *exactly eclipsed* form of the N(41)—N(42) hydrazinium ion with three hydrogens on N(42) appeared to be close ($\Sigma D = 10.372$, $\Sigma 1/D = 2.418$) to that of the *exactly staggered* form ($\Sigma D = 10.452$, $\Sigma 1/D = 2.402$). The forms with three hydrogens on N(42) (the configuration observed) were better bonded than those with three hydrogens on N(41).

The *eclipsed* form of the N(41)—N(42) hydrazinium ion has, however, an unreasonably small contact H(7) . . . H(4) = 1.44 Å with the *eclipsed* form of the N(31)—N(32) ion. The *staggered* form of the N(31)—N(32) ion has an unreasonable contact H(1) . . . H(6) = 1.62 Å with the *staggered* form of the N(41)—N(42) ion and an unreasonable contact H(4) . . . H(7) = 1.53 Å with the *eclipsed* form of N(41)—N(42). Thus, neglecting intra-ionic hydrogen replusions, the optimum exact conformations seem to be *eclipsed* for N(31)—N(32) and *staggered* for the N(41)—N(42) hydrazinium ions. These conformations are the ones observed. The main difference between predicted staggered and eclipsed forms of the same hydrazinium ion is the location of the hydrogens in the NH_2 group, not those in the NH_3 group.

Since intraionic hydrogen replusion is highest when the hydrazinium ions are exactly eclipsed and since this repulsion term is apparently low enough to allow the hydrazinium ions to deviate from being exactly staggered, hydrogen positions were then generated by rotating the ends of the ions freely in their environments. The resultant best positions for hydrogens on N(31)—N(32) ($\Sigma D = 10.390$, $\Sigma 1/D = 2.413$) agree well (average difference = 0.09 Å) with those calculated for the exactly *eclipsed* form. The best hydrogen positions for H(8), H(9), and H(10) on N(41)—N(42) agree within 0.013 Å with those of the exactly *staggered* form. For the H(6) and H(7) positions, there are two minima, one in the $\Sigma 1/D$ quantity and one in the ΣD quantity. The resultant conformations of the ions are approximately *staggered* and *eclipsed* respectively. The best H(6) and H(7) positions in the approximately *staggered* form give $\Sigma D = 10.4496$, $\Sigma 1/D = 2.4025$ for the whole N(41)—N(42) hydrazinium ion. For the approximately *eclipsed* conformation, the best hydrogen positions give $\Sigma D = 10.3608$, $\Sigma 1/D = 2.4205$. To minimize interionic interhydrogen repulsions as stated earlier, the approximately *eclipsed* form of N(31)—N(32) and the approximately *staggered* form of N(41)—N(42) are preferred. These calculated positions for hydrogen are given in table 3 and are the ones used in subsequent calculations. In general, they are near those observed although the positions of those calculated for H(1) and H(2) are slightly different (~ .5 Å) from those observed, but give better hydrogen bonds.

The environments of the hydrazinium ions are shown in figures 4 and 5. The distances in the hydrogen bonds are given in table 5 and are in the normal range. Angles showing the deviation from linearity of the hydrogen bonds are also given in table 5 and are satisfactory. According to Donohue [22] any such angle above 135° is within the normal range for a primary hydrogen bond. From table 5 and figure 3, it may be seen that O(21), O(22) and O(26) in the trinitromethide anions form very weak, if any, hydrogen bonds. The distances to their nearest neighbors (other than hydrogen atoms) in the structure are N(12) . . . O(21) = 2.926(6) Å, N(41) . . . O(22) = 2.899(8) Å, N(13) . . . O(22) = 2.990(5) Å O(13) . . . O(26) = 2.991(7) Å and N(11) . . . O(26) = 3.020(6) Å. Although none of these neighbors is unusually close, each oxygen not hydrogen bonded is near an NO_2 group and may possibly undergo van der Waals bonding with the π electrons of the NO_2 group.

A. L. Milstead of the Naval Ordnance Station visually estimated the raw intensity data. The x-ray 63

crystallographic computing system [23] was used for all crystallographic computations subsequent to the calculation of the observed structure factors from the observed data.

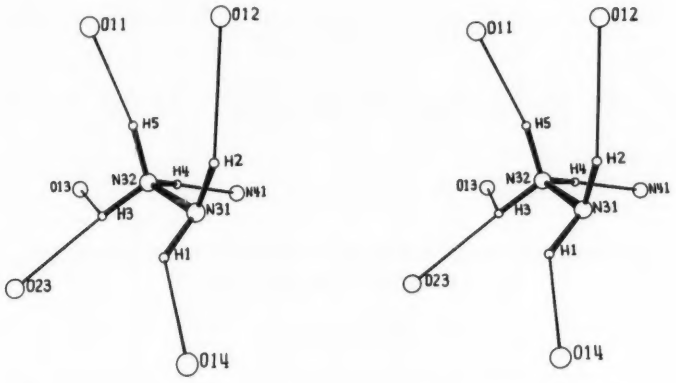

FIGURE 4. *The environment of the eclipsed hydrazinium ion* N(31)—N(32); *atoms within 2.40 Å of the hydrogens are included.*

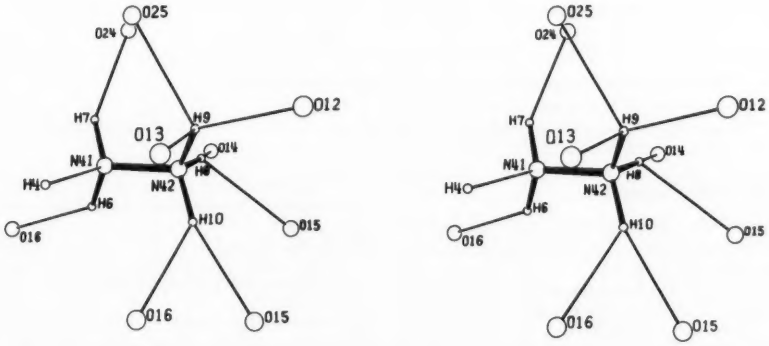

FIGURE 5. *The environment of the staggered hydrazinium ion* N(41)—N(42); *atoms within 2.40 Å of the hydrogens are included.*

TABLE 5. *Possible hydrogen bonds in* $N_2H_5^+$ $[C(NO_2)_3]^-$

	$H_R \ldots X$, Å	$H_D \ldots X$, Å	$H_C \ldots X$, Å	N—H . . . X angle		
				R, deg	*D*, deg	*C*, deg
H(1), O(14).....	2.6	2.5	2.15	113	132	138
H(2), O(12).....	2.6	2.4	2.24	138	162	149
H(3), O(23).....	2.2	2.2	2.03	154	160	152
O(13).....	2.4	2.5	2.39	103	105	100
O(16).....	2.5	2.6	> 2.4	112	109	.....
O(24).....	2.6	2.6	> 2.4	115	119	.....
H(4), N(41).....	2.1	2.2	1.91	160	162	169
O(13).....	2.5	2.6	> 2.4	98	97	....
H(5), O(11).....	2.1	2.2	2.06	160	165	151
H(6), O(16).....	2.3	2.4	2.30	115	136	136
N(31).....	2.5	2.5	> 2.4	136	137	.....
H(7), O(24).....	2.2	2.2	2.14	155	164	149
O(22).....	2.5	2.6	> 2.4	104	97	.....
O(25).....	2.5	2.5	> 2.4	103	105	.....
H(8), O(14).....	2.0	2.0	1.87	166	156	162
O(15).....	2.4	2.4	2.37	118	124	114
H(9), O(12).....	2.1	2.1	2.11	142	151	135
O(25).....	2.3	2.5	2.33	120	112	125
O(13).....	2.4	2.5	2.25	113	107	116
H(10), O(15).....	2.1	2.1	2.04	168	164	163
O(16).....	2.4	2.3	2.25	132	134	133

[R] Refers to hydrogen positions from least squares refinements.

[D] Refers to hydrogen positions from difference synthesis.

[C] Refers to hydrogen positions from calculation (see text).

5. References

[1] Hine, J., and Bailey, W. C., Jr., Substituent constants for the trinitromethyl-, 1,1-dinitroethyl-, and related groups, J. Org. Chem. **26,** 2098–2099 (June 1961).

[2] Parker, C. O., Emmons, W. D., Rolewicz, H. A., and McCullum, K. S., Chemistry of dinitroacetonitrile-I preparation and properties of dinitroacetonitrile and its salts, Tetrahedron **17,** 79–87 (1962).

[3] Boyd, R. H., Cyanocarbon chemistry. XXIII. The ionization behavior of cyanocarbon acids, J. Phys. Chem. **67,** 737–744 (1963).

[4] Hall, T. N., Reactions of nitro alcohols. I. The dissociation constants of some 2-substituted derivatives of 2,2-dinitroethanol in water, J. Org. Chem. **29,** 3587–3591 (Dec. 1964).

[5] Williams, J. K., Martin, E. L., and Sheppard, W. H., Alkyl- and aryltricyanomethanes, synthesis and properties, J. Org. Chem. **31,** 919–922 (March 1966).

[6] Dickens, B., The crystal structure of hydrazine nitroform $[N_2H_5^+C(NO_2)_3^-]$, Chem. Comm. 246–247 (1967).

[7] Dickens, B., Techniques for the low-temperature x-ray studies of sensitive materials, Report NPP/RR 66–9, Naval Propellant Plant, Indian Head, Md. 20640 (1966).

[8] Dickinson, C., Stewart, J. M., and Holden, J. R., A direct determination of the crystal structure of 2,3,4,6-tetranitroaniline, Acta Cryst. **21,** 663–669 (1966).

[9] Chastain, R. V., and Stewart, J. M., An algorithm for finding a set of phases directly from sigma two relations (centrosymmetric case), American Crystallographic Association—Winter Meeting, Abstract A8, Georgia Institute of Technology, Atlanta, Ga., Jan. 25–28, 1967.

[10] Chastain, R. V., An algorithm for finding a set of phases directly from sigma two relationships (Centrosymmetric case), In, X-ray 67-Program System for X-ray Crystallography, Technical Report 67–58, Ed. J. M. Stewart, pp. 71–75, University of Maryland, College Park, Md. (1967).

[11] Karle, I. L., and Karle, J., An application of a new phase determination procedure to the structure of cyclo (hexaglycy) hemihydrate, Acta Cryst. **16,** 969–975 (July–Dec. 1963).

[12] Karle, J., and Karle, I. L., The symbolic addition procedure for phase determination for centrosymmetric and noncentrosymmetric crystals, Acta Cryst. **21,** 849–859 (Nov.–Dec. 1963).

[13] International Tables for X-ray Crystallography **3,** 202 (the Kynoch Press, Birmingham, England, 1962).

[14] McWeeney, R., X-ray scattering by aggregates of bonding atoms. I. Analytical approximations in single-atom scattering Acta Cryst. **4,** 513–519 (1951).

[15] Coulson, C. A., The atomic radius of carbon, Victor Henri Memorial Lectures, Liege, Belgium, 15–31 (1948).

[16] Grigor'eva, N. V., Margolis, N. V., Shokhor, I. N., Mel'nikov, V. V., and Tselirskii, I. V., X-ray structure investigation of salts of trinitromethane, translated from Z. Struk. Kh. **7,** 278–280 (1966).

[17] Anderson, P., Klewe, B., and Thom, E., The crystal structure of sodium tricyanomethanide, $NaC(CN)_3$, Acta Chem. Scand. **21,** 1530–1542 (1967).

[18] Sass, R. L., and Bugg, C., The crystal structure of potassium *p*-nitrophenyldicyanomethide, Acta Cryst. **23,** 282–288 (1967).

[19] Golovina, N. I., and Atovmyan, L. O., X-ray structural study of the potassium salt of nitroform (trinitromethane), translated from Z. Struk. Kh. **8,** 307–311 (1967).

[20] Bekoe, D. A., Gantzel, P. K., and Trueblood, K. N., The crystal structure of the hexahydrated calcium salt of hexacyanoisobutylene, Acta Cryst. **22,** 657–665 (1967).

[21] Bratoz, S., Electronic theories of hydrogen bonding. Adv. Quantum Chem. **3,** 209–237 (1967).

[22] Donohue, J., Selected topics in hydrogen bonding, Book, Structural Chemistry and Molecular Biology, Ed. A. Rich and N. Davidson, pp. 443–465, (W. H. Freeman and Co., London, 1968).

(Paper 74A3–602)

JOURNAL OF RESEARCH of the National Bureau of Standards—A. Physics and Chemistry
Vol. 74A, No. 3, May–June 1970

A Refinement of the Crystal Structure of $Na_2CO_3 \cdot H_2O$

B. Dickens, F. A. Mauer, and W. E. Brown*

**Institute for Materials Research, National Bureau of Standards
Washington, D.C. 20234**

(January 28, 1970)

The crystal structure of synthetic $Na_2CO_3 \cdot H_2O$ has been refined using 1231 unique x-ray diffraction data collected by the peak height method on a diffractometer. $R = 0.034$. The unit cell is $a = 6.474(2)$, $b = 10.724(3)$ and $c = 5.259(2)$ Å with $z = 4$ and space group $P2_1ab$. The calculated density is the same as the observed density, 2.26 g·cm^{-3}. The structure contains sheets of CO_3^{2-} ions bonded to Na^+ ions and water molecules roughly halfway between the sheets. Each CO_3^{2-} bonds edgewise to both Na^+ ions. The Na^+ ions have irregular but similar coordinations of seven neighbors. Each water molecule is bonded to both Na^+ ions and forms hydrogen bonds to both neighboring CO_3^{2-} layers.

Key words: Crystal structure; hydrated carbonates; hydrogen bonding; sodium carbonate; thermonatrite; x-ray diffraction.

1. Introduction

The crystal structure of $Na_2CO_3 \cdot H_2O$ was determined except for the hydrogen positions, by Harper [1][1] in 1936 using qualitative estimates of the x-ray intensities. In our program of studies on coordination in hydrated carbonates [2] and phosphates [3], we have refined Harper's structure for $Na_2CO_3 \cdot H_2O$ using new x-ray data. $Na_2CO_3 \cdot H_2O$ is the mineral thermonatrite and often occurs with $Na_2CO_3 \cdot 10H_2O$ (natron) and $Na_2CO_3 \cdot NaHCO_3 \cdot 2H_2O$ (trona) [4, 5, 6].

2. Determination of the Structure

Formula: $Na_2CO_3 \cdot H_2O$. *Unit cell:* Orthorhombic with $a = 6.472(2)$ Å, $b = 10.724(3)$ Å, $c = 5.259(2)$ Å at 24 °C as calculated from three pairs of 2θ values of axial reflections from a single crystal and observed on a diffractometer. The standard deviations of the cell parameters are in parentheses and are estimates based on experience with the technique. *Cell volume:* 365.1 Å^3. *Wavelength used:* 0.710688 Å (Mo Kα). *Filter:* 0.025 mm Nb. *Space Group:* $P2_1ab$. *Cell contents in formula Wts:* 4. *Equivalent positions:* x, y, z; $1/2+x, -y, -z$; $1/2+x, 1/2-y, z$; $x, 1/2+y, -z$. *Reciprocal lattice extinctions:* $h0l$, $h \neq 2n$; $hk0$, $k \neq 2n$. *Observed density:* 2.255 g·cm^{-3} [7]. *Calculated density:* 2.256 g·cm^{-3}. *Habit:* Fragment from plate. *Size of crystal:* ~ 0.35 mm max. ~ 0.05 mm min. *Origin:* Evaporation of aqueous solution at 60 °C. *Linear absorption coefficient:* 4.37 cm^{-1}. *Absorption corrections:* None applied. Maximum error in any intensity from absorption is ~ 10 percent. *Number of reflections:* 2189 were collected from 2 octants and merged into a unique set of 1231 of which 1132 are "observed" reflections and 99 are less than 2σ above background and are "unobserved". *Maximum sin θ/λ for data:* 0.904 Å^{-1}. *Method used to estimate data:* peak height measurement [8] with a single crystal diffractometer [9] and some peak heights standardized against $\theta/2\theta$ scans. *Scattering factors:* Na, C, O, for neutral atoms given in reference [10]; H from reference [11]. *Least-squares refinements:* Full-matrix, with $\Sigma(w\|F_o\|-\|F_c\|)^2$ minimized. Refinements include unobserved reflections for which the calculated intensities are more than 2σ above background. *Least-squares weights:* $1/\sigma^2$ normalized so that maximum weight is 1. *Definitions:* counts in peak $= I = P - (T/2T_B)(B_L + B_H)$, $\sigma(I) = (P + (B_L + B_H)(T/(2T_B))^2)^{1/2}$, $F = ((AF)(LP)(I))^{1/2}$, $\sigma(F) = (\sigma(I)/2)(LP/I)^{1/2}$ where P = counts at the peak position, B_L and B_H = background counts at lower and higher 2θ respectively, T = time spent counting peak, T_B = time spent counting each background, AF = attenuator factor, LP = Lorentz polarization correction.

$$R_w = \left(\sum(w\|F_o|-|F_c\|)^2 \Big/ \sum(w|F_o|)^2\right)^{1/2}$$

$$R = \left(\sum\left\|F_o|-|F_c\right\|\right) \Big/ \sum\left|F_o\right|.$$

*Director, Research Associate Program of the American Dental Association at the National Bureau of Standards.

[1] Figures in brackets indicate the literature references at the end of this paper.

Final R_w: 0.029. *Final R:* 0.032. *Average shift/error for last cycle:* 0.015. *Thermal parameters:* anisotropic with form

$$\exp(-1/4(a^{*2}B_{11}h^2+b^{*2}B_{22}k^2+c^{*2}B_{33}l^2+2a^*b^*B_{12}hk+2a^*c^*B_{13}hl+2b^*c^*B_{23}kl)).$$

The structure was refined isotropically from Harper's parameters using the x-ray 67 system [12] of computer programs to $R_w=0.065$; the x parameter of Na(1) was fixed at $x=0$. The structure was refined anisotropically to $R_w=0.044$ and the hydrogens were found unambiguously as the two highest peaks in the difference synthesis in which the coefficients were weighted by the least squares weights. The two next highest peaks were less than 3/4 as high as the peaks assigned to hydrogens and were (a) halfway between C and 0(3) in the CO_3 group and (b) 0.7 Å from 0(1) of the CO_3 group. The hydrogens were included with variable positional parameters and fixed thermal parameters ($B_H=1$ Å^2) in the final refinement to $R_w=0.029$. The largest correlation coefficients are ~ 0.25 between the scale factor and the B_{11} thermal parameters of the two Na ions and ~ 0.15 between these B_{11} thermal parameters. Most correlation coefficients are less than 0.05.

The atomic parameters are given in table 1. The observed and calculated structure factors are given in table 2. The hydrogen positions obtained from the weighted difference synthesis and from the refinements differ by ~ 0.17 Å. "Calculated" hydrogen positions were derived by applying the geometry of free water (O—H = 0.958 Å, ∠H—O—H = 104.5°) with the constraint that the O—H . . . O angles be as near to linear as possible. These hydrogen positions differ from the other positions by about 0.3 Å. The three sets of hydrogen positions are compared in table 3. The distances and angles which involve hydrogen were obtained using the "calculated" hydrogen positions.

3. Description of the Structure

The structure (fig. 1) contains CO_3 anions whose planes are almost perpendicular to a and which form sheets at $x\sim 0.25$ and $x\sim 0.75$. Because the C atoms lie close to the planes of the a glides, they form columns along a at $y=0.25$, $z\sim 0.60$. Two adjacent CO_3 groups in a column are held together by both being ionically bonded to four Na ions and hydrogen bonded by one water molecule. The four Na ions and the water molecule form a pentagon roughly halfway between the CO_3 sheets. Adjacent CO_3 groups in a given sheet are linked by the Na ions that lie above and below the sheet.

3.1. The Carbonate Anion and Invironment

The dimensions in the CO_3 anion are given in table 4 and the environment is detailed in table 4 and figure 2. The CO_3 group is nearly trigonal. As can be seen in figures 1 and 2, O(2) is the only oxygen which is not hydrogen bonded, being instead ionically bonded to four Na ions. The absence of hydrogen bonding to O(2) may account for the observation that the C—O(2) bond is apparently the shortest of the three. O(1) is coordinated to three Na ions and is the acceptor in the hydrogen bond O(1) . . . H(1)—O(4) from the water molecule. O(3) is bonded strongly to two Na ions and more weakly (2.822 Å) to a third Na(2). O(3) is the acceptor in the hydrogen bond O(3) . . . H(2)—O(4) from the water molecule.

Since the planes of the CO_3 groups are all essentially perpendicular to a, this is expected to be the direction of lowest refractive index, as was found by Harper [1]. Later workers [13, 14] apparently did not permute the refractive indexes when they permuted the unit cell axes to fit crystallographic convention.

3.2. The Sodium Environments

The two crystallographically distinct Na ions in the structure are in general positions. Their environments are shown in figure 3 and are given in table 5.

Na(1) is bonded ionically to five oxygens from CO_3 groups, and strongly to one water oxygen. Four of the CO_3 oxygens, O(1), O(2′), O(3), O(3′), figure 3, define an approximate square about Na(1), and water oxygen O(4) forms the apex of a square pyramid. The fifth carbonate oxygen, O(2), is in the same CO_3 group as O(1); the CO_3 group is therefore coordinated edgewise to Na(1). The position of O(2) is such that the coordina-

TABLE 1. *Atomic parameters of* $Na_2CO_3\cdot H_2O$

Atom	x	y	z	B_{11}^*	B_{22}	B_{33}	B_{12}	B_{13}	B_{23}
Na(1)	0.0000	0.1938(1)	0.1398(1)	1.40(3)	1.54(3)	1.36(3)	0.17(3)	0.17(3)	0.08(2)
Na(2)	.0651(2)	.0020(1)	−.3786(2)	1.44(3)	1.19(3)	1.76(3)	.31(2)	.25(3)	.09(3)
C	−.2151(3)	.2556(2)	.6025(3)	.45(6)	1.11(6)	1.17(5)	−.06(5)	−.05(5)	−.03(5)
O(1)	−.2010(3)	.1381(1)	.5457(3)	1.56(6)	0.72(5)	2.72(7)	.08(5)	−.15(6)	−.47(4)
O(2)	−.2027(3)	.3369(1)	.4267(2)	1.73(6)	1.27(5)	1.24(5)	−.05(5)	−.04(5)	.47(4)
O(3)	−.2398(3)	.2876(1)	−.1639(2)	1.42(6)	2.14(6)	0.90(4)	−.28(5)	.25(4)	−.32(4)
O(4)	.0325(3)	−.0296(1)	.0683(3)	1.64(7)	1.43(6)	1.92(6)	−.21(5)	−.25(5)	.39(4)

Figures in parentheses are standard errors in last significant figure quoted, and were computed in the final cycle of full-matrix least-squares refinement.

*Thermal parameters are in Å^2.

TABLE 2. Observed and calculated structure factors for $Na_2CO_3 \cdot H_2O$ [a]

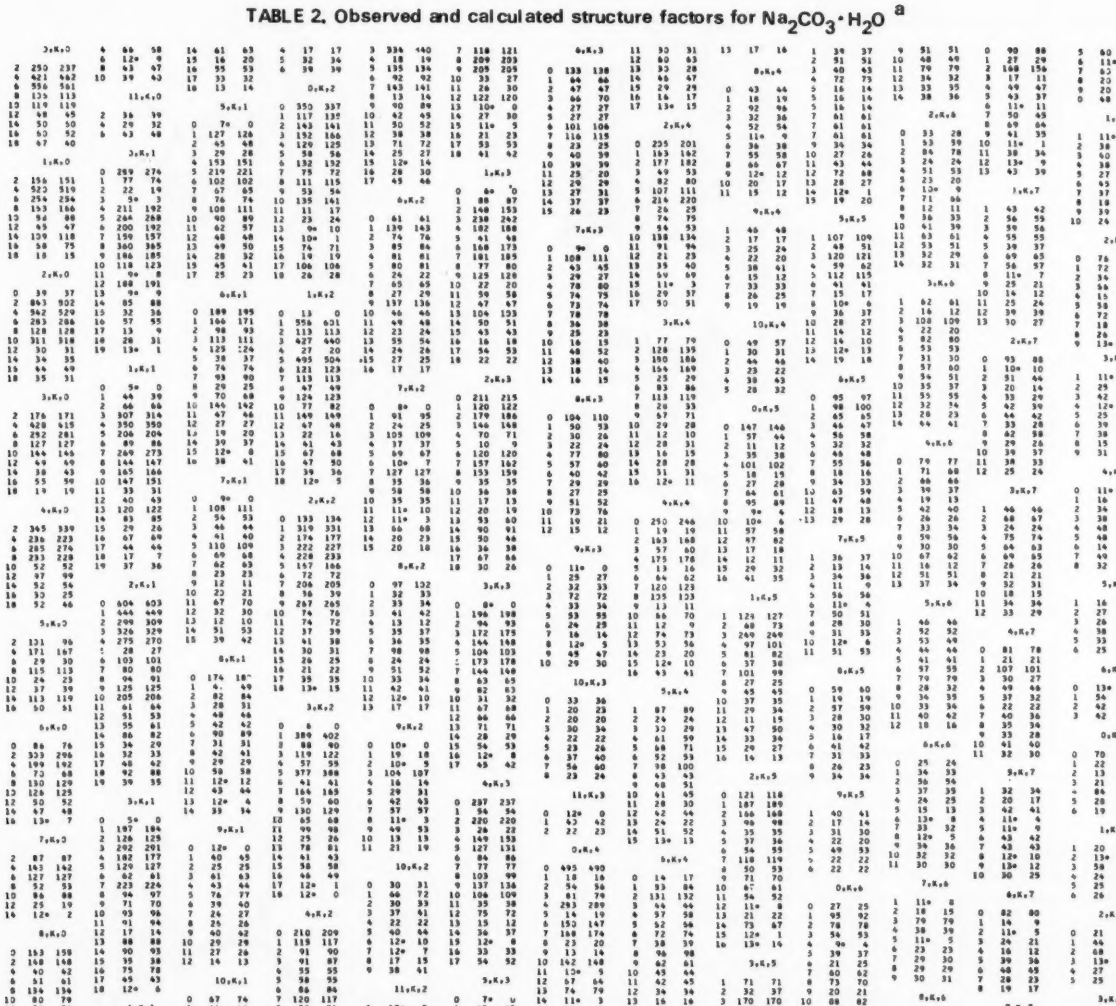

[a] The columns are k, $10F_o$, $10F_c$. "Unobserved" reflections are marked by *. F_o and F_c are on an absolute scale.

TABLE 3. *The hydrogen positions in* $Na_2CO_3 \cdot H_2O$

Atom	Weighted difference synthesis			Least squares refinements			Calculated*		
	x	*y*	*z*	*x*	*y*	*z*	*x*	*y*	*z*
H(1)	0.12	−0.07	0.14	0.11	−0.06	0.15	0.134	−0.056	0.190
H(2)	−.08	−.08	.14	−.10	−.08	.12	−.077	−.089	.084

*Assuming the geometry of free water with O—H = 0.958 Å and ∠ H—O—H = 104.5°, and making the O—H . . . O hydrogen bonds as linear as possible.

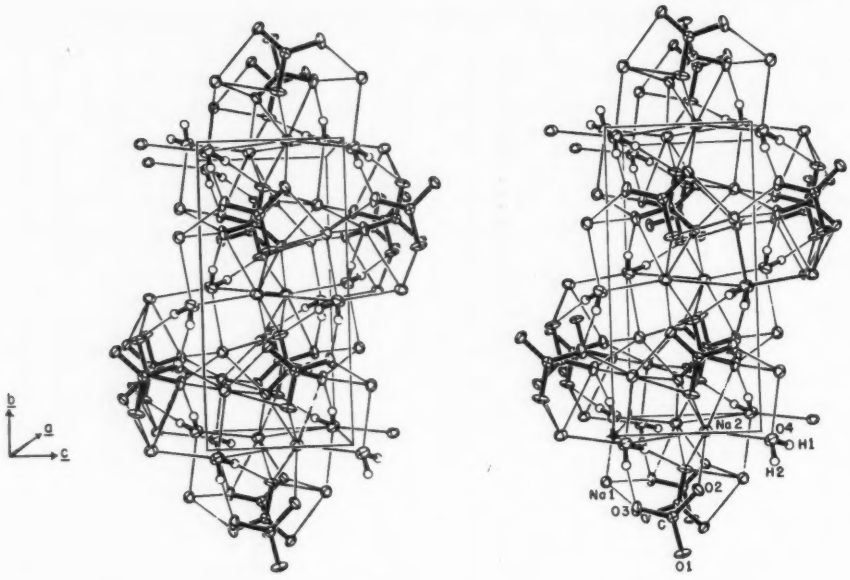

FIGURE 1. *A stereoscopic illustration of* $Na_2CO_3 \cdot H_2O$ *viewed along* a.
The origin of the unit cell is marked by the asterisk.

TABLE 4. *The* CO_3 *group*

Atoms	Distances, Å, or angle, deg.
C, O(1)	1.299(3)
C, O(2)	1.274(2)
C, O(3)	1.285(2)
O(1), O(2)	2.223(2)
O(1), O(3)	2.229(2)
O(2), O(3)	2.230(2)
O(1), C, O(2)	119.6(2)
O(1), C, O(3)	119.2(2)
O(2), C, O(3)	121.2(2)
O(1), Na(1)	2.570(2)
O(1), Na(2)	2.293(2)
O(1), Na(2′)	2.307(2)
O(1), O(4)	2.907(2)
O(1), H(1)	1.96
O(2), Na(1)	2.521(2)
O(2), Na(1′)	2.468(2)
O(2), Na(2′)	2.508(2)
O(2), Na(2)	2.491(2)
O(3), Na(1)	2.444(2)
O(3), Na(1′)	2.330(2)
O(3), Na(2)	2.822(2)
O(3), O(4)	2.685(2)
O(3), H(2)	1.74

In all tables of interatomic distances and angles, the quantities in parentheses are standard errors in the last significant figure and were computed from the standard errors in the atomic positional parameters and in the cell parameters. The primes refer to atoms in figure 2.

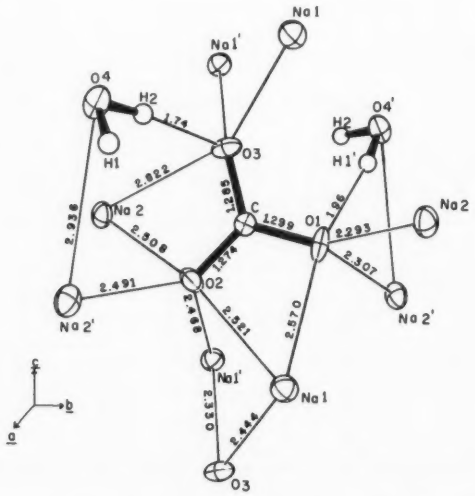

FIGURE 2. *The carbonate group environment in* $Na_2CO_3 \cdot H_2O$.
The primes refer to atoms in table 4.

tion about Na(1) cannot be considered octahedral. The next oxygen in the direction of the octahedral apex is the water oxygen O(4′), which is relatively far (3.669 Å) from Na (1).

The coordination of Na(2) is similar to that of Na(1). Na(2) is slightly displaced from the center of an approximate square of carbonate oxygens, O(1′), O(2″), O(1″), O(2‴). The displacement is towards the strongly bonded water molecule O(4), which is the

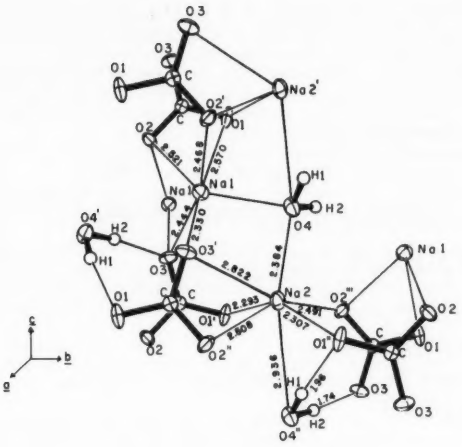

FIGURE 3. *The water and sodium environments in* $Na_2CO_3 \cdot H_2O$.
The primes refer to atoms in tables 5 and 6.

TABLE 5. *The sodium environments*

Atoms	Distance, Å
Na(1), O(1)	2.570(2) Å
Na(1), O(2)	2.521(2)
Na(1), O(3)	2.444(2)
Na(1), O(4)	2.434(2)
Na(1), O(2′)	2.468(2)
Na(1), O(3′)	2.330(2)
Na(1), O(4′)	3.669(2)
Na(2), O(4)	2.384(2) Å
Na(2), O(1′)	2.293(2)
Na(2), O(1″)	2.307(2)
Na(2), O(2″)	2.508(2)
Na(2), O(2‴)	2.491(2)
Na(2), O(4″)	2.936(2)
Na(2), O(3′)	2.822(2)

The primes refer to the atoms in figure 3.

apex of a square based pyramid (base down in figure 3). The coordination of Na(2) is completed by O(4″) (2.936 Å) which is the remaining apex of an approximate octahedron, and by O(3′) which is in the same CO_3 group as O(2″). Thus the CO_3 group is coordinated edgewise to Na(2) also, this time using O(2) and O(3) instead of O(1) and O(2), which are used to coordinate to Na(1). This edgewise coordination is shown in figure 2. The coordination to Na(2) comprises five carbonate oxygens and two water molecules instead of four carbonate oxygens and two water molecules as suggested by Harper [1] and noted by Wells [15].

3.3. The Water Environment

The water environment is given in table 6 and shown in figure 3. The water molecule is bonded to Na(1) and Na(2) with distances of 2.434 and 2.384 Å respectively, and forms hydrogen bonds to oxygens O(1) and O(3) of neighboring CO_3 groups. Na(1), Na(2), O(1), and O(3) are arranged approximately tetrahedrally about the water oxygen. The distortion of this tetrahedron is considerable as can be seen from the angles listed in table 6. The closest H . . . Na distance is H(1) . . . Na(2) = 2.42 Å, which is in the normal range.

TABLE 6. *The water environment*

Atom	Distance Å or angle, deg.
O(4),Na(1)	2.434(2) Å
O(4),Na(2)	2.384(2)
O(4),Na(2′)	2.936(2)
O(4),O(1)	2.907(2)
O(4),O(3)	2.684(2)
H(1),O(1)	1.96
H(2),O(3)	1.74
Na(1),O(4),Na(2)	91.15(6)°
O(1),O(4),Na(1)	109.70(7)
O(1),O(4),Na(2)	133.83(9)
O(3),O(4),Na(1)	129.28(9)
O(3),O(4),Na(2)	110.29(7)
O(1),O(4),O(3)	88.12(6)
O(4),H(1),O(1)	168.
O(4),H(2),O(3)	167.

The prime refers to an atom in figure 3.

The calculated hydrogen positions in table 3 were obtained using the geometry of free water and imposing the condition that the O—H . . . O angles both be as linear as possible. Because H(2) . . . O(3) is shorter (1.74 Å) than H(1) . . . O(1) (1.96 Å) it is possible that the hydrogen bond O(4)—H(2) . . . O(3) is strictly linear. Assuming the same water geometry, the hydrogens would then be $\simeq 0.14$ Å away from the positions given in table 3 at 0.145, −0.046, 0.182 for H(1) and −0.065, −0.095, 0.102 for H(2). The O(4)—H(1) . . . O(1) angle would then be 156°, and the H(1) . . . O(1) and H(2) . . . O(3) distances would be 2.01 Å and 1.73 Å, respectively. The closest H . . . Na distance would be H(1) . . . Na(2) = 2.39 Å.

Collection of the diffractometer data was made possible through the cooperation of E. C. Prince. The x-ray 67 system of computing programs (J. M. Stewart, University of Maryland, Editor) was used for most calculations. We thank Joy S. Bowen and Pamela B. Kingsbury for technical help.

This investigation was supported in part by research grant DE-00572-09 to the American Dental Association from the National Institute of Dental Research and is part of the dental research program conducted by the National Bureau of Standards, in cooperation with

the Council on Dental Research of the American Dental Association; the United States Army Medical Research and Development Command; the Dental Sciences Division of the School of Aerospace Medicine, USAF; the National Institute of Dental Research; and the Veterans Administration.

References

[1] Harper, J. P., Crystal structure of sodium carbonate monohydrate, $Na_2CO_3 \cdot H_2O$, Z. Krist. **95,** 266–273 (1936).

[2] Dickens, B., and Brown, W. E., The crystal structures of $CaNa_2(CO_3)_2 \cdot 5H_2O$, synthetic gaylussite, and $CaNa_2(CO_3)_2 \cdot 2H_2O$, synthetic pirssonite, Inorg. Chem. **8,** 2093–2103 (1969).

[3] Brown, W. E., Crystal structure of octacalcium phosphate; Nature **196,** 1048–1050 (1962).

[4] Brown, C. J., Peiser, H. S., and Turner-Jones, A., The crystal of sodium sesquicarbonate, Acta Cryst. **2,** 167–174 (1949).

[5] Bacon, G. E., and Curry, N. A., A neutron-diffraction study of sodium sesquicarbonate, Acta Cryst. **2,** 82–85 (1956).

[6] Candlin, R., Thermal changes in the structure of sodium sesquicarbonate, Acta Cryst. **9,** 545–554 (1956).

[7] Pabst, A., On the hydrates of sodium carbonate, Amer. Min. **15,** 69–73 (1930).

[8] Reimann, C. W., Mighell, A. D., and Mauer, F. A., The crystal and molecular structure of tetra isopyrazole-nickel chloride, $Ni(C_3H_4N_2)_4Cl_2$, Acta Cryst. **23,** 135–141 (1967).

[9] Mauer, F. A., and Koenig, A. L., An automatic diffractometer for off-line operation, American Crystallographic Association, Summer Meeting, Abstract E10, University of Minnesota, Minneapolis, Minn. Aug. 20–25, (1967).

[10] International Tables for X-ray Crystallography **3,** p. 202 (The Kynoch Press, Birmingham, England, 1962).

[11] McWeeney, R., x-ray scattering by aggregates of bonded atoms. I. Analytical approximations in single-atom scattering, Acta Cryst. **4,** 513–519 (1951).

[12] Chastain, R. V., An algorithm for finding a set of phases directly from sigma two relationships, In, x-ray 67-Program System for x-ray Crystallography, Technical Report 67–58, Ed. J. M. Stewart, pp 71–75, University of Maryland, College Park, Md. (1967).

[13] Palache, C., Berman, H., and Frondel, C., Thermonatrite $[Na_2CO_3 \cdot H_2O]$, The System of Mineralogy of J. D. Dana and E. S. Dana, 7th ed., **2,** p. 224 (J. Wiley and Sons, New York, N.Y., 1951).

[14] Winchell, A. N., and Winchell, H., The Microscopical Characters of Artifical Inorganic Solid Substances: Optical Properties of Artifical Minerals (Academic Press, New York, 1964).

[15] Wells, A. F., Structural Inorganic Chemistry, 3rd ed. p. 587 (Oxford University Press, London, 1962).

(Paper 74A3–603)

JOURNAL OF RESEARCH of the National Bureau of Standards—A. Physics and Chemistry
Vol. 74A, No. 3, May–June 1970

Anisotropic Reaction Kinetics of Oxygen With Pyrolytic Graphite

William S. Horton
Institute for Materials Research, National Bureau of Standards, Washington, D.C. 20234

(December 15, 1969)

Because of the possible use of pyrolytic graphite in aerospace vehicles its reaction with oxygen-containing gases is of interest, particularly with respect to chemical anisotropy. Although several authors have found different degrees of reactivity of graphite in different directions they disagree regarding the existence of a temperature coefficient. This disagreement, however, is probably due to investigators studying single crystals in some cases and pyrolytic graphite in others and in some cases different oxidizers. New data for pyrolytic graphite are presented which were obtained by oxidizing in each run several pieces of differing geometry. These together with earlier data show that the rate ratio for the two major directions is temperature dependent with an activation energy difference of about 19 kilojoules (4500 thermochemical calories) per gram atom of carbon reacted. It is shown that this difference in rates probably arises because the relative number of sites available in these directions is sufficiently different to cause a shift in which reaction step is rate-controlling. On the "faces" chemisorption is the rate controlling step followed by rapid decomposition of surface oxides. On the "edges" decomposition is the rate controlling step. This interpretation applied to the data yield 131 kJ/mol for the activation energy of chemisorption and 150 kJ/mol for decomposition (31 and 36 kcal/mol, respectively).

Key words: Chemical anisotropy; chemisorption; oxidation; pyrolytic graphite.

1. Introduction

Pyrolytic graphite is of particular interest to those studying carbon because it may be obtained as sizable specimens with its anisotropic character intact. Thus, it may be studied by some of the simpler experimental techniques. Furthermore, those studies may be considered representative of the material as used in practice rather than of special experimental material. Because of the possible use in rocket nozzles and in leading edges of reentry space vehicles, the reaction with oxygen-containing gases has received study particularly questioning the chemical anisotropy.

In an article [1][1] about carbon and "borocarbon" deposited pyrolytically, Grisdale et al. tabulated relative reaction rates as 17:1 for the "ab-direction" compared to the "c-direction." (In this paper "c-direction" and "preferred c-direction" will be used interchangeably.) No explanation, experimental description, or other information was given. The same result was again tabulated in 1953 by Grisdale [2], also without explanation. Horton reported in 1961 [3] that this ratio was judged to be about 2.5 and to increase with increasing temperature. Levy and Wong [4] in 1964 reported a ratio of about 18 although in 1962 [5] Levy had reported that the oxidation of pyrolytic graphite proceeds preferentially in the c-direction. These appear to be the only studies of the rate ratio made on pyrolytic graphite although, as mentioned later, Lang and Magnier reported values for oxidation in damp air. The work of Strickland-Constable and colleagues [6, 7] concerned itself with the oxidation rate in the c-direction only and measured it directly without reference to the ratio. Horton's work was aimed at the c-direction rate also, but required at least a rough value for the ratio in order to make a needed correction to the measurements. Both Horton and Strickland-Constable found that the c-direction rate was slower than the rate for the more usual synthetic graphites. This fact, of course, while not demonstrating a ratio different from unity, is consistent with such a possibility. These results may be contrasted with those of Gulbransen, Andrew, and Brassart [8] who found that above 1000 °C there was no difference in rate between pyrolytic and spectrographic graphites. However, they studied pyrolytic graphite only in the temperature region where gaseous diffusion controlled the rate. More recently, Lang and Magnier [24] reported rate ratios from 2.7 to 4.6 at 620 °C when pyrolytic graphite was oxidized in air containing 0.02 volume percent

[1] Figures in brackets indicate the literature references at the end of this paper.

378-324 O - 70 - 2

water vapor. A temperature coefficient determination was not reported. The rate of reaction in dry air was said to be much less.

Single crystals of graphite would also be expected to exhibit chemical anisotropy and have been studied by Hennig [9]. He stated at first that the rate ratio was 20 below 800 °C. In a later paper [18] he said the ratio must be at least 100 although the temperature was not specified. Thomas and Jones [10] found the ratio to be 26 at 800 °C. Oxidizing with nitric oxide gas they found essentially the same ratio and no essential difference for 873 or 910 °C. Patel and Bahl [11] measured rates of reaction for single crystals of Ticonderoga graphite in molten oxidizers: sodium peroxide, potassium nitrate, and sodium hydroxide between 350 and 650 °C. The ratio of about 6.7 did not vary significantly with temperature.

Although the authors all agree that the rate ratio is greater than unity, there is disagreement about the magnitude and the existance of a temperature coefficient. One can remark at the outset that only Levy and Wong [4] and Horton [3] studied the ratio itself directly on macroscopic pyrolytic graphite and with oxygen. Other studies of the ratio were on single crystals [9, 10, 11], probably on carbon films [1] or used other oxidizers [10, 11] or moist air [24]. It is not surprising that divergent results are obtained under these circumstances. The purpose of this paper is to present newer data and to examine in more detail the author's earlier data [3].

2. Experimental Details

The material used for study was from the same source as that used in 1960, i.e., it constituted part of preparation Run 34 by the General Electric Company Research Laboratory. Prepared at 2100 °C it had a density of 2.15 g cm^{-3}. The quite low impurity levels were tabulated in the early reference [3]. The crystalline and microstructural characteristics of the material were determined using a high angle Geiger counter diffractometer for powder or powder-like patterns and using a three-circle automatic-scanning single-crystal (Eulerian cradle) diffractometer to determine the degree of preferred orientation. From the 002, 004, and 006 diffraction lines c_0 was determined to be 6.8326 Å with a standard error of 0.0015 Å; a_0, from 10, 11, and 20 bands was 2.4527 Å with standard error 0.0010 Å. Heights of layer stack from broadening of the 002, 004, and 006 lines (using $L_c = 0.94\lambda/B \cos\theta$) [13] were respectively 106, 92, and 55 A. From broadening of the 10 and 11 bands (using $L_a = 1.77\lambda/B \cos\theta$) [14] the mean crystalline diameter = 146 Å, which compares reasonably with the value 128 Å obtained from the apparent change in a_0 (using [14] $L_a = 0.14\lambda/\Delta(\sin\theta)$). Using Ergun's [15] designation for disk diameter as an alternative for L_a, we obtained $D = 183$ Å. From these data the number of layers in a stack is about 29, and Franklin's [16] probability of layer misorientation, $p = 0.85$. The degree of preferred orientation, when described according to Guentert and Cvikevich [17] as $I = I_0|\cos^m \delta|$, is given by $m = 6$.

The determination of material characteristics by x-ray techniques, was initially attempted with powder obtained from filings which passed through a number 400 sieve. This was unsatisfactory because an insufficient number of lines and bands appeared. Furthermore, the thin film required absorption corrections [21] which were large, probably inaccurate, and were tedious to calculate. A solid, flat speciman was resorted to which was about 5 mm thick. Because of the preferred orientation the specimen was run twice, once with the x-ray beam incident to the "faces" and once with it incident to the "edges." Corrections were made for absorption [21], preferred orientation [22], as well as instrumental and doublet broadening [23] although the latter were quite small. The alinement of the diffracting system was checked by obtaining a pattern for a specially prepared specimen of quartz powder. This powder, with particle size about 0.15 μm, was also used to determine the magnitude of instrumental broadening.

Disk-shaped specimens were cut, as before [3], with dimensions between 0.6 and 2 cm diameter and thicknesses from 0.5 to 5 mm. Specimens were cleaved to provide fresh basal-plane surface. No pretreatment was applied before insertion in the apparatus. However, the normal course of a run required preheating in nitrogen during the time required to reach temperature. About 1 hr was required in each case to establish a steady state before the nitrogen was replaced by a reacting gas.

The specimens were oxidized in a horizontal tube furnace controlled within 1 K. The central hot zone was within ±2 K for a 2-in region. This region was carefully located and the specimens always placed in it. Temperature was measured by a platinum:platinum-10 percent rhodium thermocouple placed near the specimen and by using a type K3 potentiometer. The melting point of gold was checked satisfactorily in the same apparatus. Tank gases passed through flowmeters before going to the furnace. The gases entered the furnace through a ceramic plug about 4½ in long. The passageway through the plug made two helical revolutions before opening on the reaction chamber. The increased path length was to ensure that the gas attained the furnace temperature more closely and to avoid a cooling effect on the specimens.

In contrast to the work of 1960, in which only one specimen was run at a time, two runs were made with two specimens, seventeen were with three specimens and three were made with four specimens. Specimens run simultaneously were chosen to have divergent ratios of "faces" and "edges." Dimensions and weights were measured before and after each run. Blank runs were deemed unnecessary because thermogravimetric monitoring in the earlier work [3] showed no mass change during the pre- and post-oxidizing periods. Dimensional changes on each specimen could be used, as in the 1960 experiments, to give rate ratios. The main interest, however, was to evaluate the rate constants, k_i, in the equation

$$-\dot{m} = k_1 A_f + k_2 A. \tag{1}$$

where $\dot{m}$ is the rate of mass change, A_f and A_e are the total face and edge areas for a specimen, respectively, and k_1 and k_2 are the face and edge rates. For the case of two specimens run simultaneously a direct solution is possible. For the other cases, least squares solutions for the k's also lead to estimates of random error. Dimensions were measured with a micrometer caliper, and masses were measured with a commercial microbalance. Mass changes were from about 790 μg to 740 mg. Although specimens stayed cylindrical edges did not always remain uniformly perpendicular to the faces. However, average diameters could be used in such cases. The specimens were drilled with a small axial hole to accept a platinum wire for mounting. They were suspended on this as on a spit as shown diagramatically in figure 1. The assembly could be moved in and out of the the furnace easily as needed. Although some oxidation could be observed around the holes, the magnitude of the effect was negligible.

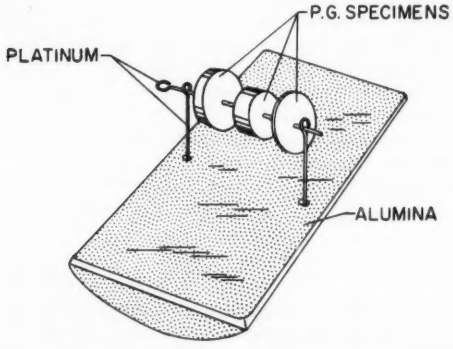

FIGURE 1. *Specimens and support assembly.*

The course of a run was as follows. Measured and weighed specimens were placed on the assembly and placed appropriately in the furnace. The gas entry plug was replaced and gas flows adjusted to be as planned. The oxidant was turned off and nitrogen allowed to continue while the furnace was heated and stabilized at the reaction temperature. At this point the oxidizing gas was turned on through a solenoid valve, simultaneously starting an electric clock. At the appropriate time the oxidizing gas was turned off, simultaneously stopping the clock. Throughout the run, readings of the gas flow and of the temperature were made. Total pressure for all runs was atmospheric. Air flows were from about 80 to 216 cm³/min. Nitrogen flows, when used, were from about 80 to 300 cm³/min. Because in the earlier work [3] flow rates changed by a factor of two had no significant effect, this factor was not investigated here. Partial pressures of oxygen were from about 1/10 to 1 atm. Times of exposure to the oxidizing gas were from 20 to 419 mins.

3. Results

The results of these experiments are shown in table 1. The least squares solutions of the rate eq (1) were performed on a high speed electronic computer with the OMNITAB program [12] which provides also the standard errors of the rate constants. All other computations reported here were performed with this programming language also. Runs 3 and 4 have no entries for error because these were performed with only two specimens. Runs 20, 21, and 22 were those performed with four specimens; all others used three. It should be noted that runs 5 to 15 and run 17 were made with air. Run 16 was with pure oxygen. Runs 1 to 4 and 20 to 22 were made with air diluted with nitrogen. When examining the rate ratios these differences are probably unimportant. However, comparison among rate constants must, no doubt, take this into account. Three ratios are negative as a result of negative face rates. These together with runs 3, 17, and 19 were not considered further. Ratios for the latter three runs were demonstrably too scattered to be considered part of the group. The remaining 16 are shown graphically in figure 2. The negative rates appear to be due to a combination of random error and small values.

As mentioned earlier sufficient dimensional data were taken to enable calculation of $\Delta D/\Delta H$ also, where D is the diameter and H the thcikness of a specimen. Of the 67 specimens 41 gave apparently usable results and these are summarized in figure 3. Of the remaining 26, twenty-one specimens gave negative results, which

TABLE 1. *Oxidation rates for pyrolytic graphite from mass changes*

Run	Temp.	Face rate, k_1	Edge rate, k_2	Std. error, k_1	Std. error, k_2	Ratio, k_2/k_1
	kelvins	mg cm^{-2}min^{-1}				
1	867	0.343−02	0.113−01	0.54−03	0.15−02	3.30
2	891	.835−02	.125−01	.11−02	.29−02	1.50
3	885	.794−03	.128−01	.....	.....	16.05
4	887	.910−02	.208−01	.....	.....	2.29
5	888	.993−02	.216−01	.22−03	.88−03	2.17
6	884	.198−01	.266−01	.33−03	.13−02	1.34
7	887	.148−01	.217−01	.20−02	.80−02	1.47
8	883	.999−02	.154−01	.83−03	.33−02	1.55
9	882	.790−02	.168−01	.64−03	.25−02	2.12
10	1214	.134+01	.729+01	.44−00	.15+01	5.46
11	1044	−.377−01	.108+01	.88−01	.34−00	−28.65
12	1045	−.149−00	.247+01	.22−00	.90−00	−16.56
13	962	.720−02	.115−01	.24−02	.67−02	1.60
14	961	.884−02	.169−01	.36−02	.98−02	1.90
15	957	.110−01	.206−01	.23−02	.65−02	1.88
16	1138	−.116+00	.352+01	.25−00	.77−00	−30.24
17	1136	.559−01	.511+01	.38−01	.24−00	91.38
18	1136	.852−00	.332+01	.38−00	.14+01	3.89
19	1137	.160+01	.391−00	.22−00	.73−00	.24
20	1047	.470−01	.139−00	.78−02	.34−01	2.96
21	1047	.623−01	.475−00	.17−01	.75−01	7.63
22	1045	.250−00	.102+01	.86−01	.37−00	4.07

Computer-modified power-of-ten expression has been used for numbers. Thus, 0.343−02 represents 0.343×10^{-2}. Precision is only roughly indicated by retained digits. The standard errors are better indicators.

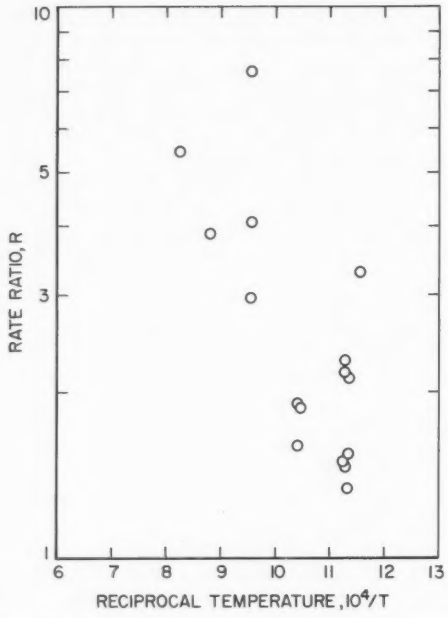

FIGURE 2. *Rate ratio versus reciprocal absolute temperatures for weight change data.*

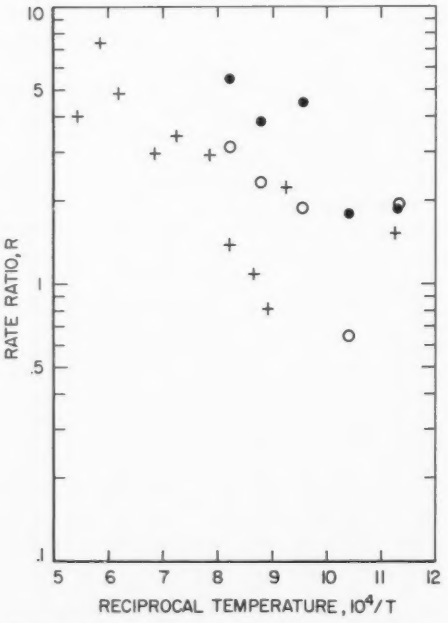

FIGURE 3. *Rate ratio versus reciprocal absolute temperature: o—mass change data; 0 dimensional change data; + dimensional change data, 1960.*

Note that within each set ratios have been averaged for closely neighboring temperatures in order to improve the clarity of the figure.

arose, no doubt, from the smallness of the dimensional changes and the precision with which the dimensions could be measured. The precision of the latter measurements is probably most influenced by the uniformity of dimension at different points on a specimen. Five results appeared too far removed from the general trend to be considered.

Although the data obtained in 1960 were not specifically focused on the rate ratio the results are interesting to compare and are also represented in figure 3. Here, there were 17 usable results out of 20. Of the discarded three, two were negative and widely divergent. In what follows it will be useful to consider this group also. The data of table 1 are also shown in this figure 3 for comparison. Within each of the three sets some points are the average of results for closely neighboring temperatures for the sake of clarity.

4. Discussion

Although the precision of the data is poor, with adequate treatment some conclusions are possible. The main question is whether these data indicate that there is a temperature coefficient. The answer may be approached by fitting the data to a temperature dependent function and determining if the parameters of the function are significant. For this purpose it is convenient to use an equation of the Arrhenius type:

$$R = \alpha e^{-\beta/T}, \tag{2}$$

where $R = k_2/k_1$. Although other forms may fit the data as well, this one corresponds to assuming that the rate ratio may be simply understood as the ratio of two rate constants, each of this form. Then α would represent the ratio of the preexponential factors and β would represent the difference in the activation energies divided by the gas constant. For the three groups of data the results are given in table 2. From the standard errors for the $\hat{\beta}$'s and the numbers of degrees of freedom (14, 39, and 15, respectively), the probabilities that each of the nonzero slopes could have been obtained accidentally as a result of random error are about 0.0016, 0.1, and 0.015, respectively. It appears to be beyond question that these data indicate the existence of a temperature coefficient for the oxidation rate ratio.

In order to understand the effect that is evident, it is

TABLE 2. *Arrhenius parameters for rate ratio*

Data set	$\widehat{\ln\alpha}$	$s(\widehat{\ln\alpha})$	$\hat{\beta}$	$s(\hat{\beta})$	$s(\widehat{\ln R})$
$\dot{m}$	4.69	0.95	−3620	910	0.36
$\Delta D/\Delta H$	2.37	1.04	−1809	1060	.70
$\Delta D/\Delta H$, 1960	3.39	.64	−3180	820	.46

The expression $s(X)$ refers to the standard error of X. The symbol $\hat{x}$ refers to the estimate of X. The units of $\hat{\beta}$ and $s(\hat{\beta})$ are kelvins. All other data in this table are dimensionless.

desirable to have a single set of values for the Arrhenius parameters. While attempting to do this, it became evident that although the three independent sets of data agree on the main conclusion there was some apparent discrepancy among them that suggested they should not be combined straight away. Further examination of the data showed that all three sets of data can be described by a single special equation. Expressed in the logarithmic form, the Arrhenius equation may be used with two intercepts and one slope:

$$\ln R = \delta_m \alpha_m + \delta_d \alpha_d + \beta/T. \tag{3}$$

In this equation δ_m is unity and δ_d is zero for mass change data, and conversely for dimensional data. This concept is essentially that of fitting a pair of parallel lines [19]. The values of the constants are given in table 3. The parameters correspond to pre-exponential factors of 26.6 and 16.1, respectively, and to an activation energy difference of −18900 J (−4500 thermochemical calories) per gram atom of carbon. Accepting this interpretation of the data suggests that the simple relationships originally assumed (eqs 6, 7, 8, and $k_2/k_1 = \Delta D/\Delta H$ of ref. [3]) are not valid.

TABLE 3. *Derived Arrhenius parameters*

Parameter	Value	Standard error
$\hat{\alpha}_m$	3.28	0.54
$\hat{\alpha}_d$	2.78	.46
$\hat{\beta}$	−2270 K	500 K

The parameters correspond to preexponential factors of 26.6 and 16.1, respectively, and to an activation energy difference of −18900 J per gram atom of carbon (−4500 thermochemical calories per gram atom). The standard error of fitting ln R to this set is 0.59

An explanation of the observed rate ratio is available in terms of the mechanism suggested by Nagle and Strickland-Constable [6]. For pressures of the order of 0.21 atm oxygen their overall rate equation at a given temperature and oxygen pressure, p, reduces to:

$$k = \frac{k_A p}{1 + k_z p}. \tag{4}$$

Only the "A-sites" are involved because at this pressure the fraction of surface sites which are the A-type is essentially unity at all the experimental temperatures. Equation (4) comes about as follows. The rate at which surface oxides are formed is given by $k_A p\,(1-\theta)$, where k_A is a rate constant for chemisorption and θ is the fraction of A-sites already covered by oxide. Sites are uncovered at a rate $k_d\theta$ where k_d is the specific rate constant for decomposition and thus $k_d\theta$ is also the rate of product formation and of carbon loss. Assuming a steady state condition whereby the fraction of covered sites do not change, the two rates must be equal, leading to

$$\theta = \frac{k_A p}{k_d + k_A p}. \tag{5}$$

Multiplying by k_d gives the rate which is seen to be eq (4) where $k_z = k_A/k_d$.

For the case at hand we assume the steady state condition for the "faces" but that decomposition is much more rapid than is adsorption. We can, therefore, assume that $k_z p \ll 1$, leading to $k_1 = k_A p$. On the "edges" we assume that adsorption is so rapid that the rate controlling step is decomposition, and that θ is proportional to p. This leads to $k_2 = k_d \kappa p$ where κ is the proportionality constant, θ/p. Correspondingly, $R = \kappa k_d/k_A = \kappa k_z^{-1}$. Although the constant, κ, was introduced to give the proportionality for the fraction of covered sites on the edges, it is easily seen that in reality one should talk about the specific number of sites in the preferred ab-direction and also in the c-direction. These are almost certainly quite different and in fact may account largely for the shift between adsorption and decomposition being rate controlling. The data of Lang and Magnier [24] suggest a value somewhere between 20 and 65 for the ratio of surface density of sites. The data of table 3 suggest about 20 for the ratio of preexponential factors. That we are probably dealing with the same kind of sites in both directions is reasonable in view of the fact that in pyrolytic graphite the "c-direction" is only a preferred direction. In as-deposited material there are still some crystallite edges available on the faces and vice versa. The constant, κ, must include a ratio of surface density of A-sites in the two directions.

Equating R proportional to k_z^{-1} requires the activation energy difference to be −17.2 kJ (4.1 kilocalories) per gram atom of carbon according to Nagle and Strickland-Constable. This is in remarkable agreement with the value reported here of −18.9, and represents the difference in activation energy for decomposition and chemisorption with that for decomposition being the higher. The activation energy for chemisorption calculated from the data of Walker et al. [20], of 117 Kj/mol (28 kcal/mol) agrees reasonably with that for k_A of Nagle and Strickland-Constable of 125 kJ/mol (30 kcal/mol). The explanation developed above also requires that the face rate, k_1, be proportional to the rate of chemisorption and to the pressure. The corresponding values from table 1 yield 131 kJ/mol with a standard error of 19 kJ/mol (31.2 and 4.6 kcal/mol, respectively) for the activation energy of chemisorption, when negative values and the widely divergent run 3 are deleted from consideration. Runs 1 to 4 and 20 to 22 must be corrected by the ratio (0.21/pressure oxygen) to refer all to the pressure of oxygen in air. These ratios were 2 for runs 1 to 4 and respectively 4, 401/101, 4045/1045 for the others, as determined from the flow rates of air and nitrogen. Using the data from this work only, the activation energy for decomposition of surface oxides is 150 kJ/mol (36 kcal/mol). The various activation energies are compared in table 4.

TABLE 4. *Activation energies*

	This research		Nagle & Strickland-Constable		Walker, Austin & Tietjen	
E_z	18.9	(4.5)	17.2	(4.1)	.....	.....
E_A	131	(31)	125	(30)	117	(28)
E_d	150	(36)	142	(34)	.....	.....

. Units are: kilojoules per gram atom; (kilocalories per gram atom).

The author is grateful to P. Minard for her assistance in making the new rate measurements and to J. L. Winick for making the x-ray characterization measurements.

5. References

[1] Grisdale, R. O., Pfister, A. C., and van Roosbroeck, W., Bell Syst. Tech. J. **30,** 271 (1951).
[2] Grisdale, R. O., J. Appl. Phys. **24,** 1288–96 (1953).
[3] Horton, W. S., Proceedings of the Fifth Carbon Conference, Vol. **2,** p. 233 (Pergamon Press, Oxford, 1963).
[4] Levy, M. and Wong, P., J. Electrochem. Soc. **111,** 1088–91 (1964).
[5] Levy, M., I & EC Product Research and Development **1,** 19–23 (1962).
[6] Nagle, J. and Strickland-Constable, R. F., Proceedings of the Fifth Carbon Conference, Vol. **1,** p. 154–64 (Pergamon Press, New York, 1961).
[7] Walls, J. R. and Strickland-Constable, R. F., Carbon **1,** 333–38 (1964).
[8] Gulbransen, E. A., Andrew, K. F., and Brassart, F. A., J. Electrochem. Soc. **111,** 626–27 (1964).
[9] Hennig, G. R., Proceedings of the Fifth Conference on Carbon, Vol. **1,** 0. 143–46. (Pergamon Press, New York, 1963).
[10] Thomas, J. M. and Jones, K. M., J. Nucl. Mtls. **11,** 236–39 (1964).
[11] Patel, A. R. and Bahl, O. P., J. Nucl. Mtls. **22,** 226–27 (1967).
[12] Hilsenrath, J., Ziegler, G. G., Messina, C. G., Walsh, P. J., and Herbold, R. J., Nat. Bur. Stand. (U.S.), Handb. 101, 284 pages (Mar. 1966), U.S. Govt. Printing Office, Washington, D.C. 20402
[13] Warren, B. E. and Bodenstein, P., Acta Cryst. **18,** 282–86 (1965).
[14] Warren, B. E. and Bodenstein, P., Acta Cryst. **20,** 602–05 (1966).
[15] Ergun, S., Carbon **6,** 7–11 (1968).
[16] Franklin, R. E., Acta Cryst. **4,** 253–61 (1951).
[17] Guentert, O. J. and Cvikevich, S. Proceedings of the Fifth Carbon Conference, Vol. **1,** p. 473–84. (Pergamon Press, New York, 1962).
[18] Hennig, G. R., Zeit. fur Elektrochemie **66,** 629–35 (1962).
[19] Dewdney, J. W. and Dewdney, S. H., Rev. Sci. Inst. **34,** 436–37 (1963).
[20] Walker, P. L., Jr., Austin, L., and Tietjen, J., Chemistry and Physics of Carbon, Vol. **1,** P. L. Walker, Jr., Ed., Chapter 6, (Marcel Dekker, New York, 1965).
[21] Keating, D. T. and Warren, B. E., Rev. Sci. Inst. **23,** 519–22 (1952).
[22] Guentert, O. J. and Cvikevich S., Carbon 1, 309–13 (1964).
[23] Klug, H. P. and Alexander, L. E., X-ray Diffraction Techniques, Chap. 9, esp. pp. 494–521 (John Wiley & Sons, New York, 1954).
[24] Lang, F. M. and Magnier, P., Chemistry and Physics of Carbon, Vol. **3,** P. L. Walker, Jr., Ed., pp 121–209 (Marcel Dekker, New York, 1968).

(Paper 74A3–604)

JOURNAL OF RESEARCH of the National Bureau of Standards—A. Physics and Chemistry
Vol. 74A, No. 3, May–June 1970

The Viscosity and Thermal Conductivity of Dilute Gaseous Hydrogen from 15 to 5000 K*

H. J. M. Hanley, R. D. McCarty,** and H. Intemann****

Institute for Basic Standards, National Bureau of Standards, Boulder, Colorado 80302

(November 26, 1969)

Measurements of the viscosity and thermal conductivity of dilute gaseous para and normal hydrogen are critically evaluated and correlated by means of dilute gas kinetic theory. Numerical results are presented from 15 to 5000 K including the dissociation region.

Key words: Dissociation; hydrogen; intermolecular potential functions; kinetic theory; quantum gas; thermal conductivity; viscosity.

We discuss the critical evaluation of the viscosity and thermal conductivity coefficients of dilute *p*-, *o*-, and *n*-hydrogen and present tables of values for para and normal hydrogen. New information—particularly with regard to experimental data from our laboratory—justifies a reevaluation of these properties of this well-known fluid. The tables given here differ significantly at the extreme temperatures from those published previously.

The coefficients are represented by standard kinetic theory expressions but the calculations are more than mere routine; to give two examples, at low temperatures, hydrogen behaves as a quantum fluid and at high temperatures it dissociates. Furthermore, to apply the theoretical expressions in practice one needs to evaluate critically experimental data in the first place, which is not a cut-and-dried problem at all.

1. Formal Equations

The required kinetic theory equations are given and briefly discussed in this section [1–4] [1].

1.1. Viscosity of Molecular Hydrogen

The viscosity, η, is given to a second approximation by

$$\eta=\eta(1)\left\{1+\frac{3}{196}\left[8\frac{\Omega^{(2,3)*}}{\Omega^{(2,2)*}}-7\right]^2\right\} \quad \text{g cm}^{-1}\ \text{s}^{-1} \tag{1a}$$

with

$$\eta(1)=\frac{5}{16}\left(\frac{\sqrt{\pi mkT}}{\pi\sigma^2\Omega^{(2,2)*}}\right) \quad \text{g cm}^{-1}\ \text{s}^{-1} \tag{1b}$$

where T is the temperature (K), m the weight of a molecule, k Boltzmann's constant, σ a cross-section parameter, and $\Omega^{(l,s)*}$ (l, $s=1$, 2, 3) are the collision integrals. Equation (1) is applicable to both classical and quantum fluids provided one properly modifies the collision integrals. For example, in the classical case the collision integrals involve the classical cross section $Q^{(l)}$ where

$$Q^{(l)}\sim\int_0^\infty(1-\cos^l\chi)bdb \tag{2a}$$

χ is the angle of deflection and b is the impact parameter, and are computed using classical statistical mechanics. In the quantum case, however, the collision integrals involve the quantum mechanical cross section given by

$$Q^{(l)}\sim\int_0^\pi(1-\cos^l\chi)I(\chi)\sin\chi d\chi \tag{2b}$$

and are computed via the quantum mechanical phase shifts. $I(\chi)$ is the differential scattering cross section. In both cases the viscosity involves the intermolecular potential function $\phi(r)$ through the scattering angle.

The integrals of eq (1) have been reduced by dividing by the values for a hard sphere of diameter σ. To agree with previous work on hydrogen [4] we define here a new parameter $\bar{\Omega}^{(l,s)*}$ by incorporating the cross section parameter with the collision integral:

$$\bar{\Omega}^{(l,s)*}=\sigma^2\Omega^{(l,s)*}. \tag{3}$$

*Work carried out at the National Bureau of Standards under the sponsorship of the Office of Standard Reference Data and the National Aeronautics and Space Administration (SNPO–C).

**Cryogenics Division, National Bureau of Standards, Boulder, Colo. 80302.

[1] Figures in brackets refer to the references given at the end of the paper.

Strictly speaking, the viscosity equation (1) applies only to a gas whose molecules interact according to a central force law and collide in a way so that the collisions are elastic. In other words, the molecules should be spherically symmetric and not have an internal structure. This is not the case for the polyatomic hydrogen, of course, but it appears that an effective spherically symmetric form of ϕ can be used for the viscosity with eq (1) and give a proper comparison with experimental data.

1.2. Viscosity of Atomic Hydrogen and the Dissociating Mixture

Dissociating hydrogen can be regarded as a mixture of molecular and atomic hydrogen, the proportions of each species depending on the pressure, p, and the temperature T via the dissociation constant K:

$$H_2 \overset{K}{\rightleftarrows} 2H. \tag{4}$$

Specifically, the mole fraction of H, x_H, is given by [5]

$$x_H = 2/\{1+[1+(4p/K)]^{1/2}\} \tag{5}$$

and

$$x_{H_2} + x_H = 1.$$

The viscosity of the dissociating mixture, η_{mix}, can be expressed by the following kinetic theory equation [1, 4, 6]:

$$\eta_{mix} = \left[\frac{x_1^2}{H_{11}} + \frac{x_2^2}{H_{22}} - \frac{2x_1x_2H_{12}}{H_{11}H_{22}}\right] \cdot \left[1 - \frac{H_{12}^2}{H_{11}H_{22}}\right]^{-1} \tag{6}$$

where

$$H_{11} = \frac{x_1^2}{\eta_1} + \left(\frac{2x_1x_2}{M_1+M_2}\right)\frac{RT}{pD_{12}}\left[1 + \frac{3M_2\langle A_{12}^*\rangle}{5M_1}\right]. \tag{7}$$

In this equation we follow the work of reference [4] and adopt the convention that the subscript 1 refers to the molecular species H_2 and the subscript 2 refers to the atomic species H.

A similar expression can be written for H_{22} with the subscripts 1 and 2 interchanged. For H_{12} we have

$$H_{12} = -\left(\frac{2x_1x_2}{M_1+M_2}\right)\frac{RT}{pD_{12}}\left[1 - \frac{3}{5}\langle A_{12}^*\rangle\right]. \tag{8}$$

In the above equations M_1 and M_2 are the molecular weights of the species and the other symbols are explained shortly. When x_2(i.e., x_H) tends to zero—negligible dissociation—eq (6) reduces to eq (1) as it should [7].

In equations (6)–(8) the entities η_1, η_2, D_{12} and $\langle A_{12}^*\rangle$ appear. η_1 is the viscosity of molecular hydrogen and involves the H_2—H_2 interaction. We already have

$$\eta_1 \sim 1/\bar{\Omega}_{11}^{(2,2)*}.$$

However, the entities η_2, D_{12}, and $\langle A_{12}^*\rangle$ involve the interactions of H—H or H—H_2, and the appropriate collision integrals need to be used. For example η_2 is given by an expression equivalent to eq (1)

$$\eta_2 \sim 1/\langle\bar{\Omega}_{22}^{(2,2)*}\rangle \tag{9}$$

and D_{12}, the diffusion coefficient is given by

$$pD_{12} = \frac{3}{16}\frac{\sqrt{2\pi k^3T^3/\mu}}{\pi\langle\bar{\Omega}_{12}^{(1,1)*}\rangle} \tag{10}$$

where μ is the reduced mass for the H—H_2 mixture and the collision integral in eq (10) is appropriate for diffusion in this H—H_2 mixture. The term $\langle A_{12}^*\rangle$ is simply the ratio of the collision integrals

$$\langle A_{12}^*\rangle = \langle\Omega_{12}^{(2,2)*}\rangle/\langle\Omega_{12}^{(1,1)*}\rangle \tag{11}$$

for the H—H_2 interactions. To explain the angular brackets: for the H—H or H—H_2 interactions the collision integrals will not be a function of a *single* potential since a single intermolecular potential energy curve will not represent a collision. Specifically one has to take into account the fact that a number of force laws will be followed as two species approach each other; each law corresponding to a different alinement of electron spins. It might be supposed that the determination of the resulting collision integrals is almost an impossible task, but the problem can be bypassed. Mason and Monchick [3], for example, show that the kinetic theory format can remain straightforward and the transport coefficient formulas can remain essentially the same, provided the appropriate collision integrals are replaced by a weighted average over the possible force laws, thus they write

$$\bar{\Omega}^{(l,s)*} \rightarrow \sum r_i\sigma_i^2\Omega_i^{(l,s)*} \equiv \langle\bar{\Omega}^{(l,s)*}\rangle \tag{12}$$

where r_i is the statistical weight of the ith force law. In the case of atomic hydrogen, r_i has the values 1/4 and 3/4 corresponding to the $^1\Sigma$ state and the $^3\Sigma$ state respectively. The same line of reasoning applies to the H—H_2 interaction (and by implication, to the H_2—H_2 interaction, although it is not necessary from a practical point of view).

1.3. *p*- and *n*-Hydrogen

In the above section we have assumed no difference between dissociating *p*-H_2 and dissociating *n*-H_2; the comments on the weighted collision integrals refer to *n*-H_2. It has thus been assumed that enough of the *p*-H_2 has already been converted to *o*-H_2 to give a normal mixture at temperatures where dissociation becomes significant [8].

In principle one should also take into account dif-

ferences in the viscosity of the undissociated isotopes since the collision integrals (i.e., the intermolecular potentials) must be different. Several authors have discussed this. In particular, if the intermolecular potential is represented by a two-parameter 12–6 function with ϵ and σ the energy and distance parameter respectively, Knaap et al. [9] show that one may expect a difference in these parameters given by $\Delta\epsilon/\epsilon \sim 0.6\times10^{-2}$ and $\Delta\sigma/\sigma \sim 0.03\times10^{-2}$. They find for the second virial coefficient a difference $(B_n-B_p)/B_n \sim 1.0\%$. A similar difference in viscosities would also be expected only with $\eta_p > \eta_n$. In fact, Becker and Stehl [10] find a small difference. Unfortunately since the scatter in experimental viscosity coefficients is ~ 2.0 percent and since a model potential function has to be used to obtain theoretical viscosity coefficients, it is difficult to judge if the difference is significant.

1.4. Thermal Conductivity of Molecular Hydrogen

The simple kinetic theory formula for the thermal conductivity, λ, of a gas with no internal structure is

$$\lambda=\frac{5}{2}c_v'\eta \tag{13}$$

where c_v' is the specific heat per gram at constant volume for the translational degrees of freedom: $c_v'=(3/2)\,k/m$. But equation (13) cannot be used directly for a polyatomic gas because the internal structure substantially influences the thermal conductivity, specifically because inelastic collisions have to be taken into account. Thus the kinetic theory treatment needs appropriate modification. The effect of inelastic collisions has been discussed formally by several authors [11] but their resulting formal equations are too esoteric for practical calculations. However, Mason and Monchick [3] have looked at the formal theory and have simplified its application. They recognized that three mechanisms contribute to the transfer of heat: (1) the translational motion of the molecules, (2) an effective internal diffusion of the internal degrees of freedom, and (3) a coupling between the translational and internal contributions. If the total conductivity is written as the sum of contributions (1) and (2), i.e.,

$$\lambda=\lambda'+\lambda'' \tag{14}$$

where λ' is the translational contribution and λ'' the internal contribution, then Mason and Monchick show that

$$\lambda'=\tfrac{5}{2}\eta(c_v'-\Delta) \tag{15}$$

$$\lambda''=\rho D_{\text{int}}(c_v''+\Delta) \tag{16}$$

where the total specific heat per gram has also been written as a sum of the translational and internal parts:

$$c_v=c_v'+c_v''. \tag{17}$$

In eq (16), D_{int} is the effective diffusion coefficient for the transfer of internal energy and Δ is a term accounting for the interchange of the translational and internal energies. From eqs (15) and (16),

$$\lambda=\frac{5}{2}\eta\left(\frac{3}{2}\frac{k}{m}\right)+\rho D_{\text{int}}c_v''-\eta\left(\frac{5}{2}-\frac{\rho D_{\text{int}}}{\eta}\right)\Delta. \tag{18}$$

One can further show that

$$\Delta=\frac{2}{\pi}\sum_k\frac{c_k''}{Z_k}\left(\frac{5}{2}-\frac{\rho D_{\text{int}}}{\eta}\right)+\text{higher terms} \tag{19}$$

where c_k'' is the internal specific heat for the kth internal mode, and Z_k is the collision number associated with that mode. Equation (18) consequently becomes,

$$\lambda=\frac{15}{4}\frac{k}{m}\eta+\rho D_{\text{int}}c_v''-\frac{2}{\pi}\eta\left(\frac{5}{2}-\frac{\rho D_{\text{int}}}{\eta}\right)^2\sum_k\frac{c_k''}{Z_k}. \tag{20}$$

Note that if the molecule has no internal structure, eq (20) reduces to eq (13) as it should.

For hydrogen, both Z_{rot} and Z_{vib} are large and the last term on the right-hand side of eq (20) can be dropped. Another simplification is possible if D_{int} is approximated to the self-diffusion coefficient, D, because

$$\frac{\rho D_{\text{int}}}{\eta}\equiv\frac{\rho D_{11}}{\eta}=\frac{6}{5}A_{11}^*. \tag{21}$$

Thus, for hydrogen,

$$\lambda=\frac{15}{4}\frac{R}{M}\eta+\frac{6}{5}A_{11}^*c_v''\eta. \tag{22}$$

The question of the validity of the general equation (18) and of the particular equation (22) has been an object of discussion for some time. A recent review is given by Sandler [12].

1.5. Thermal Conductivity of Atomic Hydrogen and the Dissociating Mixture

The thermal conductivity of a dissociating mixture is given by an expression equivalent to the formula for the viscosity, with the appropriate allowance for λ''. This is not all, however, for an additional feature appears: the dissociation process has an associated heat of reaction and this dissociation heat substantially contributes to the overall heat transfer [4, 6, 13]. The conductivity of the mixture, λ(mix), is then expressed as a sum of these contributions

$$\lambda(\text{mix})=\lambda_f(\text{mix})+\lambda(r) \tag{23}$$

where λ_f(mix) is the conductivity in the absence of the chemical reaction—called the frozen conductivity—and $\lambda(r)$ is the conductivity due to the chemical reaction. We write down the equations for these terms separately.

Frozen Thermal Conductivity: We have, following eq (14)

$$\lambda_f(\text{mix}) = \lambda'(\text{mix}) + \lambda''(\text{mix}) \tag{24}$$

where the prime and double primes refer to the translational and internal portions respectively. The expression for the first part is similar to the viscosity equation, viz.,

$$\lambda'(\text{mix}) = -4\left[\frac{x_1^2}{L_{11}} + \frac{x_2^2}{L_{22}} - \frac{2x_1x_2L_{12}}{L_{11}L_{22}}\right]\cdot\left[1 - \frac{L_{12}^2}{L_{11}L_{22}}\right]^{-1} \tag{25}$$

with

$$L_{11} = \left|-\frac{4x_1^2}{\lambda_1'} - \frac{16}{25}\frac{x_1x_2}{(M_1+M_2)^2}\frac{T}{pD_{12}}\right| \left[\frac{15}{2}M_1^2 + \frac{25}{4}M_2^2 - 3M_2^2\langle B_{12}^*\rangle + 4M_1M_2\langle A_{12}^*\rangle\right] \tag{26}$$

and a corresponding expression for L_{22} can be written with the subscripts 1 and 2 interchanged. The term accounting for the H–H_2 interactions in eq (25) is

$$L_{12} = \left[\frac{16}{25}\frac{x_1x_2M_1M_2}{(M_1+M_2)^2}\frac{T}{pD_{12}}\right]\cdot\left[\frac{55}{4} - 3\langle B_{12}^*\rangle - \langle A_{12}^*\rangle\right] \tag{27}$$

The symbols of eqs (25)–(27) have been defined when eqs (6)–(12) were discussed except for λ_i' which is given by

$$\lambda_i' = \frac{15}{4}\frac{R}{M}\eta_i \tag{28}$$

and in eqs (26) and (27) we have $\langle B_{ij}^*\rangle$ which is given by

$$\langle B_{ij}^*\rangle = \{5\langle\bar{\Omega}_{ij}^{(1,2)*}\rangle - 4\langle\bar{\Omega}_{ij}^{(1,3)*}\rangle\}/\langle\bar{\Omega}_{ij}^{(1,1)*}\rangle. \tag{29}$$

We have again used the convention that subscripts 1 and 2 refer to the molecular and atomic species respectively.

Fortunately, the internal part $\lambda''(\text{mix})$ is given by a fairly straight forward expression for hydrogen because Hirschfelder [14] has shown that this internal contribution can be depicted by

$$\lambda''(\text{mix}) = \frac{\lambda_1 - \lambda_1'}{1 + (D_{11}/D_{12})(x_1/x_2)} \tag{30}$$

where λ_1 is the total conductivity for pure hydrogen molecules. From eqs (28) and (22), we get

$$\lambda''(\text{mix}) = \frac{6}{5}A_{11}^*c_v''\eta_1/\{1 + (D_{11}/D_{12})(x_1/x_2)\} \tag{31}$$

Thus, the total frozen conductivity of the mixture $\lambda_f(\text{mix})$ is given by the sum of eqs (25) and (31).

Chemical Reaction Contribution to the Thermal Conductivity: The last term of eq (23), $\lambda(r)$, is given by [13].

$$\lambda(r) = \left[\left(\frac{pD_{12}}{RT}\right)\frac{(\Delta H)^2}{RT^2}\right]\left[\frac{x_1x_2}{(1+x_1)^2}\right] \tag{32}$$

where ΔH is the heat of reaction for the dissociation.

Hence the *total* thermal conductivity of the dissociating mixture can be determined by summing the eqs (25), (31), and (32).

1.6. *p*- and *n*-Hydrogen

In addition to the reasons mentioned in 1.3, the thermal conductivity of the two species will differ since the internal specific heat, c_v'', appears in the formulas. Between about 40 and 300 K, c_v'' for *p*-H_2 is significantly different from c_v'' for *n*-H_2[5].

2. Calculation of Mass Fraction, Heat of Reaction and Internal Specific Heat

We continue by discussing the calculation procedure we adopted. First let us consider the calculation of x, ΔH and c_v''. Actually the calculation of these properties poses no problem since the necessary variables are well known. The mass fractions at given pressures and temperatures were computed from eq (5), using values of K from reference [5]. The heat of reaction, ΔH, was also calculated from K via the Van't Hoff isobar [4, 6].

$$\frac{\Delta H}{RT^2} = \frac{d\ln K}{dT}. \tag{33}$$

The internal specific heat at constant volume was computed from values of c_p (from reference [5]) since c_v'' is given by the equation

$$c_v'' = c_p - \frac{5}{2}\frac{R}{M}. \tag{34}$$

3. The Collision Integrals

Once numerical values of c_v'', ΔH, and x are available, the only remaining unknowns in the formulas of section 1 are the collision integrals. Unfortunately, the computation of these collision integrals is the most uncertain factor in the calculation of the transport coefficients but is at the same time the most important. Except possibly, for the H–H integrals, they have to be computed from model intermolecular potential functions. The choice of the model and its parameters has to be determined from experiment and, for hydrogen, the evaluation of experimental data is not a straightforward task.

Of the collision integrals, the most important for the wide temperature range under consideration are those for the H_2—H_2 interaction. The others are needed only when dissociation becomes significant—and even at

a low pressure of 0.01 atm dissociation is not significant until about 2000 K. Further, dissociation between 2000 and 5000 K at pressures between 0.01 and 100 atm only changes the viscosity by about ±10 percent from the equivalent undissociated value. For thermal conductivity the situation is different; the conductivity of the mixture is much greater than it would be for the equivalent undissociated value, but the dominant contribution to this thermal conductivity is the contribution $\lambda(r)$ given by eq (32). This does involve the integral for the H—H_2 interaction yet, even so, the two terms $(\Delta H)^2/RT^2$ and $x_1x_2/[(1+x_1)^2]$ of eq (32) largely control the temperature *dependence* of $\lambda(r)$.

Accordingly, we did not feel it necessary to reevaluate the collision integrals for the H—H and H—H_2 interactions or comment on their selection. Consequently, the values used in these calculations were taken directly from table II of reference [4]. We concentrated on the selection of the $\bar{\Omega}_{11}^{(l,s)*}$ integrals necessary to compute the transport properties of the undissociated molecular hydrogen.

3.1. General Rules for Choosing a Model Intermolecular Potential Function

We have recently clarified the overall relation between model potential functions, theoretical expressions and experimental data [15]. We arrived at conclusions which are, in short: (1) The realistic three parameter intermolecular potential function familes are equivalent with respect to the correlation of data. By equivalent we mean that one member of all the families in common use can be found that will fit a given set of data in the same way. (2) A temperature range exists over which a property is insensitive to all sensible members of all model families. For transport properties of classical fluids this range is $2 \lesssim T_1^* \lesssim 5$ where T_1^* is the temperature reduced by the Lennard-Jones energy parameter $(\epsilon/k)_{L-J}$. This conclusion leads to the definition of a *high* temperature as a temperature above the insensitive range, and a *low* temperature as a temperature below the range. Because $(\epsilon/k)_{L-J}$ for hydrogen is ~ 40 K, one would expect that the range is 80 K $\lesssim T \lesssim$ 200 K but we are not yet clear on how quantum effects might adjust these limits [16]. (3) One member of a three parameter family is not flexible enough to simultaneously represent a property at *both* high and low temperatures. Finally, (4) a significant choice of a potential function requires that the data have a precision of about 0.5 percent at low temperatures, or about 3 percent at high temperatures. By significant choice we mean that we can distinctly select a function and attach some meaning to the selection. Of course, unless we use independent information we cannot be sure that even a distinct and proper choice does not reflect systematic error. A full discussion on these conclusions is available in reference [15].

4. Correlation of Hydrogen Data

In practice, application of the conclusions of the previous section is somewhat restricted. There are two reasons. First, we really have only one model potential with which to work at low temperatures—the quantum mechanical 12–6 (or Lennard-Jones) of Munn et al. [17]. Second, the data available often do not satisfy the criterion (4) of Section 3.

4.1. The High Temperatures Region Without Dissociation

Conclusion (1) of section 3 states that only one model function family need be considered. Since we have to use the 12–6 at low temperatures, we studied the high temperature regions with members of the m–6 family. For this family when $\phi(r)$ is the potential for two molecules separated by distance r, we have [15, 18],

$$\phi(r) = \epsilon \left[\left(\frac{\sigma}{r}\right)^m - \left(\frac{\sigma}{r}\right)^6 \right] \Big/ \left[\left(\frac{6}{m}\right)^{6/m-6} - \left(\frac{6}{m}\right)^{m/m-6} \right] \qquad (35)$$

with (in our case) $m = 9, 12, 15, 18, 21, 24$. In eq (35), ϵ is the depth of the energy well and σ is the distance separating the molecules at $\phi(r) = 0$.

a. Viscosity

We started with the viscosity equation (1b) and used it to select the potential and its parameters. The selection procedure is described in reference [19]. Basically it goes as follows: m is fixed, σ is fixed at a sensible value, and selected data for several temperatures are put into the left-hand side of equation (1b). We thus obtain experimental collision integrals as a function of temperature T. These experimental integrals are then compared with the theoretical integrals for the fixed m which are available as functions of the reduced temperature T^*, $T^* = T/(\epsilon/k)_{m-6}$. We can thus observe how ϵ/k varies with T for the given σ and m. σ is now varied until one finds a value for σ which gives the least variation of ϵ/k with T. Finally, the family parameter m is changed and the procedure repeated. Our selection of m, σ, and ϵ/k is made by finding the m and σ which give the least variation of ϵ/k with T after considering all values of m. If one member of the function family represented the data exactly, ϵ/k would be constant. The collision integrals used were those of Klein and Smith [18].

The procedure of course relies (as does any other procedure) on the data which is why criterion (4) of section 3 needs to be stated, but while several authors have investigated the viscosity (for n-hydrogen only) in the high temperature range [20–32] the amount of *reliable* data is somewhat limited. For example, there is nothing reliable at this time between about 400 and 1100 K. Other data do exist above 400 K but we have shown [33] that they are most probably incorrect (by a large amount—almost 10 percent at 2000 K. It appears that the older measurements of viscosity by the capillary flow technique are erroneous). We have pointed out that the incorrect data form the

TABLE 1. *Potential function parameters for* n- *and* p-*hydrogen selected from viscosity data*

m	A*	σ(Å)	ϵ/k (K)
High temperature			
9	....	3.06	30.4
Low temperature			
12	1.70	2.97	39.2

basis for most of the tabulations and correlations of transport properties at present in the literature. Hence the tables produced by our correlations will differ significantly from those available up to now. We refer to reference [33] for more details on this point.

Working with selected data [28–32], eq (1), and the collision integrals of reference [18], the parameters shown in table 1 were selected. The parameters were then used to compute the viscosity and a comparison of theory and experiment is shown as a deviation curve, figure 1. The curve is reasonably satisfactory. There is a small systematic deviation at the high temperatures but to remove this deviation rather unrealistic collision integrals would have to be used. It is also possible that some dissociation is occurring at the two highest temperatures.

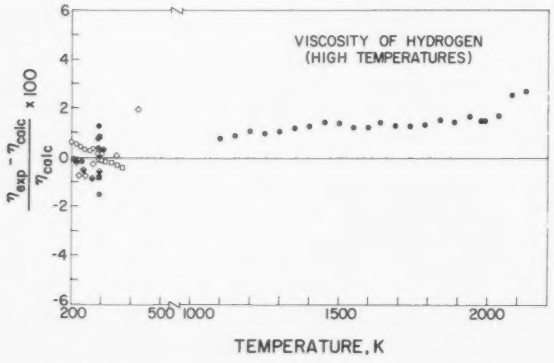

FIGURE 1. *Viscosity of hydrogen at high temperatures.*

Experimental data fitted to a 9–6 function with $\sigma = 3.06$ Å, $\epsilon/k = 30.4$ K.
Key: ⊗ [32], ◇ [30], ◒ [21], ◓ [22], ○ [24], □ [26], ◑ [27], ◆ [29], ◈ [31], ■ [28], ◆ [20].

b. Thermal Conductivity

The situation with regard to the thermal conductivity measurements is not very good [34–42], accurate data are scarce and scattered. Above 400 K four authors report results and their sets of data differ systematically by more than 20 percent [35, 36, 41, 42]. Moreover, when we use the selected potential function to compute thermal conductivity via eq (22) the deviation curve produced, figure 2, is not satisfactory. Comments are deferred until the discussion section, but we feel the conductivity data are most probably responsible for this. We cannot believe that the theoretical formulas, eqs (1) and (22), or the 9–6 function chosen to represent the viscosity are that wrong.

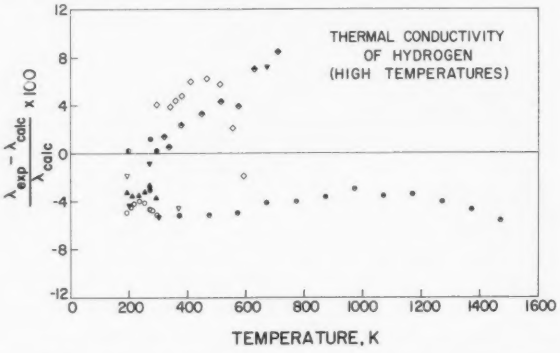

FIGURE 2. *Thermal Conductivity of hydrogen at high temperatures.*

Experimental data fitted on the basis of the viscosity correlation, see caption fo figure 1. Omitted are data from reference [35].
Key: ◓ [36], ◒ [38], ▽ [40], ○ [39], ▼ [37], ▲ [34], ◐ [52], ⊗ [60], ◇ [42], ◆ [41].

4.2. The Low Temperature Region

We have already mentioned that we have to work with the quantum mechanical 12–6 intermolecular potential. (Work is in progress to modify other functions for quantum effects, but it appears that results will not be available for some time.) Actually, this restriction may not matter much. Conclusion (3) of section 3.1, states that the model potential found from experiment to be suitable for the high temperature region will not be satisfactory when used in the low temperature region. Anyway, this might rule out the 9–6 for the low temperature region. Furthermore, our previous work with other gases using the m–6 family suggests that the parameter m compatible with the high temperature range is less than the corresponding m for the low temperature range. For example, for argon, m (high) ≈ 13, m (low) ≈ 18. While comparison of other gases with hydrogen should be made with caution, it is quite possible that if $m \approx 9$ for high temperature hydrogen, then $m \approx 12$ is reasonable for low temperature hydrogen.

a. Viscosity

Several workers have measured hydrogen below 300 K [20–25, 27, 30, 31, 43–46] but much of the data have to be considered unreliable. However, sets of viscosity data for several gases other than hydrogen [47], and one set for hydrogen [31] have recently been published and these new results tend to be somewhat lower systematically than those reported in the past. We have studied the apparent discrepancies and show there are grounds to favor the newer data [48]. In other words, while there are little, if any, direct independent evidence that the majority of hydrogen viscosities are too high, they may well nevertheless be so. To get as much new evidence as possible on

this point we re-examined the viscosity data of Diller published in 1965 [49]. Diller did not measure the dilute gas viscosities directly but rather presented the density dependence of viscosity for the dense gas and liquid state. However, by a careful analysis of his isotherms it was possible to obtain dilute gas values with reliable error limits. The analysis procedure is discussed in reference [50] and the corresponding dilute gas viscosities are listed in table 2. We find that these data are significantly lower than data published previously. Unfortunately although this result is consistent with the point made that the latter data may be too high, it does not agree with the conclusion of Knaap et al. [9], or with the experiment of Becker and Stehl [10] which suggest that $\eta(p\text{-}H_2) > \eta(n\text{-}H_2)$ at a given temperature; the existing n-H_2 data would have to be much too high if this is to be so.

TABLE 2. *Dilute gas viscosities for* p-*hydrogen obtained from dense gas data of Diller [49]*

Temperature K	Viscosity $10^6 g\ cm^{-1}s^{-1}$
33.0	16.96 ± .35
36.0	16.3 ± .2
40.0	20.0 ± .5
50.0	23.3 ± .5
60.0	28.0 ± .3
70.0	31.3 ± .1
80.0	34.9 ± .2
100.0	40.5 ± .5

After considerable manipulation of the parameters of the 12–6 function and keeping the possibilities of errors in the data in mind, we eventually concluded that the parameters shown in table 1 were the best. The deviation curve, figure 3, was plotted. We confirmed that the fit for the low temperature region matched with the fit for the high temperature region.

It should be clear that the uncertainty and scatter in the data means that one has a considerable and unwelcome latitude in choosing the parameters (conclusion (4) of section 3.1) and that several combinations

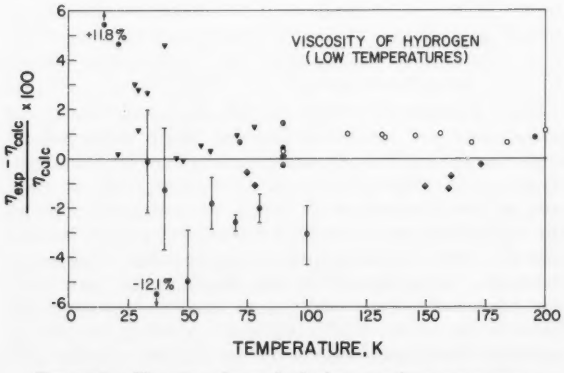

FIGURE 3. *Viscosity of* p- *and* n-*hydrogen at low temperatures.*

Experimental data fitted to a quantum mechanical 12–6 function with $\Lambda^* = 1.70$, $\sigma = 2.97$ Å, and $\epsilon/k = 39.2$ K.
Key: p-H_2, ◐ [49]; n-H_2, ◒ [20], ◒ [21], ◓ [22], ◑ [27], ○ [24], ▼ [46], ◆ [31].

are possible, Diller and Mason [51], for example, found $\epsilon/k = 37.2$ K, $\sigma = 2.97$ Å, and $\Lambda^* = 1.70$ (but by correlating the results of references 24 and 46). One should note that since $\Lambda^* = h/\sigma(2\mu\epsilon)^{1/2}$, the values of ϵ and σ should correspond to the value of Λ^* selected. This is the case for Diller and Mason, but not here.

b. Thermal Conductivity

Up to now two main sets of data existed for the thermal conductivity of hydrogen at low temperatures, those of Golubev and Kalsina [34] and of Johnston and Grilly [39]. More recently Roder and Diller have measured both para and normal hydrogen from 17 to 200 K at pressures from about 1 to 170 atm [52]. Their dilute gas values are given in table 3.

Theoretical values of the thermal conductivity for the n- and p-modifications were calculated from eq (22) using the 12–6 function and the parameters estimated from viscosity data. Values of the internal specific heat were determined from eq (34) with data from reference [5]. Theoretical conductivities were compared with experimental at the same temperature, and a deviation curve was plotted, figure 4. The fit is low overall.

TABLE 3. *Dilute gas thermal conductivity values of* p- *and* n-*hydrogen from Diller and Roder [52]*

Temperature K	p-Hydrogen	n-Hydrogen
	$mW\ cm^{-1}K^{-1}$	
17.38	[a] 0.138	
20.06	.153	
22.0	.165	
25.47	.196	
29.98	.231	
40.24	.303	
59.1		0.423 ± 0.002
59.2	.440 ± 0.001	
79.8		.561 ± .001
79.9	.599 ± .002	
99.9	.797 ± .001	.687 ± .002
122.9	1.033 ± .001	
123.0		.851 ± .001
153.0		1.052 ± .001
197.9		1.331 ± .002

[a] Values without error limits were taken to be the 1 atm value. Values with error limits were obtained by analysis of conductivity as a function of density at the given temperatures. The method of reference [50] was used.

4.3. Thermal Conductivity and Viscosity of Dissociated Hydrogen

We compute the transport properties of the dissociated hydrogen using the formulas of section 1. The collision integrals were those listed in reference [4], except for $\bar{\Omega}^{(l,s)*}$ for the H_2—H_2 interaction. These latter integrals are the same, of course, as those discussed in section 4.1a, i.e., the 9–6 integrals of reference [18]. The parameters are given in table 1.

There does not seem to be any viscosity data for the dissociated gas. Two sets of data exist for the

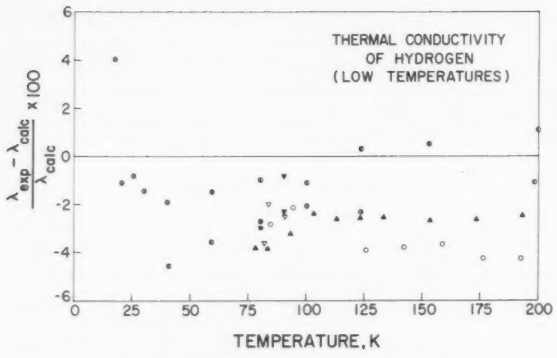

FIGURE 4. *Thermal Conductivity of* p- *and* n-*hydrogen at low temperatures, experimental data fitted on the basis of the low temperature viscosity correlation, see caption to figure 3.*

Key: p-H_2. ◑ [52]; n-H_2. ▽ [40], ○ [39], ▼ [37], ▲ [34], ◐ [52].

thermal conductivity however, those of Israel et al. [53], and those of Bethringer et al. [54]. The former set of data appears to be incorrect; dissociation seems to take place at too low a temperature. The latter data are illustrated in figure 5, together with our theoretical estimate.

5. Discussion

The deviation curves, figures 1 to 4, indicate that the fits are not completely satisfactory overall. Since we based the initial correlations on viscosity measurements, a reasonable looking deviation curve for the viscosity will always result, the disturbing fact is that the calculated values of the thermal conductivity are somewhat too high when compared with most of the experimental data especially at low temperatures. However, we feel we may explain this relatively poor correlation of experimental thermal conductivity data by blaming the experimental data itself. Our conclusion is backed by the arguments that follow.

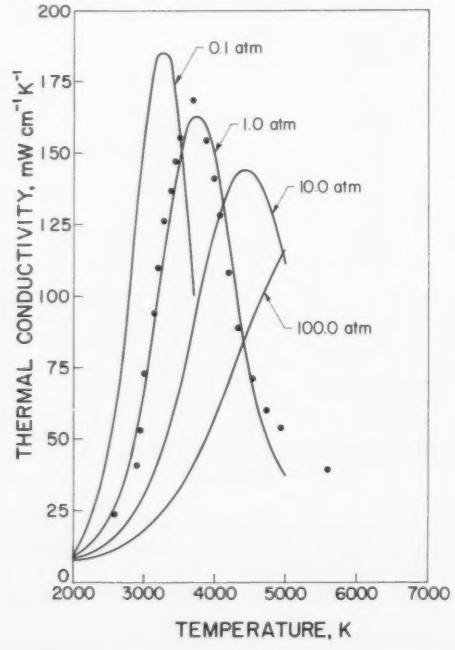

FIGURE 5. *Thermal conductivity of dissociating hydrogen at various pressures.*

See section 4.3. Data from reference [54] shown as points.

It is fairly obvious that the discrepancies between theoretical and experimental conductivities, and by discrepancies we mean first order systematic deviations between theory and experiment of about 1–2 percent, can be due to at least one of these reasons:

(a) The viscosity equation (1) is incomplete leading to an incorrect choice of a model potential function and its parameters.

(b) The viscosity equation is correct, but the viscosity data are inaccurate. As in (a) this will also mean that the selected potential function is wrong.

(c) The thermal conductivity equation (22) is incomplete.

(d) The equation (22) is correct but the thermal conductivity data are inaccurate.

(One could add to (a) and (b) that while *both* the viscosity equation and the viscosity data could be correct, the selected potential function may not be flexible enough to represent another property, such as the thermal conductivity. This cannot be the case here, however, since the same collision integrals are prominent for both viscosity and thermal conductivity.)

It should be stated that one could go a long way towards deciding which of the reasons (a) through (d) are the cause of the apparent errors if we had more independent (non-transport) information to check on the potential functions selected, or if we had definite evidence on systematic errors in the experimental measurements. For instance, we have for other gases been able to check the appropriate potential functions using results from molecular beam data, x-ray scattering data, and optical studies [33, 48]. We cannot do this for hydrogen because the necessary experiments have not been done. Hence, here we have to examine points (a) to (d) on the basis of the transport data alone which is obviously not a really satisfactory procedure. Nevertheless we will argue that for our purpose all reasons but (d) can probably be eliminated.

High Temperature Region: By and large the poor correlation of conductivities at high temperature appears to be due to random scatter in the data. Systematic deviations are not so prominent as they are at low temperatures. But it is worthwhile to go through the points (a) to (d) if only to set up our reasoning for the low temperature region. The high temperature viscosities (without dissociation) are first considered. It is assumed that the fundamental viscosity formula is valid. While such an assumption might provoke discussion, there is no evidence from any experiments for any gas that the formula is *not* correct. In fact, Klein and Hanley have demonstrated [15, 55] that from the statistical mechanical point of view the

viscosity equation is at least *consistent* with the equation for the second virial coefficient (that is, if the viscosity equation is correct, the second virial equation is also correct, and vice versa).

With regard to part (b) and the viscosity experimental data, we have confidence in at least two sets of data, those of Kestin et al. [28, 29] and of Guevara et al. [32]. The data of these authors have been found very satisfactory for other gases [33] and we see no reason why hydrogen should be an exception.

Let us now discuss point (c), i.e., the validity of the thermal conductivity equation (22)

$$\lambda = \frac{15}{4}\frac{R}{M}\eta + \frac{6}{5}A^* c_v'' \eta.$$

Note that if experimental viscosities are used, eq (22) only weakly involves the potential function through A^*. Equation (22) was obtained from the more general equations (19) and (20):

$$\lambda = \frac{15}{4}\frac{R}{M}\eta + \rho D_{\text{int}}\, c_v'' - \frac{2}{\pi}\eta\left(\frac{5}{2} - \frac{\rho D_{\text{int}}}{\eta}\right)^2 \sum_k \frac{c_k''}{Z_k}. \tag{36}$$

It is well known that this equation is not complete [12] because Mason and Monchick derived it from the Wang-Chang-Ulenbeck Theory [11], and in this theory only the first approximation expression for the thermal conductivity was obtained. In other words only one Sonine polynomial was used to compute the perturbation term in the appropriate solution of the Boltzmann equation for polyatomic molecules. If we were dealing with a monatomic gas this restriction would not be necessary and the higher approximations can be determined without too much trouble. In particular, eq (36), with the second approximation, becomes

$$\lambda = \frac{15}{4}\frac{R}{M}\eta[1 + (70/8232)y]$$

where (37)

$$y = [(8\Omega^{(2,3)*}/\Omega^{(2,2)*}) - 7]^2.$$

We write down eq (37) to show that the calculated conductivity value for a monatomic gas *increases* if eq (37) is used in preference to the first approximation eq (13). Although the effects of higher approximations on the other terms of eq (36) are not yet known, for real molecules it seems reasonable to suppose that if they were included, the calculated thermal conductivity would also increase for a polyatomic gas [56]. If this were so, the systematic deviations of figure 2 generally would be worse. Hence, neglect of higher approximations in the general equation (36) does not appear to account for the fact that the calculated thermal conductivities are generally too high when compared to most of the (presumably) more reliable data, (we exclude that data of reference [35]).

It is clear that two simplifications have been made when eq (22) is derived from eq (36); D_{int} has been taken equal to the ordinary self-diffusion coefficient D, and terms in $1/Z$, and terms with higher powers of Z, have been neglected. The two approximations can be related, however. The replacement of D_{int} by D has been a subject of some discussion and it is known that it is not a proper thing to do for many gases. This has come up again recently because Sandler [12] has compared polyatomic gas theory for model molecules with other theories such as that of Mason and Monchick [3]. One result of the comparison is the substitution,

$$D_{\text{int}} = D[1 + 0.27/Z \ . \ . \ .] \tag{38}$$

should be made rather than merely equating D_{int} with D.

This substitution also gives improved agreement of theory with experiment although one should note that gases other than hydrogen were tested.

Accepting eq (38) as a reasonable representation of D_{int}, we see that it is only necessary to drop terms in $1/Z$ to get eq (22) from eq (36). Such a step appears justified for hydrogen because all appropriate experimental evidence available indicates that Z for hydrogen is at least around 300 [3, 57]. To sum up, we feel eq (22) is satisfactory for hydrogen and thus rule out point (c). This leaves point (d) as the most likely cause for the systematic discrepancies at high temperatures.

Low Temperature Region: We are not in a particularly strong position to evaluate all the points (a)–(d) when the low temperature region is considered. Points (a) and (c) can be ruled out for the same reason as discussed above, and with regard to (c), we can further show that the question of the validity of the *particular* thermal conductivity eq (22) is not a factor of great importance when correlating data at low temperatures. Unfortunately, it is presently impossible to confidently dismiss either reason (b)—errors in viscosity *or* reason (d)—errors in thermal conductivity; we are not sure if any of the low temperature transport measurements are really reliable. Yet it *is* possible to make a sensible guess as to which of the two is more likely to be the cause of the discrepancies. Because we suspect from independent studies that the older viscosity data tend to be somewhat high [48], and because we give some weight to the apparently low results of Diller, we feel that our viscosity correlation is at least reasonable.

This all means that if a *single* factor has to be selected as a cause for the major discrepancies, we are suggesting that this factor is the experimental thermal conductivity data.

5.1. Theoretical Thermal Conductivities at Low Temperatures

The point was made above that the particular thermal conductivity expression was not too important at low temperatures. One sees this at very low temperatures because $c_v'' \approx o$ below about 40 K. Thus the terms in eq (36) involving the internal degrees of free-

dom can be dropped. The monatomic gas equation results

$$\lambda = \frac{15}{4}\frac{R}{M}\eta \tag{28}$$

[or eq (37) results if the expression is taken to the second approximation]. This type of simplification can be carried to higher temperatures if a procedure described by Harris [58] is used. It is interesting to follow this procedure up.

One can write a very general expression,

$$\lambda = \lambda'[1 + a c_v'' \delta] \tag{39}$$

where as before λ is the total thermal conductivity and λ' is the translational conductivity, a is a constant and δ is a variable. If

$$\lambda = \lambda'[1 + 2/5\ (c_v''/R)\delta] \tag{40}$$

$$\delta = \delta_H - \frac{25}{3\pi Z}\left[1 - \frac{3}{5}\delta_H\right]^2 \tag{41}$$

$$\delta_H = \frac{2}{3}\rho D/\eta \tag{42}$$

then eq (39) becomes the Mason, Monchick equation (36). But we do not require in the development that follows a or δ to have these particular forms.

We will show that eq (39) for *p*-hydrogen can be expressed in terms of experimental quantities. Consider a mixture of *o*- and *p*-hydrogen. The thermal conductivity of the mixture of *o*- and *p*-hydrogen can be expressed by the mixture equations discussed in section 1.5. Specifically,

$$\lambda_{op} = \lambda'_{op} - (\lambda_p - \lambda'_p)/[1 + (x_o/x_p)(D_{pp}/D_{op})] + (\lambda_o - \lambda'_o)/[1 + (x_p/x_o)(D_{oo}/D_{op})] \tag{43}$$

where the subscripts o, and p, or op refer to the *o*-, *p*- or *op*-mixture of hydrogen respectively. Assuming (and this is an assumption, see section 1.3) that

$$\lambda'_{op} \equiv \lambda'_o \equiv \lambda'_p = \lambda'; \qquad D_{oo} \equiv D_{pp} \equiv D_{op} \tag{44}$$

and using $x_o + x_p = 1$, eq (43) then becomes

$$\lambda_{op} = \lambda' + x_o(\lambda_o - \lambda'_o) + x_p(\lambda_p - \lambda'_p). \tag{45}$$

Writing eq (40) for *o*- and for *p*- hydrogen and using eq (45), we obtain

$$\lambda_{op} = \lambda'\left[1 + \frac{2}{5R}c_v''(o)\delta(o) + x_p b\right] \tag{46}$$

where

$$b = \frac{2}{5R}[c_v''(p)\delta(p) + c_v''(o)\delta(o)]\,. \tag{47}$$

Here the o and p in parentheses signify the particular hydrogen isotope. Now for 100 K or less, $c_v''(o) \approx o$, therefore

$$b \approx \frac{2}{5}\frac{c_v''(p)\delta(p)}{R} \quad : \quad \lambda_{op} \approx \lambda'[1 + x_p b]. \tag{48}$$

The key to the procedure is to consider two mixtures of hydrogen with different concentrations of *p*-H_2, designated as 1 and 2 respectively. One then obtains from eq (48) that

$$\lambda_{op}(1) - \lambda_{op}(2) = \lambda' b[x_p(1) - x_p(2)]. \tag{49}$$

In the special case that mixture 1 is pure *p*-hydrogen and mixture 2 is *n*-hydrogen (i.e., $x_p(2) = 0.25$),

$$\lambda_p - \lambda_n = 0.75 b\lambda'. \tag{50}$$

Hence, writing eq (46) for *p*-hydrogen, with eq (50) we find

$$\lambda_p = \lambda' + 4/3(\lambda_p - \lambda_n). \tag{51}$$

Further, if $c_v''(o) \approx 0$ we obtain from eq (48) that

$$\lambda' = 1/3(4\lambda_n - \lambda_p). \tag{52}$$

Thus the total measured thermal conductivity of *p*-hydrogen can be written in terms of itself and of the total measured conductivity of *n*-hydrogen at the same temperature:

$$\lambda_p = 1/3[4\lambda_n - \lambda_p] + 4/3[\lambda_p - \lambda_n] \tag{53}$$

This particular breakdown is only possible if $c_v''(o) \approx 0$ but $c_v''(p) \neq 0$. Equation (53) is thereby restricted to the approximate temperature range of 40 to 100 K.

It is interesting to check eq (53) with eq (22). Writing eq (53) as

$$\lambda(\text{exp}) = \lambda'\ (\text{exp}) + \lambda''\ (\text{exp}) \tag{54}$$

one obtains

$$\lambda'(\text{exp}) = 1/3\ [4\lambda_n(\text{exp}) - \lambda_p(\text{exp})] \equiv 15/4\ \frac{R}{M}\eta$$
$$\lambda''(\text{exp}) = 4/3\,[\lambda_p(\text{exp}) - \lambda_n(\text{exp})] \equiv 6/5 A^* c_v''(p)\eta. \tag{55}$$

Values for both *n*- and *p*-hydrogen are available for three temperatures between 40 and 100 K: 59.1 K, 79.1 K, and 99.8 K, see table 3. Table 4 was constructed in which we have designated (15/4) (R/M) η as λ' (calc) and (6/5) $A^* c_v''(p)\lambda$ as λ''(calc).

It is seen from table 4 that the agreement between the experimental and calculated translational and internal contributions is quite good for this limited data. It should be stressed, however, that the table does not give us definite information on the apparent discrepancy between the viscosities and thermal conductivities. Nevertheless, the rough agreement between the experimental and calculated contribu-

TABLE 4. *Comparison of thermal conductivity eqs (22) and (53)*

Temp K	λ_n(exp)	λ_p(exp)	λ_p(calc)	λ'_p(calc)	λ'_p(exp)	λ''_p(calc)	λ''_p (exp)
	$mW cm^{-1}K^{-1}$						
99.9	0.687	0.797	0.814	0.646	0.649	0.168	0.147
79.9	.561	.599	.616	.551	.549	.065	.051
59.2	.423	.440	.446	.436	.416	.010	.023

tions is encouraging, especially as eq (53) is not required to have the particular form of eq (22).

5.2. Correlation of Diffusion Data

In principle, one can check the potential and the parameters chosen by comparing calculated and experimental diffusion and thermal diffusion coefficients. But because of the lack of experimental data, such a comparison is not very significant. For the record we correlated the self-diffusion coefficients at 1 atm pressure measured by Lipsicas [59]. The appropriate deviation curve is given as figure 6. The result is satisfactory, but does not add to, or alter our previous conclusions.

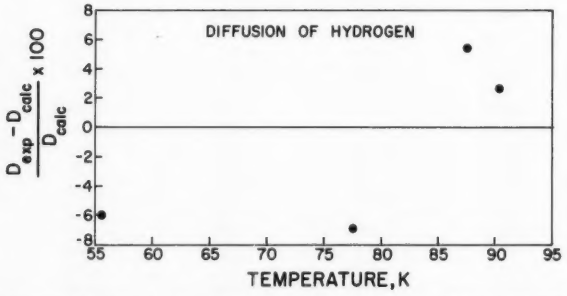

FIGURE 6. *Correlation of the self-diffusion results of Lipsicas [59] based on the viscosity correlation.*

See caption to figure 3.

6. Presentation of Results

Tables of the viscosity and thermal conductivity coefficients were constructed using the formulas and potential functions described in the previous sections. We present the results in tables 5–8. Table 5 gives the coefficients as a function of temperature in the "low temperature" region, table 6 gives the coefficients in the "high temperature" region. As previously explained, we are required at this time to use two separate functions to describe these regions—the 12–6 and 9–6 respectively. Although the regions overlap, there is a slight discontinuity at 160 K. However, we did not feel that our selection of the functions and parameters was definitive enough to justify further manipulation. Tables 7 and 8 list the coefficients for the dissociating mixture; here they are given as a function of temperature and *mole fraction* of the atomic species H. Such tables have the distinct advantage of compactness but, of course, mole fraction is not necessarily the most practical variable, one will often prefer pressure. Consequently we also show in table 9, the variation of mole fraction of H as a function of pressure and temperature. In addition, we have plotted the conductivity for several pressures in figure 5 and also include a plot of the viscosity in figure 7.

The lower limit for the pressure was chosen at 0.001 atm. For pressures below this limit, it is very likely that the dimensions of the experimental apparatus would be needed to calculate the coefficients. For pressures above the upper limit, it is unlikely that the kinetic theory expressions are valid. If an extension of this range is desired, although such an extension should be made with caution, one may compute x_H from eq (5) at the given pressure, using tabulated values of K, (see, for example, reference [5]).

The upper temperature was chosen to be 5000 K. This already represents a considerable extrapolation of the data and we did not feel that our 9–6 function could be extrapolated much further. Moreover, by not going above 5000 K it is not necessary to consider ionization [6]: ionization is not taken into account in the high temperature collision integrals.

TABLE 5. *Viscosity and thermal conductivities of hydrogen at low temperatures*

Temperature	Viscosity	Thermal conductivity (normal)	Thermal conductivity (para)
T, K	$10^3\eta$ g cm^{-1}s^{-1}	λ, mWcm^{-1}K^{-1}	
15.0	0.00740	0.114	0.114
20.0	.01023	.158	.158
25.0	.01292	.200	.200
30.0	.01549	.240	.240
35.0	.01795	.278	.278
40.0	.02025	.313	.313
45.0	.02241	.347	.347
50.0	.02451	.380	.382
55.0	.02657	.412	.417
60.0	.02852	.444	.452
65.0	.03032	.474	.489
70.0	.03215	.505	.529
75.0	.03388	.536	.571
80.0	.03562	.568	.617
85.0	.03727	.600	.664
90.0	.03889	.632	.714
95.0	.04028	.662	.763
100.0	.04179	.695	.816
105.0	.04327	.728	.869
110.0	.04487	.763	.924
115.0	.04624	.796	.977
120.0	.04765	.829	1.028
125.0	.04900	.863	1.077
130.0	.05036	.896	1.125
135.0	.05169	.929	1.171
140.0	.05298	.962	1.213
145.0	.05426	.994	1.254
150.0	.05550	1.026	1.291
155.0	.05676	1.058	1.326
160.0	.05793	1.088	1.358
165.0	.05920	1.120	1.389
170.0	.06040	1.151	1.418

378-324 O - 70 - 3

TABLE 6. *Viscosity and thermal conductivities of hydrogen at high temperatures without dissociation*

Temperature	Viscosity	Thermal conductivity (normal)	Thermal conductivity (para)	Temperature	Viscosity	Thermal conductivity (normal)	Thermal conductivity (para)
T, K	$10^3\,\eta$ g cm^{-1} s^{-1}	λ, mW cm^{-1} K^{-1}		T, K	$10^3\,\eta$ g cm^{-1} s^{-1}	λ, mW cm^{-1} K^{-1}	
140.0	0.05275	0.959	1.213	600.0	0.14338	3.050	3.050
150.0	.05540	1.026	1.294	610.0	.14499	3.085	3.086
160.0	.05799	1.092	1.365	620.0	.14660	3.121	3.121
170.0	.06052	1.157	1.427	630.0	.14820	3.156	3.156
180.0	.06299	1.220	1.482				
				640.0	.14980	3.191	3.191
190.0	.06541	1.282	1.530	650.0	.15138	3.226	3.226
200.0	.06777	1.342	1.574	660.0	.15296	3.261	3.261
210.0	.07010	1.401	1.614	670.0	.15453	3.296	3.296
220.0	.07239	1.458	1.651	680.0	.15608	3.331	3.331
230.0	.07464	1.514	1.687				
				690.0	.15765	3.366	3.366
240.0	.07686	1.569	1.723	700.0	.15920	3.401	3.401
250.0	.07904	1.622	1.758	720.0	.16228	3.470	3.471
260.0	.08119	1.674	1.793	740.0	.16532	3.540	3.540
270.0	.08332	1.725	1.828	760.0	.16836	3.609	3.610
280.0	.08541	1.774	1.863				
				780.0	.17137	3.678	3.679
290.0	.08748	1.823	1.899	800.0	.17433	3.747	3.748
300.0	.08953	1.870	1.935	820.0	.17730	3.817	3.818
310.0	.09156	1.917	1.972	840.0	.18023	3.886	3.887
320.0	.09356	1.962	2.010	860.0	.18314	3.955	3.956
330.0	.09554	2.007	2.047				
				880.0	.18604	4.025	4.026
340.0	.09749	2.051	2.085	900.0	.18891	4.095	4.096
350.0	.09944	2.095	2.123	920.0	.19175	4.165	4.165
360.0	.10137	2.137	2.161	940.0	.19459	4.235	4.236
370.0	.10326	2.179	2.199	960.0	.19740	4.305	4.306
380.0	.10516	2.220	2.237				
				980.0	.20019	4.376	4.376
390.0	.10703	2.261	2.275	1000.0	.20298	4.447	4.447
400.0	.10888	2.302	2.313	1050.0	.20984	4.623	4.623
410.0	.11073	2.342	2.352	1100.0	.21662	4.801	4.801
420.0	.11255	2.381	2.390	1150.0	.22331	4.980	4.981
430.0	.11436	2.420	2.428				
				1200.0	.22990	5.160	5.161
440.0	.11616	2.459	2.466	1250.0	.23641	5.341	5.343
450.0	.11795	2.498	2.504	1300.0	.24284	5.523	5.525
460.0	.11971	2.536	2.541	1350.0	.24921	5.707	5.708
470.0	.12148	2.575	2.578	1400.0	.25550	5.891	5.892
480.0	.12323	2.613	2.616				
				1450.0	.26172	6.075	6.076
490.0	.12497	2.650	2.653	1500.0	.26789	6.261	6.261
500.0	.12670	2.688	2.690	1550.0	.27398	6.445	6.441
510.0	.12841	2.725	2.726	1600.0	.28002	6.628	6.620
520.0	.13011	2.761	2.763	1650.0	.28601	6.812	6.800
530.0	.13181	2.798	2.799				
				1700.0	.29191	6.995	6.978
540.0	.13349	2.835	2.836	1750.0	.29781	7.178	7.158
550.0	.13516	2.871	2.872	1800.0	.30364	7.360	7.336
560.0	.13682	2.907	2.908	1850.0	.30939	7.541	7.514
570.0	.13848	2.943	2.944	1900.0	.31515	7.723	7.693
580.0	.14012	2.979	2.979				
				1950.0	.32085	7.903	7.871
590.0	.14175	3.014	3.015	2000.0	.32647	8.082	8.048

TABLE 7. *Viscosity of dissociating hydrogen, units 10^3g cm^{-1} s^{-1} presented as a function of the mole fraction of atomic hydrogen*

The asterisks at low temperatures indicate that the dissociation would occur at pressure less than 0.001 atm. The asterisks at high temperatures indicate that the atomic hydrogen could only be present at the particular mole fraction if the pressure were greater than 290 atm.

Temp (K)	Mole fraction										
	0.0	0.1	0.2	0.3	0.4	0.5	0.6	0.7	0.8	0.9	1.0
2000.0	0.32647	******	******	******	******	******	******	******	******	******	0.2528
2050.0	.33210	******	******	******	******	******	******	******	******	******	.2581
2100.0	.33766	******	******	******	******	******	******	******	******	******	.2633
2150.0	.34317	0.3447	******	******	******	******	******	******	******	******	.2687
2200.0	.34867	.3502	******	******	******	******	******	******	******	******	.2739
2250.0	.35412	.3559	0.3596	******	******	******	******	******	******	******	.2791
2300.0	.35952	.3615	.3647	******	******	******	******	******	******	******	.2844
2350.0	.36492	.3678	.3704	0.3713	******	******	******	******	******	******	.2896
2400.0	.37027	.3727	.3762	.3775	******	******	******	******	******	******	.2948
2450.0	.37557	.3781	.3819	.3834	0.3821	******	******	******	******	******	.2999
2500.0	.38086	.3837	.3887	.3893	.3883	0.3838	******	******	******	******	.3051
2550.0	.38611	.3891	.3933	.3952	.3943	.3903	0.3825	******	******	******	.3101
2600.0	.39132	.3961	.3990	.4010	.4003	.3964	.3889	******	******	******	.3151
2650.0	.39652	.3999	.4047	.4069	.4062	.4024	.3950	0.3836	******	******	.3202
2700.0	.40169	.4053	.4103	.4127	.4116	.4084	.4011	.3896	0.3735	******	.3253
2750.0	.40681	.4107	.4159	.4185	.4182	.4145	.4072	.3956	.3794	******	.3305
2800.0	.41193	.4160	.4225	.4243	.4241	.4203	.4132	.4016	.3853	******	.3357
2850.0	.41701	.4213	.4270	.4300	.4300	.4266	.4189	.4076	.3911	0.3691	.3409
2900.0	.42205	.4266	.4326	.4361	.4359	.4326	.4252	.4136	.3970	.3747	.3461
2950.0	.42709	.4318	.4380	.4417	.4418	.4386	.4314	.4195	.4029	.3803	.3513
3000.0	.43210	.4370	.4435	.4472	.4476	.4445	.4373	.4256	.4086	.3858	.3564
3050.0	.43704	.4423	.4490	.4529	.4533	.4506	.4435	.4317	.4147	.3916	.3619
3100.0	.44204	.4475	.4545	.4586	.4594	.4566	.4495	.4378	.4206	.3973	.3672
3150.0	.44698	.4526	.4599	.4642	.4653	.4620	.4555	.4437	.4264	.4029	.3723
3200.0	.45190	.4578	.4653	.4698	.4710	.4684	.4615	.4496	.4322	.4084	.3775
3250.0	.45680	.4629	.4707	.4755	.4769	.4744	.4671	.4556	.4380	.4140	.3826
3300.0	.46168	.4680	.4761	.4811	.4826	.4802	.4733	.4614	.4437	.4194	.3876
3350.0	.46653	.4731	.4814	.4866	.4883	.4861	.4792	.4671	.4494	.4248	.3925
3400.0	.47136	.4782	.4868	.4922	.4941	.4919	.4851	.4729	.4550	.4301	.3975
3450.0	.47617	.4832	.4920	.4977	.4997	.4976	.4908	.4787	.4605	.4353	.4022
3500.0	.48096	.4883	.4974	.5033	.5055	.5035	.4968	.4846	.4662	.4407	.4071
3550.0	.48572	.4933	.5026	.5087	.5111	.5092	.5025	.4902	.4716	.4458	.4118
3600.0	.49046	.4983	.5079	.5142	.5167	.5149	.5082	.4958	.4771	.4509	.4164
3650.0	.49517	.5032	.5131	.5196	.5223	.5206	.5139	.5014	.4825	.4560	.4210
3700.0	.49985	.5082	.5183	.5251	.5279	.5263	.5196	.5071	.4879	.4612	.4257
3750.0	.50451	.5131	.5235	.5305	.5335	.5320	.5253	.5127	.4933	.4662	.4303
3800.0	.50914	.5180	.5287	.5359	.5390	.5376	.5309	.5182	.4987	.4713	.4348
3850.0	.51367	.5229	.5339	.5413	.5446	.5433	.5366	.5238	.5041	.4764	.4394
3900.0	.51847	.5278	.5390	.5466	.5501	.5489	.5422	.5294	.5095	.4814	.4439
3950.0	.52310	.5327	.5442	.5520	.5557	.5545	.5479	.5350	.5148	.4864	.4485
4000.0	.52772	.5375	.5493	.5573	.5611	.5601	.5535	.5405	.5201	.4914	.4529
4050.0	.53231	.5424	.5545	.5627	.5667	.5658	.5591	.5461	.5255	.4965	.4575
4100.0	.53689	******	.5595	.5680	.5721	.5713	.5647	.5515	.5308	.5014	.4619
4150.0	.54145	******	.5646	.5733	.5776	.5769	.5703	.5570	.5361	.5064	.4664
4200.0	.54598	******	.5697	.5786	.5831	.5824	.5759	.5625	.5414	.5113	.4708
4250.0	.55050	******	.5748	.5839	.5886	.5880	.5815	.5681	.5467	.5163	.4753
4300.0	.55500	******	.5799	.5893	.5941	.5936	.5871	.5736	.5521	.5213	.4798
4350.0	.55947	******	.5848	.5945	.5994	.5991	.5926	.5790	.5573	.5262	.4842
4400.0	.56393	******	.5899	.5998	.6049	.6047	.5982	.5845	.5626	.5312	.4887
4450.0	.56836	******	.5948	.6049	.6103	.6101	.6036	.5899	.5678	.5360	.4930
4500.0	.57277	******	.5998	.6102	.6157	.6156	.6091	.5953	.5731	.5409	.4974
4550.0	.55715	******	.6049	.6155	.6211	.6212	.6147	.6009	.5784	.5459	.5019
4600.0	.58148	******	******	.6206	.6265	.6266	.6202	.6063	.5836	.5508	.5063
4650.0	.58598	******	******	.6258	.6318	.6321	.6257	.6117	.5888	.5557	.5107
4700.0	.59038	******	******	.6310	.6372	.6375	.6312	.6171	.5941	.5606	.5151
4750.0	.59476	******	******	.6362	.6426	.6431	.6367	.6226	.5994	.5656	.5195
4800.0	.59913	******	******	.6414	.6479	.6485	.6423	.6280	.6046	.5705	.5239
4850.0	.60348	******	******	.6465	.6533	.6540	.6477	.6334	.6098	.5754	.5283
4900.0	.60782	******	******	.6517	.6586	.6594	.6532	.6388	.6150	.5802	.5327
4950.0	.61215	******	******	******	.6640	.6649	.6587	.6443	.6203	.5852	.5371
5000.0	.61645	******	******	******	.6691	.6702	.6640	.6495	.6254	.5900	.5414

TABLE 8. *Thermal conductivity of dissociating hydrogen, units mW cm^{-1}s^{-1}, presented as a function of the mole fraction of atomic hydrogen*

The asterisks indicate that we would have to go beyond our chosen pressure range to compute the conductivity at the particular mole fractions. See the caption to table 7

Temp (K)	Mole fraction										
	0.0	0.1	0.2	0.3	0.4	0.5	0.6	0.7	0.8	0.9	1.0
2000.0	8.082	*******	*******	*******	*******	*******	*******	*******	*******	*******	8.702
2050.0	8.263	*******	*******	*******	*******	*******	*******	*******	*******	*******	8.424
2100.0	8.442	*******	*******	*******	*******	*******	*******	*******	*******	*******	8.375
2150.0	8.620	64.866	*******	*******	*******	*******	*******	*******	*******	*******	8.430
2200.0	8.798	61.665	*******	*******	*******	*******	*******	*******	*******	*******	8.538
2250.0	8.975	60.599	111.300	*******	*******	*******	*******	*******	*******	*******	8.671
2300.0	9.151	59.595	109.340	*******	*******	*******	*******	*******	*******	*******	8.817
2350.0	9.327	58.630	107.088	153.200	*******	*******	*******	*******	*******	*******	8.969
2400.0	9.502	57.906	105.150	150.211	*******	*******	*******	*******	*******	*******	9.124
2450.0	9.675	56.895	103.297	147.399	188.766	*******	*******	*******	*******	*******	9.281
2500.0	9.848	56.088	101.50	144.718	183.845	218.087	*******	*******	*******	*******	9.440
2550.0	10.021	55.319	99.874	142.139	180.425	211.857	232.876	*******	*******	*******	9.594
2600.0	10.192	54.57	98.208	139.78	177.171	207.991	228.088	*******	*******	*******	9.749
2650.0	10.362	53.910	96.662	137.907	174.075	204.296	223.953	226.918	*******	*******	9.906
2700.0	10.532	53.226	95.169	135.098	171.100	200.736	220.012	222.949	200.268	*******	10.064
2750.0	10.701	52.607	94.239	132.879	168.471	197.402	216.232	219.111	196.847	*******	10.223
2800.0	10.869	52.002	92.380	130.799	165.556	194.000	212.605	215.421	193.573	*******	10.383
2850.0	11.037	51.429	91.216	128.812	162.902	190.897	209.513	211.878	190.425	130.874	10.543
2900.0	11.204	50.886	89.884	126.900	160.385	187.878	205.868	208.469	187.392	128.884	10.704
2950.0	11.370	50.367	88.653	125.000	157.959	184.987	202.547	205.118	184.473	126.992	10.866
3000.0	11.536	49.872	87.516	123.328	155.804	182.186	199.443	202.026	181.663	125.158	11.026
3050.0	11.703	49.398	86.409	121.610	153.400	179.485	196.447	198.989	178.933	123.400	11.192
3100.0	11.867	48.949	85.356	119.944	151.516	176.898	193.570	196.065	176.369	121.710	11.355
3150.0	12.032	48.518	84.337	118.378	149.189	174.400	190.786	193.239	173.838	120.077	11.517
3200.0	12.196	48.106	83.358	116.851	147.115	172.218	188.100	190.506	171.409	118-500	11.676
3250.0	12.361	47.715	82.418	115.392	145.177	169.623	185.935	187.874	169.079	116.991	11.833
3300.0	12.525	47.340	81.513	113.979	143.315	167.377	183.089	185.329	166.813	115.518	11.988
3350.0	12.689	46.983	80.641	112.619	141.502	165.219	180.589	182.818	164.625	114.109	12.142
3400.0	12.854	46.616	79.754	111.235	139.670	163.004	178.132	180.309	162.402	112.671	12.293
3450.0	13.018	46.312	78.989	110.029	138.064	161.064	175.987	178.182	160.454	111.411	12.443
3500.0	13.182	46.000	78.209	108.803	136.434	159.101	173.796	175.954	158.449	110.131	12.591
3550.0	13.346	45.701	77.457	107.817	134.854	157.193	171.675	173.790	156.568	108.891	12.735
3600.0	13.510	45.416	76.734	106.472	133.328	155.353	169.626	171.702	154.705	107.692	12.879
3650.0	13.674	45.143	76.033	105.363	131.846	153.564	167.632	169.674	152.891	106.530	13.023
3700.0	13.839	44.882	75.357	104.291	130.414	151.833	165.706	167.709	151.147	105.417	13.165
3750.0	14.003	44.634	74.706	103.256	129.029	150.158	163.839	165.809	149.464	104.325	13.307
3800.0	14.168	44.397	74.079	102.256	127.689	148.536	162.032	163.968	147.826	103.264	13.449
3850.0	14.330	44.171	73.471	101.284	126.386	146.959	160.273	162.175	146.234	102.252	13.590
3900.0	14.501	43.954	72.885	100.345	125.124	145.430	158.568	160.437	144.690	101.263	13.731
3950.0	16.672	43.747	72.318	99.435	123.901	143.948	156.914	158.752	143.193	100.303	13.871
4000.0	14.836	43.551	71.773	98.555	122.718	142.512	155.310	157.117	141.742	99.373	14.010
4050.0	14.998	43.364	71.244	97.701	121.567	141.115	153.751	155.527	140.329	98.471	14.149
4100.0	15.172	*******	70.733	96.872	120.451	139.758	152.235	153.981	138.958	97.596	14.288
4150.0	15.340	*******	70.242	96.072	119.370	138.445	150.767	152.484	137.629	96.749	14.426
4200.0	15.508	*******	69.765	95.294	118.317	137.165	149.336	151.024	136.334	95.924	14.564
4250.0	15.676	*******	69.301	94.536	117.290	135.915	147.938	149.598	135.069	95.120	14.702
4300.0	15.843	*******	68.854	93.800	116.293	134.701	146.578	148.210	133.839	94.340	14.839
4350.0	16.011	*******	68.420	93.085	115.321	133.516	145.253	146.858	132.639	93.580	14.976
4400.0	16.177	*******	68.002	92.394	114.380	132.368	143.967	145.545	131.476	92.843	15.113
4450.0	16.343	*******	67.595	91.720	113.462	131.246	142.711	144.262	130.339	92.125	15.250
4500.0	16.509	*******	67.203	91.065	112.569	130.155	141.488	143.014	129.232	91.426	15.387
4550.0	16.672	*******	66.823	90.429	111.699	129.091	140.294	141.794	128.152	90.745	15.522
4600.0	16.834	*******	*******	89.815	110.855	128.058	139.135	140.610	127.103	90.086	15.661
4650.0	16.999	*******	*******	89.212	110.031	127.048	138.001	139.452	126.077	89.442	15.797
4700.0	17.160	*******	*******	88.630	109.231	126.066	136.898	138.324	125.079	88.816	15.933
4750.0	17.318	*******	*******	88.065	108.453	125.111	135.824	137.227	124.107	88.207	16.069
4800.0	17.475	*******	*******	87.519	107.698	124.182	134.780	136.159	123.161	87.616	16.205
4850.0	17.628	*******	*******	86.987	106.962	123.275	133.758	135.114	122.236	87.039	16.340
4900.0	17.777	*******	*******	86.471	106.245	122.392	132.764	134.096	121.335	86.477	16.475
4950.0	17.923	*******	*******	*******	105.551	121.534	131.797	133.106	120.459	85.932	16.610
5000.0	18.064	*******	*******	*******	104.877	120.700	130.856	132.142	119.606	85.404	16.747

TABLE 9. *The mole fraction of atomic hydrogen presented as a function of temperature and pressure*

Note: Since the reference dissociation constant is given with pressure units of atmospheres we use atmospheres here. To convert pressure to the S. I. system the following conversion is required:

1 atm. = 0.101325 MN/m^2.

Temp (K)	Pressure (atm)									
	0.001	0.002	0.003	0.004	0.005	0.006	0.007	0.008	0.009	0.010
2000.0	0.050	0.036	0.029	0.025	0.023	0.021	0.019	0.018	0.017	0.016
2050.0	.069	.049	.041	.035	.032	.029	.027	.025	.024	.022
2100.0	.094	.067	.055	.048	.043	.039	.037	.034	.032	.031
2150.0	.125	.090	.074	.064	.058	.053	.049	.046	.043	.041
2200.0	.163	.118	.098	.085	.076	.070	.065	.061	.058	.055
2250.0	.209	.153	.127	.111	.100	.091	.085	.080	.075	.072
2300.0	.263	.194	.162	.142	.128	.117	.109	.102	.097	.092
2350.0	.324	.243	.203	.179	.161	.148	.138	.130	.123	.117
2400.0	.392	.298	.251	.222	.201	.185	.173	.163	.154	.147
2450.0	.465	.359	.305	.271	.246	.228	.213	.201	.190	.182
2500.0	.539	.426	.365	.326	.298	.276	.258	.244	.232	.222
2550.0	.613	.495	.430	.386	.354	.329	.310	.293	.279	.267
2600.0	.683	.565	.497	.450	.415	.387	.365	.347	.331	.317
2650.0	.746	.634	.564	.515	.478	.449	.425	.404	.387	.371
2700.0	.801	.698	.630	.581	.543	.512	.486	.464	.446	.429
2750.0	.847	.756	.692	.644	.606	.575	.549	.526	.506	.489
2800.0	.883	.806	.748	.704	.667	.636	.610	.587	.567	.549
2850.0	.912	.848	.798	.757	.723	.694	.669	.646	.626	.608
2900.0	.934	.882	.840	.804	.773	.747	.723	.702	.682	.665
2950.0	.950	.909	.874	.844	.817	.793	.771	.752	.734	.718
3000.0	.963	.930	.902	.877	.854	.833	.814	.796	.780	.765
3050.0	.972	.947	.924	.903	.884	.866	.850	.835	.820	.807
3100.0	.979	.959	.941	.924	.909	.894	.880	.867	.855	.843
3150.0	.984	.969	.954	.941	.928	.916	.905	.894	.883	.873
3200.0	.988	.976	.965	.954	.944	.934	.924	.915	.906	.898
3250.0	.990	.981	.972	.964	.956	.948	.940	.933	.925	.918
3300.0	.993	.985	.978	.972	.965	.959	.952	.946	.940	.935
3350.0	.994	.989	.983	.978	.972	.967	.962	.957	.952	.948
3400.0	.995	.989	.984	.979	.974	.970	.965	.960	.956	.951
3450.0	.996	.993	.989	.986	.983	.979	.976	.973	.969	.966

TABLE 9. *The mole fraction of atomic hydrogen presented as a function of temperature and pressure*—Continued

Note: Since the reference dissociation constant is given with pressure units of atmospheres we use atmospheres here. To convert pressure to the S. I. system the following conversion is required:

1 atm. = 0.101325 MN/m^2.

Temp (K)	Pressure (atm)									
	0.010	0.020	0.030	0.040	0.050	0.060	0.070	0.080	0.090	0.100
2250.0	0.072	0.051	0.042	0.036	0.033	0.030	0.028	0.026	0.024	0.023
2300.0	.092	.066	.054	.047	.042	.039	.036	.034	.032	.030
2350.0	.117	.084	.069	.060	.054	.050	.046	.043	.041	.039
2400.0	.147	.106	.088	.076	.069	.063	.058	.055	.052	.049
2450.0	.182	.132	.109	.095	.086	.079	.073	.069	.065	.062
2500.0	.222	.163	.135	.118	.106	.097	.091	.085	.080	.076
2550.0	.267	.197	.164	.144	.130	.119	.111	.104	.099	.094
2600.0	.317	.237	.198	.174	.157	.145	.135	.127	.120	.114
2650.0	.371	.281	.236	.208	.189	.174	.162	.152	.144	.138
2700.0	.429	.329	.278	.246	.224	.206	.193	.182	.172	.164
2750.0	.489	.380	.324	.288	.263	.243	.227	.214	.203	.194
2800.0	.549	.435	.374	.334	.305	.283	.265	.250	.238	.227
2850.0	.608	.481	.425	.382	.350	.326	.306	.290	.276	.264
2900.0	.665	.547	.479	.433	.398	.372	.350	.332	.316	.303
2950.0	.718	.602	.533	.485	.448	.420	.396	.377	.360	.345
3000.0	.765	.655	.586	.537	.499	.469	.444	.424	.406	.390
3050.0	.807	.705	.638	.589	.551	.520	.494	.472	.453	.436
3100.0	.843	.751	.687	.639	.601	.570	.543	.521	.501	.483
3150.0	.873	.791	.732	.686	.649	.618	.592	.569	.549	.531
3200.0	.898	.827	.773	.730	.694	.664	.638	.616	.595	.577
3250.0	.918	.857	.809	.770	.737	.708	.683	.661	.641	.623
3300.0	.935	.883	.841	.806	.775	.748	.725	.704	.684	.667
3350.0	.948	.905	.868	.837	.809	.785	.763	.743	.725	.708
3400.0	.951	.911	.876	.846	.819	.796	.774	.755	.737	.721
3450.0	.966	.937	.910	.887	.865	.845	.827	.810	.795	.780
3500.0	.973	.948	.926	.906	.887	.870	.854	.839	.825	.811
3550.0	.978	.958	.939	.922	.906	.891	.877	.863	.851	.839
3600.0	.982	.966	.950	.935	.922	.909	.896	.885	.873	.863
3650.0	.986	.972	.959	.947	.935	.924	.913	.903	.893	.883
3700.0	.988	.977	.966	.956	.946	.936	.927	.918	.910	.901
3750.0	.990	.981	.972	.963	.955	.947	.939	.931	.924	.917
3800.0	.992	.984	.977	.969	.962	.955	.949	.942	.936	.929
3850.0	.993	.987	.981	.974	.968	.962	.957	.951	.946	.940
3900.0	.994	.989	.984	.979	.973	.968	.964	.959	.954	.949
3950.0	.995	.991	.986	.982	.978	.973	.969	.965	.961	.957
4000.0	.996	.992	.988	.985	.981	.977	.974	.970	.967	.964

TABLE 9. *The mole fraction of atomic hydrogen presented as a function of temperature and pressure*—Continued

Note: Since the reference dissociation constant is given with pressure units of atmospheres we use atmospheres here. To convert pressure to the S. I. system the following conversion is required:

1 atm. = 0.101325 MN/m^2.

Temp (K)	Pressure (atm)									
	0.100	0.200	0.300	0.400	0.500	0.600	0.700	0.800	0.900	1.000
2500.0	0.076	0.055	0.045	0.039	0.035	0.032	0.030	0.028	0.026	0.025
2550.0	.094	.067	.055	.048	.043	.039	.037	.034	.032	.031
2600.0	.114	.082	.068	.059	.053	.048	.045	.042	.040	.038
2650.0	.138	.099	.082	.071	.064	.059	.054	.051	.048	.046
2700.0	.164	.119	.098	.086	.077	.071	.066	.061	.058	.055
2750.0	.194	.142	.117	.102	.092	.084	.078	.074	.070	.066
2800.0	.227	.167	.139	.121	.109	.100	.093	.087	.083	.078
2850.0	.264	.195	.162	.142	.128	.118	.110	.103	.097	.093
2900.0	.303	.226	.189	.166	.150	.138	.128	.120	.114	.108
2950.0	.345	.260	.218	.192	.174	.160	.149	.140	.133	.126
3000.0	.390	.296	.250	.220	.200	.184	.172	.162	.153	.146
3050.0	.436	.335	.284	.251	.228	.211	.197	.185	.176	.168
3100.0	.483	.376	.320	.284	.259	.239	.224	.211	.200	.191
3150.0	.531	.418	.358	.320	.292	.270	.253	.239	.227	.217
3200.0	.577	.461	.398	.356	.326	.303	.284	.269	.255	.244
3250.0	.623	.505	.439	.395	.363	.337	.317	.300	.286	.274
3300.0	.667	.549	.481	.435	.400	.373	.352	.334	.318	.305
3350.0	.708	.592	.523	.475	.439	.411	.387	.368	.352	.337
3400.0	.721	.606	.536	.488	.452	.423	.399	.380	.363	.348
3450.0	.780	.673	.604	.555	.517	.487	.462	.440	.422	.406
3500.0	.811	.711	.644	.595	.556	.525	.499	.477	.458	.441
3550.0	.839	.745	.681	.633	.595	.563	.537	.514	.495	.477
3600.0	.863	.777	.716	.669	.632	.601	.574	.551	.531	.514
3650.0	.883	.806	.749	.704	.667	.637	.611	.588	.567	.549
3700.0	.901	.832	.779	.736	.701	.671	.646	.623	.603	.585
3750.0	.917	.855	.806	.766	.733	.704	.679	.657	.637	.619
3800.0	.929	.875	.831	.794	.762	.735	.711	.689	.670	.652
3850.0	.940	.892	.853	.819	.789	.764	.741	.720	.701	.684
3900.0	.949	.908	.872	.842	.814	.790	.768	.748	.730	.714
3950.0	.957	.921	.889	.861	.836	.814	.794	.775	.758	.742
4000.0	.964	.932	.904	.879	.856	.836	.817	.799	.783	.768
4050.0	.969	.941	.917	.894	.874	.855	.838	.822	.807	.792
4100.0	.974	.950	.928	.908	.890	.872	.857	.842	.828	.815
4150.0	.977	.957	.937	.920	.903	.888	.873	.860	.847	.835
4200.0	.981	.963	.946	.930	.915	.902	.888	.876	.864	.853
4250.0	.983	.968	.953	.939	.926	.914	.902	.890	.880	.869
4300.0	.986	.972	.959	.947	.935	.924	.913	.903	.894	.884
4350.0	.988	.976	.964	.954	.943	.933	.924	.915	.906	.897
4400.0	.989	.979	.969	.959	.950	.941	.933	.925	.917	.909
4450.0	.991	.982	.973	.964	.956	.948	.941	.933	.926	.919
4500.0	.992	.984	.976	.969	.962	.955	.948	.941	.935	.928
4550.0	.993	.986	.979	.973	.966	.960	.954	.948	.942	.936
4600.0	.994	.988	.982	.976	.970	.965	.959	.954	.949	.944
4650.0	.994	.989	.984	.979	.974	.969	.964	.959	.954	.950
4700.0	.995	.990	.986	.981	.977	.972	.968	.964	.959	.955
4750.0	.996	.992	.987	.983	.979	.975	.971	.968	.964	.960
4800.0	.996	.992	.989	.985	.982	.978	.975	.971	.968	.964

TABLE 9. *The mole fraction of atomic hydrogen presented as a function of temperature and pressure*—Continued

Note: Since the reference dissociation constant is given with pressure units of atmospheres we use atmospheres here. To convert pressure to the S. I. system the following conversion is required:

1 atm. = 0.101325 MN/m^2.

Temp (K)	Pressure (atm)									
	1.000	2.000	3.000	4.000	5.000	6.000	7.000	8.000	9.000	10.000
2800.0	0.078	0.056	0.046	0.040	0.036	0.033	0.030	0.028	0.027	0.026
2850.0	.093	.066	.055	.047	.043	.039	.036	.034	.032	.030
2900.0	.108	.078	.064	.056	.050	.046	.042	.040	.038	.036
2950.0	.126	.091	.075	.065	.059	.054	.050	.047	.044	.042
3000.0	.146	.106	.087	.076	.068	.062	.058	.054	.051	.049
3050.0	.168	.122	.101	.088	.079	.072	.067	.063	.059	.056
3100.0	.191	.139	.115	.101	.091	.083	.077	.072	.068	.065
3150.0	.217	.159	.132	.115	.104	.095	.088	.083	.078	.075
3200.0	.244	.180	.150	.131	.118	.108	.101	.094	.089	.085
3250.0	.274	.203	.169	.148	.134	.123	.114	.107	.101	.097
3300.0	.305	.227	.190	.167	.151	.138	.129	.121	.115	.109
3350.0	.337	.253	.212	.187	.169	.155	.145	.136	.129	.123
3400.0	.348	.262	.220	.194	.175	.161	.150	.141	.134	.127
3450.0	.406	.309	.261	.231	.209	.193	.180	.170	.161	.153
3500.0	.441	.339	.288	.255	.232	.214	.200	.188	.178	.170
3550.0	.477	.371	.315	.280	.255	.236	.220	.208	.197	.188
3600.0	.514	.402	.344	.307	.279	.259	.242	.229	.217	.207
3650.0	.549	.435	.374	.334	.305	.283	.265	.251	.238	.227
3700.0	.585	.468	.404	.362	.332	.308	.289	.273	.260	.249
3750.0	.619	.501	.435	.391	.359	.334	.314	.297	.283	.271
3800.0	.652	.534	.466	.421	.387	.361	.340	.322	.307	.294
3850.0	.684	.566	.498	.451	.416	.388	.366	.347	.332	.318
3900.0	.714	.598	.529	.481	.445	.416	.393	.374	.357	.342
3950.0	.742	.629	.560	.511	.474	.445	.420	.400	.383	.367
4000.0	.768	.659	.590	.541	.503	.473	.448	.427	.409	.393
4050.0	.792	.686	.620	.570	.532	.501	.476	.454	.436	.419
4100.0	.815	.715	.648	.599	.561	.530	.504	.482	.462	.446
4150.0	.835	.740	.676	.627	.589	.558	.531	.509	.489	.472
4200.0	.853	.764	.702	.654	.616	.585	.559	.536	.516	.498
4250.0	.869	.786	.727	.680	.643	.612	.586	.563	.543	.525
4300.0	.884	.807	.750	.705	.669	.638	.612	.589	.569	.551
4350.0	.897	.826	.772	.729	.693	.663	.637	.614	.594	.576
4400.0	.909	.843	.792	.751	.717	.687	.662	.639	.619	.601
4450.0	.919	.859	.811	.772	.739	.710	.686	.663	.644	.626
4500.0	.928	.873	.829	.792	.760	.732	.708	.687	.667	.649
4550.0	.936	.886	.845	.810	.780	.753	.730	.709	.690	.672
4600.0	.944	.898	.859	.827	.798	.773	.750	.730	.711	.694
4650.0	.950	.908	.873	.842	.815	.791	.769	.750	.732	.715
4700.0	.955	.918	.885	.856	.831	.808	.788	.769	.751	.735
4750.0	.960	.926	.896	.869	.846	.824	.804	.786	.770	.754
4800.0	.964	.933	.906	.881	.859	.839	.820	.803	.787	.772
4850.0	.968	.940	.915	.892	.871	.852	.835	.819	.803	.789
4900.0	.972	.946	.923	.902	.883	.865	.848	.833	.819	.805
4950.0	.975	.951	.930	.911	.893	.877	.861	.846	.833	.820
5000.0	.977	.956	.937	.919	.903	.887	.873	.859	.846	.834

TABLE 9. *The mole fraction of atomic hydrogen presented as a function of temperature and pressure*—Continued

Note: Since the reference dissociation constant is given with pressure units of atmospheres we use atmospheres here. To convert pressure to the S. I. system the following conversion is required:

1 atm. = 0.101325 MN/m^2.

Temp (K)	Pressure (atm)									
	10.000	20.000	30.000	40.000	50.000	60.000	70.000	80.000	90.000	100.000
3200.0	0.085	0.061	0.050	0.043	0.039	0.036	0.033	0.031	0.029	0.028
3250.0	.097	.069	.057	.049	.044	.041	.038	.035	.033	.032
3300.0	.109	.078	.065	.056	.050	.046	.043	.040	.038	.036
3350.0	.123	.088	.073	.063	.057	.052	.048	.045	.043	.041
3400.0	.127	.092	.076	.066	.059	.054	.050	.047	.044	.042
3450.0	.153	.111	.092	.080	.072	.066	.061	.057	.054	.051
3500.0	.170	.124	.102	.089	.080	.073	.068	.064	.060	.057
3550.0	.188	.137	.114	.099	.089	.082	.076	.071	.067	.064
3600.0	.207	.152	.126	.110	.099	.091	.084	.079	.075	.071
3650.0	.227	.167	.139	.121	.109	.100	.093	.087	.083	.079
3700.0	.249	.201	.153	.134	.120	.110	.103	.096	.091	.087
3750.0	.271	.261	.167	.147	.132	.121	.113	.106	.100	.095
3800.0	.294	.219	.183	.160	.145	.133	.124	.116	.110	.105
3850.0	.318	.238	.199	.175	.158	.145	.135	.127	.120	.114
3900.0	.342	.257	.216	.190	.172	.158	.147	.139	.131	.125
3950.0	.367	.278	.234	.206	.186	.172	.160	.151	.143	.136
4000.0	.393	.299	.252	.223	.202	.186	.173	.163	.155	.147
4050.0	.419	.321	.271	.240	.218	.201	.187	.176	.167	.159
4100.0	.446	.343	.291	.258	.234	.216	.202	.190	.181	.172
4150.0	.472	.366	.311	.276	.251	.232	.217	.205	.194	.185
4200.0	.498	.389	.332	.295	.269	.249	.233	.220	.209	.199
4250.0	.525	.412	.353	.315	.287	.266	.249	.235	.224	.213
4300.0	.551	.436	.375	.335	.306	.284	.266	.251	.239	.228
4350.0	.576	.460	.397	.355	.325	.302	.283	.268	.255	.243
4400.0	.601	.484	.419	.376	.345	.320	.301	.285	.271	.259
4450.0	.626	.508	.441	.397	.365	.339	.319	.302	.288	.275
4500.0	.649	.531	.464	.418	.385	.359	.337	.320	.305	.292
4550.0	.672	.554	.486	.440	.405	.378	.356	.338	.322	.309
4600.0	.694	.577	.508	.461	.426	.398	.375	.356	.340	.326
4650.0	.715	.600	.530	.482	.446	.418	.394	.375	.358	.344
4700.0	.735	.622	.552	.504	.467	.438	.414	.394	.376	.361
4750.0	.754	.643	.574	.525	.487	.458	.433	.412	.395	.379
4800.0	.772	.664	.595	.546	.508	.478	.453	.431	.413	.397
4850.0	.789	.684	.615	.566	.528	.497	.472	.451	.432	.416
4900.0	.805	.703	.636	.586	.548	.517	.491	.470	.451	.434
4950.0	.820	.721	.655	.606	.568	.537	.511	.489	.469	.452
5000.0	.834	.739	.674	.626	.587	.556	.530	.507	.488	.471

TABLE 9. *The mole fraction of atomic hydrogen presented as a function of temperature and pressure*—Continued

Note: Since the reference dissociation constant is given with pressure units of atmospheres we use atmospheres here. To convert pressure to the S. I. system the following conversion is required:

1 atm. = 0.101325 MN/m^2.

Temp (K)	Pressure (atm)									
	100.000	110.000	120.000	130.000	140.000	150.000	160.000	170.000	180.000	190.000
3750.0	0.095	0.091	0.087	0.084	0.081	0.079	0.076	0.074	0.072	0.070
3800.0	.105	.100	.096	.092	.089	.086	.084	.081	.079	.077
3850.0	.114	.109	.105	.101	.098	.095	.092	.089	.087	.084
3900.0	.125	.119	.115	.110	.107	.103	.100	.097	.095	.092
3950.0	.136	.130	.125	.120	.116	.112	.109	.106	.103	.101
4000.0	.147	.141	.135	.131	.126	.122	.118	.115	.112	.109
4050.0	.159	.153	.147	.141	.137	.132	.128	.125	.122	.118
4100.0	.172	.165	.158	.153	.148	.143	.139	.135	.131	.128
4150.0	.185	.178	.171	.165	.159	.154	.150	.146	.142	.138
4200.0	.199	.191	.184	.177	.171	.166	.161	.157	.153	.149
4250.0	.213	.205	.197	.190	.184	.178	.173	.168	.164	.160
4300.0	.228	.219	.211	.203	.197	.191	.185	.180	.176	.172
4350.0	.243	.234	.225	.217	.210	.204	.198	.193	.188	.184
4400.0	.259	.249	.240	.232	.224	.217	.211	.206	.201	.196
4450.0	.275	.264	.255	.246	.239	.232	.225	.219	.214	.209
4500.0	.292	.281	.270	.261	.253	.246	.239	.233	.227	.222
4550.0	.309	.297	.286	.277	.268	.261	.254	.247	.241	.236
4600.0	.326	.314	.303	.293	.284	.276	.268	.262	.255	.250
4650.0	.344	.331	.319	.309	.300	.291	.284	.277	.270	.264
4700.0	.361	.348	.336	.326	.316	.307	.299	.292	.285	.279
4750.0	.379	.366	.353	.342	.332	.323	.315	.307	.300	.293
4800.0	.397	.383	.371	.359	.349	.340	.331	.323	.316	.309
4850.0	.416	.401	.388	.376	.366	.356	.347	.339	.331	.324
4900.0	.434	.419	.406	.394	.383	.373	.364	.355	.347	.340
4950.0	.452	.437	.423	.411	.400	.390	.380	.372	.363	.356
5000.0	.471	.455	.441	.429	.417	.407	.397	.388	.380	.372

TABLE 9. *The mole fraction of atomic hydrogen presented as a function of temperature and pressure*—Continued

Note: Since the reference dissociation constant is given with pressure units of atmospheres we use atmospheres here. To convert pressure to the S. I. system the following conversion is required:

1 atm. = 0.101325 MN/m^2.

Temp (K)	Pressure (atm)									
	200.000	210.000	220.000	230.000	240.000	250.000	260.000	270.000	280.000	290.000
3900.0	0.090	0.088	0.086	0.084	0.083	0.081	0.079	0.078	0.077	0.075
3950.0	.098	.096	.094	.092	.090	.088	.087	.085	.084	.082
4000.0	.107	.104	.102	.100	.098	.096	.094	.093	.091	.089
4050.0	.116	.113	.111	.108	.106	.104	.102	.100	.099	.097
4100.0	.125	.122	.120	.117	.115	.113	.111	.109	.107	.105
4150.0	.135	.132	.129	.127	.124	.122	.120	.117	.115	.114
4200.0	.145	.142	.139	.136	.134	.131	.129	.127	.124	.122
4250.0	.156	.153	.150	.147	.144	.141	.139	.136	.134	.132
4300.0	.168	.164	.160	.157	.154	.151	.149	.146	.144	.141
4350.0	.179	.175	.172	.168	.165	.162	.159	.156	.154	.151
4400.0	.191	.187	.183	.180	.176	.173	.170	.167	.164	.162
4450.0	.204	.200	.196	.192	.188	.185	.181	.178	.176	.173
4500.0	.217	.212	.208	.204	.200	.197	.193	.190	.187	.184
4550.0	.230	.226	.221	.217	.213	.209	.205	.202	.199	.196
4600.0	.244	.239	.234	.230	.226	.222	.218	.214	.211	.208
4650.0	.258	.253	.248	.243	.239	.235	.231	.227	.223	.220
4700.0	.273	.267	.262	.257	.252	.248	.244	.240	.236	.233
4750.0	.287	.282	.276	.271	.266	.262	.257	.253	.249	.245
4800.0	.302	.296	.291	.285	.280	.276	.271	.267	.263	.259
4850.0	.318	.311	.305	.300	.295	.290	.285	.281	.276	.272
4900.0	.333	.327	.320	.315	.309	.304	.299	.295	.290	.286
4950.0	.349	.342	.336	.330	.324	.319	.314	.309	.305	.300
5000.0	.364	.358	.351	.345	.339	.334	.329	.324	.319	.314

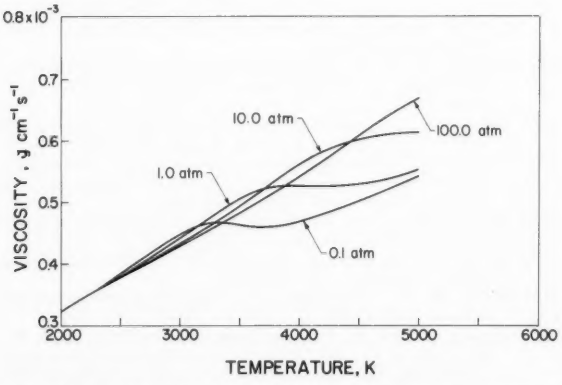

FIGURE 7. *The viscosity of dissociating hydrogen at various pressures.*

We place an error bar on the values tabulated of ±3 percent up to 2000 K for viscosity and 4 percent for thermal conductivity, and ±10 percent on both coefficients for the dissociating mixture.

7. Conclusion

We have correlated the viscosity and thermal conductivity coefficients of normal and para hydrogen. We hope we have reduced the considerable uncertainties and variations in data which existed in the literature until recently but clearly the situation is not very satisfactory. However, the state of the art is such that experimental measurements could be produced which would be superior to those available, both in extended temperature range and in accuracy.

This work was supported by the Office of Standard Reference Data. In addition, R. D. McCarty was partially supported by the National Aeronautics and Space Administration (SNPO–C), Contract No. R–45.

We are very grateful to D. E. Diller and H. M. Roder, NBS–Cryogenics Division, for valuable discussions and for allowing us to use their data prior to publication. We also acknowledge the help given us by reading the relevant publications of E. A. Mason of Brown University and of R. Brokaw at NASA Lewis Research Center.

8. References and Notes

[1] Hirschfelder, J. O., Curtiss, C. F. and Bird, R. B., Molecular Theory of Gases and Liquids (John Wiley & Sons, New York, N.Y., 1964).

[2] Mason, E. A., Prediction of Transport Properties of Dilute Gases, pp. 21–30, Proc. 4th Symposium on Thermophy, Prop. (ASME, New York, 1968).

[3] Mason, E. A. and Monchick, L., Heat conductivity of polyatomic and polar gases, J. Chem. Phys. **36**, 1622–1639 (1962).

[4] Vanderslice, J. T., Weissman, S., Mason, E. A., and Fallon, R. J., High-temperature transport properties of dissociating hydrogen, Phys. Fluids **5**, 155–164 (1962).

[5] Woolley, H. W., Scott, R. B. and Brickwedde, F. G., Compilation of thermal properties of hydrogen in its various isotopic

and ortho-para modifications, J. Res. NBS **41,** 379–475 (1948) RP 1932.

[6] Grier, N. T., Calculation of Transport Properties and Heat Transfer Parameters of Dissociating Hydrogen, NASA Tech Note D–1406 (Oct. 1962).

[7] Note that the pressure enters into the dilute gas formulas which are supposedly pressure independent. Of course, the pressure enters only into the dissociation part, but one might question the validity of equation (6) when applied to dissociation at high pressures. However, we would estimate [Childs, G. E. and Hanley, H. J. M., Applicability of Dilute Gas Transport Property Tables to Real Gases, Cryogenics **8,** 94–97 (1968)] that the dilute gas equation (1) would be applicable to pressures of at least 100 atmospheres at temperatures when dissociation becomes important.

[8] This assumption appears to be justified. See A. Farkas, Light and Heavy Hydrogen (Cambridge University Press, Cambridge, 1935).

[9] Knaap, H. F. P., Hermans, L. J. F., Jonkman, R. M. and Beenakker, J. J. M., Interactions between the hydrogen isotopes and their ortho and para modifications, Discussions Faraday Soc. No. **40,** 135–139 (1965).

[10] Becker, E. W. and Stehl, O., Viscosity difference between ortho and para hydrogen at low temperatures, Z. Physik **133,** 615–628 (1952).

[11] See, for example, Wang Chang, C. S. and Uhlenbeck, G. E., Transport Phenomena in Polyatomic Gases, Univ. of Mich. Eng. Rept. No. CM–681 (1951).

[12] Sandler, S. I., Thermal conductivity of polyatomic gases, Phys. Fluids **11,** 2549–2555 (1968).

[13] Brokaw, R. S., Thermal conductivity of gas mixtures in chemical equilibrium II, J. Chem. Phys. **32,** 1005–1006 (1960).

[14] Hirschfelder, J. O., Heat transfer in chemically reacting mixtures, J. Chem. Phys. **26,** 274–281 (1957).

[15] Hanley, H. J. M. and Klein, Max, On the selection of the intermolecular potential function: application of statistical mechanical theory to experiment, Nat. Bur. Stand. (U.S.), Tech. Note 360, 85 pages (Nov. 1967).

[16] This range may have to be modified for quantum gases. Our conclusions were based on three parameter potential function families (e.g., the exp: 6 family with α, σ, and ϵ). For quantum gases another parameter is required. This extra parameter (although it is not independent) might introduce extra sensitivity, that is, decrease the insensitive range, particularly at the lower end.

[17] Munn, R. J., Smith, F. J., Mason, E. A., and Monchick, L., Transport Collision Integrals for Quantum Gases Obeying a 12–6 Potential, J. Chem. Phys. **42,** 537–539 (1965).

[18] Klein, Max and Smith, F. J., Tables of collision integrals for the $(m, 6)$ potential function for ten values of m, Nat. Bur. Stand. (U.S.), **72A** (Phys. and Chem.), No. 4, 359–423 (July–Aug. 1968).

[19] Hanley, H. J. M., Comparison of the Lennard-Jones, exp-6 and Kihara potential functions from viscosity data of dilute argon, J. Chem. Phys. **44,** 4219–4222 (1966).

[20] Sutherland, B. P. and Maass, O., Measurement of the viscosity of gases over a large temperature range, Can. J. Res. **6,** 428–443 (1932).

[21] Van Itterbeek, A. and Keesom, W. H., Measurements of the viscosity of oxygen gas at liquid oxygen temperatures, Physica **2,** 97–103 (1935).

[22] Van Itterbeek, A., and Van Paemel, O., Measurements of the viscosity of gases for low pressures at room temperature and at low temperatures, Physica **7,** 273–283 (1940).

[23] Van Itterbeek, A. and Claes, A., Viscosity of hydrogen and deuterium gas between 293 degrees and 14 degrees K, Physica **5,** 938–944 (1938).

[24] Johnston, H. L. and McCloskey, K. E., Viscosities of several common gases between 90 K and room temperature, J. Phys. Chem. **44,** 1038–1058 (1940).

[25] Van Itterbeek, A., and Van Paemel, O., Measurements on the viscosity of neon, hydrogen, deuterium and helium as a function of the temperature between room temperature and liquid hydrogen temperatures, Physica **7,** 265–272 (1940).

[26] Wobser R., and Muller, Fr., The viscosity of gas vapors and their measurements in a Hoppler viscosimeter, Kolloid-Beih. **52,** 165–276 (1941).

[27] Rietveld, A. O., and Van Itterbeek, A., Viscosity of mixtures of H_2 and HD between 300 K and 14 K, Physica **23,** 838–842 (1957).

[28] Kestin, J., and Leidenfrost, W., An absolute determination of the viscosity of eleven gases over a range of pressures, Physica **25,** 1033–1062 (1959).

[29] Kestin, J. and Nagashima, A., The viscosity of the isotopes of hydrogen and their intermolecular force potentials, Phys. Fluids **7,** 730–734 (1964).

[30] Barua, A. K., Afzal, M., Flynn, G. P., and Ross, J., Viscosity of hydrogen, deuterium, methane and carbon monoxide from −50° C up to 150° C below 200 atmospheres, J. Chem. Phys. **41,** 374–378 (1964).

[31] Gracki, J. A., Flynn, G. P., and Ross, J., Viscosity of nitrogen, helium, hydrogen and argon from −100° C to 25° C up to 150–250 atmospheres, to be published.

[32] Guevara, F. A., McInteer, B. B., and Wageman, W. E., High temperature viscosity ratios for hydrogen, helium, argon and nitrogen, to be published.

[33] Hanley, H. J. M., and Childs, G. E., Discrepancies between viscosity data for simple gases, Science **159,** 1114–1117 (1968)..

[34] Golubev, I. F., Kalsina, M. V., Thermal conductivity of nitrogen and hydrogen at temperatures from 20 to −195 °C and pressures from 1 to 500 atmospheres, Gaz. Prom. **9,** 41–43 (1964), Trans. avail. from SLA Translation Center, No. LA–TR–65–1.

[35] Blais, N. C., and Mann, J. B., Thermal conductivity of helium and hydrogen at high temperatures, J. Chem. Phys. **32,** 1459–1465 (1960). Also Mann, J. B., private communication.

[36] Geier, H. and Schafer, K., Thermal conductivity of pure gases and gas mixtures between 0° and 1200° C, Allgem. Waermetech. **10,** 70–75.

[37] Bromley, L. A., Thermal Conductivity of Gases at Moderate Pressures, Calif. Univ. Radiation Lab. Berkeley, Rept No. 1852 (1952).

[38] Ubbink, J. B., Thermal conductivity of gaseous hydrogen and of gaseous deuterium, Physica **14,** 165–174 (1948).

[39] Johnston, H. L., and Grilly, E. R., The thermal conductivities of eight common gases between 80 and 380 K, J. Chem, Phys. **14,** 233–238 (1946).

[40] Eucken, A., On the temperature dependence of the thermal conductivity of several gases, Physik Z. **12,** 1101–1107 (1911).

[41] Vargaftick, N. B., and Parfenov, E. D., Thermal conductivity of hydrogen, Zh. Eksptl. Teor. Fiz. **8,** 189–197 (1938).

[42] Gregory, H. S., The Effect of Temperature on the Thermal Conductivity and Accomodation Coefficient of Hydrogen, Proc. Roy. Soc. (London) **A 149,** 35–56 (1935).

[43] Keesom, W. H., and MacWood, G. E., The viscosity of liquid hydrogen, Physica **5,** 745–749 (1938).

[44] Keesom, W. H., and Keesom, P. H., The viscosity of hydrogen vapour, Physica **7,** 29–32 (1940).

[45] Becker, E. W., and Misenta, R., Viscosity of HD and of He^3 between 14 K and 20 K, Z. Physik **40,** 535–539 (1955).

[46] Coremans, J. M. J., Van Itterbeek, A., Beenakker, J. J. M., Knaap, H. F. P., and Zandbergen, P., The viscosity of gaseous He, Ne, H_2, and D_2 below 80 K, Physica **24,** 557–576 (1958).

[47] Clarke, A. G., and Smith, E. B., Low-temperature viscosity of argon, krypton and zenon, J. Chem. Phys. **48,** 3988–3991 (1968).

[48] Hanley, H. J. M., and Childs, G. E., Dilute gas viscosities at low temperatures, J. Chem. Phys. **50,** 4600–4601 (1969).

[49] Diller, D. E., Measurements of the viscosity of para hydrogen, J. Chem. Phys. **42,** 2089–2100 (1965).

[50] Hanley, H. J. M., McCarty, R. D., and Sengers, J. V., Density dependence of experimental transport coefficients of gases, J. Chem. Phys. **50,** 857–870 (1969).

[51] Diller, D. E., and Mason, E. A., Low temperature transport properties of gaseous H_2, D_2, and HD, J. Chem. Phys. **44,** 2604–2609 (1966).

[52] Diller, D. E., and Roder, H. M., Thermal Conductivity Measurements on Fluid Hydrogen at 17 to 200 K and Pressures to 100 atm, Paper presented at Cryogenic Engineering Conference 15th, Los Angeles, Calif. (June 16–18, 1969).

[53] Israel, S. L., Hawkins, T. D., and Hyman, S. C., Thermal Conductivity of Hydrogen from 2000° to 4700° F., United Nuclear

Corp., White Plains, N.Y., Rept No. NASA–CR–403, (Mar 1966) Contr. No. NAS3–3205, 65 p., NASA 66 19386.

[54] Bethringer, K., Kollman, W., and Mentel, J., Thermal conductivity of hydrogen between 2000 and 7000 K., Z. Physik **215,** 127–151 (1968).

[55] Hanley, H. J. M., and Klein, Max, to be published.

[56] Sandler, S. I., University of Delaware, Private communication; Steele, W. A., Pennsylvania State University, private communication. See also, Sandler, S. I., and Dahler, J. S., Transport properties of polyatomic fluids II: A dilute gas of spherocylinders., J. Chem. Phys. **44,** 1229 (1966).

[57] Barua, A. K., Manna, A., and Mukhopadhyay, P., Thermal conductivity and rotational relaxation in some polar gases, J. Chem. Phys. **49,** 2422–2425 (1968); Healy, R. N., and Storvick, T. S., Rotational collision number and Eucken factors from thermal transpiration measurements, J. Chem. Phys. **50,** 1419–1427 (1969).

[58] Harris, L. B., Determination of Eucken factor from relative change in thermal conductivity of gas mixtures; ortho-para hydrogen mixtures at 77 K., J. Chem. Phys. **49,** 206–211 (1968). Erratum: J. Chem. Phys. **50,** 1909 (1969).

[59] Hartland, A., and Lipsicas, M., Quantum symmetry effects in hydrogen gas., Phys. Letters **3,** 212–213 (1963); Lipsicas, M., private communication.

[60] Van Dael, W., and Cauwenbergh, H., Measurements of the thermal conductivity of gases I., experimental method. Data for pure gases., Physica **40,** 165–172 (1968).

(Paper 74A3–605)

JOURNAL OF RESEARCH of the National Bureau of Standards—A. Physics and Chemistry
Vol. 74A, No. 3, May–June 1970

Temperature Classification of the Spectra of Dysprosium (Dy I , Dy II)

Arthur S. King,* John G. Conway, Earl F. Worden,*** and Charlotte E. Moore**

Office of Standard Reference Data, National Bureau of Standards, Washington, D.C. 20234

(January 13, 1970)

The Temperature Classifications are listed for 4584 lines of Dy I and Dy II, as taken from an unpublished manuscript of the late A. S. King. In recording his observations, King used a wavelength list compiled mostly from the early literature. A homogeneous and extensive line list based on new observations has been prepared at the Lawrence Radiation Laboratory (LRL). King's data have been edited and adjusted by the present authors to fit the new wavelength list.

In the Table, King's estimated intensities of Dy lines in the spectra of the Arc, Spark, and Furnace are given along with the Temperature Classification. Some of his earlier published work has been used to fill the gaps in this manuscript, which was forwarded to the late W. F. Meggers in 1956.

Key words: Intensity estimates, Dy spectra; dysprosium spectra, temperature classification; temperature classification, Dy I and Dy II; spectra, Dy I and Dy II.

Upon completion of Volume III of "Atomic Energy Levels" in 1958 attention was focused more sharply on rare-earth spectra in preparation for Volume IV, the last of the series. Many of these spectra are complex and have overlapping configurations. The early observations are so fragmentary that it has been necessary to observe the spectra with modern sources and prepare new, homogeneous line lists having spectra of different stages of ionization clearly separated.

In addition, two types of observations are particularly helpful with the interpretation, namely Zeeman Effect and Temperature Classification. The latter subject is uniquely associated with the name of the late A. S. King, who initiated and carried out the extensive program at the Mount Wilson Observatory on estimated line intensities observed in Arc and Spark Spectra and in Furnace Spectra at various temperatures, for many elements. His numerous papers on this subject have helped to lay the foundation of our present knowledge of the structure of complex spectra. An excellent illustration may be found in his work on Gd spectra [1][1], which enabled H. N. Russell to extend the analyses without the aid of Zeeman data [2].

The present paper is concerned with the first and second spectra of the rare-earth element Dy ($Z=66$), for which new line lists are available and, also, an extensive list of Temperature Classifications by A. S. King which was unpublished at the time of his death. With the cordial support of R. B. King, the present authors have felt that the material should be published without further delay. They have assembled the data in Table A, which contains in the first two columns, respectively, the new wavelengths and the spectrum, from the list prepared at the Lawrence Radiation Laboratory (LRL). The following columns are from A. S. King's material; they contain, respectively, his estimated intensities in the Arc, Spark, and High, Medium and Low Temperature Furnace Spectra and the Temperature Classification. The last column contains special notes.

The LRL Line List. The two authors from LRL (J.G.C. and E.F.W.) have selected from their extensive line list the wavelengths and spectral assignments that correspond to the lines observed by King.

The spectra were photographed with the 9.15m Spectrograph at Argonne National Laboratory [3]. The sources were electrodeless lamps containing $^{162}DyI_3$ prepared and operated as described in references [4] and [5]. The plates were measured on a Grant comparator with photoelectric setting. A thorium comparison spectrum provided the standards. A description of the wavelength reductions may be found in the paper by F. S. Tomkins and M. Fred [6]. The wavelengths are standard air values. They have been rounded off to three decimal places and are listed in column 1 of Table A. The standard deviation ranges from about ± 0.001 Å at 3000 Å to ± 0.01 Å at 9375 Å.

Two methods were used to separate Dy I and Dy II lines: (1) the comparison of relative intensities of lines emitted by electrodeless lamps operated at low and high pressure [5]; (2) the comparison of lines emitted by a spark between Dy metal electrodes and by an electrodeless lamp operated at high Dy vapor pressure. The LRL assignment of the spectrum is entered in column 2 of Table A.

*Deceased.
**Present address: Lawrence Radiation Laboratory, Berkeley, Calif. 94720.
***Present address: Lawrence Radiation Laboratory, Livermore, Calif. 94550.
[1] Figures in brackets indicate the literature references at the end of this paper.

The King Line List. This list extends from 3000 Å to 9375 Å. It was forwarded by A. S. King to W. F. Meggers in hand-written manuscript form, in April 1956, evidently with the idea of assisting with the analyses of these complex Dy spectra. Some years later Meggers expressed his desire to one of the present authors (C.E.M.) to have the paper published, but he wished to fill a gap in the observations from λ3807 to λ3903 before publishing it. He did not live to accomplish this. The present authors have utilized two of King's earlier papers [7] and [8] to help cover this gap and another one from λ3407 to λ3463.

A few general remarks about the 1956 list are available from correspondence. In a letter to Meggers dated April 4, 1956, King states that "In the first section, λ3000–3800, I did not try to pick out Dy II lines, but I think the criterion will be that Dy I lines maintain their strength in the furnace better than Dy II lines. At higher wavelengths the difference is more pronounced, and I have made the distinction in the 'Class' column."

In a later letter he writes "The λ's are in general those of Eder throughout the spectrum, in order to have a basic list. Major λ lists are those of J. M. Blank . . . and Harrison, from M.I.T. λ's. . . . The section 3900–4700 was photographed in the second order and is improved in number of lines by later first-order spectrograms. However, the data from the second-order plates [7] can be used with little change except for improved wavelengths . . .".

A considerable amount of editing has been done in fitting the earlier King list to the later much more complete LRL line list. In many cases the disagreement in wavelength is large, amounting in some cases to tenths of an Angstrom. In fact, within the King line list itself, for a given line several wavelengths are occasionally entered that differ appreciably. These appear to be taken from the earlier literature. Lines for which discrepancies in wavelength exist between the two line lists are indicated by note 3 in the last column of Table A. This note is used for differences exceeding ± 0.05 Å in case King lists the wavelength to two decimals, and for differences exceeding ± 0.1 Å when he lists the wavelength to only one decimal. In spite of large tolerances in Δλ, it is felt that the fitting of the lines from the LRL list to the King list is essentially reliable.

Most of the published papers on Temperature Classification of rare-earths contain only Arc and Furnace intensities. In earlier papers, however, such as one on Ti, King describes in detail the temperature stages and estimated intensities as observed in the High, Medium, and Low Temperature Furnace [9]. In the case of Dy, Arc intensities (column 3, Table A) are given for all lines, and High Temperature Furnace intensities (column 5) for most lines. Intensities from the Medium and Low Temperature Furnace (columns 6 and 7)-exposures are given for only a few of the strongest lines. The Spark intensities in column 4 are all from [7], as indicated by note 1. This reference has been used, also, for two gaps in the 1956 list: λλ3407 to 3463 and λλ3809 to 3831. Users are reminded that in these intervals the intensity scales may not fit smoothly with the rest of Table A.

For lines appearing in both the 1956 list and in reference [7], the arc intensities are the same in many cases; for these the published spark intensity [7] is quoted in Table A, Column 4. In case the 1956 arc intensity differs from that in the 1943 list, the spark intensity published in [7] has been adjusted approximately to the 1956 scale and entered in parentheses in Table A. Examples are as follows:

	λ	Arc	Spark	λ	Arc	Spark
Ref. 7	3849.388	25	25	4111.343	125	80
1956		15			150	
Table A		15	(15)		150	(100)

The gap from λ3836 to λ3902 has been covered in Table A as completely as possible by material from King's 1930 paper [8]. Again, the scale may not fit smoothly on to that of his 1956 ledger, but note 2 in the last column indicates to users that this break exists in the 1956 list. The High Temperature Furnace intensities given in the 1956 list supersede those of 1943 except for the gaps mentioned above.

All lines in the 1943 paper [7] are lines of Dy II according to King. With only one or two exceptions this agrees with the LRL listing. For these lines "E" has been entered in Table A in column 8, which contains the Temperature Classification assigned by A. S. King.

Braces are included in column 8 for lines indicated by King to be double or triple, but unresolved in his list. For example, the pair at λ6879.015 to λ6879.157 is clearly resolved in Table A, but the intensity estimates apply to one line in King's list.

A number of lines are blends of Dy I and Dy II. For example, the estimated intensities of the pair at λ5471.913 and λ5471.961 are entered as blends in Table A. An asterisk in column 5 or 6 indicates that the intensity in the High or Medium Temperature Furnace applies to the Dy I line.

General Comments. A number of King's lines have been omitted from Table A. They fall into three categories: (1) lines for which an Arc intensity is given but no Furnace intensity or Temperature Classification is entered; (2) lines not seen on the new spectrograms used for the LRL list; (3) lines rejected as impurities.

For those lines in King's list where there is a Furnace intensity but no Temperature Classification, a Classification has been added in column 8, on the basis of King's assignments for similar lines and in accordance with the known analysis. Parentheses indicate throughout the entries that have been furnished by the present authors, i.e. entries not taken from the 1956 or earlier lists by King.

The total number of lines in Table A is 4584. Had King lived to edit his list and compare it with the new line list from LRL, the present contribution could have been improved and greatly extended. An earnest effort has been made to interpret and present his data as reliably as possible.

This work could not have been done without the friendly encouragement of R. B. King, which is greatly appreciated. The authors are, also, most grateful to Isabel D. Murray for her painstaking care in preparing the press copy of the Table.

TABLE A. *Temperature classification of dysprosium lines*

Wavelength (Air)	Spectrum	Intensity					Temp. Class	Notes
		Arc	Spark	Furnace				
				High	Medium	Low		
3001.088	I	4					V	
3001.649	II	2					V	
3002.384	II	30	25				VE	1
3002.862	II	3					V	
3003.756	II	40	20				VE	1
3004.178	II	4					V	
3005.045	II	1					V	
3005.935	II	4					V	
3007.032	II	5					V	
3007.526	II	2					V	
3008.814	II	10					V	
3010.034	II	2					V	
3011.157	II	1					V	
3012.296	II	2					V	
3012.629	II	3					V	
3013.363	II	2					V	
3013.452	II	2					V	
3013.698	II	4					(V)	
3014.279	I	1		5			IV	
3015.068	II	30	25				VE	1
3015.684	II	60	50				VE	1
3016.598	II	1					V	
3016.951	II	40	60				VE	1
3017.720	II	3					V	
3018.272	II	1					V	
3018.956	II	1					V	
3020.340	II	3					V	
3021.780	II	8					V	
3022.087	II	3					V	
3022.627	II	3					V	
3023.053		1					V	3
3024.604	II	1					V	
3025.412	II	1					V	
3025.588	II	25		1			IV	
3025.746	II	5					V	
3026.157	II	150	60	15			IVE	1
3027.337	II	2					V	
3027.562	II	8					V	
3028.453	II	2					V	
3028.912	II	1					V	
3029.314	II	1					V	
3029.813	II	50	80				VE	1
3030.064	II	1					V	
3030.397	II	15					V	
3030.786	II	1					V	
3031.194	II	10					V	
3031.532	II	1					V	
3031.923	II	1					V	
3032.522	II	1					V	
3032.820	II	1					V	
3033.194	II	20					V	
3033.822	II	1					V	
3034.484	II	3					V	
3035.033	II	1					V	
3035.944	II	1					V	
3036.698	II	30	15	2			IVE	1
3037.387	II	2					V	
3038.285	II	300	300	5			IVE	1
3039.804	II	1					V	
3040.262	II	10					V	
3041.638	II	12					V	
3042.087	II	5					V	
3042.238	II	2					V	
3043.135	II	80	80	2			IVE	1
3043.426	II	30	20	1			IVE	1
3043.540	II	10					V	
3044.541	II	8					V	
3045.231	II	1					V	
3046.318	II	1	2				IV	
3046.379		5						
3046.736	II	3					V	
3047.560	II	60	50	2			IVE	1
3048.224	II	6					V	
3048.394	II	8					V	
3049.119	II	40	30	2			IVE	1
3049.638	II	1					V	
3050.499	II	3					V	
3051.239	II	1					V	
3051.454	II	60	20	5			IVE	1
3051.818	I			3			IV	3
3052.318	II	40	60				VE	1
3052.731	II	3					V	
3053.198	II	1					V	
3053.686	II	1					V	
3054.427		1					V	
3054.672	II	4					V	
3055.126	II	1					V	
3055.858	II	1					V	
3056.964	II	20					V	
3057.118	II	4					V	
3058.178	II	1					V	
3058.793	II	3					V	
3059.473	II	15					V	
3060.019	II	20					V	
3060.312	II	8					V	
3060.644	II	80	80	1			VE	1
3061.365	II	30	30				VE	1
3061.492	II	20	15				VE	1
3062.185	II	20					V	
3062.616	II	100	80	10			IVE	1
3063.248	II	1					V	
3063.547	II	1					V	
3063.880	II	2*d*					V	
3064.034	II	10					V	
3064.565	II	3					V	
3065.174	II	4					V	
3065.633	II	2					V	
3066.986	II	60	60	1			VE	1
3067.437	II	3					V	
3068.938	II	6					V	
3069.695	II	10					V	
3070.458	II	8					V	
3071.908	II	80	40	15			IVE	1
3072.380	II	2					V	
3072.735	II	4					V	
3072.916	II	8					V	
3073.539	II	80	80	2			IVE	1
3073.999	II	2					V	
3074.391	II	1					V	
3075.074	II	4					V	
3075.178	II	2					V	
3075.500	II	6					V	
3075.894	II	5					V	
3076.344	II	1					V	

378-324 O - 70 - 4

TABLE A. *Temperature classification of dysprosium lines* — Continued

Wavelength (Air)	Spectrum	Intensity					Temp. Class	Notes
		Arc	Spark	Furnace				
				High	Medium	Low		
3076.888	II	20		4			IV	
3078.207	I	15		5*			IV	3
3078.330	II							
3078.682	II	80	60	2			IVE	1
3079.329	II	50	40	1			VE	1
3080.006	II	2					V	
3080.282	II	4					V	
3080.918	II	15					V	
3081.911	II	1					V	
3082.510	II	50	15	6			IVE	1
3083.443	II	2					V	
3083.557	II	2					V	
3084.468	II	3					V	
3084.641	II	15*d*					V	
3084.684	II	3					V	
3085.783	II	3					V	
3086.627	II	12					V	
3087.511	II	10		1			IV	
3088.206	II	1					V	
3088.412	II	5					V	
3088.970	II	1					V	
3089.416	II	2					V	
3089.597	II	10					V	
3089.775	II	4					V	
3090.188	II	10					V	
3090.529	II	2					V	
3090.818	I	1		4			IV	
3090.872	I							
3091.930	I	2		2			IV	
3092.216	II	1					V	3
3093.101	II	60	20	2			IVE	1
3093.458	II	1					V	
3093.730	I	25		1*			IV	3
3093.822	II							
3094.543	II	3					V	
3095.024	II	10					V	
3095.615	II	4					V	
3095.745	II	40	30				VE	1
3096.290	II	2					V	
3096.898	II	2					V	
3096.995	I	3?		2*			IV	3
3097.278	II	1						
3097.579	II	3					V	
3097.655	II	1					(V)	
3098.037	II	10					V	
3098.523	II	3					V	
3098.566	II	1					V	
3099.908	I	1		2			IV	3
3100.915	II	6					V	
3101.381	II	2					V	
3101.878	II	20	80	20			IIIE	1
3101.932	II	50						1
3102.197	II	8					V	
3102.786	II	1					V	
3103.240	II	60	30	15			IIIE	1
3103.828	II	60	60	4			IVE	1
3104.109	II	10		1			IV	
3104.992	II	40	50				VE	1
3106.046	II	1					V	
3106.619	II	1					V	
3106.970	II	5		2*			V	3
3107.041	I							
3108.241	II	1					V	3
3109.295	II	4					V	
3109.760	II	150	100	10			IVE	1
3110.315	II	2					V	
3110.715	I	15		2*			IV	
3110.745	II							
3111.544	II	4					V	
3111.854	II	2					V	
3112.080	II	3					V	
3112.778	I	5		1*			IV	3
3112.870	II							
3113.104	II	10		3*			IV	3
3113.179	I							
3113.441	II	1					V	
3114.297	I	1					V	
3115.660	II	1					V	
3115.921	II	3					V	
3116.426	II	1					V	
3116.867	II	5					V	
3117.423	II	2					(V)	3
3117.504	II	20					V	
3117.960		1					(V)	
3117.986	II	8					V	
3118.648	II	1					V	
3118.963	II	2					V	
3119.450	II	1					V	
3120.180	II	80	80	1			VE	1
3120.509	II	3		1			IV	
3121.423	II	1					V	
3121.987	II	6					V	
3122.115	II	4					(V)	
3122.452	I	3*d*		15			IV	
3122.943	II	3					V	
3123.004	II	1					(V)	
3124.896	II	2					V	
3126.196	II	50	30	2			IVE	1
3126.714	I	6		1*			IV	3
3126.801	II							
3127.259	II	5					V	
3127.475	II	4					V	
3128.406	II	150	125	5			IVE	1
3128.757	II	5					V	3
3129.302	I	3		20			IV	
3129.764	II	1					V	
3130.154	II	8					V	
3130.561	II	2					V	
3131.204	II	2					V	
3131.467	II	1					V	
3132.121	II	6					V	
3132.600	II	3					V	
3132.663	II	2					(V)	
3133.026	II	6					V	
3133.499	II	1					V	
3133.815	I	2		25			III	
3134.474	II	2					V	
3135.385	II	500	500	30			IVE	1
3135.690	II	6					V	
3136.011	I	1		20			III	3
3136.394	II	2					V	
3136.692	II	10		1			IV	
3137.558	II	1					V	
3138.127	II	4*d*					V	

TABLE A. *Temperature classification of dysprosium lines* – Continued

Wavelength (Air)	Spectrum	Intensity					Temp. Class	Notes
		Arc	Spark	Furnace				
				High	Medium	Low		
3138.965	II	2					V	
3139.497	II	5					V	
3139.887	II	2					V	
3140.036	II	3					V	
3140.413	II	4					V	
3140.642	II	150	150	5			IVE	1
3141.140	II	200	60	40			IIIE	1
3141.934	II	1					V	
3142.295	II	40	40	1			IVE	1
3142.624	I			5			IV	3
3143.176	II	15					V	
3143.835	II	50	50	1			IVE	1
3144.224		1					V	3
3144.500	II	1					V	
3145.218	II	25		6			III	
3146.160	II	60	80	2			IVE	1
3146.544	II	1					V	
3146.885	II	3		1			IV	
3147.531	II	30	30				VE	1
3147.694	I	1		20			III	
3148.164	II	1					V	
3149.075	II	3					V	
3149.277	II	3					V	
3149.872	II	8					V	
3150.172	II	25					V	
3150.470	II	6					V	
3150.663	I	4		5			IV	
3151.310	II	2					V	
3151.527	I	2		1			IV	
3151.890	II	50	25	5			IVE	1
3152.223	II	8					V	
3152.374	II	30					V	
3153.312	II	20					V	
3153.828	I	1		10			IV	3
3154.068	II	5					V	
3154.526	II	3					V	
3154.659	II	5					V	
3155.380	II	1					V	
3156.522	II	500	500	20			IIIE	1
3157.206	II	8					V	
3157.551	II	15					V	
3157.976	II	3					V	
3158.249	II	2					V	
3159.289	I	5		3			IV	
3159.304	II	3					V	
3159.750	II	1					V	
3159.962	II	1					V	
3160.503	II	40	15	5			IVE	1
3161.031	II	20		2			IV	
3161.314	II	1					V	
3162.833	II	250	250	10			IVE	1
3163.457	II	1					V	
3164.041	II	10					V	
3164.134	II	15		1			IV	
3164.917	II	6					V	
3165.264		1					V	3
3165.616	I	1		5			(IV)	
3166.304	II	2					V	3
3166.832	II	1					V	3
3167.471	II	25					V	
3167.850	II	15		1			IV	3
3168.151	II	20		3			IV	
3168.637	II	5					V	
3168.954	I	6		30			IV	
3169.558	II	8					V	
3169.994	II	300	100	100			IIIE	1
3170.102	II	40?					V	
3170.750	II	40	40	1			IVE	1
3170.971	II	20		2			IV	
3171.471	II	20		2			IV	3
3172.086	II	4					V	
3172.426	I	2		1			IV	
3172.694	II	2					V	
3173.017	II	2					V	3
3173.366	II	1					V	3
3174.017	II	3					V	
3174.284	II	1					V	
3174.883	II	30		1			IV	
3175.538	II	1					V	3
3176.125	II	2					V	
3176.462	II	4					V	
3176.709	II	3					V	
3177.213	II	1					V	
3177.522	II	10					V	
3177.888	II	125	125	2			IVE	1
3178.374	II	60	20	15			IIIE	1
3179.030	II	8					V	
3180.274	II	3					V	
3180.692	II	5					V	
3181.089	II	3					V	
3181.636	II	3					V	3
3181.939	II	15		3			IV	
3182.482	II	2					V	
3183.195	II	8					V	
3183.946	II	2					V	3
3184.190	II	5					V	
3184.271	II	10					V	3
3184.552	II	4		1*			IV	3
3184.600	I							
3184.787	II	40	25	10			IVE	1
3185.405	I	2		1*			IV	3
3185.464	II							
3185.967	II	1					V	
3186.377	II	80	60	4			IVE	1
3187.246	II	5					V	
3187.680	II	60	60	2			IVE	1
3188.372	II	2					V	
3188.666	II	5					V	
3189.067	II	5					V	
3189.803	II	4					V	
3190.108	II	1					V	
3190.180	II	3					V	
3190.656	II	4					V	
3191.561	II	1					V	
3192.035	II	5		1*			IV	3
3192.139	I							
3192.222	II	2					V	
3192.695	II	2					V	
3193.304	II	80	25	25			IIIE	1
3193.659	II	3					V	
3193.868	II	3					V	
3194.445	II	1					V	
3194.799	II	1					V	
3195.886	II	3					V	

TABLE A. *Temperature classification of dysprosium lines* – Continued

Wavelength (Air)	Spectrum	Intensity					Temp. Class	Notes
		Arc	Spark	Furnace				
				High	Medium	Low		
3196.278	I	4		2*			IV	3
3196.429	II							
3197.067	II	1					V	
3197.595	II	5					V	
3198.148	I	1*d*		4			IV	
3198.787	II	2					V	
3199.233	II	8		1			IV	
3199.587	I	3		8			IV	
3200.321	I	1		3*			IV	3
3200.632	II							
3200.926	II	1		3*			IV	3
3201.196	I							
3201.301	II	15		2			IV	
3201.660	II	20		1			IV	
3202.218	I	2		10			IV	
3202.597	II	20					V	
3202.848	II	8					V	
3203.339		1					V	
3203.842	II	5					V	
3204.299	I	6		2			IV	
3204.357	II	3					V	
3204.944	II	3					V	
3205.459	II	30					V	
3206.405	II	80	80	1			VE	1
3206.642	II	20					V	
3207.123	II	60	60	3			IVE	1
3207.340	II	2					V	
3207.774	II	1					V	
3208.312	II	5					V	
3208.813	II	80	60	5			IVE	1
3208.847	II							
3209.284	II	8		1			IV	
3210.066	II	2					V	
3210.333	I	3		2			IV	
3210.724	II	1					V	
3212.045	II	20		1			IV	
3212.443	II	15					V	
3212.683	II	20					V	
3213.173	II	4					V	
3213.205	II							
3213.587	II	1					V	
3213.706	I	2		3			IV	
3214.633	II	25		3			IV	
3215.193	II	125	125	10			IVE	1
3215.978	II	6		1			IV	
3216.237	II	3					V	
3216.627	II	150	200	12			IVE	1
3217.151	II	1					V	
3217.377	II	15					V	
3218.012	II	1					V	
3218.779	II	1					V	
3218.839	II	2					V	
3219.542	II	8					V	
3220.128	II	5					V	
3220.464	II	25					V	
3221.069	I	1		4			IV	
3221.494	II	50	50	1			IVE	1
3221.637	II	50*d*	25	3			IVE	1
3221.884	II	6					V	
3222.550	II	1					V	
3222.875	II	2					V	
3223.284	II	80	80	4			IVE	1
3223.840	II	1					V	3
3224.075	II	3					V	
3224.595	II	1					V	
3225.079	II	25	15	10			IVE	1
3225.153	II	10					IVE	
3225.367	II	2					V	
3225.947	II	80	60	6			IVE	1
3226.380	II	15					V	
3227.033	II	1					V	
3227.419	II	2					V	
3227.499	II	2					V	3
3227.712	II	5					V	
3228.154	II	2					V	
3228.598	I	1					V	
3228.972	II	15					V	
3229.363	II	15					V	
3229.748	II	1					V	
3229.939	II	20		8			IV	
3230.320	II	6					V	
3230.663	I	1					V	
3230.950	II	1					V	
3231.076	II	1					V	
3231.291	II	1					V	
3232.092	II	5					V	
3232.154	II	3					V	
3232.645	II	30		8			IV	
3233.413	II	3					V	
3234.093	II	5					V	
3234.416	I	2					IV	
3235.085	II	1					IV	
3235.360	II	1					V	3
3235.816	II	120	(100)	8			IVE	3
3235.894	II	100					IVE	1
3236.078	II	4					V	
3236.693	II	80	80	6			IVE	1
3237.089	II	5		1			IV	
3237.857	II	1					V	
3238.170	II	4					V	
3238.290	II	4					IV	3
3238.693	II	6					IV	
3238.800	II	6					IV	3
3239.190	II	1					V	
3239.457	II	2					V	3
3239.585	II	6					V	
3240.037	II	8					V	
3240.385	II	2					V	
3240.721	II	4					V	
3240.861	II	30	30	1			IVE	1
3241.309	II	3					V	
3241.717	II	1					V	
3242.088	II	2*d*					V	
3242.292	II	2					V	
3242.498	II	6					V	
3243.119	II	2					V	
3243.723	II	15*d*					V	
3243.784	II							
3244.189	II	2					V	
3244.797	I	1		6			IV	
3245.124	II	100	(100)	3			IVE	1
3245.666	II	1		3*			IV	3
3245.741	I							
3245.877	II	4					V	

TABLE A. *Temperature classification of dysprosium lines* — Continued

Wavelength (Air)	Spectrum	Intensity					Temp. Class	Notes
		Arc	Spark	Furnace				
				High	Medium	Low		
3246.178	II	2					V	
3246.685	II	4					V	
3246.802	I	1		5			IV	3
3247.272	II	1					V	
3248.359	II	50	40	1			IVE	1
3248.893	II	2					V	
3249.331	II	2					V	
3249.414	II	2					V	
3249.904	II	1					V	
3249.994	II	1					IV	
3250.548	II	2					V	
3250.987	II	6		1*			IV	3
3251.084	I							
3251.268	II	300	300	15			IVE	1
3251.376	I	20		10*			IV	
3251.407	II							
3251.898	II	50	25	2			IVE	1
3252.189	II	50	50	2			IVE	1
3252.638	II	1					V	
3253.223	II	1					V	
3253.366	II	1					V	
3253.573		1					V	
3253.910	II	12					V	
3254.483	II	15		1			IV	
3255.148	I	2		3*			IV	3
3255.241	II							
3255.666	I	1		6			IV	3
3256.259	II	80	60	1			IVE	1
3257.174	I	15		6*			IV	3
3257.226	II							
3257.366	II	20					IV	
3258.039	II	2					V	
3258.283	II	2					V	
3258.890	II	1					V	
3260.021	II	3		8?			IV?	
3260.701	II	50	25	10*			IVE	1
3260.718	I							
3261.008	II	2					V	
3261.215	II	30	40				VE	1
3261.607	II	1					V	
3261.954	II	2					V	
3262.042	II	4		1			IV	
3262.278	II	6		1			IV	
3263.076	II	3					V	
3263.186	I	1		10			IV	
3263.581	II	1					V	
3263.908	II	1					V	
3264.300	II	5		1			IV	
3264.744	II	4					V	
3265.159	II	4					V	
3265.523	II	10		2			IV	
3265.998	II	60	80	1			IVE	1
3266.024	II							
3266.210	II	80	125	1			IVE	1
3266.608	II	1					V	
3267.259	II	1					V	
3267.756	II	8		1			IV	
3267.787	II							
3268.075	II	3					V	
3268.278	II	6					V	
3268.644	I	2		2			IV	
3269.108	II	100	30	15			IVE	1
3269.540	II	3					V	
3269.947	II	1					V	
3270.444	II	1					V	
3270.939	II	3					V	
3271.307	II	2		2*			IV	3
3271.426	I							
3271.666	II	1					V	
3272.032	II	4					V	
3272.090	II	10					V	
3272.730	II	80	60	1			IVE	1
3272.961	I			15			IV	3
3273.624	II	1					V	
3274.208	II	1					V	
3274.570	II	1					V	3
3274.609	II	1					V	
3274.962	II	2					V	
3275.743	II	30					V	
3275.928	II	40		2			IV	
3276.176	II	1					V	
3276.839	II	1					V	3
3277.588	II	6					V	
3277.646	II	4					V	
3278.330	II	6					V	
3278.396	II	1					V	3
3278.587	II	1					V	
3279.453	II	30					V	
3279.511	II							
3279.696	II	80	60	4			IVE	1
3280.092	II	250	100	30			IIIE	1
3280.442	II	1					V	
3280.664	II	2					V	
3280.982	II	1					V	
3281.650	II	10		1			IV	
3282.059	II	1					V	
3282.504	II	3					V	
3282.775	II	100	150	1			VE	1
3283.083	I			30			?	3
3283.158	II	6		2			IV	
3283.556	II	2					V	
3283.714	II	4		2			IV	
3283.743	II							
3284.008	II	3					V	
3284.256	II	1					V	3
3284.365	II	8					V	
3284.862	I	3		3			IV	
3284.878	II	2					V	
3285.443	II	1					V	
3285.635	II	1					V	
3286.151	II	2					V	
3286.575	II	10		5			IV	
3287.096	I							
3287.154	II	2*d*		2*			IV	
3287.170	II							
3287.621	I	1		2*			IV	3
3287.807	II							
3287.944	II	50	30	1			VE	1
3288.624	I	30		10			IV	
3289.103	I	6		1*			IV	
3289.144	II							
3289.336	II	5					V	
3289.969	I	1		6			IV	
3290.213	II	1					V	

TABLE A. *Temperature classification of dysprosium lines* — Continued

Wavelength (Air)	Spectrum	Intensity					Temp. Class	Notes
		Arc	Spark	Furnace				
				High	Medium	Low		
3290.647	II	1					V	
3291.121	II	15					V	
3292.168	I	1		3			IV	
3292.615	II	3					V	
3293.426	II	1					V	
3293.805	II	40	15	8			IVE	1
3293.876	II	2					V	
3294.203	II	2					V	
3294.670	II	1					V	
3294.916	II	6*d*					V	
3294.976	II							
3295.202	II	5					V	
3295.405	II	2					V	
3295.606	II	1					V	
3295.830	I	2		6			IV	
3295.875	II			4			V	
3296.302	II	40	30	1			VE	1
3296.868	II	1					V	
3297.175	II	2					V	
3297.603	II	30	40	4			IVE	1
3298.038	II	1					V	
3298.245	II	10		3*			IV	3
3298.362	I							
3299.149	II	4		1*			IV	
3299.208	I							
3299.856	II	1					V	
3300.310	II	1					V	
3300.923	II	15					V	
3301.490	II	2					V	
3301.723	II	3					V	
3302.016	II	2					V	
3302.062	I	1					V	
3302.401	II	5					V	3
3302.470	II	2					V	
3303.170	II	2					V	
3303.183	II							
3303.667	II	2					V	
3303.715	II	1					V	3
3304.012		1					V	
3304.069	II	1					V	
3304.294	II	6					V	
3304.706	II	1					V	
3305.400	II	40	30	1			IVE	1
3305.513	II	50	40	1			IVE	1
3306.188	II	50	50	1			IVE	1
3306.794	II	4					V	
3307.427	II	1					V	
3308.057	II	3					V	
3308.287	I	1		6			IV	
3308.794	II	150	100	3			IVE	1
3308.884	II	300	200	10			IVE	1
3309.392	II	1					V	
3309.863	II	1					V	
3310.732	II	1					V	
3310.967	II	10					V	
3311.263	II	1					V	
3311.513	II	5					V	
3312.328	II	3					V	
3312.719	II	100	50	15			IVE	1
3312.931	I	3		2*			IV	3
3313.023	II							
3313.150	II	4					V	
3313.312	II	15					V	
3313.854	II	1					V	
3313.990	II	1					V	
3314.212	I			4			IV	
3314.583	II	1*d*					V	
3314.949	II	15		1			V	
3315.480	II	3					V	
3315.742	II	4					V	
3316.316	II	150	60	20			IVE	1
3316.672	II	4					V	
3317.116	II	40	30	6			IVE	1
3317.565	II	6*d*					V	
3317.601	II							
3318.128	I	10		2			IV	
3318.174	II	2					IV	
3318.206	II							
3318.424	I	8		1*			IV	
3318.483	II							
3318.728	II	2					V	
3319.038	II	1					V	
3319.424	II	8					V	
3319.682	II	3					V	
3319.878	II	400	100	40			IVE	1
3320.060	I	1		6			IV	3
3320.878	II	1					V	
3321.033	II	4					V	
3321.435	II	1					V	
3321.878	II	2					V	
3322.309	II	1					V	
3322.925	II	1					V	
3323.275	I	10		3			IV	
3323.396	I	1		1			(IV)	3
3323.715	II	3					V	
3323.932	II	8					V	
3323.962	II							
3324.174	II	10					(V)	
3324.215	II	3					(V)	
3324.282	II	5					(V)	3
3324.872	II	2					V	
3325.277	II	4					V	
3325.505	II	2					V	
3325.590	II	4					V	
3325.867	II	1					V	
3326.192	II	50	25	8			IVE	1
3326.419	II	8?					V	
3326.521	II	6					V	3
3326.987	II	1					V	3
3327.084	II	20	(7)	5			IVE	1
3327.297	II	12					V	
3327.793	II	2*d*					V	
3327.932	II	4		1			IV	
3328.796	II	15		2			IV	
3329.308	II	1					V	
3329.798	II	1					V	3
3330.204	II	2					V	
3330.599	II	10					V	
3331.196	II	4					V	
3331.275	II	12		2			IV	
3332.046	II	3					V	
3332.778	II	3					V	
3333.037	II	2					V	
3333.547	II	5					V	

TABLE A. *Temperature classification of dysprosium lines* – Continued

Wavelength (Air)	Spectrum	Intensity					Temp. Class	Notes
		Arc	Spark	Furnace				
				High	Medium	Low		
3333.980	I			4			IV	3
3334.137	II	30	25	1			IVE	1
3334.448	II	15					V	
3334.861	I	6		3			IV	
3335.460	II	2*d*					V	
3335.826	II	8					V	
3335.973	II	2*d*					V	
3336.029	II							
3336.515	II	1					V	
3336.654	I	3		3			IV	3
3336.833	II	1		1			IV	
3337.114	II	4					V	
3337.789	II	4					V	3
3338.026	II	2					V	
3338.224	II	3					V	
3338.613	I	4		1			V	
3339.066	II	1					V	
3339.509	II	50	30	8			IVE	1
3340.404	II	1					V	3
3340.614	II	20		2			IV	
3340.995	II	200	200	12			IVE	1
3341.429	I	40	10	10*			(IV)	
3341.445	II						IVE	1
3341.545	II	2					V	
3341.885	II	80	30	12			IVE	1
3342.616	I	6		2*			IV	
3342.644	II							
3343.166	II	1					V	
3343.367	II	2					V	
3343.510	II	4		4*			IV	
3343.524	I							
3343.769	I	2		6			IV	3
3344.483	I	4		5			IV	
3344.826	II	1					V	
3345.372	II	10					V	
3345.798	II	10					V	
3346.144	II	12					V	
3346.641	I	5		1*			IV	
3346.662	II							
3347.258	II	2					V	
3347.828	II	40	30	4			IVE	1
3348.027	II	10					V	
3348.876	II	4					V	
3349.589	II	1					V	
3350.298	II	3		1			IV	
3350.659	II	5					V	
3350.965	II	3					V	
3351.286	II	2					V	
3351.736	I	1		5			V	
3352.217	II	6					V	
3352.688	II	50	60	1			VE	1
3353.234	II	2					V	3
3353.586	II	125	50	25			IVE	1
3353.913	II	1					V	
3354.211	II	4					V	
3354.686	I	1		5			IV	
3355.015	II	6					V	
3355.063	II	10					V	
3355.340	II	3					V	
3355.593	II	5					V	
3356.212	II	40	40	1			IVE	1
3356.478	II	2					V	
3356.752	II	2*d*					V	
3357.311	I	1		2			IV	
3357.600	II	4		1			IV	
3357.922	II	3					V	
3358.224		15		2			IV	
3358.300		15		2			IV	
3358.602	II	50	15	10			IVE	1
3358.952	II	4					V	
3359.094	II	2					V	
3359.462	II	40	40	1			IVE	1
3360.124	I	1					V	
3360.218	II	1					V	
3360.560	II	1					V	
3360.654	II	5					V	
3360.936	I	1		5			IV	
3361.141	II	1					V?	3
3361.414	II	4					V	
3361.612	II	2					V	
3361.846	II	1		3			IV	
3362.170	II	4					V	
3362.568	II	2		3*			IV	
3362.600	I							
3362.911	II	1					V	
3363.382		8		1			IV	
3363.481	II	3					(V)	
3363.946	II	1					V	
3364.099	I	12		10*			IV	3
3364.337	II							
3364.624	II	2					V	
3365.020	II	2					V	
3365.155	II	1					V	
3365.806	II	30	30	1			IVE	1
3366.235	II	3					V	
3366.703	II	1					V	
3367.207	II	4					V	
3367.527	II	10		1			IV	
3368.106	II	150	50	40			IVE	1
3368.524	II	2					V	
3368.640	II	1					V	3
3369.283		10		1			IV	
3369.638		8		1			IV	
		2						
3369.935	I							
3370.030	II	2		1*			IV	
3370.098	II							
3370.373	II	4		1			IV	
3370.851	II	40	50	1			IVE	1
3370.222	II	1					V	
3371.512	II	2					V	
3371.692	II	40	40	1			IVE	1
3371.806	II	40	40	2			IVE	1
3372.116	I	1		8			IV	
3372.312	II	2					V	
3372.779	II	8					V	
3373.781	II	2					V	3
3374.291	II	8					V	
3374.958	II	1					V	
3375.254	II	1					V	
3375.739	II	20		1			IV	
3375.998	II	15		3			IV	
3376.183	II	2					V	
3376.296	II	10					V	

TABLE A. *Temperature classification of dysprosium lines* – Continued

Wavelength (Air)	Spectrum	Intensity					Temp. Class	Notes
		Arc	Spark	Furnace				
				High	Medium	Low		
3376.370	II	10					V	
3376.548	I			6			IV	
3376.620	II	15					V	
3376.927	II	1					V	3
3377.101		10		3			IV	
3377.236	II	1					V	
3377.744	II	} 2		2*			IV	
3377.788	I							
3378.207	II	20		1			IV	
3378.416	II	40	30	4			IVE	1
3378.879	II	25	40	8			IVE	1
3379.085	II	1					V	3
3379.458	I			3			IV	
3379.906	II	4					V	
3380.164	II	3					V	
3381.538	II	20		1			IV	
3381.917	II	10					V	
3382.345	II	1					V	
3382.718	II	5					V	
3383.409	I	1		8			IV	3
3383.670	II	1					V	
3384.017		10		1			(IV)	3
3384.092	II	8					(V)	
3384.126	II	4					(V)	
3384.797	I	{ 10 } { 3 }		8			IV	3
3385.015	II	600	400	100	5		IIIE	1
3385.674	II	1					V	
3386.348	I			5			IV	
3386.568	II	60	80	1			VE	1
3386.967		3		1			IV	
3387.212	II	} 15		1			IV	
3387.272	II							
3387.780	II	12		1			IV	
3388.076	II	10		1			IV	
3388.366	II	1					V	
3388.850	II	100	60	15			IVE	1
3389.444	II	20*d*					V	
3389.832	II	1					V	
3390.084	II	1					V	
3390.513	II	2					V	
3390.786	II	5					V	
3391.056	II	30		3			(IV)	
3391.162	II	25		1			IV	
3391.280	II	4					V	
3391.620	II	1					V	
3391.966	II	30		1			IV	
3392.517	I			4			IV	
3392.772	II	} 4					V	
3392.822								
3392.973	II	5					V	
3393.363		15		3			IV	
3393.568	II	400	250	80	4		IIIE	1
3393.979	II	25		1			IV	
3394.443	II	1					V	
3394.841	II	4		1			IV	
3395.493	II	1					V	
3396.157	II	200	150	50			IVE	1
3396.562	I	1		3			IV	
3396.800	II	2				}	IV	
3396.863		4		1				
3397.445	I	1		3			IV	
3397.726	I	1		2			IV	
3397.962	I	} 3		5*			IV	
3397.979	II							
3398.324		12		2			IV	
3398.789	II	5					V	
3399.057	I	} 12*d*		8*			IV	3
3399.175	II							
3399.357	II	8					V	
3399.586	II	1					V	
3399.954	I			6			IV	3
3400.432	II	3					V	
3400.913	II	4		1			IV	
3401.278	II	6					V	
3401.687	I	2		10	1		III	
3401.980	II	} 10		8*			IV	
3402.009	I							
3402.264	II	1					V	
3402.461	II	2					V	
3402.732	II	6					V	3
3402.870	II	4					V	
3403.176	I	} 20		4*			IV	3
3403.244	II							
3403.428	II	15					V	
3403.810	II	1					V	
3404.600	II	1					V	
3404.944	I	5	}	15*			IV	
3404.987	II	20						
3405.314	II	1		1			IV	
3405.496	II	6		1			IV	
3405.653	II	25		6			IV	
3406.758	II	8		1			IV	
3406.911	II	2					V	
3407.159	II	40	30	10			IVE	1
3407.596	II	1					V	
3407.795	II	800	500	150			E	1
3408.144	II	60	60	2			E	1
3413.785	II	150	80	40			E	1
3414.821	II	40	30	5			E	1
3417.129	II	20	20	1			E	1
3418.103	II	20	20	1–			E	1
3419.631	II	50	40	5			E	1
3422.864	II	25	25	1			E	1
3425.056	II	50	20	6			E	1
3429.443	II	60	60	3			E	1
3431.788	II	30	30	1–			E	1
3432.575	II	25	15	4			E	1
3434.368	II	250	150	60			E	1
3438.944	II	40	40	1			E	1
3440.928	II	60	80	2			E	1
3441.447	II	150	60	25			E	1
3445.574	II	300	150	80			E	1
3446.993	II	60	40	6			E	1
3449.892	II	30	20	5			E	1
3454.318	II	200	150	40			E	1
3454.510	II	40	40	2			E	1
3456.559	II	125	80	10			E	1
3460.968	II	300	150	60			E	1
3463.873	II	20	10	3			E	1
3468.430	II	60	40	8			IVE	1
3468.562	II	6					V	
3468.784	II	10		1			IV	

TABLE A. *Temperature classification of dysprosium lines* — Continued

Wavelength (Air)	Spectrum	Intensity					Temp. Class	Notes
		Arc	Spark	Furnace				
				High	Medium	Low		
3469.132	II	2					V	
3469.148	II							
3469.882	II	5					V	
3470.176	II	15		1			IV	
3470.198	II							
3470.577	I	1		3			IV	3
3471.077	II	60*d*	40	6			IVE	1
3471.138	II							
3471.527	II	40	20	3			IVE	1
3471.606	II	50	30	5			IVE	1
3471.803	I	4		8	6		III	
3471.951	II	5					V	
3472.242	II	6					V	
3472.595	II	1					V	
3472.927	I	4		4*			IV	
3472.946	II							
3473.300	II	5		1*			IV	
3473.360	I							
3473.696	II	50	40	6			IVE	1
3474.269	II	30*d*	50	8			IVE	1
3474.296	II							
3474.703	II	3		1			IV	
3475.336	II	3					V	
3475.414	II	2					V	
3475.657	II	4					V	
3476.363	II	8					V	
3476.723	II	6					V	
3477.067	II	150	100	50			IVE	1
3477.400	II	2					V	
3477.528	II	4					V	
3477.927	II	10		1			IV	
3478.177	I	3		25	5		III	
3478.283	II	6					V	
3478.478	II	10		1			IV	
3478.761	II	3					V	
3478.877	I	1		6			IV	
3479.417	II	2					V	
3479.760	II	6		1			IV	
3480.050	II	1					IV	
3480.419	II	8		2			IV	
3480.811	II	20	20	3			IVE	1
3481.144	II	1					V	
3481.604	I	3		1*			IV	
3481.623	II							
3482.102	II	20*d*					V	
3482.400	II	1					V	
3482.433	I	1					V	
3482.772	II	10					V	
3483.073	II	1					V	
3483.315	I	3		8			IV	
3483.556	II	1					V	
3484.190	I	3*d*		15	2		III	
3484.522	II	8					V	
3484.676	II	40	30	3			IVE	1
3484.881	II	5					V	
3485.408	II	1					V	
3485.436	II	3					V	
3485.660	II	1					V	
3485.918	II	20		1			IV	
3486.146	II	3					V	
3486.945	II	3					V	
3487.197		15		3			IV	
3487.570	II	30*d*?	40	3			IVE	1
3487.605	II							
3487.921	II	1					V	
3488.192	I	3		8			IV	3
3488.308	II	2					(V)	
3488.859	II	4					V	
3488.994	II	10		1			IV	
3489.543	I	2		10			IV	
3489.897	II	2					V	
3490.649	II	10					V	
3490.880	II	3					(V)	
3490.945	II	2					V	
3491.286	II	4					V	
3492.299	I	2		2			IV	
3492.503	II	4					V	
3493.086	II	3					V	
3493.243	I	3		6			IV	
3493.637	II	1					V	
3493.946	II	3					V	
3494.127	II	15	(15)	1	2		IVE	1
3494.491	II	300	150	100			IVE	1
3494.742	I	3		15			IV	
3495.322	II	3					V	
3496.228	II	4					V	
3496.339	II	50	30	10			IVE	1
3496.712	II	3		1			IV	
3497.113	I	2		1*			IV	
3497.134	II							
3497.343	II	1		1*			IV	
3497.378	I							
3497.813	II	40	25	3			IVE	1
3498.172	I	1		1			IV	
3498.707	II	100	40	5			IVE	1
3498.934	II	30	15	8			IVE	1
3499.620	I	4		1			IV	
3499.862	II	10		1			IV	
3499.964	I	8		3			IV	
3500.512	II	5		5			IV	
3500.812	II	1					V	
3501.288	II	1					V	
3501.429	II	4	(4)				VE	1
3501.859	II	10		1			IV	
3502.091	I	4		4			IV	
3502.143	II	6					(V)	
3502.640	I	2		2			IV	
3502.847	I	3		1			IV	
3503.025	II	2					V	
3503.174	II	20*d*		3			IV	
3503.238	II							
3503.365	II	3					V	
3503.663	II	2					V	
3503.784	II	1						3
3504.116	II	1					V	3
3504.498	II	80*d*?	80	8			IVE	1
3504.529	II							
3504.936	II	4					V	
3505.171	II	3					V	
3505.420	II	50	40	8			?E	1
3505.453	II			5				
3505.561	II	3					V	
3505.844	II	20	10	5			IVE	1
3506.038	II	2					V	
3506.247	II	3		1			IV	

TABLE A. *Temperature classification of dysprosium lines* – Continued

Wavelength (Air)	Spectrum	Intensity					Temp. Class	Notes
		Arc	Spark	Furnace				
				High	Medium	Low		
3506.638	II	1					V	
3506.813	II	150	50	30			IVE	1
3507.534	II	2		2*			IV	
3507.694	I							
3508.031	I	1		1*			IV	3
3508.095	II							
3509.012	II	3					V	
3509.231	II	20		3			IV	3
3509.434	II	4					V	
3510.053	II	3					V	
3510.155	II	3					V	
3510.872	II	2					V	
3511.014	I	5		25	15	5	II	
3511.368	II	2					V	
3511.685	II	20		1			IV	
3511.974		4		1			IV	
3512.078	II	4					V	
3512.556	II	20	20	1			IVE	1
3512.699	II	30	40	1			VE	1
3513.046	II	2					V	
3513.208	II	2					V	
3513.516	I			5			IV	
3513.734	II	2					V	
3513.891	I	3		4			IV	
3514.131	II	5					V	
3514.536	II	1		1*			IV	3
3514.591	I							3
3514.732	I	1		1*			IV	
3514.795	II							
3515.097	I	2		3			IV	
3515.614	II	4					(V)	
3515.769	I	1		25	3		III	
3516.112		1					V	
3516.511	II	1					V	
3517.050		1					V	3
3517.261	II	60	50	8			IVE	1
3517.625	I	2		8			IV	
3517.934	II	1					V	
3518.721	II	1					IV	
3519.104	II	1					V	
3519.665	II	6					(V)	
3519.765	II	6					(V)	
3519.903	II	8					(V)	
3520.349	II	1					V	
3521.157	I	15		25	6		III	
		20						
3521.491	I	4		3			IV	3
3521.879	II	6		1			IV	
3521.897	II							
3522.277	II	10d		2			IV	
3522.672	II	2					V	
3522.861	II	15		3			IV	
3523.208	II	2?		15	1*		IV	
3523.254	I	2						
3523.455	I	1		10	2		III	
3523.982	II	400	300	100	2		IVE	1
3524.574	II	2					IV	
3524.633	I	6		3			IV	
3524.930	II	8?d					V	
3525.746	II	15		3			IV	
3526.566	II	2					(V)	
3526.637	II	5					V	
3526.839	II	4					(V)	
3526.905	II	8					V	
3527.088	II	8		10	3*		III	3
3527.178	I							
3527.707	I	1		15	1		IV	3
3527.993	II	6		1			IV	
3528.472	II	2					V	
3528.861	I	3		1*			IV	
3528.896	II							
3529.030	II	6					V	
3529.148	II	15					V	
3529.563	II	1		2			IV	
3530.047		1					V	
3530.371	I	2		20	4		III	
3530.566	II	8					V	
3530.954	II	3					V	
3531.706	II	2000	1500	500	100	5	IIIE	1
3532.427	I	4		1			IV	
3532.536	I	3		1			IV	
3532.884	I	1		3			IV	
3533.262	I	1		3			IV	
3533.638	I	3		5*			IV	
3533.749	II							
3534.033	I	4		15	4		III	
3534.450	II	20		4*			IV	
3534.508	I							
3534.959	II	200	100	80	8		IIIE	1
3535.186	II	2					V	
3535.630	II	2					V	
3536.019	II	400	400	80	3		IVE	1
3536.512	II	15					(V)	
3536.585	I	2		3			(IV)	
3536.860	II	2					V	
3537.174	II	1					V	
3537.665	II	6					IV	
3537.763	I	2		3			IV	
3538.056	II	1					V	
3538.517	II	300	150	100	6		IIIE	1
3538.852	II	1					V	
3539.368	II	30	20	15*			IVE	1
3539.386	I							
3539.643	II	10		1			IV	
3539.896	I	4		4			IV	
3540.232	I	2		5			IV	3
3540.687	II	8		1			IV	
3541.301	II	3		1			IV	
3541.579	II	1					V	
3541.824	II	4		1			IV	
3542.327	II	150	100	30			IVE	1
3542.420	I			4			IV	3
3542.865	II	5		1			IV	
3543.132	II	2					V	
3543.826	II	3					V	
3544.038	II	4					V	
3544.204	II	25	20	4			IVE	1
3544.347	II	20	20	3			IVE	1
3544.992		30		4			IV	
3545.259	II	1					V	
3545.625	II	2					V	
3545.768	II	5					V	
3546.002	II	1					V	
3546.105	II	1					V	

TABLE A. *Temperature classification of dysprosium lines* – Continued

Wavelength (Air)	Spectrum	Intensity					Temp. Class	Notes
		Arc	Spark	Furnace				
				High	Medium	Low		
3546.831	II	100	50	50	2		IVE	1
3547.008	II	3					V	
3547.538		10		1			IV	
3547.912	II	1					(V)	
3547.962	I	6		6	3		III	3
3548.192	II	15	(15)	2			IVE	1
3548.717	II	8		1			IV	
3549.248		8		2			IV	
3550.218	II	300	200	80	2		IVE	1
3550.986	II	2					V	
3551.148	I	5		6			IV	
3551.616	II	150	100	30			IVE	1
3552.021	II	2	3				IV	
3552.289	II	1					V	
3553.160	II	2	4	4			IV	
3553.208		2						
3554.855	II	2					V	
3555.328	I	2		3			IV	
3555.677	II	3					V	
3555.970	II	10		1			IV	
3556.420		1					V	
3556.550	I	1		1			IV	3
3556.842	I	2		8*			IV	3
3557.010	II							
3557.181	I	2		10			IV	
3557.622	II	10		1			IV	
3558.117	II	2					V	
3558.232	II	8		5			IV	
3558.511	I	3		3			IV	
3559.295	II	15		2			IV	
3559.564		1		1			IV	
3560.139	II	10		4*			IV	
3560.207	I							
3560.409	II	1		5			IV	
3561.263	II	2					V	3
3562.696		5		2			IV	
3563.148	II	200	100	40	1		IVE	1
3563.395	I	1		3			IV	
3563.692	II	40	50	3			IVE	1
3564.237	I	8		15			IV	
3564.561	II	2					V	
3564.768	II	1					V	
3565.116	II	1					V	
3565.269	II	1					V	3
3565.686		5		1			IV	
3566.055	II	4					V	
3566.099	II	1					V	
3566.561	II	2					V	
3566.785	I	2		3			IV	
3566.886	II	2					V	
3567.299	I	3		1			IV	
3567.620	I	1		4			IV	
3568.035	II	3					V	
3568.363	II	5					V	
3568.408	II	3					V	
3568.727	I	1		8			IV	
3568.739	I							
3569.010	II	4					V	
3569.332	I	2		6			IV	3
3569.660	II	20	10	8			IVE	1
3571.023	II	3		1*			IV	
3571.063	I							
3571.438	I	1		30	10	4	III	
		3						
3571.667	II	6		10	1*		IV	
3571.740	I							
3572.094	II	1					V	
3572.389	I	1		5			IV	
3572.654	II	2					V	
3573.026	I	6		1*			IV	
3573.063	II							
3573.318	I	1		8	2		III	3
3573.830	II	60	50	4			IVE	1
3574.006	I			2			IV	
3574.153	II	100	60	15			IVE	1
3574.620	II	1					V	
3574.903	II	1					V	
3575.379	II	2					V	
3575.600	I	2		3			IV	
3576.004	I	10		3			IV	
3576.244	II	300	200	50	1		IVE	1
3576.580	II	5					V	
3576.866	II	150	100	25	1		IVE	1
3577.460	II	1					V	
3577.649	II	4					V	
3577.982	II	60	30	25			IVE	1
3578.501	I	3		2			IV	
3578.832	I	3		3			IV	
3579.113	I	5		5			IV	
3579.437	I	2		1			IV	
3580.035	II	40	30	8			IVE	1
3581.847	II	1					V	
3582.021	II	10	(10)	2			IVE	1
3583.459	I			10	2		III	3
3584.417	II	40	40	3			IVE	1
3585.058	II	250	100	50	3		IVE	1
3585.778	II	150	80	20			IVE	1
3586.112	II	50	30	10			IVE	1
3589.457	I				5		(III)	3
3590.074	II	30	25	2			IVE	1
3590.658	II	25	20	2			IVE	1
3591.415	II	125	80	20			IVE	1
3591.811	II	40	40	5			IVE	1
3591.982	I	1		10			IV	
3592.107	II	30	30	10			IVE	1
3592.667	II	2					V	3
3593.047	II	1		1			IV	3
3593.160	I	4		1			IV	
3593.676	II	2		20	1*		IV	
3593.773	I							
3594.283	II	2					V	
3594.480	I	4		5			?	
3594.560	I	5		30	8		III	
3595.036	II	125	125	20			IVE	1
3595.283	II	6		1			V	
3595.648	II	1		1			IV	
3596.058	II	40	30	6			IVE	1
3596.481	II	6		1			IV	
3596.987	II	1					V	3
3597.284	I	3		25	3		III	
3597.537	I				1		(III?)	
3597.742	II	1					(V)	
3597.936	II	8		1			IV	
3598.256	II	10		6*			IV	
3598.319	I							

TABLE A. *Temperature classification of dysprosium lines* — Continued

Wavelength (Air)	Spectrum	Intensity					Temp. Class	Notes	Wavelength (Air)	Spectrum	Intensity					Temp. Class	Notes
		Arc	Spark	Furnace							Arc	Spark	Furnace				
				High	Medium	Low							High	Medium	Low		
3598.726	I	1		2			IV		3622.350	I	}						3
3599.038	II	3		1			IV		3622.560	II	4		2*			IV	
3599.471	II	4		1			IV		3622.588	II	}						
3600.253	II	} 15		10			IV	}	3622.769	II	4					V	
3600.297	II	}							3623.127	I	1		8			IV	
3600.376	II	50*d*?	40	30			IVE	} 1	3623.385	I	2		15	2		III	
3600.632		1					V		3624.267	II	30	30	1			IVE	1
3600.946	II	1					V	3	3624.900	II	2					V	
3601.372	I	{ 2	}	6			IV		3625.528	I	2		6			IV	
		{ 1	}						3625.739	II	4		3			IV	
3601.899	II	1					V		3626.340	II	1		10			IV	
3602.178	I	1		2			IV		3626.711	I	} 3		8*			IV	
3602.823	II	20	(15)	3			IVE	1	3626.783	II	}						
3603.162	I	10		1			IV		3626.872	I	3		15	3		III	
3603.329	I	1		20	6	2	II		3627.127	I	1		2			IV	
3603.655	II	2					V		3627.359	II	3		1			IV	
3603.755	I	1		5			III		3627.897	I	2		6			IV	
3604.342	I	4		3			IV		3628.018	I	3		3			IV	
3604.482	I	1		5			IV	3	3628.565	I	1		15	1		IV	3
3604.873	II	4					V		3629.418	II	100	80	8			IVE	1
3605.120	II	2					V		3630.237	II	250	150	100	3		IVE	1
3606.118	II	150	100	50			IVE	1	3630.476	II	10	(6)	4			IVE	} 1
3606.385	II	2					V		3630.552	I	10		5			IV	} 3
3606.944	I	4		5			IV		3630.843	II	5		2			IV	
3607.141	II	1		1			IV		3632.776	II	25	20	–	}		IIIE	1
3607.688	II	2					V		3632.803	I	5		10				
3608.038	I	} 4		4*			IV		3633.018	II	15	25	1			IVE	1
3608.089	II	}							3633.274	II	8		1			IV	
3609.247	I	8		1			IV		3633.758	II	10		1			IV	
3610.795	II	1					V		3634.322	II	10					(V)	}
3610.915	I			15	4		III		3634.409	I	12		12			III	} 3
3610.989	I			10	2		III		3634.777	I	} 2		1*			IV	
3611.228	I	3		25	6		III		3634.838	II	}						
3611.946	II	3					V		3635.267	II	30	25	5	1		IVE	1
3612.362	I	1*d*		10	1		IV		3635.633	II	} 1		1*			IV	3
3612.780	II	25	(35)	1			IVE	1	3635.742	I	}						
3613.079	II	15	20	1			IVE	1	3636.254	II	15		3			IV	3
3613.618	I	1		1			IV		3637.275	II	20	(12)	6			IVE	1
3614.074	II	30	(30)	1			VE	1	3638.535	II	2					V	
3614.702	II	} 5		30	1*		IV		3638.801	I	} 2		3*			IV	
3614.774	I	}							3638.917	II	}						
3614.947	II	} 6		30	1*		III?		3639.814	II	6	}	1			IV	
3615.052	I	}						3	3639.902	II	4	}					
3615.186	II	1					V		3640.248	II	100	60	40			IVE	1
3615.564	II	1					V		3640.830	II	10					V	
3616.078	I	8		3			IV		3641.072	II	2		1			IV	
3616.366	I	5		1			IV		3641.633	II	3					V	
3617.203	I	4		2			IV		3641.830	I	4		25	6		III	
3617.633	I	5		1			IV		3641.984	I			3			IV	
3617.780	II	3					V		3642.623	I	3		3			IV	
3618.104	II	30	(30)	3			IVE	1	3643.524	I	3		30	6		III	
3618.509	II	30	(12)	30			IVE	1	3643.923	II	40*d*	15	20			IVE	1
3619.451	II	6	(4)	2			IVE	1	3644.181	II	1					V	
3619.975	II	10	(10)	1			IVE	1	3644.498	I	2*d*		1			IV	
3620.161	II	60	40	8			IVE	1	3644.899	II	1					V	
3620.544	I	} 6		4*			IV		3645.398	II	1000	800	100	30		IIIE	1
3620.575	II	}							3545.860	II	30	20	3			IVE	1
3621.090	I	3		12			IV	3	3646.294	I	1		3			IV	
3621.566	II	1					V	3	3646.612	II	15	15				VE	1
3621.792	I	1		15			IV		3646.895	I	3		1			IV	
3622.045	I	} 1		{ 3			(IV)		3647.258	II	1					V	
3622.123	I	}		{ 15			IV		3647.600	I	2*d*		10	3		III	

TABLE A. *Temperature classification of dysprosium lines*—Continued

Wavelength (Air)	Spectrum	Intensity					Temp. Class	Notes
		Arc	Spark	Furnace				
				High	Medium	Low		
3647.977	I	3		8	1		IV	
3648.365	II	4		1			IV	
3648.459	II	5						
3648.785	II	60	50	3			IVE	1
3650.052	II	6*d*		1			IV	
3650.415	II			5			IV	
3651.133	II	1					V	
3651.742	II							
3651.866	I	2		5*			IV	3
3651.966	I							3
3652.292	I	2		15	1		IV	
3652.828	II	2					V	
3653.278	I	1		1			IV	
3653.727	II	2					V	
3653.874	II	4*d*					V	
3653.898	II							
3654.184	II	8		1			IV	
3654.876	II	10		1			IV	
3655.618	I	6		10	2		III	
3655.907	II	2					V	
3656.358	I	3		1			IV	
3656.877	II	4		6*			IV	3
3656.956	I							
3657.795	II	2,2					V	
3658.151	II	2		1			IV	
3658.502	I	1		15	4		III	
3658.712	I	2		4			IV	3
3658.943	I			3			IV	
3659.299	II	1					V	
3659.848	I	3		6	1		III	
3660.251	II	1					V	
3660.674	I	1		4			IV	
3661.080	II	2					V	
3661.235	I	3		2*			IV	
3661.268	II							
3661.780	II	15	15	1			IVE	1
3662.261	I	2		3			IV	
3662.851	II	1					V	
3663.347	I	1		8			IV	
3663.739	II	1					V	
3664.248	II	1					V	
3664.615	II	6*d*	50	4			VE	1
3664.680	II			3				
3664.985	I	1		25	6		III	
3665.008	I							
3665.233	II	30	30				VE	1
3665.401	I	5		5			IV	
3666.031	I	1		1*			IV	
3666.053	II							
3666.333	II	4		1*			IV	
3666.364	I							
3666.839	I	6		30	15	3	III	
3666.998	II	3*d*					V	
3668.093	I	1		4			IV	
3668.542	II	3					V	
3668.726	II	2					V	
3668.903	II	6	(4)	2			IVE	1
3669.175	I	1		3			IV	
3669.664	II	1					V	
3670.515	I	1		3			IV	
3670.903	II	1					V	
3671.689	II	20	15	3			IVE	1
3672.300	II	125	80	15			IVE	1
3672.700	II	40	20	10			IVE	1
3672.920	I	1		6			IV	
3673.140	II	40	15	8			IVE	1
3673.768	I	2		1*			IV	
3673.814	II							
3674.085	II	250	60	80	1		IVE	1
3674.452	I	8		4	12	2	III	
3675.137	II	1					V	
3675.383	II	1					V	
3675.569	I	2		3			IV	
3676.023	II	4					V	
3676.430	II	10*d*		5			IV	
3676.590	II	250	60	60			IVE	1
3677.042	I			4			IV	
3677.266	I	4		3			IV	
3678.019	II	3					V	
3678.121	I	1		1			IV	
3678.357	II	2?					V	3
3678.507	I	10		10	15	3	II	
				4				
3679.119	II	1					V	
3679.273	II	2					V	
3680.613	II	2		2*			IV	3
3680.655	I							
3680.804	II	1		1			IV	
3681.038	II	2					V	
3681.420	II	1					V	
3681.710	II	1					V	3
3681.951	II	2					V	
3682.612	II	2		4			IV	
3683.089	I	2		8	1		IV	
3683.402	II	10*d*					V	
3684.400	II	2		1			IV	
3684.853	I	8*d*		3	3		(IV)	
				12				
3685.782	I	30		30	30	8	II	
				50				
3686.441	II	1					V	3
3686.890	II	1					V	
3687.151	I	1		2			IV	
3687.440	I	1		8			IV	
3687.659	I	1		4			IV	
3688.306	I	5		10	1		IV	
3688.593	I			6	1		IV	
3689.031	II	3					V	
3689.300	I			8			IV	
3689.465	I	3		5	1		IV	
3689.888	I	1		5	1		IV	
3690.297	II	2*d*					V	
3690.361	II							
3690.576	I	3		4			IV	
3691.236	I	4		2			IV	3
3691.584	II	1					V	3
3692.076	II	3					V	
3692.260	II	3					V	
3692.289	I	3		8			IV	
3692.484	I			10	2		III	
3692.986	I	2		1			IV	
3693.531	I	1		6			IV	3
3693.874	I	4		20	3		III	
3693.970	II	2					V	

TABLE A. *Temperature classification of dysprosium lines* – Continued

Wavelength (Air)	Spectrum	Intensity					Temp. Class	Notes
		Arc	Spark	Furnace				
				High	Medium	Low		
3694.371	II	25*d*	20	1			IVE	1
3694.415	II							
3694.810	II	500	300	60	5		IIIE	1
3695.658	II	6		1			IV	
3696.083	I	2		1			IV	
3696.587	II	1					V	
3696.885	II							
3696.947	II	10*d*		8	1*		III	
3696.962	I							
3697.314	II	30	20	2			IVE	1
				5				
3697.637	I	1		5			IV	3
3697.958	II	3					V	
3698.207	II	60	50	5			VE	1
3698.304	I	?		1			IV	
3698.714	I	2		4*d*			IV	
3698.980	I	5		6			IV	
3699.723	I	1		3			IV	3
3700.577	II	10		8	1*		III	
3700.727	I							3
3701.627	II	40	30	3			IVE	1
3701.903	II	2					V	
3703.235	I	1		15	2		III	
3704.526	I	2		6*d*			IV	
3704.699	I							
3705.807	I	5		5	1		III	
3705.830	II	2					(V)	
3706.385	I	1		1			IV	
3706.798	I	2		20	1		IV	
3707.212	I	1		2			IV	
3707.404	II	30	20	5			IVE	1
3707.573	II	20	(15)	15			IVE	1
3708.220	II	40	30	10			IVE	1
3710.071	II	30	25	3			IVE	1
3710.744	II	10					V	
3711.662	II	30	20	2			IVE	1
3711.814	I	1		2			IV	
3713.843	II	15	10	15	3*		IIIE	1
3713.865	I							
3714.430	I	1		4			IV	
3715.313	II	15	10	1			VE	1
3716.941	II	20	20	1			VE	1
3717.284	I	2		30	8	2	III	
3718.135	II	8		1			IV	
3718.691	II	4					V	
3718.919	I	1		12			(III)	
3719.431	I	4		6	1		IV	
3720.834	I	2		25	10	5	III	
3721.712	I	2*d*		3			IV	
3721.809	I	1		3			IV	
3722.672	II	15					V	
3722.784	I	1		5			IV	
3724.446	II	150	80	50	1		IVE	1
3724.891	I	2		8	1		III	
3725.441	II	15		1			V	
3725.935	I	4		40	5	1	III	
3726.178	I	2		20	2		III	
3726.548	II	3					V	
3727.091	II	2					V	
3727.999	I	5		50	8	3	III	
		8						
3728.432	II	3					V	
3728.467	II	4					V	

Wavelength (Air)	Spectrum	Intensity					Temp. Class	Notes
		Arc	Spark	Furnace				
				High	Medium	Low		
3729.270	II	2					V	
3730.606	II	12		10	1*		IV	
3730.673	I							
3731.139	II	4		1			IV	
3731.292	I	4		5			IV	
3732.075	I	1		3			IV	
3733.336	I	2		8	1		IV	
		3						
3734.269	I	5*d*		15	2		III	3
3734.378	II	4					V	
3735.993	I	2		6			IV	
3738.292	II	3					V	
3738.594	II	3					V	
3739.344	I	20		60	20	10	III	
3739.858	II	5					V	
3740.064	I	12		40	15	8	II	
3740.379	II	1		2*			IV	
3740.529	I	1						
3741.201	I	8		15	5	1	III	
3741.894	I	15*d*					V	
3742.350	I	1		10	1		IV	
3743.053	II	2		2	2*		II	
3743.115	I							
3743.868	I	1					V	
3744.930	I	3		4			IV	
3745.497	I	5		15*			IV	
3745.540	II							
3745.819	II	8					V	
3747.817	II	100	40	20			IVE	1
3748.056	II	20	20				VE	1
3748.550	I	1		6			IV	
3748.779	I	1					V	
3750.316	II	15	15				VE	1
3750.346	II							
3751.802	II	20		1			IV	
3752.382	I	2		5			IV	
3752.808	I	2		40			IV	
3753.506	II	150	60	15			IVE	1
3753.749	II	200	100	4			IVE	1
3754.809	I	8*d*		10	1		IV	
3755.137	II	3					V	
3755.381	I	4		10			IV	
3756.094		2		3	1		III	
				2				
3757.054	I	8		20	30	20	II	
3757.372	II	500	300	60	2		IVE	1
3758.988	II	5		1			IV	
3760.086	II	2		1			IV	
3760.362	I	2					V	
3760.850	II	1					V	
3761.407	I	2		5	2		(III)	3
3761.517	I	1		6	1		III	
3762.234	II	8*d*		1*			IV	
3762.274	I							
3762.691	II	10*d*					V	
3762.766	II							
3764.316		8		1			IV	
3764.835	I	6		8			IV	
3765.969	I	1		5	1		IV	
3766.214	I	3		8	2		III	
3767.628	I	15		30	20	8	II	
3768.507	I	1		1			IV	

TABLE A. *Temperature classification of dysprosium lines* – Continued

Wavelength (Air)	Spectrum	Intensity					Temp. Class	Notes
		Arc	Spark	Furnace				
				High	Medium	Low		
3769.095	I	1		10			IV	
3769.370	I	1		8	–1		IV	
3770.701	I			3			IV	
3771.107	I	4		15	6	2	II	
3771.164	I	2		8?	2		III	
3772.105	I	2		2			IV	
3772.642	I	2		12	3	1	II	
3773.052	I	115		40	20	8	II	
3773.303	II	25	20	6	1		IVE	1
3773.766	I	1		4	1		III	
3774.843	II	10		1			IV	
3775.937	I	} 2		1*			IV	
3776.030	II							
3776.921	II	4					V	
3777.434	I	5d?		25?	2		III	
3779.032	II	3					V	3
3779.232	II	10	(8)	1			IVE	1
3779.671	I	1		6			IV	
3780.308	I	3		20	4		III	
3780.944	I	2		15	4		III	
3781.468	I	10		12	6		III	
3782.154	II	1					V	
3782.871	II	10	(5)	4			IVE	1
3783.595	II	12					V	
3783.941	I	} 8		6	1*		IV	
3783.972	II							
3784.559	I	2		4	1		III	3
3785.214	I	2		2			IV	
3785.411	II	15	(8)	4	1		IIIE	1
3786.176	II	300	150	100	5	1	IIIE	1
3786.826	I	2		8	2		III	
3787.256	II	5		1			IV	
3788.436	II	150	80	80	?		IIIE	1
3789.850	I	} 2		2*			IV	
3789.894	II							
3791.871	II	50	25	8			IVE	1
3793.513	II	2					V	
3794.222	II	3					V	
3795.428	II	3					V	
3795.989	I	} 1		2?*			IV	
3796.048	II							
3796.817	I	2		15	4	1	III	
3797.750	I	3		12	6	1	III	
3798.312	II	2					V	
3798.567	I	2		6	2		III	
3799.014	II	2					V	
3799.564	II	3					V	
3799.903	I	1		4	2		III	
3800.404	I	2					V	
3801.571		2					V	
3801.926	II	5					V	
3802.693	II	1		1			IV	
3803.549	I	1		8	2		III	
3804.142	II	40	20	10	2		IIIE	1
3804.352	I	4			1		IV	
3805.832	I	1		3	1		IV	
3806.271	II	50	100	1?			IVE	1
3807.474	I	2		?			?	
3809.020	II	25	20				E	1
3813.672	II	40	30	3			E	1
3816.762	II	200	150	10			E	1
3822.580	II	20	15	5			E	1

Wavelength (Air)	Spectrum	Intensity					Temp. Class	Notes
		Arc	Spark	Furnace				
				High	Medium	Low		
3825.680	II	30d	15	?			E	1
3825.951	II	20?	30				E	1
3831.641	II	20	15	5			E	1
3836.504	II	60	(35)	5?			IIIE	1,2
3838.658	II	5					VE	2
3840.894	I	10		5?			II	2
3841.310	II	40	(25)	3			IVE	1,2
3842.004	I	20		2?			III	2
3844.363	I	6		3			II	2,3
3846.342	II	15	(10)				VE	1,2
3847.022	I	8		6			II	2
3848.398	I	2		3			III	2
3849.388	II	15	(15)				VE	1,2
3850.036	II	5					VE	2
3850.420	II	4					VE	2
3850.515	II	5					VE	2
3853.027	II	50	(35)	3			IVE	1,2
3854.935	II	4					VE	2
3855.636	II	5					VE	2
3858.104	II	5					VE	2
3858.404	I	15		8?			II	2
3862.700	I	5		3			III	2
3863.245	II	4					VE	2
3865.482	II	8					VE	2
3866.580	II	20	(15)				VE	1,2
3867.855	II	5					VE	2
3868.450	II	25	(15)	2?			IVE	1,2
3868.808	I	50		12?			II	2
3869.137	II	3					VE	2
3869.424	II	10	(6)				VE	1,2
3869.864	II	25	(12)	?			VE	1,2
3871.628	II	10	(7)				VE	1,2
3872.107	II	300	(250)	?			IVE	1,2
3873.986	II	40	(25)	?			IVE	1,2
3875.179	II	4					VE	2
3877.943	II	2					VE	2
3879.058	II	20d	(20)				VE	1,2
3881.993	II	12	(10)				VE	1,2
3883.066	II	4					VE	2
3887.540	I	8		1			IV	2
3888.426	II	6	(8)				VE	1,2
3888.951	I	12		2			IV	} 2
3889.013	II	20	10	6			(IV)E	} 1
3891.865	II	3					VE	2
3891.969	I	6		5			III	2
3892.901	I	12		8?			II?	2
3893.382	I	1		6			IIIA	2
3894.530	I	2		6			IIIA	2
3895.373	II	15	(18)				VE	1,2
3896.218	I	1		6			IIIA	2
3896.651	I	2		6			IIIA	2
3898.529	II	300	(240)	20			IVE	1,2
3899.120	I	} 6		{ 4			III	} 2
3899.169	I			{ 6			III	
3902.400	II	2					VE	2
3903.072	II	1					(?)	
3903.330	I	8		15			III	
3904.084	I	2		8			III	
3904.210	II	20	15	1			VE	1
3905.172	I	1		2			(IV)	
3905.598	II	?		1?			VE	
3905.941	I	3		10			III	

TABLE A. *Temperature classification of dysprosium lines* —Continued

Wavelength (Air)	Spectrum	Intensity					Temp. Class	Notes
		Arc	Spark	Furnace				
				High	Medium	Low		
3907.573	I	1		4			(III)	
3909.135	II	2		1			(IV)	
3910.106	I	4*d*		12			III	
3910.547	II	2					VE	
3911.672	I	2		5			III	
		3		5				
3912.298	I	2		5			(III)	
3912.545	I	10		10			III	
3912.866	II	5					VE	
3913.062	I			2			(III)	
3913.625	I	10		20			III	
3913.974	II	5	(7)				VE	1
3914.866	II	40	(20)	3			IVE	1
3915.594	II	40	(20)	4			IVE	1
3917.292	I	30		30			III	
3917.376	I	20		15			III	
3917.985	I	1		1			(IV)	
3918.555	II	6					VE	
3919.125	I	5*d*		5			(III)	
3919.156	I			15			III	
3920.114	I	2		5			III	
3920.860	I	4		6			III	
3921.313	I	1		2			(III)	
3922.049	I	2		5			(III)	
3922.617	II	2					(V)	
3923.291	II	3					VE	
3923.380	II	10	(10)				VE	1
3924.409	I	4		(6?)			IIIA	2
3924.466	II	3					VE	
3925.261	I	1		3			(III)	
3925.563	II	3*d*					(V)	3
3926.771	I	2		3			(III)	
3927.300	II	1					(V)	
3927.861	I	10		8			III	
3928.005	II	3					V	
3929.333	II	5	(7)				VE	1
3929.716	II	2					(V)	
3930.146	I	15		8			III	
3931.281	II	8	(6)	2			IVE	1
3931.524	II	150	125	5			IVE	1
3932.078	II	3					(V)	
3932.216	II	10	(10)				VE	1
3932.995	II	6					VE	
3934.207	II	8	8				VE	1
3934.373	I	3		5			(III)	
3936.054	II	5	(5)				VE	1
3936.295	II	4					VE	
3936.700	I	10		8			III	
3937.164	I	4		5			III	
3937.984	I	3		5			III	
3938.046	II	4					VE	
3938.203	I	6		4			III	
3938.842	I	1		1			IV	
3939.260	I	1		3			IV	
3939.794	I	2		6			IV	
3942.045	II	3					VE	
3942.527	II	25	(20)	2			VE	1
3944.683	II	600	(450)	50			IIIE	1
3945.634	II	1					(V)	
3945.913	I	3		4			IV	
3946.343	I	2		5			(III)	
3946.929	II	15	(20)				VE	1
3949.248	I	1		2			(III)	
3949.700	I	1		2			(III)	
3950.389	II	20	(20)	1			VE	1
3951.342	I	1		1			(IV)	
3951.837	I	1		2			(III)	
3952.135	I	1		3			(III)	
3952.481	II	1					(V)	
3953.128	II	3					(V	
3953.191	I			3			(III)	
3953.500	I	4		6			III	
3953.970	I	1		1			(IV)	
3954.552	II	20	(15)				VE	1
3955.100	I	2		2			(IV)	
3955.353	I	1		1			(IV)	
3955.484	II	1					(V)	
3956.252	I	2		4			(III)	
3956.809	II	3					(V)	
3957.240	II	3					(V)	
3957.790	II	30	(30)	1			VE	1
3957.996	I	2		4			III	
3958.832	II	1					(V)	
3959.380	II	4					VE	
3959.700	II	2					(V)	
3960.827	II	1					(V)	
3961.802	I	5		5			III	
3962.152	I	1		1*			(IV)	3
3962.454	II							
3962.590	I	10		8			III	
3962.791	I	2		2			(IV)	
3963.165	I	3		4			(III)	
3963.807	II	4					VE	
3964.712	II	3					VE	
3965.155	I	1		2			(III)	
3966.356	I	5		6			III	
3967.512	I	10		10			III	
3968.391	II	1000	800	20			IIIE	1,2
3969.227	I	10		5			III	
3971.214	I	8		10			III	
3971.613	I	2		3			(III)	
3972.415	I	4		6			III	
3973.313	I	1		1			(IV)	
3973.877	I	12		10			III	
3975.075	I	2		5			(III)	
3976.962	I	2		4			III	
3978.566	II	250	200	5			IVE	1
3979.471	II	10	(6)	2			VE	1
3979.945	I	2		4			(III)	
3980.369	I	1		1			(IV)	
3980.695	I	1		1			(IV)	
3981.366	I	3		20			III	
3981.924	II	100	80	2			IVE	1
3982.512	I	2		?			(?)	
3982.843	I	1		1			(IV)	
3983.652	II	100	(70)	4			IVE	1
3984.210	II	60	(40)	1			IVE	1
3984.691	II	3		1			VE	
3985.356	I	2		4			III	
3986.059	I	4		6			III	
3987.070	II	3					VE	
3987.541	I	1		2			(III)	
3988.207	I	2		4			(III)	

TABLE A. *Temperature classification of dysprosium lines* – Continued

Wavelength (Air)	Spectrum	Intensity					Temp. Class	Notes
		Arc	Spark	Furnace				
				High	Medium	Low		
3988.880	I	6*d*		5?			III	
3988.931	I							
3989.683	I	2		5			(III)	
3990.336	II	3					VE	
3990.734	I	1		1			(IV)	
3991.316	II	30	25				VE	1
3991.849	II	3					VE	
3992.457	I	1		1			IV	
3993.274	II	1					VE	
3993.571	I	8		6			III	
3993.680	I			2			(III)	
3993.854	I	1		3			III	
3994.531	I	4		6			III	
3995.333	I	1		1			(IV)	
3995.757	II	3					(V)	
3995.990	I	5		8			III	
3996.688	II	150	100	4			IVE	1
3996.920	I	2		5			III	
3998.060	II	3					VE	
3998.204	I	2		4			(III)	
3998.938	I	1		5			III	
3999.847	II	2					(V)	
4000.450	II	800	600	10			IIIE	1
4000.589	I	1		4			III	
4001.188	I	1		1			(IV)	
4001.521	I	2		4			III	
4002.179	I	1		3			(III)	
4004.297	I	3		5			(III)	
4004.452	I	1		2			III	
4005.838	I	12		8			III	
4006.071	I	10		8			III	
4006.444	I	2		6			(III)	3
4006.738	II	4					(V)	
4007.136	I	4		6			III	
4007.759	II	6					VE	
4008.478	I	2		5			(III)	
4009.330	I	1		3			(III)	
4009.855	I	3		5			(III)	
4010.067	II	5					VE	
4011.161	I			1			(III)	
4011.288	II	20	(15)				VE	1
4011.816	I	1		2			III	
4012.524	I	2		5			III	
4012.816	II	2*d*					(V)	
4013.826	I	15		40*r*			II	
4014.097	I	1		6			III	
4014.704	II	20	(12)	1			VE	1
4015.172	II	4					VE	
4016.748	I	2		1*			(IV)	3
4016.895	II							
4017.054	I	3		5			III	
4017.752	II	1					(V)	
4018.476	I	1		1			(IV)	
4019.396	II	2					VE	
4019.548	II	2					VE	
4020.032	I	1		1			(IV)	
4020.868	II	5					VE	
4020.897	I	1		5			III	
4022.554	I	1		2			(III)	
4023.587	I	2		5			(III)	
4023.713	I	10		15			III	
4024.428	II	10					VE	
4024.899	I	8		6			III	
4025.391	I	2		4			III	3
4025.603	I	4		4			III	
4026.054	I	1		2			(III)	3
4026.754	I	1		2			(III)	3
4027.779	II	15	(12)				VE	1
4028.316	II	8					VE	
4028.412	I	12		10			II	
4031.075	I	3		8			III	
4032.471	II	30	(30)	1			VE	1
4032.840	I	4		2			III	
4033.551	I	1		2			III	
4033.655	II	10					VE	
4036.325	II	15					VE	
4037.624	I	3		2			III	
4038.512	II	8					VE	
4038.708	I	1		5			III	
4038.828	I	4		3			III	
4040.771	I	2		3			(III)	
4041.975	II	10					VE	
4043.035	I	1		3			IIIA	2
4043.388	II	2*d*					(V)	
4045.271	I	2		4			III	
4045.971	I	400		200			II	
4047.391	II	2					(V)	
4047.731	II	3		2			III	
4048.377	II	3*d*?					(V)	
4048.931	I	5		5			III	
4049.362	I	5		8			II	
4050.564	II	150	(90)	3			IVE	1
4052.448	I	1		3			III	
4054.988	I	8		5			III	
4055.144	II	30	(20)				VE	1
4057.373	II	3					VE	
4057.441	II							
4058.159	I	2		1			(IV)	
4060.566	II	5					VE	
4061.045	I	2		3			III	
4065.158	I	2		2			III	
4065.391	I	4		5			III	
4066.745	I	2		4			III	
4067.960	I	2		4			III	
4071.021	I	3		4			III	
4072.609	II	3					VE	
4073.116	II	150	80	10			IVE	1
4073.985	II	3					VE	
4077.340	I	2		3			IV	
4077.964	II	800	500	20			IIIE	1
4079.258	I	3		5			III	
4079.586	I	3		5			III	
4081.730	I	2		2*			(IV)	
4081.835	II							
4083.100	I	4		6			III	
4083.802	I	2		4			III	
4085.130	I	15		15			III	
4085.336	I	20		20			III	
4087.199	II	15	(12)				VE	1
4087.381	I	5		6			III	
4089.502	I	3		5			III	
4090.389	I	1		3			III	
4091.520	II	10	(8)				VE	1
4091.759	II	6					VE	

378-324 O - 70 - 5

TABLE A. *Temperature classification of dysprosium lines* – Continued

Wavelength (Air)	Spectrum	Intensity					Temp. Class	Notes
		Arc	Spark	Furnace				
				High	Medium	Low		
4093.638	I	3		5			III	
4095.244	I	1		3			III	
4096.099	I	20		15			III	
4096.624	I	{ 2 2 }		5			III	
4099.880	I	4		10			II	
4101.393	I	2		4			III	
4101.840	I	1		3			III	
4101.933	II	2					VE	
4103.304	II	600	400	150			IVE	1
4103.874	I	60		6?			III	
4105.017	I	?		5			III	
4105.035	II	8	(6)				VE	1
4105.256	I	3					(V)	
4105.804	I	2		3			III	
4105.988	I	2		2			(III)	
4106.378	II	5					VE	
4106.679	II	3					VE	
4107.170	II	2					(V)	
4107.359	II	3					VE	3
4109.134	I	1		1			(III)	
4111.343	II	150	(100)	40			VE	1
4113.054	I	5		8			III	
4114.052	II	{ 4*d*					VE	
4114.117	II	}						
4114.642	I	3		6			IV	
4119.310	II	10	(8?)				VE	1
4120.652	I	1		4			III	
4124.626	II	20	(10)	2			IVE	1
4126.086	I	8		15*r*			II	
4128.238	II	20	(10)	1			IVE	1
4129.117	I	10		15*r*			II	
4129.422	II	100	50	3			IVE	1
4130.351	I	10		12*r*			IIA	2,3
4131.021	II	6					VE	
4132.835	II	3					VE	
4133.353	II	6					VE	
4133.849	I	15		8			III	
4134.146	I	10		4			III	
4134.708	I	4		4			III	
4136.901		1					IV	
4137.349	II	4					(V)	
4138.539	I	4		6			III	
4139.558	I	4		6			III	
4141.385	I	3		6			III	
4141.505	II	20	(8)	2			IVE	1
4143.099	II	300	(160)	5			IVE	1
4145.621	II	2					VE	2
4146.060	I	100		30*r*			II	
4147.968	I	3		4			III	
4148.957	I	2		4			(III)	
4149.776	I	2		4			III	3
4152.424	II	8					VE	
4153.122	I	5		4			III	
4153.375	I	4		5			III	
4154.202	II	5					VE	
4154.242	I	3		4			III	
4154.515	I	3		4			III	
4156.361	I	4		3			III	
4156.952	I	5		6			III	
4157.862	II	4					VE	
4158.055	I	6		5			III	
4159.313	I	8		8			III	
4160.247	I	3		3			III	
4162.246	I	4		4			III	
4164.732	I	3		4			III	
4166.234	I	4		3			III	
4167.225	II	2	}				(VE)	3
4167.552	II	2						
4167.974	I	400		100*R*			II	
4169.043	I	3		5			III	
4169.247	II	5					VE	
4170.317	I	2		5			III	
4170.562	I	3		4			IV	
4171.930	I	6		8			III	
4172.002	I	8		8			III	
4176.601	I	4		3			III	
4176.784	I	3		3			III	
4177.766	I	3		3			III	
4178.086	I	6		4			III	
4181.269	I	3		5			III	
4182.404	II	3					VE	
4183.599	I	8		10?			III	
4183.723	I	30		30*r*			II	
4186.818	I	600		300*R*			II	
4189.396	I	3		4			III	
4190.939	I	10		8			III	
4191.642	I	100		50*R*			II	
4194.845	I	500		200*R*			II	
4195.254	I	8		?			III	
4198.019	I	25		15			II	3
4201.027	I	3		5			III	
4201.304	I	15		15			III	
4201.372	II	10					VE	
4202.241	I	20		20*r*			II	
4204.001	I	2		4			III	
4205.062	I	15		10			III	
4206.542	II	30	(15)	6			IVE	1
4207.696	I	6		6			III	
4211.239	I	15		30*r*			II	
4211.715	I	1200		600*R*			II	
4213.179	I	60		50*R*			II	
4214.410	I	5		12			III	
4215.159	I	80		100*R*			II	
4216.985	I	2		4			III	
4218.091	I	200		150*R*			II	
4218.574	II	4					VE	
4221.108	I	250		200*r*			II	
4222.210	I	20		15			III	
4224.672	I	3		4			III	
4225.155	I	150		100*r*			II	
4232.024	I	30		15			II	
4234.132	I	3		4			III	
4234.831	I	5		4			III	
4236.264	I	2		4			III	
4236.579	I	1		4			III	
4237.523	II	3					VE	
4237.945	I	2		3			III	
4238.070	II	2					VE	
4238.455	II	3					VE	
4239.852	I	40		30*r*			II	
4240.685	I	1		2			III	
4240.850		1		5			III	

TABLE A. *Temperature classification of dysprosium lines* – Continued

Wavelength (Air)	Spectrum	Intensity					Temp. Class	Notes
		Arc	Spark	Furnace				
				High	Medium	Low		
4241.818	I	1		5			III	
4242.716	I	3		4			III	
4242.990	I	3		4			III	
4243.435	I	5		10			III	
4244.792	II	2					VE	
4245.912	I	30		20			III	
4247.345	II	10	(8)				VE	1
4248.451	II	3					VE	
4248.893	I	1		2			III	
4250.337	I	3		3			III	
4250.459	I	2		5			III	
4251.319	I	3		8			III	
4251.733	I	5		6			III	
4252.122		1		3			III	
4254.923	I	1		3			III	
4255.955	II	2					VE	
4256.205	II	5					VE	
4256.330	II	15	(5)	3			IVE	1
4257.698	II	1					VE	
4257.785	I	1		10			III	
4258.149	I	5		10			III	
4258.514	I	1		5			III	
4258.577	I	10		10			III	
4259.768	I	1		3			III	
4259.831	I	1		3			III	
4260.715		1		2			III	
4264.834	I	1		2			III	
4265.789	II	2					VE	
4266.007	I	1		4			III	
4267.870	I	4		3			IV	
4268.264	I	5		10			III	
4269.545	I	6		8			III	
4272.976	I	3		4			III	
4273.133	II	5					VE	
4274.954	I	4		6			III	
4275.405	I	3		3			III	
4275.918	I	1		3			III	
4276.688	I	15		15			III	
4277.715	I	1		3			III	
4279.730	I	6		8			III	
4282.057	I	1		3			III	
4283.259	I	1		5			III	
4283.575	I	2		5			III	
4284.232	I	1		3			III	
4288.019	I	1		3			III	
4288.185	I	1		2			III	
4288.719	I	2		3			III	
4290.442	I	5		8			III	
4290.952	II	1		3			III	
4291.955	I	8		15			III	
4294.456	I	1		2			III	
4294.928	II	10	(10)				VE	1
4295.036	I	25		8			III	
4296.353	I	1		3			III	
4297.775	I	1		3			III	
4298.518	I	5		3			III	
4298.910	I	2		5			III	
4300.380	II	3					VE	
4300.634	II	1		4			III	
4300.736	II	3					VE	
4301.340	I	1		2			III	
4302.581	II	12					VE	
4302.714	II	8					VE	
4306.766	I	1		3			III	
4308.349	I	2		5			IIIA	2
4308.626	II	200	100	8			IVE	1
4311.946	I	2		4			III	
4312.431	I	1		4			III	
4313.880	II	2					VE	
4313.931	I	6		6			III	
4315.603	I	1		4			III	
4318.356	I	1		4			III	
4318.991	I	6		4			III	
4322.184	II	5					VE	
4322.367	I	1		4			III	
4322.533	II	8					VE	
4323.795	I	4		5			III	
4324.661	II	1					VE	
4325.108	II	20	(15)				VE	1
4326.375	I	15		4			III	
4328.668	I	1		2			III	
4328.902	II	15	(8)				VE	1
4329.886	II	2 3					VE	
4334.052	I	1		3			III	
4334.358	I	1		6			III	
4335.995	I	1		6			III	
4338.459	I	2		1			(IV)	
4339.622	II	20	(25)				VE	1
4339.654	II							
4340.407	II	2					VE	
4346.371	II	10					(VE)	2
4347.708	I	15		6			III	
4356.109	I	2		6			III	
4356.747	I	3		3			III	
4358.443	II	40	(15)	2			IVE	1
4360.186	II	6					(V)	
4361.343	II	8					VE	
4364.046	II	5					VE	
4364.204	II	15	(20)				VE	1
4365.612	I	2		11			III	
4366.722	I	8		12			III	
4368.256	I	1		2			III	
4369.541	I	2		6			III	
4374.235	II	40	(12)	3			IVE	1
4374.764	II	30	(20)	2			IVE	1
4375.308	II	10	(12)				VE	1
4379.338	I	2		2			(III)	3
4380.221	II	6					VE	
4380.469	I	2		5			III	
4384.295	II	8					VE	
4385.272	II	5					VE	
4389.774	I	5		3			IV	
4390.306	I	1		2			III	
4390.926	I	2		5			III	
4393.265	I	1		3			III	
4394.978	II	15	(6)	5			VE	1
4397.490	I	1		4			III	
4399.713	I	2d?		4			III	
4400.077	II	6					VE	
4403.957	I	1		4			III	
4408.034	II	10					III?	
4409.378	II	100	(50)	5			IVE	1

TABLE A. *Temperature classification of dysprosium lines* – Continued

Wavelength (Air)	Spectrum	Intensity					Temp. Class	Notes
		Arc	Spark	Furnace				
				High	Medium	Low		
4409.909	I	1		2			III	
4411.353	I	3		3			IV	
4411.669	I	1		3			III	
4414.172	I	1		3			III	
4418.095	II	5					(V)	
4421.683	II	4					VE	
4426.866	I	5		3			III	
4430.991	II	15					VE	
4435.774	II	3					VE	
4436.627	II	3					VE	
4444.576	I	25		12			III	
4448.185	II	20					VE	
4449.130	II	10					VE	
4449.702	II	200	(100)	8			IVE	1
4454.332	I	2		4			III	
4455.598	II	20					VE	
4467.870	II	6	(5)				VE	1
4468.137	II	30	(10)	3			IVE	1
4479.464	I	5					(V)	
4480.680	I	8		10			III	
4481.956	II	5					(V)	
4482.290	I	5		2*			IV	
4482.316	II							
4484.357	I	10		10			III	
4486.222	II	5					(V)	
4487.857	I	1		2			III	
4492.144	I	1		5			III	
4493.091	I	5					(V)	
4496.361	I	2		2			IV	
4499.259	I	3		2			III	
4502.602	II	10					(V)	
4503.232	II	50	(30)				VE	1
4503.372	I	1		4			III	
4505.622	II	5					(V)	
4506.063	II	4					(V)	
4506.939	II	8		2			IV	
4508.086	I	?		3			IV	
4513.586	I	4		12			III	
4516.838	I	20		5*			III	
4516.952	II							
4518.506	II	3	(6)				VE	1
4519.815	II	10					VE	
4522.704	I	1		4			III	
4523.075	I	2		3			(III)	
4525.110	I	4		3			IV	
4526.083	I	4		3			IV	
4527.761	II	10?	40?	3			VE	1
		50?						
4531.552	I	5		15			II	
4538.730	II	20	15	3			VE	1
4539.134	II	3		6			IV	
4541.663	II	30	40				VE	1
4545.322	II	6					VE	
4546.424	I	2		2			IV	
4546.760	I	1		3			III	3
4550.866	II	2	(3)	1			VE	1
4553.130	I	4		8			III	
4555.007	I	3		4			III	
4555.219	I	8		8			III	
4556.439	II	4					VE	
4557.324	I	2		4			III	
4559.582	I	3		3			III	
4565.091	I	50		20*r*			II	
4565.937	I	1		5			III	
4566.216	I	6		3			IV	
4567.044	I	5		8			III	
4568.415	I	3		3			III	
4573.850	II	20					VE	
4576.584	II	25					VE	
4577.776	I	200		40*R*			II	
4585.703	I	3		5			III	
4585.959	I	3		4			III	
4586.184	II	3		3			III	
4586.620		10		1			IV	
4587.906	II	40	30				VE	1
4589.088	I			12			III	
4589.355	I	400*d*		150*R*			II	
4590.553	I	5		3			III	
4591.658	I	2		3			III	
4591.776	II	12					VE	
4595.127	II	5					VE	
4599.845	I	8*d*		6			IV	
4601.550	I	1		4			IV	
4602.513	I	3		4			IV	
4604.298	II	4		1			IV	
4606.037	I	10		10			IV	
4611.692	II	1					VE	
4612.258	I	300		100			II	
4613.827	I	6		6			IV	
4614.822	I	10		10			IV	
4615.564	II	5					VE	
4616.929	I	1		2			IV	
4617.264	II	30	20				VE	1
4618.719	II	1					VE	
4620.034	II	60	40	1			VE	1
4620.378	II	1					VE?	
4620.969	I	2		2			IV	
4621.411	II	3					VE	
4622.370	II	5					VE	
4622.732	I	1		5			III	
4624.118	I	6		6			IV	
4624.439	II	4					VE	
4625.661	I	1–		3			IV	
4626.021	I	2		1			IV	
4627.394	I	1		10			IV	3
4628.066	II	5					VE	
4631.489	I	10		12			III	
4634.762	I	2		2			IV	
4635.292	I	5		5			III	
4637.126	I	6		3			IV	
4637.579	II	4					VE	
4638.800	II	5					VE	
4641.072	I	2		6			III	
4642.205	I	1		3			IV	
4642.237	I							
4642.767	II	2					VE	
4643.438	I	6		3			IV	
4644.105	II	1					VE	
4646.714	I	3		2			IV	
4647.281	II	4		4*			IV	3
4647.397	I							

TABLE A. *Temperature classification of dysprosium lines* — Continued

Wavelength (Air)	Spectrum	Intensity					Temp. Class	Notes
		Arc	Spark	Furnace				
				High	Medium	Low		
4649.466	II	2					VE	
4650.148	I	6		15			III	
4651.523	II	15					VE	
4653.406	II	2		1?			IV	
4654.761	II	6					VE	
4655.880	II	2					VE	
4657.445	II	5					VE	
4659.500	I	4		2			IV	
4660.823	I	5		2			IV	
4661.916	II	4					VE	
4662.146	I	4		4			IV	
4662.725	I	8		10			III	
4663.074	II	2					VE	
4664.659	II	80	40	2			IVE	1
4665.893	I	1		3			IV	
4666.532	II	5					VE	
4667.778	II	2					VE	
4668.089	I	2		1*			IV	
4668.162	II							
4669.108	I	1		1			IV	
4669.388	II	2		2			IV	
4671.125	II	2*d*					VE	
4671.528	II	2					VE	
4672.471	I	3		2			IV	
4673.596	II	15					VE	
4674.598	I	2		1			IV	
4675.789	I	8		2			IV	
4679.061	II	1					VE	3
4680.175	I	2		2			IV	
4680.739	I	1		5			III	
4680.961	I	2		4			IV	
4681.863	I	4		4			IV	
4682.028	II	8					VE	
4683.775	II	6					VE	
4685.986	I	1		2			IV	
4689.751	II	40	50				VE	1
4690.243	I	2		2			IV	
4691.596	I	1		1			IV	
4692.728	I	2		2			IV	
4693.659	II	2					VE	
4693.956	I	1		1			IV	
4694.336	II	4		6*			IV	
4694.389	I							
4695.240	II	8					VE	
4697.169	II	1					VE	3
4698.684	II	60	60?				VE	1
4699.297	I	1		3			IV	
4703.471	I	10		6			IV	
4705.729	I	1		1			IV	
4706.773	I	5		8			IV	
4707.791	II	5*d*					VE	3
4709.223	II	6					IVE	
4711.065	I	2		2?			IV	
4711.595	II	2		2?			IV	
4712.505	II	2		1			IV	
4714.789	II	2		?			IV?	
4716.876	II	1		1			IV	
4718.500	I	1		1			IV	
4718.818	I	3		?			IV	
4721.225	I	30		8			IV	
4723.154	II	2					VE	
4723.916	I	5		12			III	
4724.224	I	3		3			IV	
4726.194	II	2					VE	3
4726.352	I	4		6			IV	
4726.765	I	1		3			IV	
4727.127	II	50	150				VE	1
4728.344	II	2					VE	
4728.869	I	6		5			III	
4729.087	I	2		2			IV	
4731.846	II	150	80	10?			VE	1
4732.097	I	5?		4?			IV	
4734.379	I	2		?			IV?	
4734.617	I	1		?			IV?	
4738.466	I	2		3			IV	
4740.926	I	6		6			IV	
4741.538	I	5		5			IV	
4742.397	I	1		1			IV	
4743.018	II	15					VE	
4744.910	I	1		8			III	
4745.784	II	30	25				VE	1
4747.870	I	1		1			IV	
4749.529	I	1		2*d*?			IV	
4754.990	II	20	20				VE	1
4756.672	II	15	10				VE	1
4757.408	I	2		1			IV	
4758.375	I	1		1			IV	3
4760.046	II	50	30	1			VE	1
4761.307	I	2		1			IV	
4762.400	I	1		1			IV	
4763.835	II	3					VE	
4764.365	II	2					VE	
4764.652	I	2		3			IV	3
4765.585	II	1		1			IV	
4767.151	II	2					VE	
4769.622	II	6					VE	
4770.798	II	1					VE	
4771.937	I	20		15			III	
4772.444	I	1		1			IV	
4773.151	II	1					VE	
4774.286	II	2*d*					VE	
4774.804	I	6		3			IV	
4775.789	I	30		20			III	
4776.841	II	1					VE	
4778.813	I	1		1			IV	
4780.145	I	1		1			IV	
4781.023	II	2					VE	
4781.814	I	5		4			IV	
4784.576	I	1		1			IV	
4784.900	II	12					VE	
4785.295	I	4		2			IV	
4786.241	II	2					VE	
4786.919	II	50	25	?			VE	1
4788.393	I	1		15?			IV?	
4789.911	I	1		1			IV	
4790.455	I	1		1			IV	
4791.289	I	30		50			III	
4791.920	I	2		1			IV	
4792.563	I	1		1			IV	
4792.843	I	4		3			IV	
4794.845	I	2		3			IV	
4797.572	II	2					VE	
4798.420	I	2		1			IV	

TABLE A. *Temperature classification of dysprosium lines* – Continued

Wave-length (Air)	Spectrum	Intensity					Temp. Class	Notes	Wave-length (Air)	Spectrum	Intensity					Temp. Class	Notes
		Arc	Spark	Furnace							Arc	Spark	Furnace				
				High	Medium	Low							High	Medium	Low		
4800.639	I	6		6			IV		4875.927	I	3		1			IV	
4802.142	II	1					VE		4877.115	I	1		1			IV	3
4804.512	I	5		5			IV		4879.170	I	1		1			IV	
4806.950	I	1		8			?		4880.161	I	30		30			II	
4807.942	I	12		15			III		4881.981	II	3*d*					VE	
4808.739	I	2		2			IV		4884.152	I	3		10			III	
4810.276	I	3		3			IV		4884.551	I	6		3			IV	
4810.802	II	1		1			IV		4886.144	I	2		2			IV	
4812.801	I	8		30			III		4888.081	I	40		60			III	
4814.150	I	1		12			III	3	4889.327	II	50	60				VE	1
4816.517	I	1		2			IV		4889.783	II	1					VE	
4817.069	I	1		1			IV		4890.102	II	60	15	1			VE	1
4817.464	I	1		1			IV		4892.592	II	2					VE	
4818.203	I	-2		8			IV		4893.676	I	8		6			IV	
4819.041	I	10		10			III		4895.850	I	5		6			IV	
4820.275	I	1		2			IV		4897.121	II	2					VE	
4821.293	I	5		4			IV		4899.245	I	5		3			IV	
4821.907	I	1		1			IV		4901.941	I	6*d*?		25			III	
4823.723	I	2		8			IV		4903.682	I	1		5			IV	
4824.964	I	12		6			IV		4906.252	I	5		30			III	
4826.555	II	5					VE		4907.479	I	2		2			IV	
4828.880	I	8		6			IV		4909.003	II	1					VE	
4829.130	II	2					VE		4909.799	I	2					VE	
4829.682	II	20	20				VE	1	4911.167	I	1		5			IV	
4830.879	II	1					VE		4911.480	II	1					VE	
4832.377	I	15		15			IV		4912.547	II	2					VE	
4833.754	II	15	15				VE	1	4914.729	I	5		40			III	
4836.947	I	1		2			IV		4916.409	I	15		6			IV	
4837.683	I	2*d*		1			IV		4917.175	I	3		20			III	
4839.677	I	1		1			IV		4918.242	I	5		5			IV	
4840.169	I	1					VE		4919.554	I	1		1			IV	
4840.461	II	10		8			IV VE		4921.492	I	2		2			IV	
									4922.221	II	25	50				VE	1
4841.082	I	1		3			IV		4923.160	II	60	25				VE	1
4841.752	I	8		3			IV		4927.332	II	2					VE	
4842.192	I	1		1			IV		4929.322	II	2					VE	
4843.422	II	2					VE		4931.031	I	3		3			IV	
4843.767	I	1					VE		4932.474	I	1		1			IV	
4844.824	II	1					VE		4933.028	I	1		2			IV	3
4845.778	I	2*d*		4			IV	3	4933.845	II	8					VE	
4850.952	I	1		3			IV		4936.108	I	2		2			IV	
4851.435	I	2		2			IV		4936.832	I	1		1			IV	
4852.517	I	2		2			IV		4940.425	I	1		10			IV	
4854.978		1		3*d*			IV		4941.159	I	2		1			IV	
4855.136	I							3	4942.849	I	2		3			IV	
4855.578	I	2		2			IV		4945.502	II	1					VE	
4856.239	II	20	20				VE	1	4946.262	II	4					VE	
4857.373	I	1		1			IV	3	4948.217	I	3		4			IV	
4858.971	I	1		15			III		4949.319	I	1		2			IV	3
4859.150	I	1					VE		4951.016	I	2		1			IV	
4860.051	I	1		1			IV		4951.431	I	2		3			IV	
4861.701	I	1		1			IV		4953.366	I	1		3			IV	
4861.798	I								4954.349	II	2					VE	
4865.682	I	2		1			IV		4957.338	II	1500	500	50			IVE	1
4867.756	I	1		1			IV		4959.587	I	6		5			IV	
4868.050	II	15	15				VE	1	4961.742	I	1		8			IV	3
4868.650	I	1		2			IV	3	4963.081	II	2					VE	
4868.832	I								4964.659	I	1					VE	
4869.660	I	1		1			IV		4969.859	I	2*d*?		10			IV	
4872.476	I	1		1			IV		4971.768	I	4		3			IV	
4873.159	I	3		3			IV		4973.568	I	6		6			IV	
4875.460	II	(?)					VE		4974.990	II	6	(8)				VE	1

TABLE A. *Temperature classification of dysprosium lines* – Continued

Wavelength (Air)	Spectrum	Intensity					Temp. Class	Notes
		Arc	Spark	Furnace				
				High	Medium	Low		
4976.444	I	1		1			IV	
4980.126	I	2		?			IV	
4981.964	I	1		1			IV	
4983.818	I	1		1			IV	3
4984.622	I	1					VE	3
4985.068	I	2		2			IV	3
4985.523	I	10		6			IV	
4988.112	I	1*d*?		3			IV	
4991.819	I	1		1			IV	
4993.518	I	2		8			IV	
4994.808	I	3		2			IV	
4995.359	II	8					VE	
4996.771	I	1*d*?		4			IV	
4997.630	I	1		3			IV	3
4998.462	I	3		10			IV	
4998.976	II	4*d*?					VE	
4999.048				1			IV	
5000.108		1					VE	
5000.925	I	1*d*		5			IV	
5003.867	I	20		25			IV	
5004.285	II	50					VE	
5005.888	I	1		1			IV	
5007.418	II	8					VE	
5009.415	I	1		4			IV	
5010.606	I	4		3			IV	
5011.529	I	1		1			IV	
5012.156	I	2*d*		2			IV	
5012.579	I	1		6			IV	
5017.986	II	10	(8)				VE	1
5019.319	I	1					VE	
5021.835	I	1		30			III	
5022.118	I	50		80			III	
5024.032	I	5		6			IV	
5024.536	I	6		25			III	
5027.874	I	6		6			IV	
5029.233	II	3					VE	
5032.660	I	5		6			IV	
5032.996	I	6		6			IV	
5034.353	I	1*d*		2			IV	
5036.901	I	1		1			IV	
5037.702	I	1*d*		6			IV	
5039.046	I	3		15			III	
5040.529	II	2					VE	
5042.038	I	2		1			IV	
5042.634	I	100		100			III	
5043.624	I	2		3			IV	
5045.498		1		1			IV	
5046.300	II	4					VE	
5047.249	I	8		20			III	
5049.521	I	2*d*		4?			IV	
5050.215	I	10		6			IV	
5051.241	I	1		1			IV	
5052.010	I	4		10			IV	
5053.189	I	2					V	
5053.352	I	5		5			IV	3
5055.462	I	4		3			IV	
5055.859	I	1		2			IV	
5056.180	II	2*d*					VE	
5060.732	I	1		1			IV	
5061.594	II	5					VE	
5063.435	I	3		6			III	
5065.537	I	2		1			IV	
5065.760	I	3		1			IV	
5067.157		1					VE	
5070.678	I	60		80			III	
5071.761	I	1		2			IV	
5072.954	II	1					VE	3
5073.809	I	1		1			IV	
5074.274	I	2					VE	
5077.669	I	60		80			II	
5080.172	II	4					VE	
5084.947	I	2		?			IV	
5086.864	I	2					VE	
5088.419	II	5					VE	
5090.386	II	50	25	1			VE	1
5092.203	II	8	(8)				VE	1
5099.844	II	2					VE	
5102.350	I	4		10?			IV	
5105.331	I	2		5			IV	
5106.347	I	8					VE	
5106.882	I	5		8			IV	
5107.983	II	20	20				VE	1
5108.454	I	2		4			IV	
5110.321	I	15		8			IV	
5112.713	I	1		15			III	
5113.415	II	3					VE	
5120.036	I	100		80			III	
5122.408	I	4		?			IV	
5123.119	I	3		2			IV	
5125.534	I	2*d*?		?			IV	3
5127.487	I	3					VE	
5128.292	I	5		?			IV	
5129.846	II	15	15				VE	1
5130.336	I	2		?			IV	
5131.068	II	4*d*					VE	3
5131.121	I			1			IV	3
5131.928	I	2		3			IV	
5132.221	I	2					VE	
5133.603	I	1					V	3
5135.023	I	15		30			III	
5136.292	II	8					VE	
5139.598	II	200	80	6			IVE	1
5141.524	I	2*d*		8			IV	3
5141.652	I							
5145.212	II	15	20				VE	1
5146.978	I	2		8			IV	
5147.192	I	3		3?			IV	
5148.976	I	2		?			IV	
5149.642	I	1		2			IV	
5150.137	I	6*d*?					VE	
5151.299	I	1					VE	
5151.607	I	2		4			IV	
5154.582	I	1		2			IV	
5155.305	I	60		30			IV	
5156.031	I	1		4			IV	3
5156.805	I	3		4?			IV	3
5157.805	I	1		?			IV	
5158.917	II	4					VE	
5159.162	I	6		25			III	
5161.027	II	25	25				VE	1
5162.338	I	2*d*?		?			IV	
5164.116	II	25	30				VE	1
5165.073	I	1		1			IV	3
5165.338	I	15		15?			IV	
5165.390	I							

TABLE A. *Temperature classification of dysprosium lines* — Continued

Wavelength (Air)	Spectrum	Intensity					Temp. Class	Notes	Wavelength (Air)	Spectrum	Intensity					Temp. Class	Notes
		Arc	Spark	Furnace							Arc	Spark	Furnace				
				High	Medium	Low							High	Medium	Low		
5166.845	II	30					VE		5247.742	I	10*d*?					VE	
5168.110	I	2		2			IV		5248.141	II	20					VE	
5169.584	I	?		10			IV		5248.454	I	5					VE	
5169.688	II	150	60				VE	1	5250.804	I	2		2			IV	3
5170.193	II	5					VE		5254.158	II	1		1			IV	
5171.919	I	4		60			III	3	5255.047	II	15	20				VE	1
5172.895	II	5					VE	3	5255.326	I	1		1			IV	
5173.833	I	5		5			IV		5258.372	II	25	15				VE	1
5175.079	I	8*d*		6			IV		5259.880	I	30		20			III	
5177.575	I	1		1			IV		5260.558	I	100		80			III	
5180.105	I	3*d*		3			IV		5262.519	I	1		1			IV	
5182.231	I	1		1			IV	3	5263.546	I	?		2			IV	
5184.506	I	3		25			III	3	5264.354	I	6		5			IV	
5185.158	I	30		25			III		5265.746	I	2?		1			IV	
5185.615	I	1		1			IV		5267.111	I	80		100			II	
5186.984	II	2					VE		5268.949	I	3		5			IV	
5188.452	II	15	10	3			VE	1	5270.765	I	4		4			IV	
5190.529	I	1–		4			IV	3	5272.248	II	80	30				VE	1
5192.496	I	?		2			IV		5274.068	I	20		60			II	
5192.865	II	1000	400	30			IVE	1	5275.291	II	100	100				VE	1
5194.053	I	1		3			IV	3	5275.916	I	2					VE	
5196.814	I	6		8			IV		5276.846	I	1		4			IV	
5196.969	I			2			IV	3	5277.377	II	15					VE	
5197.664	II	150	80	2			IVE	1	5277.684	I	4		6			IV	
5199.511	I	1*d*		4			IV		5277.883	I	8		6			IV	
5200.826	I	2*d*		2			IV		5278.327	I	3		3			IV	
5202.334	II	2					VE		5279.698	II	125	100				VE	1
5203.449	II	1					VE		5280.391	I	2		2			IV	
5205.663	I	10*d*?		10			IV		5281.594	I	1		1			IV	
5206.857	II	2					VE		5282.072	I	60		100			II	
5212.033	I	3*d*		40			IV		5282.360	I	3		4			IV	
				?			?		5283.296	II	2					VE	
5212.402	I	3		2			IV		5283.753	I	2		2			IV	
5214.428	II	6*d*					VE	3	5284.987	II	50	30				VE	1
5215.412	II	4					VE		5287.967	I	3		3			IV	
5216.212	I	1		6			IV	3	5290.034	I	5		20			III	
5216.427	I	1		4			IV	3	5292.713	I	2		2			IV	
5217.270	I	1		2			IV		5295.610	I	2		3			IV	3
5220.322	II	(1?)					VE		5297.817	II	60	50	50			IIIE	1
5220.704	II	3					VE		5299.039	I	1		1			IV	
5221.980	I	10		60			IV		5300.298	II	20	8				VE	1
5224.228	I	1		5			IV		5300.884	I	5		50			III	
5225.028	I	1		1			IV		5301.576	I	300		200			I	
5225.867	I	1		1			IV		5303.170	I	3		1			IV	
5226.919	I	15		20			IV		5305.727	I	1		1			IV	3
5227.411	I	1		2			IV		5306.600	I	4		2			IV	
5227.827	I	3		3			IV		5308.830	I	4		4			IV	
5229.530	I	2		1			IV	3	5309.015	II	150	150				VE	1
5231.948	I	2*d*?		1			IV		5309.377	I	1		1			IV	3
5232.973	II	5					VE		5310.086	I	4		4			IV	
5234.275	I	1		1			IV	3	5311.849	I	3		15			IV	
5235.488	I	1		1			IV	3	5312.162	II	3					VE	
5236.253	I	25		150			I		5312.627	I	12		8			IV	
5238.372	I	5		50			III		5313.750	I	1		4			IV	
5240.894	I	2		1			IV		5315.991		4*d*?		0			VE	3
5241.463	I	2		1			IV		5316.150	I			1			IV	
5242.071	I			4			IV		5316.981	I	3		15			IV	
5242.485		3					VE		5318.108	I	4		3			IV	
5245.158	II	2					VE		5319.202	I	4		6?			IV	3
5246.387	I	2		3			IV		5319.945	II	1					VE	3
5246.944	II	20	20				VE	1	5320.619	I	1		1?			IV	
									5321.689	I	8		6			IV	

TABLE A. *Temperature classification of dysprosium lines* — Continued

Wavelength (Air)	Spectrum	Intensity					Temp. Class	Notes
		Arc	Spark	Furnace				
				High	Medium	Low		
5322.233	I	6		50			III	
5324.695	II	125	125	2			VE	1
5325.780	I	1		4			IV	
5326.688		3					VE	
5328.938	I	5		25			IV	
5330.734	I	4	(10)				VE	1
5333.083	I	5		5			IV	
5334.085	I	1		1			IV	
5335.053	I	6		6			IV	
5336.513	I	2		2			IV	
5336.786	I	4		12			IV	
5337.432	II	30	20				VE	1
5340.300	I	100		80			III	
5343.154	I	4		20			IV	
5343.557	I	5		25			IV	
5345.562	I	2		1			IV	
5347.561		1					VE	
5348.353	II	4					VE	
5350.295		1					VE	
5352.114	I	40		150			II	
5353.245	I	3		3			IV	
5354.993	I	3		?			IV	
5356.142	I	6		3			IV	
5360.665	II	2					VE	
5361.349	I	3		3			IV	3
5364.852	I	2		1			IV	
5368.085	I	3?		2			IV	
5368.197	II	30					VE	
5369.245	II	5	(12)				VE	1
5370.588	I	8		30			III	
5372.980	I	4					VE	
5376.099	I	10		6?			IV	
5380.660	I	4		8			III	
5381.358	I	2		25			III	
5381.878		2					VE	
5384.844	II	4					VE	3
5385.629	II	40	(14)				VE	1
5386.673		1		1			IV	3
5389.580	II	300	(60)	3			VE	1
5389.744	I	?		15			IV	
5390.092	II	4					VE	
5391.199	I	3		4			IV	
5392.044	I	15		50			II	
5395.126	II	1		1			IV	3
5395.572	I	60		150			I	
5399.934	II	20	10				VE	1
5401.354	I	6*d*?		4			IV	
5404.192	I	40		200			I	
5407.749	I	10		8			IV	
5409.681	I	3		3			IV	
5410.766	II	4*d*					VE	3
5412.474		2		?			VE?	
5416.559	I	1		1			IV	3
5416.938	I	3		2			IV	
5418.722	I	4		3			IV	
5419.133	I	80		60			III	
5419.298	I	?		10			IV	
5420.770	I	8		60			III	
5421.989		2		3			IV	
5423.319	I	150		200			I	
5424.273	I	20		20			III	
5424.699	I	2		1			IV	
5425.304	I	2		1			IV	3
5426.336	II	2					VE	
5426.700	II	80	100	2			VE	1
5428.823	I	1		1			IV	3
5431.489	I	3		3			IV	3
5434.961	I	1		4			IV	
5436.678	II	4		1			IV	
5442.226	I	1		1			IV	3
5443.344	II	30	30				VE	1
5449.416	I	1		1			IV	3
5449.965	I	2		4			IV	
5451.109	I	300		200			I	
5453.597	II	2					VE	
5454.249	I	2		3			IV	
5455.466	II	40	40				VE	1
5455.711	I	3		10			IV	
5458.114	I	2		1			IV	
5459.340	I	2		1			IV	
5460.605	I	6		4			IV	
5465.642	I	2		8			IV	
5468.641	I	1		1			IV	3
5469.106	II	40	20				VE	1
5471.913	II	15	(8)	20*			IVE	1
5471.961	I						(IV)	
5472.632	I	2		2			IV	
5474.888	I	2		2			IV	
5477.253	I	4					VE	
5478.577	I	2		2			IV	
5479.925	I	3		2			IV	
5481.112	I	1		2			IV	3
5481.637	I	2		?			IV?	
5483.853	I	3		2			IV	
5486.382	I	3		2			IV	3
5486.834	I	2		8			IV	3
5488.700	I	3		3			IV	3
5489.184		1					VE	3
5490.336	I	3		2			IV	
5491.809	I	3		15			IV	
5496.181	I	1		1			IV	
5496.830	I	20		20			IV	
5497.288	I	2		5			IV	3
5499.552	I	2		2			IV	
5501.858	I	1		1			IV	
5502.794	I	20		40			III	
5503.927		2					VE	
5506.515	I	20		10			IV	
5508.301		5*d*?		2			IV	
5511.313	I	4		3			IV	
5511.895	I	3		4			IV	
5515.407	II	30	15	2			VE	1
5519.925	I	5*d*?		2			IV	
5521.762	I	2					VE?	3
5522.336	I	2		2			IV	3
5527.259	I	1					V	3
5527.443		3					VE	
5528.012	I	30		80			III	
5530.548	II	3		1			IV	
5532.078	I	5*d*?		5			IV	
5534.367	I	4		4			IV	
5535.216	I	8		5			IV	
5538.231	I	3		6			IV	
5539.100	I	1		2			IV	

TABLE A. *Temperature classification of dysprosium lines* – Continued

Wave-length (Air)	Spectrum	Intensity					Temp. Class	Notes
		Arc	Spark	Furnace				
				High	Medium	Low		
5542.195	I	8		4			IV	
5544.047	I	1		1?			IV	
5544.679	I	2		1			IV	
5546.383	I	2		2			IV	3
5547.268	I	300		300			I	
5552.861	I	2		2			IV	3
5554.691		4		10			IV	3
5555.627	I	2		1			IV	
5557.453	I	2		2			IV	3
5559.119	II	8					VE	
5562.481	I	10		10			IV	
5563.169	II	8					VE	
5564.061	I	2		3			IV	3
5564.783	I	2					VE	
5566.302	I	5					VE	
5567.222		3		5			IV	
5568.150	I	5		4			IV	
5573.943	I	1		1			IV	3
5574.337	I	1		1			IV	
5575.951	I	2					V	
5576.611	I	2		40			III	
5577.817	I	1					V	
5579.432	I	1					V	
5579.901	I	2		12			III	
5582.799	II	1					V	3
5583.195	I	8	(8)	30			III	1
5584.347	I	2		2			IV	
5585.562	I	1		6			IV	
5591.642	I	3		3			IV	
5592.314	II	5	(8)				VE	1
5594.338	I	6		4			IV	
5596.055	I	2					V	3
5597.350	II	5	(5)				VE	1
5598.338	I	2?					V	
5598.799	I	1		3			IV	
5600.652	II	200	(80)				VE	1
5600.800	I	?		4			IV	
5602.426	II	2					V	
5605.629	I	20		20			III	
5609.866	I	2		4			IV	
5613.229	I	60		30			IV	
5618.453	II	1					V	3
5620.618	I	1		8			IV	
5622.498	I	3		4			IV	
5624.996	I	2		2			IV	
5626.135	I	3		10			IV	
5627.490	I	20		200			II	
5629.714	II	3					V	
5634.714	II	6					VE	
5635.976	II	2					V	
5637.160	I	1		4			IV	
5637.578	I	1					V	3
5639.498	I	500		400			I	
5641.504	II	25	(10)	2			IVE	1
5645.520	I	4					V	
5645.990	I	100		80			III	
5649.766	II	3					V	
5651.469	I	1		2			IV	
5652.009	I	300		250			I	
5653.488	I	2		2			IV	3
5654.543	I	1		1			IV	3
5654.749	II	2		0			VE	3
5656.327	I	1		4			IV	3
5658.785	I	2		4			IV	
5660.308	II	3	(5)				VE	1
5661.380	I	1		1			IV	
5663.873	II	8d	(4)	5*			VE	1
5663.954	I						IV	
5664.412	I	3		60			II	
5665.560	II	3					V	
5666.428	I	6		4			IV	
5669.268	I	1		1			IV	
5670.308	I	2		2			IV	
5671.250	I	20		20			IV	
5673.026	I	2		4			IV	
5677.683	I	30		40			IV	
5678.344	II	6					VE	
5683.032	I	4		10			IV	
5685.583	I	40		300			II	
5687.625	I	2					IV	
5690.436	I	4		4			IV	
5690.959	I	2		4			IV	3
5692.352	I	4		2			IV	
5695.889	II	12	(8)	4			IVE	1
5698.718	II	15	(15)				VE	1
5699.332	I	20		200			II	
5702.908	I	30		150			II	
5704.458	I	1		2			IV	
5707.031	I	3		3			IV	3
5707.808	I	20		25			IV	
5711.025	I	4		15			IV	
5713.848	I	2		5			IV	
5717.686	I	3		4			IV	
5714.925	I	2		2			IV	3
5718.461	I	100		50			III	
5719.978	II	3					VE	
5727.451	I	8		50			III	
5732.912	I	15		12			IV	
5733.360	I	3		3			IV	
5737.704	I	3		3			IV	
5740.204	I	50		50			III	
5745.529	I	80		300			II	
5748.010	I	2		3			IV	
5750.219	I	1?		6			IV	
5750.484	I	10		6			IV	
5753.648	I	5		2			IV	
5754.261	I	5		40			III	
5758.226	I	8		10			IV	
5758.793	I	25		300			II	
5759.780	I	4		2			IV	
5760.223	I	1		1			IV	
5761.853	I	4		4			IV	
5763.524	II	5					VE	
5766.350	I	4		2			IV	3
5766.973	II	5					VE	
5771.276	I	2		2			IV	3
5784.026	I	4		6			IV	
5787.197	I	5		5			IV	
5789.280	II	5					VE	
5800.689		1					IV	3
5802.617	I	8		80			III	
5805.554	I	30		100			III	
5807.658	I	15		60			III	
5813.101	I	8		?			VE?	

TABLE A. *Temperature classification of dysprosium lines* – Continued

Wavelength (Air)	Spectrum	Intensity					Temp. Class	Notes
		Arc	Spark	Furnace				
				High	Medium	Low		
5824.920	I	1		2			IV	
5827.426	I	2		3			IV	
5829.292	I	2		8			III	
5831.378	I	1		1			IV	3
5838.869	I	2		1			IV	
5840.125	I	5		8			IV	
5840.339	I	5		1			IV	
5845.360	II	8					VE	
5846.157	I	4					VE	
5850.131	I	4		8			IV	
5852.460	I	4		6			IV	3
5856.082	II	6	(6)				VE	1
5856.976	I	2		10			III	3
5858.054	I	2		3			IV	
5859.566	II	4					VE	
5864.025	I	15		20			IV	
5868.106	II	150	25	4			VE	1
5874.086	I	4		3			IV	3
5876.312	I	1		4			IV	
5883.216	I	2		8			IV	
5884.189	I	4		50			III	
5887.497	II	4					VE	
5893.098	I	4		30			III	3
5893.308	I	6		20				
5897.670	II	5					VE	
5902.448	II	10	(10)				VE	1
5903.295	I	5		6			IV	
5905.185	II	3					VE	
5907.262	I	2		3			IV	
5909.167	II	12	(7)				VE	1
5915.163	II	100	(65)				VE	1
5916.619	I	5		5			IV	
5922.360	I	6		6			IV	
5923.970	I	3					IV	
5924.562	II	30	10	2			VE	1
5927.812	I	5		3			IV	3
5929.111	I	1		2			IV	
5929.521	I	5		6			IV	
5929.591	I							
5933.177	I	6		40			III	
5935.269	I	1		1			IV	
5935.567	I	1		1			IV	
5936.597	I	3		3			IV	
5938.816	II	2					VE	
5941.464	I	3		25			III	
5943.674	I	8		150			II	
5945.803	I	200		300			II	
5948.633	I	1		1			IV	3
5949.481	I	2		2			IV	
5951.614	I	2		2			IV	3
5954.358	I	1		1			IV	3
5955.514	II	5	(8)				VE	1
5958.803	I	1		1			IV	
5961.272	I	5		5			IV	
5964.464	I	100		400			II	
5964.713	I	20?	15	40			III	1
5965.052	I	1		12			IV	
5965.426	I	1		2			IV	
5966.486	II	10					VE	
5970.032	I	15		20			IV	
5970.719	II	4					VE	
5974.487	I	300		300			I	
5978.248	II	2	(2)				VE	1
5979.996	I	5		200			I	
5982.501	I	3		5			III	
5984.102	I	1		3			IV	
5984.862	I	30		30			IV	
5985.990	I	15		100			II	
5988.562	I	800		500			I	
5989.671	II	2					VE	
5990.505	I	1		3			IV	
5991.674	I	8		50			III	
5992.638	II	2					VE	
5994.952	I	1		8			IV	
5996.581	I	1		1			IV	
6000.838	I	10		10			IV	
6001.214	II	1					VE	3
6003.262	I	15		30			III	
6006.842	I	3		2			IV	3
6007.753	I	1					VE	
6008.351	I	1		3			IV	
6008.938	I	40		250			II	
6009.331	I	2		20			III	
6010.815	I	200		400			I	
6013.638	II	3					VE	
6017.263	I	20		150			II	
6018.542	I	4		15			III	
6021.564	I	3					VE	
6023.593	I	1		4			IV	
6025.074	I	2		3			IV	
6030.980	I	25		300			II	
6036.180	I	1		2			IV	
6038.700	II	8					VE	
6040.443	I	1		5			III	3
6040.556	I			15				
6042.966	I	1		1			IV	3
6044.480	II	4	(3)				VE	1
6047.051	I	1		2			IV	
6050.061	II	6	(4)				VE	1
6052.040	I	2		2			IV	
6052.914	II	4					VE	
6053.201	I	1		5			IV	
6058.176	I	60		400			II	
6058.790	I	1		1			IV	
6063.561	II	8	(8)				VE	1
6067.895	I	10		150			II	
6073.775	II	6	(6)				VE	1
6074.605	II	6	(4)				VE	1
6075.020	I	5		20			IV	
6076.942	I	2		2			IV	3
6079.843	I	1		1			IV	3
6083.362	I	2		4			IV	
6084.043	I	6		4			IV	
6084.372	I	1		2			IV	3
6085.056	I	100		500			II	
6088.261	I	500		400			I	
6089.300	I	6		40			II	
6090.432	I	1		1			IV	
6090.889	I	10		200			II	
6091.270	I	2					VE	
6093.464	I	1		4			IV	3
6097.357	I	3		25			III	
6099.646	I	6		80			II	

TABLE A. *Temperature classification of dysprosium lines* – Continued

Wavelength (Air)	Spectrum	Intensity					Temp. Class	Notes
		Arc	Spark	Furnace				
				High	Medium	Low		
6103.375	I	10		125			II	
6103.648		8					VE	
6106.201	I	1		3			IV	
6107.621	I	10		15			IV	
6107.886	I	1		12			IV	
6111.337	I	1		15			III	3
6113.927	I	15		50?			II	
6114.074	I	10		200?				3
6115.276	I	15		150			II	
6115.676	I	10		80			III	
6117.025	I	1		2			IV	
6119.630	I	20		200			III	
6121.612	I	1		3			IV	
6124.830	I	2		8			IV	
6125.931	I	1		4			IV	
6126.487	I	30		40			IV	
6127.155	I	40		150			III	
6132.238	I	1		1			IV	
6133.645	I	60		300			III	
6138.362	I	8		40			III	3
6142.211	I	1		10			III	
6143.016	I	1		2			IV	
6144.879	I	2		1			IV	
6145.537		2		2			IV	3
6146.441	I	1		2			IV	
6150.604	I	10		40			III	3
6150.772	I	8		80			III	
6151.488	I	3		2			IV	
6152.770	I	1		2			IV	
6158.282	I	50*d*		400			II	
6158.838	I	1		5			IV	
6163.984	I	1		8			IV	
6165.555	I	80		400			II	
6167.981	I	1		2			IV	
6168.431	I	600		1000			I	
6169.639	I	2		2			IV	3
6170.317	I	3		3			IV	3
6170.525	I	3		3			IV	
6172.701	I	1		8			III	
6173.454	I	2		6			IV	
6175.173	I	2		2			IV	
6177.039	I	2		2			IV	
6184.704	II	4	(3)				VE	1
6189.706	I	10		100			III	
6191.718	I	1		?			VE?	3
6196.231	II	50	(25)				VE	1
6199.212	II	15					VE	
6203.382	I	2		1			IV	
6204.016	I	4		3			III	
6205.120	I	1					V	
6206.322	I	2		1			IV	
6207.977	I	3		3			III	
6210.767		2		3			IV	
6212.665	I	10		2			IV	
6213.426	I	5		3			III	
6215.209	I	2					VE	
6216.562	II	6	(4)				VE	1
6220.371	I	1		1			IV	3
6221.640	II	2					VE	
6225.371	I	3					VE	
6229.740	II	40					VE	
6230.590	I	10*d*		2			III	
6230.779	II						VE	3
6232.328	I	2					VE	3
6236.572	I	1					VE	
6237.391	II	2					VE	3
6238.268	I	3		6			II	3
6239.248	II	8					VE	
6240.171	II	3					VE	
6244.126	I	1					VE	
6246.847	I	40		8			III	
6250.003	II	5	(5)				VE	1
6250.654	I	10*d*		5			II	
6251.265	I	5		10			III	
6254.309	I	6					VE	
6255.446	I	15		4			III	
6255.921	I	3					VE	
6259.088	I	1000		1200			I	
6260.364	I	100		80			II	
6260.444	I							
6261.091	II	2*d*		1			IV	
6263.440	I	1		1			IV	
6265.552	I	4		1?			IV?	
6266.734	I	2		2			IV	3
6270.759	I	40					VE	
6271.102	I	20		3			III	
6272.897	I	5		2			IV	3
6273.800	I	15		4			IV	3
6274.618	I	1		1			IV	
6281.273	I	4		8			III	3
6283.738	II	1					VE	
6288.730	I	2		1			IV	3
6290.485	II	5					VE	
6291.651	I	50		40			II	
6298.902	I	3					VE	
6299.281	I	4		5			II	
6300.230	II	6*d*					VE	3
6301.013	I	4		2			IV	
6302.652	I	5					VE	
6303.038	II	3					VE	3
6304.202		2		2			IV	
6305.150	I	2					VE	
6305.626	I	1		20			III	
6310.524	I	2		1?			IV?	
6311.829	I	4					VE	
6316.632	II	5	(5)				VE	1
6317.228	II	40	(20)				VE	1
6318.705	I	3					VE	
6320.180	II	6					VE	3
6320.456	I	2					VE	
6321.464	I	5					VE	
6322.793	I	3		1?			IV?	3
6323.210	I	30		2?			IV?	
6326.912	I	6		5			III	3
6329.216	I	8		6			III	
6329.591	I	3					VE	
6331.086	I	30					VE	
6331.234	I	?		3			III	
6331.988	I	4		2			IV	
6333.354	I	2*d*?					VE	
6333.814	I	4		4			IV	
6334.232	I	3		1			IV	
6336.121	I	1					V	
6338.083	I	50		60			I	

TABLE A. *Temperature classification of dysprosium lines* – Continued

Wavelength (Air)	Spectrum	Intensity					Temp. Class	Notes
		Arc	Spark	Furnace				
				High	Medium	Low		
6339.318	II	5					VE	
6341.362	I	15		3			III	
6341.877	I	3					V	
6342.518	II	6					VE	
6343.325	I	150		4			III	
6344.689	I	3					V	
6348.356	I	3		?			V	
6349.002	I	2		1?			IV?	
6351.251		3					VE	
6352.630	I	15		10			III	
6353.090	I	15		2			IV	
6353.631	II	20	15				VE	1
6358.495	I	10		15			III	
6359.702	I	12		2			IV	
6359.897	I	3					V	
6361.496	II	5					VE	
6366.885	I	1					V	
6368.009		3					V	3
6369.590	I	80					VE	
6371.997	I	1		1			IV	
6373.157	I	2					V	3
6374.439	I	3					V	
6375.010	I	12		12			II	
6376.905		2					VE	3
6377.712	I	60					VE	
6379.323	I	5		2			IV	
6379.750	I	3		4			III	
6381.368	I	5					V	3
6382.163		1					V	
6386.796	I	400		300			I	
6387.532	I	15		4			III	
6388.388	I	10		2			IV	
6390.641	II	10	(10)				VE	1
6396.411	I	?		?			II	
6396.604	II	200	200				VE	1
6402.009	I	10					V	3
6402.300	I	50					V	
6407.531	II	5					V	
6408.274	I	3					V	
6410.397	I	2					V	
6413.500	I	6		1?			IV?	
6414.806	I	2					V	
6415.630	I	4		5			II	
6418.239	I	3?		1			IV }	3
6418.426	II	30					VE }	
6421.917	I	600		500			I	
6423.070		2					V	
6427.282	I	60		100			II	3
6427.768	II	6	(4)				VE	1
6431.180	I	3		2			IV	
6432.399	I	1					V	
6432.965	I	20		10			III	
6434.354	II	4					VE	
6435.013	I	4					V?	
6435.626	II	8	(8)				VE	1
6436.547	I	60					VE	
6436.736	I	2?		2			IV	
6441.815	II	6	(12)				VE	1
6442.639	I	2					V	
6443.085		1					V	
6443.696	II	40	40				VE	1

Wavelength (Air)	Spectrum	Intensity					Temp. Class	Notes
		Arc	Spark	Furnace				
				High	Medium	Low		
6444.149	I	10		2?			IV?	
6445.489	I	1					V	
6449.509	I	1					V	3
6449.974	I	10					V	3
6450.501	I	20					V	
6453.476	II	3					V	
6454.587	I	1					V	
6454.886	II	1					V	
6456.019	I	3		2?			IV	3
6459.260	I	3					V	
6460.048	I	1		1			IV	
6460.829	I	300		200			II	
6467.943	I	2					V	3
6468.497	I	?		4			III	
6468.576	II	150	(150)				VE	1
6471.976	II	50	(35)				VE	1
6474.005	I	1					V	
6474.915	I	125		1			VE	
6478.218	II	15					V	
6480.961	II	4					V	
6482.546	I	3		1?			IV?	
6483.586	II	300	(120)				VE	1
6486.595	I	800		50			III	
6487.165	I	2					V	
6489.477	I	4		2?			IV?	
6496.265	I	1					V	3
6498.528	I	2					V	
6499.119	I	1					V	
6503.472	I	1					V	
6504.274	I	3		1			IV	3
6505.318	I	5					V	3
6509.334	II	3					V	3
6511.474	I	1					V	
6512.135	I	2					V	3
6513.126	I	15					V	
6513.599	I	1					V	3
6515.898	I	3					V	
6516.527	II	3					VE	3
6517.909	I	1					V	3
6519.130	II	50	(35)				VE	1
6522.301	II	4					V	
6526.026	I	4					V	
6527.963	I	3					V	3
6529.453	II	4					VE	
6532.339	II	10	25				VE	1,3
6534.454	I	2					V	3
6536.646	I	5					V	3
6539.452	II	8					VE	
6542.608	I	10		15			II	
6548.258	II	200	(100)				VE	1
6550.750	I	5		4			IV	3
6553.194	II	8					V	
6554.824	I	1					V	
6556.969	I	2					V	
6558.023	I	500		400			I	
6563.166	I	1					V	
6563.994	II	5					V	
6565.114	I	150		10			IV	
6570.196	I	3		2			IV	
6574.299	II	20					V	
6575.486	I	3					V	3
6579.367	I	2000		500			I	

TABLE A. *Temperature classification of dysprosium lines* —Continued

Wavelength (Air)	Spectrum	Intensity					Temp. Class	Notes	Wavelength (Air)	Spectrum	Intensity					Temp. Class	Notes
		Arc	Spark	Furnace							Arc	Spark	Furnace				
				High	Medium	Low							High	Medium	Low		
6582.048	I	2					V		6709.519	I	1					V	
6582.979	I	3					V		6711.567	I	4		1			IV	
6583.523	I	1					V		6713.046	I	} 30		15			III	3
6585.079	II	2					V	3	6713.157	I							
6587.503	I	5		5			IV		6716.200	I	2					V	
6591.678	I	15		2			IV		6718.266	I	3		2			IV	
6594.145	II	80	(65)				VE	1	6719.411	I	1					VE	3
6595.299	I	4		1?			IV?		6720.216	I	1		1			IV	
6595.581		1					V		6721.704	I	3		2			IV	3
6600.546	I	1					V		6722.238	I	1					V	3
6604.502	I	10					V		6723.210	I	1		2			IV	
6607.051	I	1		2			IV	3	6723.442	I	2		2			IV	
6611.729	II	15					V		6724.706	I	20		5			III	
6614.707	I	3					V		6726.884		1					V	
6614.911	I	20					V		6727.619	I	1					V	
6616.200	II	2					V		6730.337		1					V	
6617.683		3					V		6733.823	I	3*d*?		2			III	3
6622.567	I	1					V	3	6736.069	I	15		20			III	
6623.742	I	1					V	3	6736.963	I	2		2			III	3
6625.490	I	15*d*?		6			IV		6738.569	I	3					VE	3
6626.972	I	2					V		6739.860	I	3		4			III	
6628.288	I	3		2			IV		6740.470	I	2		1			IV	
6632.961	I	1		5			III		6741.219	I	4					V	
6639.213	I	30		5			III		6742.274	I	5		5			III	
6641.450	I	2		2			III		6742.782	I	2		2			IV	
6643.373	I	200		250			I		6743.680	I	10					VE	3
6645.475	I	2		2			III		6744.439	I	8		2			IV	3
6649.522		2		2			IV		6747.930	I	300		100			II	
6650.290	I	3		2			III		6748.686	I	1					V	
6654.232	II	8	(8)				VE	1	6750.212	I	30		40			II	
6654.542	I	1					V		6751.581	I	2		3			IV	
6658.039	I	10		40			III	3	6752.778	I	1					V	
6658.360	I	300		40			III		6753.052	I	1		1			IV	3
6660.090	I	1		3			III	3	6757.623	I	60		20			III	
6661.639	I	300		150			III		6758.489	I	1		1			IV	
6662.806	II	2					VE		6759.113	I	8		10			III	
6666.937	I	6		4			III		6764.778	I	15		30			II	
6667.858	I	1200		800			II		6765.894	I	600		300			II	
6670.161	I	30		40			II		6767.499	I	1		1			IV	
6672.061	I	1		1			IV		6768.037	I	2		2			IV	
6676.707	I	2		1			IV		6768.436	I	1		2			IV	
6682.094	I	3		2			IV		6769.790	I	2		1			IV	
6683.247	II	3					VE		6770.877	I	1		1			IV	
6683.498	I	2		20			II		6772.188	I	5		6			III	
6684.776	II	2					VE		6772.630	I	1		2			III	
6686.381	I	6		5			III		6774.088	I	1		3			III	3
6687.837	I	2					VE		6774.590	I	4		5			III	
6688.068	I	10		15			III		6775.078	I	1		1			IV	
6691.133	I	3		1			IV		6776.407	I	2		1			IV	
6692.351	I	2					V		6777.044	I	15		30			II	
6692.729	I	4*d*?		2			IV	3	6777.646		6					V	
6694.072	I	2					V		6778.435	I	1					V	3
6694.568	I	3		2			IV	3	6780.997	I	1		1			IV	3
6697.028	II	1					V		6782.471	I	2		1			IV	
6698.122	I	1					IV		6783.082	I	3		1			IV	
6698.401	I	4		2			IV	3	6783.942	I	1		1			IV	3
6700.044	I	(1)					V		6785.000	I	3					V	3
6700.636	II	20	(15)				VE	1	6785.701	I	4		15			III	
6701.582	II	1					VE	3	6787.370	I	25		20			III	
6704.333	I	2					V		6790.298	I	30		200			I	
6704.724		1					V		6794.229	I	30		50			II	

TABLE A. *Temperature classification of dysprosium lines* — Continued

Wavelength (Air)	Spectrum	Intensity					Temp. Class	Notes
		Arc	Spark	Furnace				
				High	Medium	Low		
6795.167	I	1					V	
6795.538	I	2		1			IV	
6797.294	I	2					V	
6797.552	I	5					VE?	
6798.937		2					V	3
6799.579		2					V	
6800.010	II	6					V	
6800.419	I	2		1			V	
6803.066	II	8	(8)				VE	1
6803.324	I	6		1			IV	3
6805.545	I	40		30			III	3
6807.312		6	(5)				VE	1
6808.409	I	2		1			IV	
6811.782	I	1		1			IV	3
6814.839		4					VE	
6815.330	I	8		10			III	
6816.769	I	2					V	3
6817.299	II	1					VE	3
6818.205	I	80		80			II	
6818.680	II	2					VE	
6820.820	I	4		1			IV	
6821.780	I	200		40			III	
6822.546		2					V	3
6822.687								
6824.703	I	1					V	
6826.438		1		1			III	
6827.072	I	30		6			III	
6828.347	II	6	(6)				VE	1
6829.130	I	2		1			IV	3
6832.914		1					V	
6833.652	I	8		8			III	
6835.418	I	2000		500			I	
6835.862	I	8?		8			IV	
6838.902	I	1					V	
6839.563	I	3					VE	
6841.191	I	1		1			IV	
6841.802	I	3					V	
6842.751		1					V	
6843.747	I	8		2			III	
6844.970		2					VE	
6845.761	I	40		20			III	
6848.321		1					VE	
6849.593		2					V	
6850.565	I	3					VE	
6850.803	I	1		1			IV	
6851.992	I	20		4			III	
6852.964	I	1500		400			II	
6855.768	I	4		4			III	3
6856.458	I	300		80			III	
6857.356	I	1					V	
6857.902	I	3		10			II	
6860.386		2		1			IV	3
6861.470	I	2					V	
6861.872	I	1					V	3
6863.394	I	1					VE	
6865.558	I	1					V	
6868.109	I	(?)					IV	
6870.893	I	8		3			IV	
6871.446	I	4		1			V	
6871.819		2		1			V	3
6873.020		1					VE	
6873.636	I	2		3			IV	
6874.944	I	3		3			III	3
6875.122	I	10		2			III	
6875.823	I	2		2			IV	3
6876.798		1					VE	
6879.015	I	2		3			III	3
6879.157	I	2		1			IV	
6882.313	I	3		1			IV	
6884.315		1					V	
6885.939	I	1		1			IV	
6886.399	I	15		4			III	
6888.565	I	6?		6?			IV?	3
6888.833	I	200		300			I	3
6889.859	I	1		1			IV	
6890.679	I	3		3			III	
6891.205		1					VE	
6894.516	I	25		10			III	
6895.228	I	1					V	3
6895.509	I	30		40			III	
6895.953	I	2					V	
6896.905		1		1			IV	
6897.968	II	40	(25)	1			VE	1
6898.923	I	20		8			III	3
6899.321	II	1500	1000	10			IVE	1
6900.040	I	1		6			III	
6900.235	I	1					V	3
6900.700	I	8		8			III	
6902.046	II	4	(4)				VE	1
6904.076		1					V	
6905.949	I	3		15			III	
6906.443	I	200	(110)	200*			II	1
6906.534	II						VE	
6908.419		1					V	3
6908.886		1		1			IV	
6910.386	I	3		2			IV	
6912.198	II	10	(8)				VE	1
6912.677	II	2					V	
6914.002	II	2					VE	
6915.340	I	2		1			IV	
6915.784	II	1					IV	
6917.213	II	1					V	
6917.801	II	2					V	
6918.014	I	2		2			IV	
6919.669	II	4					VE	
6921.980	I	1		1			IV	
6922.845	I	1					IV	
6923.204	II	1					VE	
6925.261	I	5		1			IV	3
6925.494	I	10		3			III	3
6927.664	I	1		1			IV	3
6929.550	I	200		500			I	
6931.517	I	1		1			IV	
6932.452	II	20	(16)	1			VE	1,3
6933.865		1		1			IV	
6935.778	I	5		2			III	
6936.963		1		1			IV	
6939.650	I	6		3			III	
6940.242	I	2		4			III	3
6940.428	I	2					V	
6942.114	I	15		25			III	
6945.263	I	20		150			II	
6946.432	I	3		1			IV	

TABLE A. *Temperature classification of dysprosium lines*—Continued

Wavelength (Air)	Spectrum	Intensity					Temp. Class	Notes
		Arc	Spark	Furnace				
				High	Medium	Low		
6948.622	I	6		1			IV	
6950.280	II	100	(80)	2			IVE	1
6951.417	I	50		8			III	
6952.203	I	3		1			IV	
6952.933	II	10	(7)				VE	1, 3
6956.414	I	2		2			IV	
6957.483	I	10		6			III	
6958.084	I	1000		1000			I	
6959.687	I	1					V	
6961.674	I	3		2			IV	
6963.947	II	1					V	
6966.138	II	1					VE	
6966.984	I	8		1			IV	3
6968.778	I	4		4			III	
6970.427	I	80		100			II	
6971.062	I	1		6			III	3
6972.871		1					V	3
6973.594	I	10		2			IV	
6974.677		1					V	3
6974.918	I	2		2			IV	
6975.436	I	4		2			III	
6977.340	II	3					VE	
6977.932	II	6					VE	3
6978.740	I	1					V	3
6982.435	I	150		60			III	
6984.364	I	2					VE	
6985.506	I	2		2			IV	
6986.191	I	3		3			III	
6990.077		2		1			IV	
6991.304	I	250		500			I	
6992.168	II	1					VE	
6993.160	I	6		2			III	
6994.914	I	3		1			IV	
6996.450	II	1					VE	
6998.095	I	1500		800			II	
6999.035	I	4		4			III	
7002.732	II	1					VE	
7004.894	I	5		6			III	
7006.069	II	2					VE	
7009.437	I	3		2			IV	3
7012.303	II	3					VE	
7014.640	II	8	(8)				VE	1
7015.608	I	2		1			IV	
7017.416	I	400		200			II	
7019.196	I	3		2			III	
7020.164	I	2		1			IV	
7020.907	I	2		2			IV	
7021.783	I	5		10			III	
7022.098	II	1					VE?	
7023.284	II	2					V	
7026.032		2					V	
7026.786	II	1					VE	
7027.283	I	6		6			III	
7029.145	I	1					V	
7031.088		2*d*					V	
7033.186	I	8		3			III	
7033.962	I	1		6			III	
7034.675	I	3		1?			IV	
7035.649	I	1					V	
7036.375	I	20		30			III	
7037.535	I	150		300			II	
7039.194	I	1		2			III	
7040.118	I	1					V	

Wavelength (Air)	Spectrum	Intensity					Temp. Class	Notes
		Arc	Spark	Furnace				
				High	Medium	Low		
7040.673	I	8		10			III	
7043.622	I	10		15			III	
7046.522		1					V	
7047.485	II	3					VE	
7048.061	I	3		2			III	
7049.446	I	3		1			IV	
7050.448	I	1					V	
7053.577	I	6		1			IV	
7053.738	I	6		8			III	
7054.338	I	4		5			III	
7054.644	I	3					V	
7055.398		1		1			IV	
7055.952	II	250	200	4			IVE	1
7057.061	II	1					VE	
7059.680	I	1					V	3
7061.160	II	1					V	3
7061.814	I	2		2			III	
7062.297	I	80		40			III	
7063.307	I	4		2			IV	
7063.887	I	1		1?			IV?	
7066.863	I	2		1			IV	
7067.840	II	2					VE	
7073.036	I	4		4			III	
7073.683	II	1		1?			IV?	
7074.683		1		1			IV	3
7075.139	II	150	100	5			IVE	1
7075.761	II	2					VE	
7078.951	I	1		1			IV	
7079.661	I	2		2			III	
7080.043	I	1					V	
7081.414	II	1					VE	
7082.090	II	1					V	
7084.228		1					VE	
7084.998	I	10		1			IV	3
7086.245	I	2		1			IV	3
7087.590		1					V	3
7090.250		2					VE	
7091.733	I	5		2			IV	
7093.695	I	1					V.	
7095.649	I	2		5			III	
7095.858	I	4		2			III	
7097.791	I	3		3			III	
7098.060	II	1?					VE	
7098.800	II	1					V	3
7099.180	I	3					VE	
7099.725	I	1					V	
7100.542	II	10	(10)				VE	1
7101.663	II	30	15				VE	1
7103.516	I	3					VE?	
7105.628	I	2					V	
7107.005	II	1					V	
7107.357	I	2		1			IV	
7107.650	II	1					V	3
7109.258	II	100	60	15			IVE	1
7110.079		1					VE	
7110.987	I	2					V	3
7111.611	I	2		1			IV	
7113.054	I	3					V	
7114.710	II	1					V	3
7116.289	II	5					VE	
7117.531	I	1					V	
7120.810	II	30					VE	

TABLE A. *Temperature classification of dysprosium lines* – Continued

Wavelength (Air)	Spectrum	Intensity					Temp. Class	Notes
		Arc	Spark	Furnace				
				High	Medium	Low		
7121.232	I	150		500			I	
7121.895	II	1					VE	
7123.281		1					V	3
7125.363	I	2		1			III	
7126.251	I	1					V	3
7127.509	II	1					V	3
7128.388	I	3		2			III	
7129.694	I	10		6			III	
7131.368		1					V	
7132.577	I	2		3			III	
7133.381	I	6		4			III	
7135.430		2					VE	3
7135.896	I	3		1			IV	3
7137.521	I	4		4			III	
7137.788	I	3		1			IV	
7139.809	II	4*d*?					VE	
7140.371		3					V	3
7141.216	I	2		1			IV	
7141.515	II	4	(3)				VE	1
7143.504	I	3		2			III	
7145.066	II	4	(4)				VE	1
7147.251	I	1					VE	
7149.302	II	6	(4)				VE	1
7153.308		1					V	
7155.838	I	2					V	
7156.478	I	40		15			III	
7157.300	I	1		1			IV	
7158.742	I	3		3			III	
7162.046	I	6		10			III	
7163.100	I	1		2			III	
7166.502	I	15		20			III	
7167.253	I	2					V	
7170.008	II	1					VE?	
7170.478	I	3					V	
7172.298	I	3		3			III	
7172.690	II	2					VE	3
7175.107	II	60	(50)	1			VE	1
7177.791	I	2		1			IV	
7181.372	I	2		3			(III)	
7184.102	I	1		3			III	3
7185.064	I	3		2			III	3
7187.312	I	1		1			IV	
7190.080	I	2		1			IV	
7190.423	I	1		2			III	
7192.657	I	20		5			III	
7194.830	I	40		80			II?	
7196.709	II	1					(V)	
7198.653	I	10		150			III	
7200.266		1					V	
7204.248	I	1					V	
7206.279		1					VE	3
7206.767	I	40		60			III	
7207.328	I	40		100			II	
7208.147	I	1		1			IV	3
7213.274	I	150		200			II	
7213.899		1		1			IV	
7215.056	I	1					V	
7215.513	I	15		5			III	
7215.940	I	10*d*		5			III	3
7216.064	I			–			VE	
7217.744	I	4		15			III	
7220.788	I	4*d*?		1			IV	
7222.010	I	2		4			IV	
7222.520	I	10		1			IV	
7222.901	I	15		100			II	
7224.178		1					V	3
7226.366	I	2		2			III	
7229.388	I	1		1			IV	3
7230.044	I	600		400			II	
7231.591	I	1					V	3
7232.563	I	1					V	
7233.270	I	1					V	
7234.450	I	1		1			IV	
7234.679	II	8	?				VE	1
7237.664	II	1					V	3
7238.139	II	1					V	
7238.565	II	1					V	3
7241.049	I	1					V	
7243.051	II	2					VE	
7244.830	I	2					IV	
7245.870		1					IV	
7246.190	I	1					V	3
7247.001	I	1		1			IV	3
7250.010	I	300		400			I	
7253.398	II	1					VE	
7254.601	I	3		2			III	
7257.183	II	1					V	
7258.210	I	2		2			IV	
7258.562	I	4		2			IV	
7260.180	I	1		3			III	
7261.738	I	50		200			I	
7263.599		3					VE	
7264.538	II	1					VE	3
7265.576	I	1		1			IV	
7265.889	II	2					VE	
7271.848	II	2					VE	
7273.573	II	20	(12)				VE	1
7273.948	II	2					VE	
7274.249	I	2		5			III	
7275.508	I	1					V	
7276.579	II	1					V	
7277.309	II	1					VE	
7278.597	I	1		1			IV	
7278.918	II	2					VE	
7279.710	I	2					VE	
7279.905	I	8		20			III	
7283.196	I	1		6			III	
7285.224	I	3		4			III	
7288.238	II	20	(12)				VE	1
7288.921	I	12		60			II	
7289.518	I	2		3			III	
7289.774	I	2		1			IV	
7291.048	I	3		2			III	
7291.140								
7291.613	I	5		20			II	
7293.324	I	1					VE	
7295.496	II	1					VE	
7297.897	II	2					VE	
7298.662	I	2					V	3
7299.253	II	2					VE	3
7300.276	I	30		40			III	
7302.224	I	3					V	3
7303.114	II	1					V	
7303.348	I	1					VE	

378-324 O - 70 - 6

TABLE A. *Temperature classification of dysprosium lines* – Continued

Wavelength (Air)	Spectrum	Intensity					Temp. Class	Notes
		Arc	Spark	Furnace				
				High	Medium	Low		
7303.988	II	1					V	3
7308.976	II	1					V	3
7311.425	I	1					VE	3
7311.655	II	1					VE	3
7312.807	I	1					VE?	3
7313.079	I	1					V	
7313.405	I	2		1			IV	3
7314.706	II	2					VE	
7318.170	II	1					V	3
7318.704	II	2					V	
7321.735	I	1		2			IV	
7322.269		2					VE	3
7324.195	I	3		1			IV	
7326.843	II	1					VE	
7328.785	II	2					VE	
7332.758	I	4		4			III	
7334.559	I	1					V	3
7336.886	I	2		2			IV	
7337.454	I	1					V	
7338.080	I	3		1			IV	
7339.750	II	2					V	
7340.081	I	4		4			III	
7341.077	I	15		4			III	
7342.301	I	6		4			III	
7345.132	II	150	(30)	20			IIIE	1
7347.153	I	2		1			IV	
7349.147	I	1		1			IV	
7349.643	II	3					V	
7350.475	I	2					VE	
7351.031		1					VE	3
7353.582	I	20	80				II	
7354.394	II	6					VE	
7355.574	II	1					V	
7357.065	I	5*d*		4			III	
7360.221	I	4		1			(IV)	
7361.578	II	8	(6)				VE	1
7362.779	II	6					VE	
7363.590	I	1		1			IV	
7365.868	II	1					VE	
7367.564	I	2		2			IV	
7368.566	I	2					V	3
7369.045	I	15		60			II	
7370.234	II	50	(35)	1			VE	1
7370.447	I	3		8			III	3
7372.754	I	5		1			IV	
7376.038	I	600		1000			I	
7377.530	II	1					VE	
7378.831	I	2		1			IV	
7380.167		1					VE?	
7380.865	II	2					VE	3
7381.566	I	150		300			II	
7381.959	I	1					V	
7386.184	II	3		1			IV	
7387.837	II	1					VE	
7388.166	I	2		1			IV	
7389.815	II	2					V	
7391.172	I	2*d*					V	3
7391.547	I	2		1			IV	
7394.964	I	2					V	
7398.276	I	(?)					III	3
7400.660	I	3		30			III	
7401.069	I	1		1			IV	
7401.853	I	3		5			III	
7403.103	I	100	(70)	150*			(II (VE)	1
7403.194	II							
7404.016	I	50		125			III	
7407.595	I	150		500			I	
7409.381	I	2		2			IV	
7409.708	I	2*d*					V	
7412.369	I	400		300			II	
7413.778	II	1					VE	
7415.453	II	2					VE	
7418.945	I	2		2			IV	3
7422.561	I	2		1			IV	3
7425.219	I	3		1			IV	
7426.194	I	3		2			IV	
7426.863	II	300	(120)	15			IIIE	1
7427.553	II	1					VE	
7427.889	I	20		40			III	
7428.538	I	30		8			III	
7429.370	I	3		2			IV	
7431.238	I	1					VE?	
7433.140	I	6*d*		2			IV	3
7434.963	I	4*d*		3			IV	3
7436.568	II	3					V	
7437.493	I	4		4			III	
7440.169	I	2					VE?	
7440.565	I	3					V	
7449.502	I	4					V	
7450.489	I	6*d*		1			IV	
7451.115	II	30	(15)				VE	1
7451.802	I	3		2			III	
7454.058	I	2					V	
7454.760	I	4					V	
7455.558	I	3		5			III	
7457.047	II	100	60	3			IVE	1
7457.864	I	5		2			IV	
7459 988	I	60		50			III	
7461.759	I	3		25			III	
7462.158		1					V	
7464.028	I	4					V	
7464.904	I	3					V	
7467.320	I	4		4			IV	
7469.261		2					V	
7474.145	I	1		1			IV	
7476.976		1					V	
7483.027	I	100		30			III	
7485.348	I	1		1			IV	
7487.479	II	6		–			VE	
7487.551	I			6			III	
7490.790	I	10		2			IV	
7493.771	I	12		10			III	
7495.045	I	4		5			III	
7496.184	I	3					V	
7497.378	I	10		10			III	
7502.865	II	3					VE	
7503.296	I	3					V	
7503.872	I	20		6			III	
7504.716	I	5					V	
7506.475	II	8					(VE (?)	
7507.900		1					V	
7509.596	I	25		100			II	
7510.154	I	3		1			IV	

TABLE A. *Temperature classification of dysprosium lines* — Continued

Wavelength (Air)	Spectrum	Intensity					Temp. Class	Notes
		Arc	Spark	Furnace				
				High	Medium	Low		
7512.580	I	1		3			III	
7516.613	II	15	(90)	3			IVE	1
7519.469	I	4		5			III	
7521.460	I	30		25			III	
7521.964	II	1					VE	
7522.684	I	6		30			III	
7523.863	II	4					VE	
7528.506	II	3					VE	3
7529.595	I	3*d*					V	
7531.352	I	4		5			III	
7532.666	I	6		30			II	
7533.160	I	100*d*		40			III	
7533.698	I	3		4			III	
7536.714	I	2					VE?	
7538.921	I	4		1			IV	
7539.847	I	1		4			III	3
7540.340	I	2					VE	
7541.987	I	5		10			III	
7543.729	I	2000		1000			II	
7544.483	I	2		1			IV	
7544.992	I	2		2			III	
7545.916	I	3					V	
7548.693	I	3		3			III	
7553.000	I	300		100			III	
7557.852	I	80		150			II	
7559.036	I	1		2			III	3
7559.782	I	250		600			I	
7562.965	II	200	(160)	4			IVE	1
7564.258	I	10		2			III	
7565.055	I	12*d*?		3			III	
7566.979	I	8		8			III	
7571.370	II	2					VE	
7572.194	II	1		1			IV	
7577.462	II	200	(120)	3			VE	1
7578.454	I	5		1			IV	
7580.548	I	2		1			IV	
7583.334	I	4		1?			IV	
7584.748	II	1					V	
7585.364	II	3					VE	
7587.764	I	25		15			III	
7591.305	I	300		200			II	
7593.849	I	4					VE?	
7594.859	I	60		15			III	
7595.408	I	4		1			IV	
7596.280	I	5		5			III	
7596.714	II	1					VE	
7598.350	II	2					VE	
7598.686	II	1					VE	
7603.724	I	2*d*		1			IV	
7606.506	I	5		1			IV	
7609.175	I	30		6			III	
7609.702	I	6		2			III	
7611.555	I	150		60			III	
7612.725	I	15		4			III	
7613.433	II	1					V	
7614.322	I	4		1			IV	
7615.683	II	1					VE	
7616.215	I	50		15			III	
7617.702	I	100		15			III	
7620.869	I	2					V	
7624.290	II	4					VE	
7625.030	I	2		1			IV	
7626.587	I	4		1			IV	
7627.513	I	1		2			IV	3
7629.575	I	15		2			III	
7631.270	I	25		4			III	
7633.618	II	2					VE	
7635.320	I	40		4			III	
7638.171	I	2		5			III	
7639.298	I	30		15			III	
7640.004	I	4		1			IV	
7641.093	I	800		600			II	
7641.226	I							3
7644.273	I	3		4			III	
7645.162	I	15		3			III	
7645.866	I	150		150			II	
7646.637	I	80		40			III	
7647.153	I	1					V	
7648.113	II	8	(7)				VE	1
7650.435	II	1					VE	
7652.249	I	5					V	
7655.467	II	?					VE	
7661.478	I	?		200			I	
7662.358	I	?		400			I	
7666.310	I	?		2			IV	
7666.784	II	(15)?	(10)?				VE	1
7672.748	I	?		5			III	
7675.994	I	?		2			III	
7676.687	I	40		40			III	
7677.481	I	2?		2			IV	
7680.039	I	?		2			IV	
7681.904	I	8		2			IV	
7682.715	I	8		8			III	
7688.665	I	?		2			IV	
7690.738	I	?		3			IV	
7692.015	I	5?		5			III	
7693.865	I	8?		8			III	
7696.540	I	?		15			III	
7699.838	I	?		3			III	
7701.779	I	?		2			III	
7706.666	I	?		3			III	
7707.286	II	(2)?	(2)?				VE	1
7710.137	I	?		4			III	
7711.912	II	8	(5)				VE	1
7715.327	I	500		300			II	
7717.430	II	1					V	3
7721.122	I	30*d*?		20			III	
7722.085	I	25		25			III	
7724.378	I	2*d*					IV	
7725.582	I	3		3			III	
7728.020	I	5					V	
7728.758	I	4		2			III	
7729.764	II	200	(150)	8			IVE	1
7732.516	I	20*d*		15			III	
7732.674	I							
7737.538	I			2			IV	
7739.381	II	8	(5)				VE	1
7739.586	I	3		2			IV	
7740.531	I	6		10			III	
7741.916	I	2					V	
7742.456	I	1		1			IV	
7745.818	I	4		4			III	
7746.671	I	2		2			IV	
7746.836	I							

TABLE A. *Temperature classification of dysprosium lines* – Continued

Wave-length (Air)	Spec-trum	Intensity					Temp. Class	Notes
		Arc	Spark	Furnace				
				High	Medium	Low		
7750.148	I	50		150			II	
7751.616	II	250	(125)	50			IIIE	1
7753.115	I	1					V	
7753.548	I	3		3			III	
7754.844	I	6		2			III	
7757.324	I	40		150			II	
7760.083	I	12		6			III	
7764.412	II	2					V	3
7767.119	II	2					VE	
7772.805		2					V	3
7773.424		10		5			III	
7775.783		5		40			II	
7777.808	I	8		15			III	
7780.890	I	100		40			III	
7785.811	II	2					V	
7786.981	I	2		2			IV	
7790.020	I	500		300			II	
7792.853	II	3					VE	
7793.590	I	4		4			III	
7798.012	I	30		40			III	
7799.247	I	2					V	
7801.618	I	4		4			III	
7806.967		1		8(?)			III	
7807.256	I	8					VE	
7808.114	I	3		4			III	
7812.055	I	1000		300			II	
7814.598	I	30		40			III	
7815.115	I	4		2			III	
7815.641	I	3		3			III	
7817.765	II	1					V	
7819.675	II	1					V	
7821.103	I	4		1?			IV?	
7823.154	I	1					V	
7824.357	I	1					V	
7827.569	II	3					VE	
7828.052	I	2		1			IV	
7829.060	II	2*d*?					VE	
7829.111	II							
7830.893	I	1					V	3
7831.679	I	1		2			IV	
7832.767	I	60		200			II	
7833.877	I	20		40			III	
7835.522	II	20	(15)				VE	1
7836.012	I	1		1			IV	
7836.817	I	20		40			II	
7838.607	II	3					VE	
7842.679	II	5					VE	
7843.290	I	1		1			IV	
7844.658	II	4					VE	
7850.748	I	1		1			IV	
7851.765	I	5		5			III	
7858.624	I	2		2			IV	
7860.768	I	8		6			III	
7864.309	II	30	(40)				VE	1
7864.965	I	100		80			III	
7866.099	I	1		1			IV	3
7866.577	I	1		1			IV	
7867.617	II	3					VE	3
7870.638	I	10		2			IV	
7870.744	I	8					VE(?)	
7871.146	I	4		6			III	
7874.934	I	3		2			IV	
7877.142	II	3					VE	3
7881.946	II	2		1			IV	
7889.419	I	4		2			IV	
7893.992	I	2					V	3
7899.750	I	5		40			II	
7900.783	II	–*d*?					VE	
7902.526	I	20		15			III	
7904.520	II	3		–			VE	3
7904.629	I			2			IV	
7908.860	I	?		4			III	3
7909.386	I	300		150			II	
7911.548	I	2		2			III	
7916.739	I	30		200			I	
7922.884	I	8*d*?					VE	
7934.335	I	1		4			III	
7934.976	I	40		250			I	
7940.672	II	6	(5)				VE	1
7948.742	II	5					VE	
7952.244	II	3					VE?	
7954.178	I	8		8			III	
7954.728	I	2		3			IV	
7955.914	I	1		2			IV	
7962.772	I	40		200			II	
7965.413	II	5					VE	
7968.627	I	125		80			III	
7973.134	I	80		50			III	
7982.854	II	50	(40)				VE	1
7983.415	I	3					V	
7990.087	II	4					VE	
7997.764	II	2					V	
8004.474	II	3					VE	
8008.706	II	30	(20)				VE	1
8010.194	I	40		50			III	3
8016.845		4					VE	
8025.312	I	80		400			I	
8027.216	I	50		20			III	
8034.837	II	25	15	1			(V)E	1,3
8035.767	II	2					VE	
8036.043	I	1		4			III	
8040.090	I	50		50			III	
8042.664	I	2		30			II	
8047.277	I	30		60			II	
8050.070	II	10	(6)				VE	1
8050.853	I	30		40			II	
8057.988	I	4		1			IV	
8059.959	II	2					VE	
8065.130	I	2		4			III	
8070.903	II	40	(20)				VE	1
8075.833	I	2		2			IV	3
8077.919	II	8	(8)				VE	1
8098.335	II	8	(20)				VE	1
8106.308	I	15		25			III	
8106.697	I	1		1			IV	
8108.430	II	50	(30)				VE	1
8110.378	I	2		10			III	
8112.624	I	2		3			III	
8116.901	II	30	(20)				VE	1
8121.354	I	3		6			III	3
8123.707	I	6		3			III	
8128.971	I	3		2			IV	
8139.706	I	5		4			III	
8140.724	II	4					VE	

TABLE A. *Temperature classification of dysprosium lines* — Continued

Wavelength (Air)	Spectrum	Intensity					Temp. Class	Notes
		Arc	Spark	Furnace				
				High	Medium	Low		
8142.100	II	3					VE	
8144.295	II	6	(5)				VE	1
8147.288	I	200		300			I	
8149.341	I	1		2			III	3
8150.809	I	1		2			IV	3
8153.797	I	3					V	
8158.684	I	3		6			III	
8160.317	I	5		8			III	3
8169.055	II	6*d*?					VE	
8171.486	I	1		3			III	
8175.156	I	4?		3			III	
8186.400	I			2			III	
8190.482	II	2?					VE?	
8197.290	I	2		2			III	
8198.770	II	80	(25)	2			IVE	1
8201.573	II	300	(120)	30			IIIE	1
8204.928	II	1					(V)	
8208.339	II	8	(5)				VE	1
8210.189	II	2					(V)	
8210.470	II	2					(V)	
8217.042	II	40					VE	1
8218.623	II	125					VE	1
8224.531	II	3					VE	
8225.130	I	5		150			I	
8233.557	II	40					VE	1
8235.379	II	2					V	
8238.398	II	5*d*?					V	
8240.376	I	1		10			III	
8240.948	I	20		40			III	
8242.239		1					V	
8243.906	II	40*d*?					VE	1
8244.535	I	40		100			II	
8245.334	II	1		3			IV	
8246.867	I	10*d*		5			III	
8249.360	I	6*d*?		2			IV	
8255.076	I	1					V	
8255.392	I	1					V	
8257.377	II	8					V	
8264.004	I	4		4			III	
8265.528	I	200		600			I	
8271.628	I	1					V	
8272.407	I	3		2			III	
8284.146	I	3*d*		2			III	
8295.323	I	3		1			IV	3
8302.283	I	2		5			IV	3
8307.823	I	2?		2			IV	3
8314.524				2			III	
8322.186	I			15			III	3
8323.849	I			60			III	
8323.973		10					(V)	3
8324.522	II	10					(V)	
8326.103	I	150		1000			I	3
8335.313	II	3					V	3
8341.519	II	2					V	3
8343.669	I	5		30			III	3
8344.351	II	4					V	3
8346.571	I	3		1			IV	3
8388.526	I	12		60			III	
8392.008	II	200					VE	
8395.776	II	6					V	
8405.854	II	50					VE	
8416.641	II	150					VE	
8424.557	II	3					V	
8435.476	II	1					V	
8438.583	II	150					VE	
8441.444	II	6					V	3
8444.461	II	60					VE	
8448.860	I	5		5			III	3
8455.503	II	5					V	
8461.670	I	2		4			IV	
8462.225	II	1					V	3
8464.362	II	8*d*?					V	
8472.580	II	40					VE	3
8473.566	II	2					V	
8477.784	I	4		15			III	
8480.662	II	20					VE	3
8490.149	I	12		40			III	
8492.370	II	10					VE	3
8506.608	II	1					V	3
8507.817	II	1					V	
8510.792	II	150					VE	
8513.273	II	30					VE?	3
8517.683	II	30					VE?	
8521.105	I	3?		5			III	
8523.386	I	1		20			III	
8525.732	II	100					VE	
8527.295	I	1					V	
8528.326	II	40					VE	
8537.398	I	1		10			III	3
8540.832	II	} 3					V	3
8540.958								
8548.931	II	50					VE	
8554.052	I	1		5			III	
8557.786	II	50					(VE)	
8559.262	I	2		10			III	3
8563.430	I	2		20			III	3
8567.968	II	30					VE	
8573.013	I	1?		2			III	3
8575.577	II	40					VE	
8578.664	I	5		6			III	
8582.638	I	5		40			III	
8586.803	II	8?					V	
8593.202	II	12					VE	
8605.201	II	1					V	
8610.794	I	2		3			III	
8618.521	I	4		4			IV	
8622.556	II	6					V	3
8625.315	I	2		3			IV	
8630.118	I	25		80			III	3
8632.429	II	4					V	
8635.778	II	60					VE	3
8637.215	II	3					V	
8655.935	II	400					(V)	
8657.678	II	200					(V)	
8667.375	II	50					(V)	
8672.617	I	15		30			(III)	3
8678.490	II	200					(V)	3
8685.256	I	4		50			(III)	3
8696.829	II	50					(V)	3
8715.949	II	25					(V)	3
8728.538	I	1		5			(III)	3
8744.098	I	2*d*?		10			(III)	3
8750.400	II	50					(V)	3

TABLE A. *Temperature classification of dysprosium lines* — Continued

Wavelength (Air)	Spectrum	Intensity					Temp. Class	Notes	Wavelength (Air)	Spectrum	Intensity					Temp. Class	Notes
		Arc	Spark	Furnace							Arc	Spark	Furnace				
				High	Medium	Low							High	Medium	Low		
8753.513	II	3		2			(IV)	3	8912.567		8					(V)	
8759.043	II	6					(V)	3	8919.219		5					(V)	3
8762.120	I	2		3			III		8923.817		12					(V)	3
8773.444	I	3		2			IV		8924.814		10					(V)	3
8780.831	I	25		60			(II)	3	8942.854	II	15					(V)	3
8782.496	I	1		4			(III)		8970.763	I	8		3			(IV)	3
8783.524	I	3		4			(IV)	3	8972.248	II	10					(V)	3
8790.978	I	?		20			(III)	3	8985.667		5					(V)	3
8791.389	II	100					(V)		8988.507	I	6		10			(III)	3
8798.378	I	2		3			(IV)		8994.150		2					(V)	
8805.409	I	10		15			(III)	3	9005.619		4					(V)	3
8809.869	I	1		3			(IV)	3	9014.103	II	25					(V)	3
8813.492	I	3		4			(IV)		9020.789	II	200					(V)	3
8817.786	I	5		15			(III)	3	9038.596	I	25		50			(III)	3
8822.240	I	1		2			(IV)		9079.314	II	8					(V)	
8826.543		3					(V)	3	9100.495	I	3*d*					(V)	
8832.811	II	5					(V)	3	9111.168	II	200					(V)	
8833.083	II	20					(V)	3	9136.428	II	4					(V)	
8836.202	I	5		1?			(IV)	3	9169.436	II	20					(V)	3
8836.863	I			2			(IV)		9171.587	II	600					(V)	
8842.633		4					(V)	3	9180.740	II	1					(V)	
8850.374	II	100					(V)	3	9182.318	I	15		10			(IV)	
8866.698	II	10					(V)	3	9200.275	II	15					(V)	3
8868.050	I	2		2			(IV)	3	9251.157	II	8					(V)	3
8873.610		4					(V)	3	9257.664	I	6					(V)	3
8897.212	I	10					(V)	3	9373.326	II	5					(V)	3
8905.748	II	80					(V)	3	9375.806	II	15					(V)	3

Notes to Table A

Column 8

The Temperature Classification scheme used by King is as follows. (See Astrophys. J. **68,** 200 (1928).

I The more decided low-temperature lines.

II Lines that strengthen rapidly at medium temperature.

III, IV, V } Lines requiring successively higher temperatures.

A Denotes a neutral line that is relatively much stronger in the furnace than in the arc.

E Denotes lines of ionized atoms (Dy II).

Column 9

1. See, also, A. S. King and C. E. Moore, Astrophys. J. **98,** 33 to 42 (1943); "E" entered by present authors in Column 8 for lines from this reference, λ3002 to λ8243. This reference used for gap in 1956 list from λ3407 to λ3463 and λ3809 to λ3831.
2. See A. S. King, Astrophys. J. **72,** 244 to 249 (1930); this reference used for gap in 1956 line list: λ3836 to λ3902.
3. Discordance in wavelength, LRL versus A.S.K. listing, exceeds ±0.05 Å for wavelengths given to 2 decimal places by A. S. K.; ±0.1 for those given to one decimal place.

References

[1] A. S. King, Astrophys. J. **97,** 323–380 (1943).
[2] H. N. Russell, J. Opt. Soc. Am. **40,** 550–575 (1950).
[3] F. S. Tomkins and M. Fred, Spectrochim. Acta **6,** 139–143 (1954).
[4] F. S. Tomkins and M. Fred, J. Opt. Soc. Am. **47,** 1087–1091 (1957).
[5] E. F. Worden, R. G. Gutmacher and J. G. Conway, Appl. Opt. **2,** 707–713 (1963).
[6] F. S. Tomkins and M. Fred, Appl. Opt. **2,** 715–725 (1963).
[7] A. S. King and C. E. Moore, Astrophys. J. **98,** 33–42 (1943).
[8] A. S. King, Astrophys. J. **72,** 244 (1930).
[9] A. S. King, Astrophys. J. **59,** 155–176 (1924).

(Paper 74A3–606)

Symposium on Electronic Density of States

Electronic Density of States was the subject of the 3d Materials Research Symposium, sponsored by, and held at the National Bureau of Standards, Gaithersburg, Md. on November 3–6, 1969. Attention was focussed on the correlation of various experimental and theoretical techniques such as optical methods; photoelectron, soft x-ray, and ion neutralization spectroscopy; specific heat; Knight shift; and magnetic susceptibility. Band theory and many-body effects, as they relate to the electronic density of states, were included.

Approximately 100 papers were presented at these sessions, including 16 invited presentations. Six of these invited papers were published in the March–April 1970 issue of the Journal, five are being published in this issue, and five will appear in the July–August issue. All of the papers presented at the symposium will be published by the National Bureau of Standards as Special Publication 323 which will appear later this year.

JOURNAL OF RESEARCH of the National Bureau of Standards—A. Physics and Chemistry
Vol. 74A, No. 3, May-June 1970

Optical Density of States Ultraviolet Photoelectric Spectroscopy*[1]

W. E. Spicer

Stanford Electronic Laboratory, Stanford University, Stanford, California 94305

(October 10, 1969)

The use of ultraviolet photoemission to determine the density of valence and conduction states is reviewed. Two approaches are recognized. In one, the photoemission as well as other studies are used to locate experimentally a limited number of features of the band structure. Once these are fixed, band structure calculations could be carried out throughout the zone and checked against other features of the photoemission data. If the agreement is sufficiently good, the density of states is then calculated from the band structure. The second method depends only on experimental data. Using this approach, features of the density of states are determined directly by the photoemission experiment without recourse to band calculations. In cases where bands are wide and **k** clearly provides an empirically important optical selection rule, this is possible only for portions of the bands which are relatively flat. Successful determinations of this type are cited for PbTe, and GaAs. In metals with narrow *d* bands such as Cu, it has been found empirically that one may explain fairly well the experimental energy distribution curves in terms of transitions between a density of initial and final states (the optical density of states, ODS) requiring only conservation of energy.

The ODS determined by such ultraviolet photoemission studies have more strong detailed structure than the density of states determined by any other experimental method. Studies on a large number of materials indicate that the position in energy of this structure correlates rather well with the position in energy of structure in the calculated density of states. It is suggested, following the very recent theoretical work of Doniach, that **k** conservation becomes less important (and nondirect transitions more important) as the mass of the hole becomes larger. This is due to the change in **k** of electrons in states near the Fermi level as they attempt to screen the hole left in the optical excitation process. These electrons take up the excess momentum. One would expect the **k** conservation selection rule to play an increasingly important role as the mass of the hole decreases. This is in agreement with experiment.

Key words: Copper; copper nickel alloys; density of states; GaAs; Ge; nondirect transitions; optical density of states; PbTe; ultraviolet photoemission.

1. Introduction

Photoemission can give a great deal of detailed information about the optically excited electronic spectra of solids. Adequate interpretation of photoemission data can produce detailed information on the electronic structure and, assuming that Koopmans' theorem [1] holds, on the ground state density of states.

The utility of photoemission lies in two factors: (1) The ability to determine the distribution in energy of electrons excited by monochromatic light, and (2) the ability to study the valence bands of solids over their entire widths. Difficulties arise in correcting for inelastic scattering and electron escape probability and in interpreting the data so corrected. Correction for scattering and escape probability seems to have been rather successfully done in a number of cases [2,3,4,5,6]. There are still detailed questions open in interpreting the data; however, as will be shown in this paper, it is clear that considerable information on the density of states can be obtained from photoemission data independent of these questions.

Let us look in more detail at the essence of optical excitation in solids and the photoemission experiment.

* An invited paper presented at the 3d Materials Research Symposium, *Electronic Density of States*, November 3-6, 1969, Gaithersburg, Md.

[1] Work supported by NASA, NSF, U.S. Army Night Vision Laboratories, U.S. Army—Durham, and the Advanced Research Projects Agency through the Center for Materials Research at Stanford University.

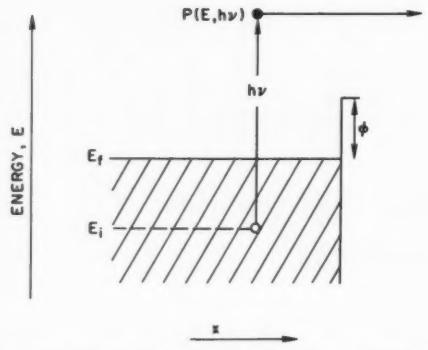

FIGURE 1. *Energy diagram for a metal.* P(E, hν) *is the probability of a photon of energy* hν *exciting an electron to final energy* E. ϕ *is the work function,* E_i *is the initial energy of the excited electron,* E_f *is the Fermi energy.*

Consider the probability, $P(E,h\nu)$, of a photon, of energy $h\nu$, exciting an electron to a final state of energy E (see fig. 1). The excitation spectrum in the solid is then given by the values of $P(E,h\nu)$ for all values of energy. The external photoemission energy distribution $N(E,h\nu)$ would correspond exactly to $P(E,h\nu)$ if all excited electrons escaped without inelastic scattering. Thus,

$$P(E,h\nu) \rightarrow N(E,h\nu). \tag{1}$$

In contrast, the optical constants $\omega\sigma$ or ϵ_2 (from which attempts are often made to determine the electronic structure) are related to the integral of $P(E,h\nu)$ over all possible final states

$$\epsilon_2 \rightarrow \int P(E,h\nu)dE. \tag{2}$$

ϵ_2 is the imaginary part of the frequency dependent dielectric constant and σ is the optical conductivity, $\sigma = \epsilon_2/\omega$. For the relations in eqs (1) and (2), it can be seen that photoemission contains much more detailed information than do the optical constants. This is illustrated by figure 2a, b, and c.

In figure 2a the imaginary part of the dielectric constant for Cu is plotted versus photon energy [7]. The arrows call attention to two values of photon energy, 5.0 and 10.2 eV. A maximum appears in ϵ_2 at $h\nu = 5.0$ eV. There has been considerable discussion [3,4,8,9,10] concerning the optical transition or transitions responsible for this peak. There is no measurable peak in ϵ_2 at 10.2 eV; rather, the curve is almost flat. In figure 2b and 2c, energy distribution curves, EDCs, are presented for $h\nu$ equal to 5.0 and 10.2 eV. The striking thing about these curves is the large amount of structure which is present in them. Whereas only one peak was present in the ϵ_2 curve near 5.0 eV and none was present near 10.2 eV, several pieces of structure are present in the EDCs for each value of $h\nu$.

From the energy at which the structure appears, the initial and final states involved in the optical transition can be quickly identified. In the present case, the electrons within 2 eV of the high energy cutoff, E_{max}, are excited from the almost free-electron-like conduction states lying within 2 eV of the Fermi level; whereas, the sharp structure lying more than 2 eV below E_{max} is due to excitation from the d states.

By noting the manner in which EDC structure moves with $h\nu$, the relative importance of initial and final states can be determined and information can be obtained about selection rules and/or matrix elements. For example, it was possible to determine that the peak in figure 2b at about 2.7 eV was due to a direct transition from states near the Fermi level with a threshold at about 4.4 eV [3]. Examination of band calculations showed that the transition must be centered near the L symmetry point. We will return later to the discussion of the interpretation of photoemission data. In fact, such discussion will provide the central theme for this paper; however, it is first useful to briefly review experimental techniques and the effects of scattering on photoemission data.

2. Experimental Techniques

As was suggested in the Introduction, a large amount of information can be obtained from the photoemission energy distribution curves. A second useful measurement is that of the spectral distribution of quantum yield. Let us briefly review the experimental methods for obtaining such data. In so doing, we will not attempt an exhaustive list of references, but rather will attempt to refer to recent articles representative of the various techniques. Because of his closeness to the work at Stanford, the author will draw particularly heavily on this work.

For many years EDCs were obtained by measuring an I-V curve and differentiating it by hand. The most important modern advancement was the replacement of this tedious and demanding practice by various schemes which yield EDCs directly from the experiment. Most popular are methods which add a small alternating voltage to the retarding voltage so that the derivative is taken electronically [11,12]. By slowly (typically 1 volt/minute) sweeping out the retarding voltage, a complete derivative curve can be obtained. Recently [13,14], measurements have been made at the second harmonic of the alternating voltage to obtain

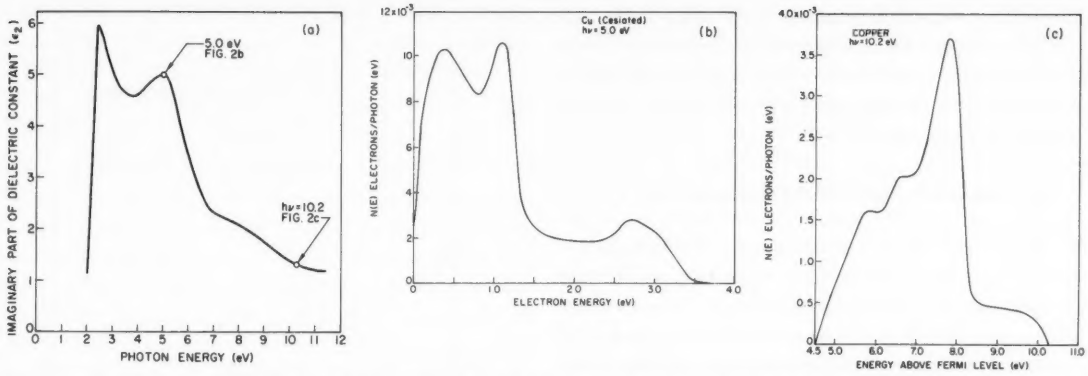

FIGURE 2. (a) ϵ_2 *for Cu.* (b) *EDC obtained from Cu with Cs on the surface for* $h\nu = 5$ *eV. Note that this curve has several pieces of structure in it, whereas the* ϵ_2 *curve had only one peak at 5 eV.* (c) *EDC for clean Cu.* $h\nu = 10.2$ *eV. Note that several pieces of structure occur in the EDC, whereas there is no strong structure near 10.2 eV in the EDC.*

the second derivative of the I-V curve. In this way weak structure in the EDCs can be detected and studied. A second approach is to take a I-V curve and then to either differentiate it electronically [15,16] or by means of a computer.

The geometry and other details of the energy analyzer are also of considerable importance. Because of ease of construction, wide use has been made of a cylindrical approximation [11] to the more ideal spherical geometry of the collector. This has given an energy resolution of between 0.1 and 0.3 eV, depending on the kinetic energy of the emitted electrons, the details of the emitter geometry, the uniformity of the collector work function, and other factors. Of particular importance for small electron kinetic energies are differences in work function between the face of the emitter and its sides. DiStefano and Pierce [17] have recently made an overall study of the factors limiting resolution. They conclude that a spherical collector with a spherical grid providing a field-free drift region should provide a significant increase in resolution provided that effects of the earth's magnetic field are properly minimized. Preliminary measurements with this geometry support these conclusions.

In principle, the measurement of the spectral distribution of quantum yield is much simpler than the energy distribution measurement. All that is needed is a standard detector of known response to which the emission of the sample under study can be compared. In the visible and near infrared spectral ranges, this is fairly easy to achieve because of the high light intensities available and the large number of suitable detectors. It is considerably more difficult in the ultraviolet where light intensity may be low and there are considerable problems with detectors [18]. Groups at the National Bureau of Standards, Stanford University, and other laboratories are cooperating in an attempt to establish good standards on a national-wide basis.

Another very necessary condition for successful photoemission experiments is the ability to provide emitter surfaces which are atomically clean. One must be able to provide such surfaces and insure that they do not contaminate in the course of study (pressures better than 10^{-8} or 10^{-9} Torr are usually necessary). Depending on the material, surfaces may be provided by cleaving [19], evaporation [4,6,20], heating [21], sputtering [22], or a combination of these methods. In covalent semiconductors such as Ge, it is well known that care must be taken to preserve crystalline perfection; however, in metals such considerations seem much less important. In fact, for Cu and Ni, which have been studied both as single crystals and evaporated films, the evaporated samples have given to date as good or better results than have sputtered and/or heat-cleaned samples [21,23]. This is despite the fact that some evaporated samples may have very small crystallite sizes (for example, about 100 Å in the case of Ni [6,20]). The insensitivity to crystallite size is due to the escape length for photoexcited electrons often being much less than 100 Å.

It is often useful to reduce the threshold for photoemission by placing a layer of cesium on the surface of a material. Ideally the cesium will only form a monatomic layer which reduces the work function without affecting any other properties of the solid. However, since Cs may chemically combine, amalgamate, or interact in other ways with the material under study, one must take care. The best procedure is to obtain EDCs from clean material over a photon energy range of several eV or more before placing the cesium on the

surface. Then, after the cesium is placed on the surface, EDCs should be obtained from the same photon energy range. By comparison of the two sets of EDCs, an estimate can be obtained of any extraneous changes produced by the cesium.

3. Electron Scattering Phenomena

As mentioned in the Introduction, one must understand the effects of electron scattering in order to properly interpret photoemission data. Two principal scattering mechanisms are electron-electron and electron-phonon scattering. In the first type of event, the scattered electron loses a large fraction of its original energy to a second electron, which is thus excited. The electron-electron event is characterized by a mean-free path which decreases rapidly as the primary electron energy is increased in the range $E < 12$ eV. The energy loss in the phonon-scattering event is much smaller than that in the electron-electron event and, since this energy loss varies roughly as the Debye temperature, it will be much smaller for the material containing heavier atoms than for those with lighter atoms. There is no evidence that the phonon mean-free path is highly dependent on electron energy as is the case for electron-electron scattering. Kane [24] has pointed out that the electron-phonon scattering will be enhanced for final states having low group velocity (*i.e.*, states associated with a high density of states). Eastman [25] has made the same observation for the electron-electron event. However, it does not appear that massive distortion of the energy distributions are produced by these effects.

There is a threshold for pair production in semiconductors and insulators of about the forbidden band gap energy (*i.e.*, the electron must be above the conduction band minimum by this amount before it can produce a secondary). Thus, only phonon scattering is possible below this threshold. In a metal there is no such threshold. However, as mentioned previously, in both semiconductors above threshold and in metals the electron-electron scattering length decreases quite fast with increasing electron energy. In figure 3 we present values [5,26,27,28] for Au obtained by several different methods. Note that the mean-free path drops by two orders of magnitude within a few eV. The electron-electron scattering effects have been taken into account quantitatively in interpreting photoemission data [3,4,6]. In fact, photoemission measurements can be used to determine the electron-electron mean-free path. The solid curve in figure 3 was deduced from such measurements by Krolikowski and Spicer [4].

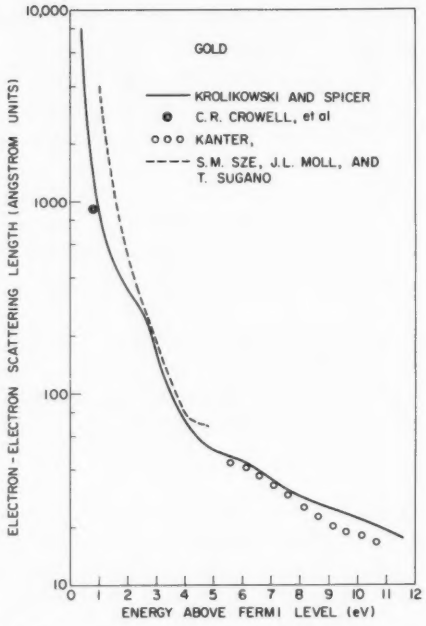

FIGURE 3. *Electron-electron scattering length for Au as obtained by several workers* [5,26,27,28].

More recently, Eastman [29] has developed a direct method for obtaining electron-electron mean-free paths from photoemission measurements. This is based on a variation of sample thickness.

For electron energies below the threshold for pair production in semiconductors, photoemission has been used extensively by James and Moll [30] to study the scattering of electrons by phonons in GaAs. This is of particular interest because of its importance in the Gunn effect. DiStefano and Spicer [31] have developed special photoemission techniques to study the scattering of hot electrons in alkali halides by phonons.

We give the examples listed above to illustrate the degree to which scattering of excited electrons in the photoemission experiment has been studied and is understood. This is not to say the processes are understood in all detail. This is not the case; however, a good, first-order understanding does seem to exist. There are other possible scattering phenomena which are less well understood. These include scattering from: (1) Bulk imperfections (such as grain boundaries), (2) the sample surface, and (3) scattering from oxide or other "crude" layers on the surface [19].

4. Interpretation of Photoemission Data: Direct and Nondirect Transitions

The present author and his coworkers have suggested [2,19,32] that, for excitation from *certain*

quantum states characterized by low mobility holes, conservation of **k** may not provide an important selection rule and that only conservation of energy need be considered in interpreting the photoemission data. Such transitions were called nondirect.

The suggestion of nondirect transitions was prompted by the character of the photoemission data obtained from states of this character. Based on this data, it was further suggested that a measure of the density of states could be obtained directly from analysis of the photoemission data. Of course, such a strong departure from accepted theory was met with considerable skepticism. Recently, band calculations [25,33,34,35], as well as new photoemission data (much of which will be reported at this meeting), have shown that there are certain strong similarities between the experimental EDCs interpreted as nondirect and the EDCs calculated using band structure results and **k** conservation when broadening effects were included in the calculation. However, other important systematic differences do remain, which may have considerable significance. In this paper, I will place particular emphasis on this discussion since it is central to the experimental determination of the density of states from uv photoemission.

Before proceeding further with this discussion, it should be recognized and emphasized that there were a number of materials in which direct transitions were clearly identified and many in which *only* direct transitions were seen; for example, the column IV and III-V semiconductors [36]. It should also be recognized that the criterion of peaks "moving with $h\nu$" (or the criteria of peaks which are stationary independent of $h\nu$) has been considered a necessary, but not sufficient, condition for identifying a nondirect transition [36,37,38]. In particular, abrupt appearance or disappearance or strong modulation of *peaks* has been taken as suggestive of direct transitions even when peaks "*move with hν*" [38]. PbTe [37], GaAs [36], CdTe, CdSe, and CdS [38] provide examples of this.

Another method for attempting to distinguish, experimentally, between direct and nondirect transitions is to examine the effects of reducing or destroying the periodicity of the lattice. Since **k** conservation is imposed by the periodicity of the lattice, destroying that periodicity should remove any importance of **k** conservation as an optical selection rule. Examples will be given of cases where periodicity is reduced or destroyed by alloying, melting, or forming an amorphous solid. Brust [39] has recently pointed out the possibility of explaining these changes by introducing an uncertainty in **k** rather than removing it completely as a selection rule.

Neville Smith has played a key role in the development of calculations of photoemission from *d* bands at Stanford [33]. A paper describing some of his work is included in this conference as is work on indium and aluminum by Koyama and Spicer [40]. The group of Janak, Eastman, and Williams [41] has also completed calculations assuming direct transitions for Pd which they will report at this meeting. I will not attempt to summarize these papers; but rather I will attempt to emphasize certain points.

The nondirect transition model was developed empirically since it appeared to give a good first approximation to the behavior of experimental photoemission data in a number of cases, including Cu. This model has been described in detail elsewhere [2,3]. The essence of it is that the optical transition probability, $P(E,h\nu)$, is given by the product of the optical densities of states (ODS) at energies E and $E-h\nu$:

$$P(E,h\nu) \rightarrow \eta(E)\eta(E-h\nu). \qquad (3)$$

Here $\eta(E)$ is the optical density of empty states at an energy, E; and $\eta(E-h\nu)$ is the filled ODS at an energy $h\nu$ below E. The term "optical density of states" is used since this density of states is obtained from the optical transitions as seen in photoemission. It is also appropriate since the optical density of states may be modified from the true density of states by optical matrix elements.

Let us examine direct and nondirect models for Cu as well as the experimental data used most recently. Copper is most appropriate for a number of reasons. First, its band structure seems to be as firmly established as any of the noble or transition metals. Second, it possesses relatively narrow *d* bands which might provide nondirect transitions; and third, experimentally Cu has been studied as thoroughly or more thoroughly than any of the other noble and transition metals so that the experimental data now seems to be on a very good footing.

Let us now examine photoemission from clean Cu for $6.0 \leqslant h\nu \leqslant 11.6$ eV. In figure 4 we present EDCs for Cu from the work of Krolikowski and Spicer [4]. More recently, Eastman [42] and Smith [43] have reproduced these curves; thus, the experimental data seems quite reliable. This data has all of the characteristics which lead to the assumption of nondirect transitions. For one thing, the peaks superimpose when they are plotted against $E-h\nu$, *i.e.*, against the *initial* state energy. Thus, it is apparent that the EDC struc-

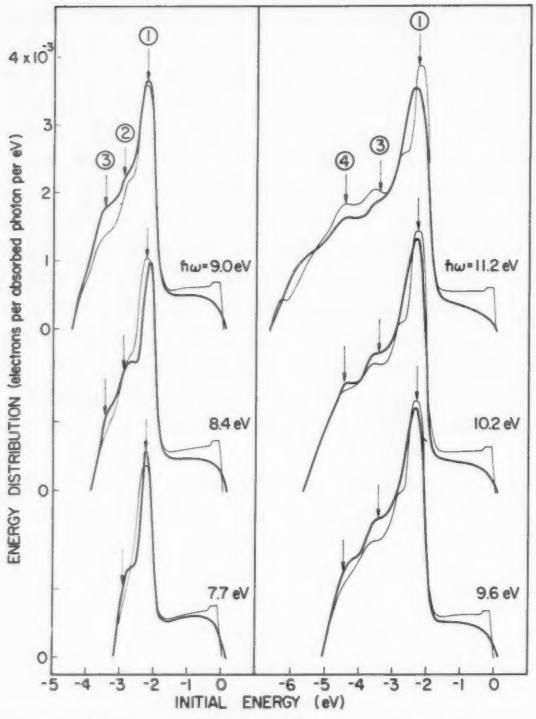

FIGURE 4. *EDCs for clean Cu plotted versus the initial energy. The solid curve indicates the experimental curve and the thin full curve gives the energy distribution calculated using the nondirect model for the values of photon energy indicated. The arrows indicate the position in energy of structure in the ODS.*

ture is due to the same structure in the initial ODS. Note also that the structure in the EDC varies very monatonically with photon energy. As we shall show later, a striking characteristic of the direct transitions calculations is the relatively larger amount of modulation which they predict in the peak strengths as a function of photon energy.

As described by Krolikowski and Spicer [4], the ODS was obtained from the photoemission and optical data. The ODS so obtained is presented in figure 5a and b. From this ODS, the thin full curves in figure 4 were obtained from this ODS using the nondirect, constant matrix element model. As can be seen, the agreement is rather good particularly since it is on an absolute basis. The notable difference is that the first peak broadens and the second peak appears to merge into it at higher photon energies.

In figure 5a and b, the ODS obtained from the photoemission studies is compared to the density of states from two band calculations [44,45]. As can be seen, rather good agreement is obtained between the locations of the major pieces of structure in the ODS and the calculated density of states. However, there is no such agreement between the relative strengths of the structure. This may be due to the effects of optical matrix elements, to difficulties in the band calculations (note the difference between the two calculated density of states), or to other effects.

In figure 6, the results [33] of calculations based on the direct-transition model for clean Cu are presented. These calculated curves have strong similarities to the experimental data. However, in order to obtain such agreement it was necessary to include a Lorentzian broadening of 0.4 eV for the calculated curve. Other calculations [34,35] use broadenings of between 0.3 and 0.7 eV. If the broadening is not used, much too much sharp structure appears in the calculated EDCs and this structure is modulated much too strongly and fast. The use of the broadening function finds partial justification in several factors—the instrumental and lifetime broadening, the finite lifetime of the excited carriers, and the inaccuracy in the band calculations. However, it is important that we keep the broadening in mind since it tends to make the direct and nondirect calculations more similar and also since it may provide an empirical method of making correction for many body effects. In the limit of flat initial bands, the direct and nondirect models would be identical. As the bands become less flat, increased broadening will still tend to keep the agreement between EDCs calculated on the direct and nondirect models.

Let us now examine the EDCs calculated by the direct method. In figure 6 we show the results of the calculations of Smith and Spicer and in figure 7 we compare the results of these calculations to experimental data. Again, the comparison is on an absolute basis. Several things are noteworthy about these results: (1) The position in energy of peaks in the direct calculations is constant on the $E-h\nu$ plot, (2) the position of structure corresponds rather well with the position observed experimentally (the numbered lines correspond to the position of structure found experimentally and in the ODS), and (3) the modulation of peak heights and widths is much stronger than anything seen experimentally. If, in fact, such strong modulation was observed experimentally, this would have been attributed to the effects of direct transitions or matrix elements effects despite the constant position in $(E-h\nu)$ of the peaks. Such identification was made, for example, in the II-VI compounds [38], GaAs [36] and PbTe [37] where strong modulation was observed experimentally.

The constant position in energy of the direct structure in figure 6 and its agreement with experiment is

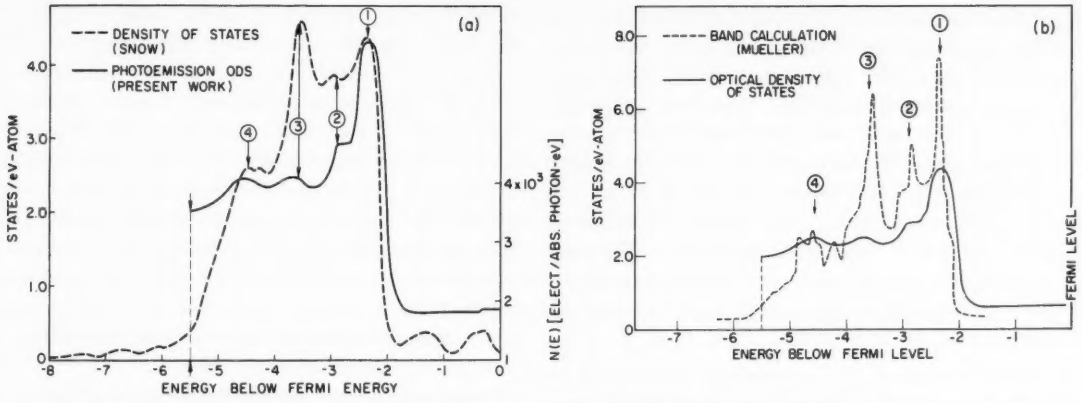

FIGURE 5. (a) *Comparison of the ODS with the density of states calculated by Snow* [44] *using an 5/6* $\rho^{1/3}$ *exchange term. Snow's density of states have been shifted by 0.2 eV to place the Fermi level to* d*-band energy in exact agreement with experiment. The absolute scale was placed on the ODS by placing 11 electrons within 5.5 eV of the Fermi level. Note that the four pieces of numbered structure coincide rather well in energy. The numbered arrows correspond to those in figure 4.* (b) *Comparison of the ODS with the density of states calculated by Mueller* [45].

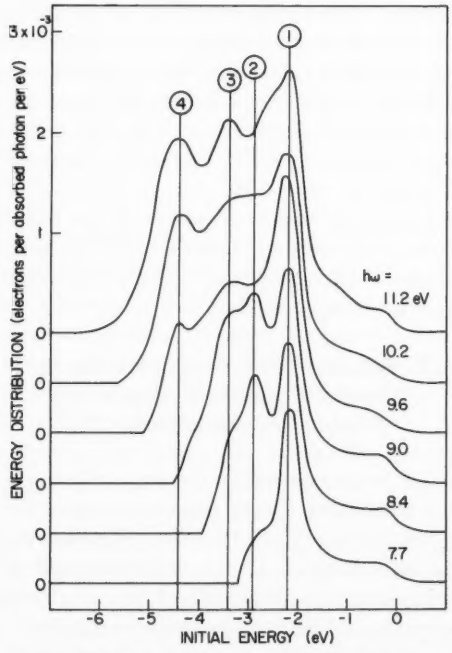

FIGURE 6. *The EDCs calculated for Cu by Smith and Spicer assuming direct transitions.*

not surprising in retrospect in view of the agreement between the ODS and band calculations shown in figure 5. It would appear, at least for the limited range of $h\nu$ covered by this study, that the Cu bands are sufficiently flat and that the broadening effects are sufficiently large so that the **k** conservation condition does not impose overwhelming constraints on the optical excitation process. The fact that the nondirect model gives better detailed agreement with the experimental data than the direct model, suggests that many body effects may still be important in bringing in a range of **k** rather than a delta function in the optical absorption process.

In another paper, presented at this meeting, Neville Smith [34] will show new experimental data which give

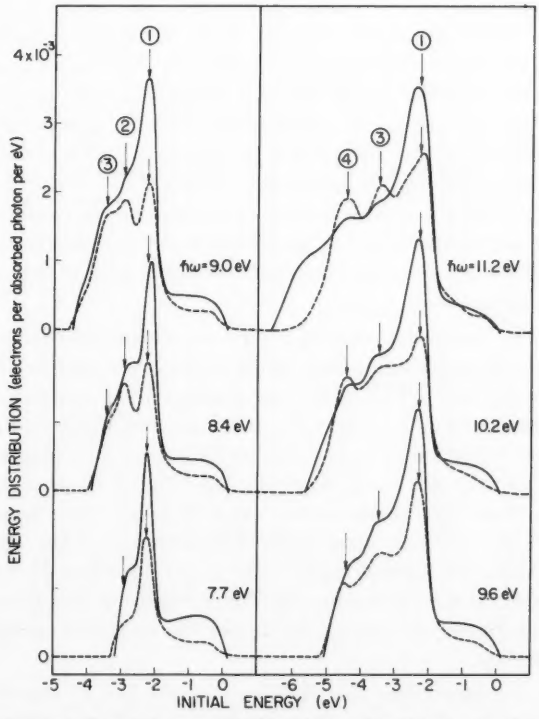

FIGURE 7. *Comparison of the EDCs calculated for Cu using the direct transition model with the experimental EDCs. The full line gives experimental and the dashed line calculated EDCs.*

clear evidence of direct transitions in cesiated Cu. The transitions originate from states 2.8 to 3.8 eV below the Fermi level. It is in this region that the *d* bands have greatest curvature. Recognizing that this curvature should provide the most easily detectable evidence for direct transitions, Berglund and Spicer [3] looked especially for direct transitions in this region. Apparently poorer sample preparation conditions prevented them from seeing the transitions. The success of Smith is a tribute to him and to the advances in vacuum and preparation techniques made at Stanford and elsewhere in recent years.

Smith has also made direct transition calculations of the EDC for cesiated Cu. These show the effects found experimentally; however, despite the inclusion of a 0.3 eV broadening factor, the predicted modulation is considerably stronger than that observed experimentally.

There is perhaps a good analogy between the present situation in this matter and that with regard to x-ray emission spectroscopy for many years. The simple and popular view of the latter field was that one could always explain the x-ray emission spectra just in terms of single particle transitions so that the valence band density of states could be obtained directly from the emission spectra if "atomic-like" matrix elements were properly taken into account. With the simple metals fair agreement was obtained between experiment and theory on this model, although certain nagging inconsistencies remained. The situation has changed drastically in the last few years since theorists have had success in treating the many body effects of the hole in the core state. I will not attempt to review this work since it will be discussed in some detail at this conference. However, there may be a parallel with regard to the uv photoemission work.

At Stanford, Doniach [46] has been expanding his investigation of many body effects in the x-ray photoemission effect to include the many body effects associated with screening of the valence band hole in the uv optical excitation process [32]. Preliminary results suggest that such effects exist, producing a spread in possible **k** in the optical transitions, and increase in importance as the effective mass of the hole increases. Thus, the flatter the valence band is, the larger the effect. If one looks at the Cu results with this in mind, one notes that the flatter the bands, the better the nondirect model works.

In concluding this section, I would like to remark that the direct transition model is based on a rather idealistic assumption which applies best where the bands have good curvature; empirically, this model seems to work very well for a wide range of materials of this type. On the other hand, the nondirect, ODS, model should work best in materials with quite flat bands. It may never be completely correct (we must understand the physics better before it is possible to pass quantitative judgment); however, its great simplicity may make it a good first approximation when it can be successfully applied, *i.e.*, when the EDCs based on the ODS are in relatively good agreement with experiment. Certainly the success with Cu, Ni, and similar material, suggests that it may give us the best first approximation to the densities of states of these materials which can be obtained solely from experiment.

There may be an intermediate range of bands and materials in which neither the direct nor the nondirect model applies with great accuracy. In this case, detailed understanding can only be obtained when theories such as that of Doniach are fully developed. In the meantime, it is probably well to keep open the possibility of transitions occurring over a range of **k** and not just at a given value. It would be extremely nice if in the direct calculations, a broadening could be put in by a distribution in **k** before searching the zone rather than over energy after the vertical transitions have been tabulated.

Experimentally, it is important to obtain data over a wider range in energy to test the selection rules with more rigor. Eastman [29] has already begun to do this with very interesting results.

5. Effect of Reducing or Destroying Crystal Periodicity: Liquid In, Alloys, and Amorphous Ge

Another way of testing for the importance of **k** as an optical selection rule is to reduce or destroy the long-range order of a crystal. Clearly as the solid becomes increasingly disordered, any dependence of **k** must become less and less well defined, *i.e.*, a single value of **k** can no longer be used to define a quantum state. Rather, if a description in terms of **k** is used, it must contain a distribution of **k**; a single **k** will be insufficient. In the limit of complete disorder, **k** will lose meaning as a quantum number.

5.1. Indium

Indium has been studied experimentally by Koyama [18] in the crystalline, amorphous and liquid forms. Note that, since it contains no *d* electrons, In would not be expected to fall within the class of nondirect materials. In addition, Koyama has made calculations based

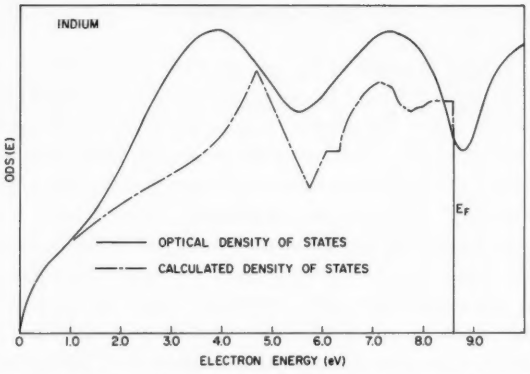

FIGURE 8. *Comparison of the ODS for In with the density of states obtained from band calculations [40].*

on direct as well as nondirect models. These calculations will be described in detail in a separate paper of this conference [40]. Koyama's findings for crystalline indium are quite interesting: (1) Both the direct and nondirect transition models fit the experimental data fairly well (as they do for Al), (2) the EDCs for In are characterized by two broad peaks separated by a minimum which correlates [47] well (in either model) with a large band gap in the band structure of Ashcroft and Lawrence [48] (see fig. 8), and (3) the principal features of the EDC (the two peaks) were seen to persist in liquid indium despite highly increased electron scattering. Since there seems, at least at present, to be less physical justification for the nondirect model in In than in Cu, it is tempting to assume for this material that direct transitions dominate in the crystalline material and that nondirect transitions occur in the liquid. Even then a question would arise as to why the density of states structure due to crystalline potentials persists into the liquid. (Shaw and Smith [49] have found theoretical evidence of such effects in Li.) Koyama [18] has suggested that this is due to the dominance of short-range interactions in determining the electronic structure and thus the density of states of both liquid and crystalline In. Clearly studies of In at higher resolution and for a wider range in $h\nu$ should prove very worthwhile.

In any case for both Al and In, the density of states obtained by the nondirect analysis seems to be in fair agreement with the results of band calculations. As the direct transition calculations show, this may be due to the large range in **k** space from which direct transitions can take place and thus not be a true indication that **k** vector is unimportant (although, again, some uncertainty in **k** is probably important in bringing the direct and nondirect models into agreement). The sensitivity of the calculated EDCs to the electronic structure is illustrated by the fact that, whereas Ashcroft and Lawrence's band structure for In agreed with experiment, other proposed band structures [49] did not give agreement with the ODS.

Mosteller, Huen and Wooten [50] have recently studied the photoemission from Zn as a function of temperature and found that the quantum yield decreased significantly on cooling the sample from room to liquid N_2 temperature. Based on this, they note the possibility that in Zn the ultraviolet optical transitions may be indirect, *i.e.*, phonons conserve **k**. Such temperature dependence has not been observed for other semiconductors and metals such as Cu, Gd [51] and Cr [52] which have been studied as a function of temperature. The Zn results are mentioned here because of the similarity between the In and Al band structure and that of Zn and because In and Al have not been measured below room temperature.

5.2. Amorphous and Crystalline Ge

In contrast to In, Ge provides a striking case of a material whose optical properties and uv EDCs change drastically when the long-range order is destroyed by forming amorphous Ge. Photoemission studies show clearly the direct nature of the transitions in crystalline Ge [36] in agreement with analysis of optical data [53]. Thus, differences between crystalline and amorphous Ge are of considerable importance.

Figure 9 indicates ϵ_2 for the amorphous and crystalline material [54,55] and figure 10 indicates EDCs for

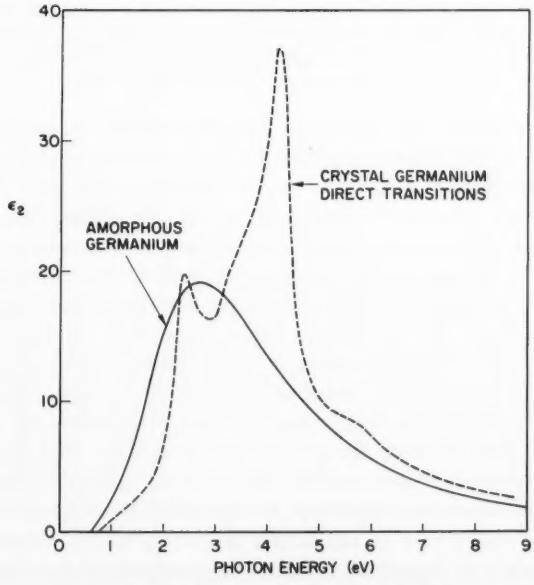

FIGURE 9. ϵ_2 *for amorphous and crystalline Ge.*

378-324 O - 70 - 7

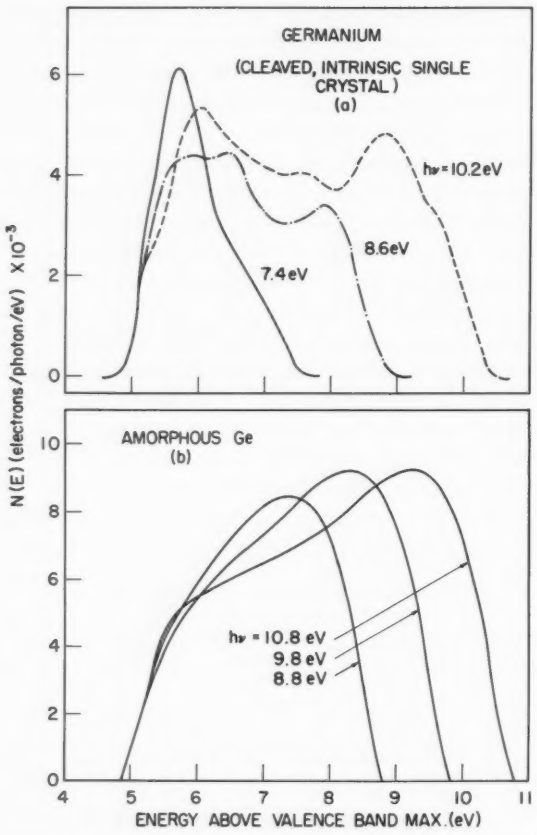

FIGURE 10. *Photoelectron energy distributions for Ge surfaces. (a) Cleaved, intrinsic, single crystal. (b) Amorphous film. The vertical axis gives the number of electrons per absorbed photon per eV. The horizontal axis gives the electron energy relative to the maximum in the valence band. The sharp structure in (a) is due to direct transitions in specific regions of the zone. The single broad peak in (b) is due to a peak in the valence-band optical density of states.*

crystalline and amorphous Ge [54,55,56,57]. As can be seen, the changes in ϵ_2 and the EDCs which accompany the change in form of Ge are first order. The loss of sharp structure is clearly due to the loss of long-range order. In their studies of amorphous Ge, Donovan and Spicer have used a nondirect analysis with considerable success to treat data from the amorphous material. In figure 11 the ODS obtained from these studies is compared to the density of states obtained from band calculations [58]. Brust is approaching the problem of amorphous Ge from calculated band structures by a method in which there is a spread in **k** associated with the optical transitions and thus is intermediate between the direct and nondirect models [59]. Because of its flexibility due to the possibility of assigning various values to the spread in **k**, this approach clearly has certain advantages over the pure nondirect approach.

5.3. Cu-Ni Alloys

A third example of the effect of disorder is in the alloys such as those between the noble and transition metals. Here the lattice periodicity is not destroyed. Rather, atoms with two different potentials are arranged at random, or almost at random (it appears that clustering effects are negligible [21]) within the periodic lattice. Since the potentials are quite different (for example the transition metal typically produces a virtual-bound state when dissolved in a noble metal), the effect on the periodicity should be considerable. Despite this, the effect on the ϵ_2 and on the EDCs of the host metal does not appear to be drastic. The principal effect is in the production of a virtual-bound state under the proper circumstances. Such states have been and are being qualitatively studied through the use of photoemission [21,23,60,61,62,63].

In figure 12, the optical parameter $\omega\sigma$ is presented for the Cu-Ni alloys studied by Seib and Spicer [21,23]. Except for $h\nu<2$ eV in the Cu-rich alloys where the change is due to the formation of a virtual-bound Ni state, the changes are much less than those found in the crystalline to amorphous transformation of Ge.

As outlined in the Introduction, photoemission can give a more detailed look at the optical transition than can the optical data. Examination of EDC data from the alloys shows that the direct transition from the *s-p*-derived bands near the Fermi surface at L is not detectable in the alloys [21]. However, the transitions from the d states are much less affected. In fact, the EDCs from Ni and Ni-Cu alloys with up to 19 percent

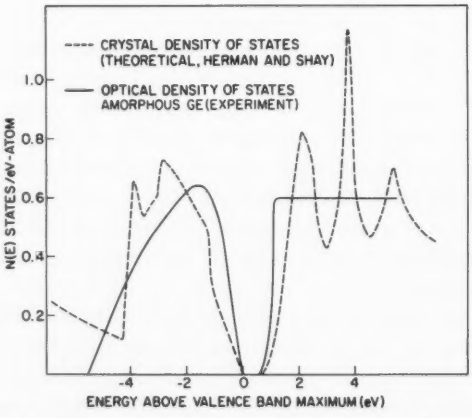
CRYSTAL DENSITY OF STATES (THEORETICAL, HERMAN AND SHAY)
OPTICAL DENSITY OF STATES AMORPHOUS GE (EXPERIMENT)
N(E) STATES/eV-ATOM
ENERGY ABOVE VALENCE BAND MAXIMUM (eV)

FIGURE 11. *Optical density of states for amorphous Ge as determined by photoemission compared with the electronic density of states for crystalline Ge calculated by Herman and Shay. The vertical axis is in units of states per eV per atom for the crystal density of states and in arbitrary units for the optical density of states. The energy zero in both cases is taken at the maximum of the valence band.*

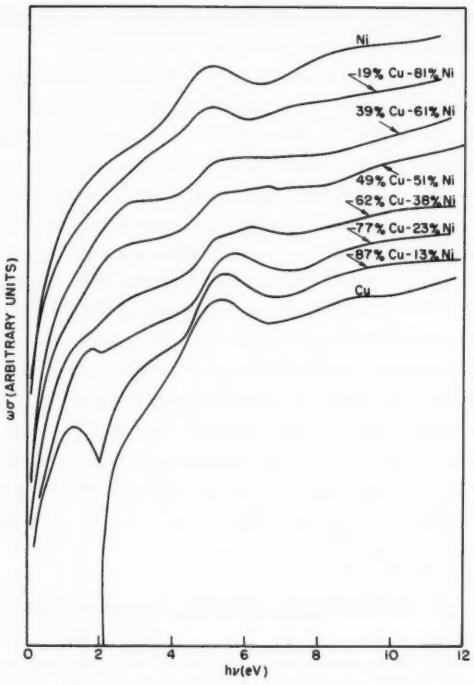

FIGURE 12. *The optical constant ωσ for pure Ni and Cu and a series of Ni-Cu alloys.*

Cu (atomic present) are almost indistinguishable except for effects due to the change in work function. This is shown by the data in figure 13. Even for 39 percent Cu, the position of the two strong peaks in the EDC were unchanged [23].

Let us next examine the Cu-rich alloys. In figure 14 we present data for pure Cu and Cu containing 13 and 23 percent Ni [21]. As can be seen, the Cu *d* edge is little changed and the position in energy of structure from the *d* bands is similar to that in the pure material; however, the relative strengths of the peaks are changed.

The contrast in optical properties and EDCs between these alloys and Ge in its crystalline and amorphous forms is striking. For the alloys, the changes are relatively small whereas, for Ge, they are much larger. **k** conservation clearly plays the dominant role in determining the optical transition probabilities in crystalline Ge; thus, destroying the long-range order completely changes the optical properties. The insensitivity of Cu and Ni to disruption of the long-range order suggests that the optical transitions from the *d* states of pure Cu and Ni are, on the average, much less strongly affected by the **k** conservation condition; however, the *L* transition from the *s*- and *p*-derived states is clearly a direct transition and this disappears in the alloys studied.

6. Methods of Determining the Density of States from Ultraviolet Photoemission Data

Two extreme approaches can be taken in using photoemission data to determine the density of states of solids. One is to use the photoemission results to provide input into band calculations. This approach is not necessary if first-principles band calculations give exact results. If this is not the case, the band calculations can be adjusted to give agreement with the experimental data. Such correction is often necessary and, in addition to overcoming uncertainty in the potential used in the band calculation, the empirical correction may correct for departures from Koopmans' theorem as, for example, suggested by Herman [66]. One approach is to parameterize the calculation and use experimental data. de Haas-van Alphen data or optical data could also be used for adjusting the band calculations. Since the de Haas-van Alphen data give experimental data only at the Fermi surface, it is not very sensitive to energy shifts from the Fermi level. Unambiguous interpretation of structure in the optical constants, such as ϵ_2, has proven very difficult. Piezoreflection has proven to be very powerful in Cu [10] but despite considerable effort, so far has not been successfully applied to Ni [67]. A difficulty in piezoreflection also lies in estimating the absolute or relative strength of optical transitions whose symmetry is determined by these measurements.

If first-principles band calculations were thought to be sufficiently good, the photoemission studies would

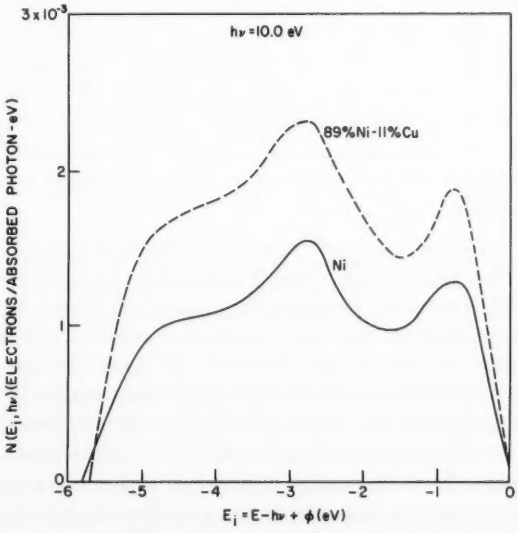

FIGURE 13. *The EDCs at hν = 10 eV obtained from pure Ni and a Cu-Ni alloy containing 11 atomic percent Ni.*

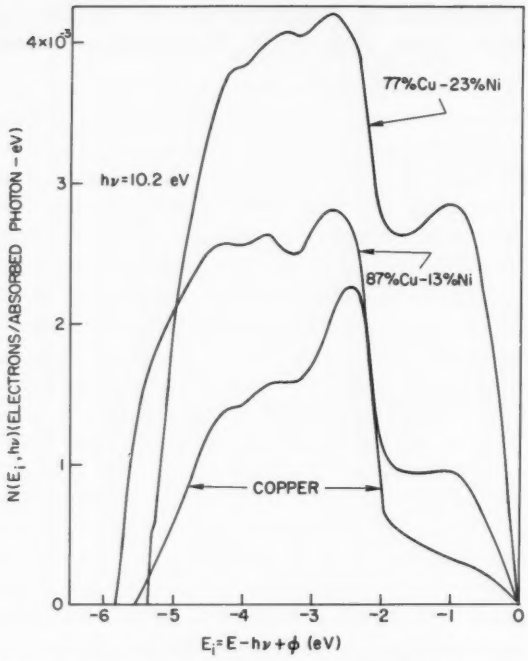

FIGURE 14. *EDCs from pure Cu and two different Cu-Ni alloys. Note that the Cu* d *edge and the position in energy of the* d *peaks is essentially unaffected by the alloy.*

simply serve as a check. For best results, this approach requires two conditions. First is a fairly accurate and well-advanced band theory. Without this, it is difficult to relate the photoemission data to the band structure in a meaningful way. Second is photoemission data which shows dramatic band structure effects such as the onset of the L transition in copper or the Γ transition in CdTe [38]. For materials like GaAs in which **k** conservation dominates the optical transition probability, Eden has developed a systematic method for comparing photoemission results and the results of band calculations. This will be reviewed briefly in the next section.

A second approach is to attempt to obtain density of states information directly from the photoemission data. The more apparent the connection between the photoemission data (*i.e.*, the optical transition probability) and the density of states, the more efficient is this approach. As we will see in the next section, it is very difficult to obtain density of states information from photoemission data for a material such as GaAs where **k** conservation provides a dominant optical selection rule; however, in a case such as copper where **k** conservation does not play such a dominant role, the nondirect method of analysis gives a good mechanism for obtaining the principal features of the density of states from experimental data.

The nondirect transition [3,4] model provides a simple way to analyse the photoemission data to obtain an ODS. Once this is done, EDCs can be calculated and compared with experiment. In this way, the consistency of the nondirect approach can be judged. Only where reasonable consistency is obtained can the nondirect approach be used in a meaningful way. However, even when clear evidence is obtained that some structure is due to direct transitions, useful density of states information can apparently be obtained from the nondirect approach when EDCs calculated using the ODS reproduce closely enough the major strengths in the experimental EDCs. (Cu [3,33,34] and Au [5] appear to be examples of this.) By major strengths, we mean attention should not be focused on relatively weak structure which is clearly direct, but on the overall amplitudes in the EDCs.

7. A Sampling of Experimental Data

Since this paper is already lengthy, we will not attempt a comprehensive survey of the photoemission literature; rather, we will attempt to present only a few representative results which have not been presented previously in this paper in order to illustrate and amplify the remarks made earlier.

Photoemission measurements and the nondirect analysis has been made on a fairly large number of transition and noble metals other than those mentioned earlier. Eastman, in particular, has obtained the ODS for a wide range of transition metals [6,20,29]. In figure 15 we present the ODS obtained by Eastman for ten metals [68]. For the sake of comparison, the density of states from band calculations are also given [68,69]. Although the agreement between experiment and calculation is not perfect, it is encouraging, particularly when one realizes that the band calculations were not highly refined and in some cases were just obtained from the calculation for a different material using a rigid-band approximation. The agreement obtained suggests that there is a meaningful relationship between the ODS and density of states obtained from band calculations, as does the agreement found for Cu [3,4], Ag [3,62,70], Ni and other transition [6,52] and rare earth metals [71].

In section 4, it was suggested that the narrower the bands the more valid the nondirect approach and thus the ODS of the correct density of states. If this is true, the situation within the transition metals should become less favorable as the atomic weight of the metal

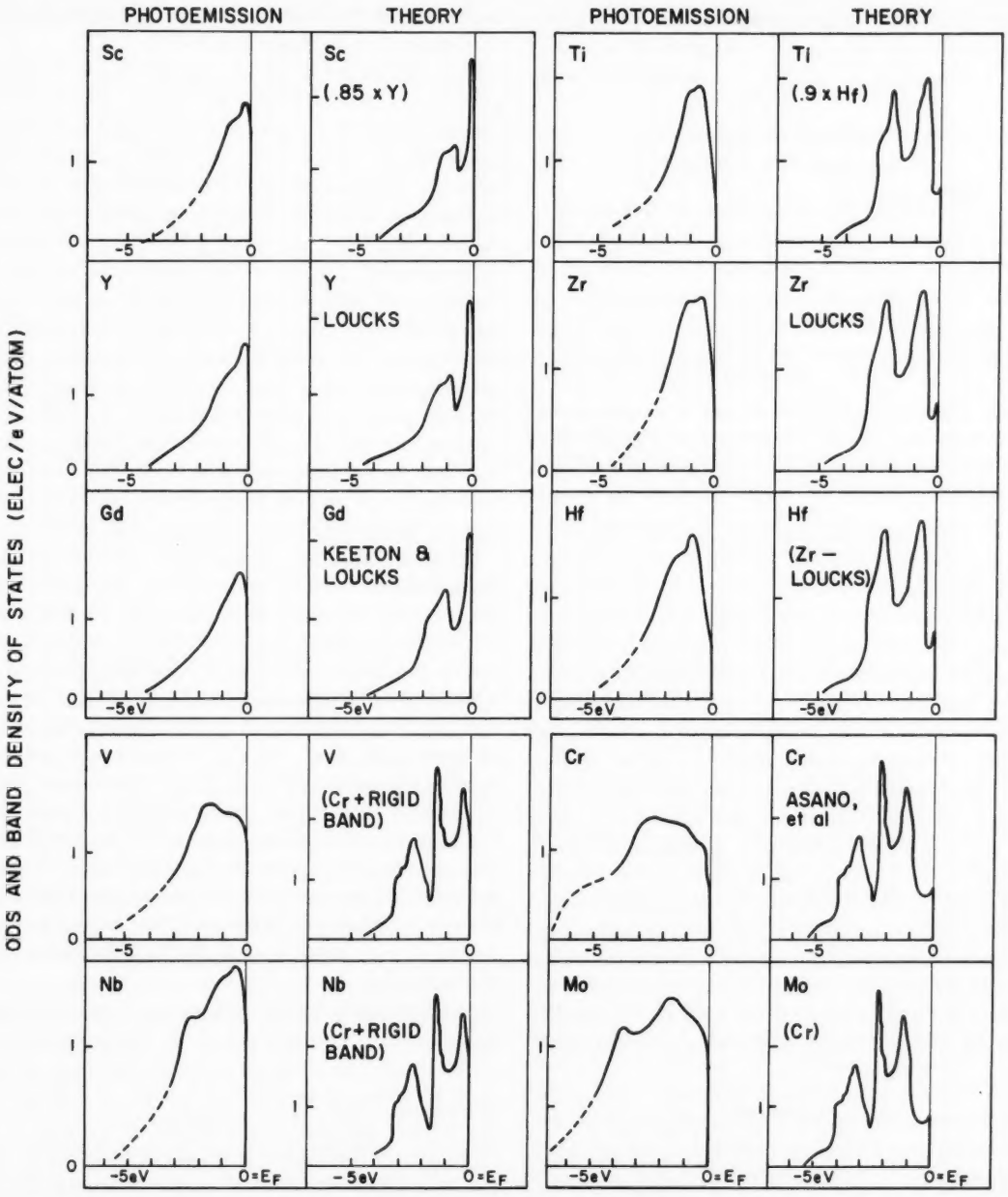

FIGURE 15. *Optical density of states obtained by Eastman as compared to the density of states obtained from band calculations. This figure is taken from ref. 68.*

increases since relativistic effects will broaden the bands. For example, the *d*-band width of Au is about twice that of Cu. Krolikowski and Spicer [5] have also studied clean Au in good vacuum for $5.4 \leq h\nu \leq 11.6$ eV and in poor vacuum for $h\nu$ values of 16.8 and 21.2 eV. From this work the ODS presented in figure 16 was obtained. As can be seen in figure 16, the ODS is in rather good agreement with the EDCs obtained from soft x-ray photoemission work [72]. The photoemission results also have been found by Ballinger and Marshall [73] to correlate rather well with their band calculations. On the other hand, work by Eastman at photon energies of 16.8 and 21.2 eV in good vacuum gives strong evidence that direct transitions are important in

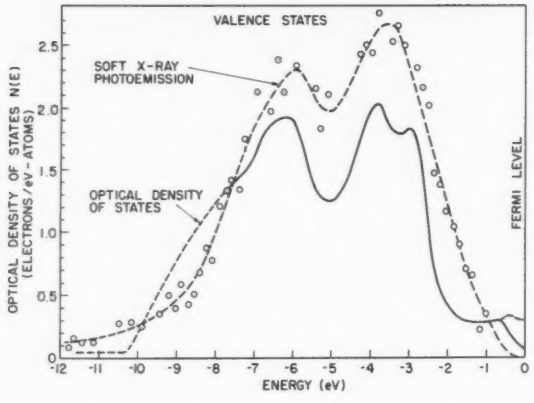

FIGURE 16. *Comparison of the ODS and the soft x-ray photoemission results of Siegbahn, et al. [72]. The x-ray results have been shifted to lower energy by 0.6 eV to obtain the best fit. (It is difficult to set the absolute zero of energy in the x-ray experiment.)*

Au. This series of results suggest that quite useful density of states information can be obtained from the relatively narrow bands of noble and transition metals by the ODS type of analysis even when direct transitions are important and that the broadening of the *d* band in going to Au does not make the ODS approach useless.

Up to this point we have concentrated to a large extent on materials for which the nondirect analysis can be used. In order to give perspective, let us now examine GaAs in which **k** conservation has been found to provide a dominant optical selection rule as it has been found for Ge, Si, and other III-V compounds [36]. If structure in the EDCs is due to peaks in the initial or final density of states, this can be detected by plotting the EDCs against initial energy ($E-h\nu$) or final energy (E) respectively. This argument holds even if the transitions are direct. The distinction between direct and nondirect transitions is made on the basis of modulation of the strengths of the peaks with particular attention being paid to evidence for them appearing or disappearing as photon energy is varied [36,37].

With this in mind, let us examine figure 17a and b where two typical EDCs for GaAs [36,74,75] are plotted versus final, figure 17a, and initial state energy, figure 17b. As can be seen, these EDCs are particularly strong in structure. Despite this, there is little tendency for the structure to fall at the same energy either on initial ($E-h\nu$) or final, energy plot. This shows clearly that **k** conservation provides an important selection rule. As a result, it is difficult to obtain density of states information directly from such plots. Eden [74] and Eden and Spicer [75] have derived a reasonable way of analyzing such data. This is done by making a plot of the final state energy of structure in the EDC, E, of structure versus the photon energy. Such a plot is shown in figure 18 for cesiated GaAs. One can obtain from band calculations theoretical plots of the same type for the symmetry directions of the crystal. By superimposing the two plots, it is possible to make identifications of the structure in the EDC. Such identification is indicated in figure 18. Further details are available elsewhere [36,74,75]. To obtain information on the density of states, it is sufficient to note two features: (1) A horizontal set of points for $E \approx 5$ eV labeled, "Final States Near L_3,W;" and (2) the 45° line between final state energies of about 4.5 and 8 eV labeled, "Transition II from Band 3 Minimum." Since (1) is a fixed, final state, it would suggest a peak in the final density of states at about 5 eV. In figure 19 we present a band structure for GaAs by Cohen and Bergstresser [76] along with the density of states calculated from it by Shay and Herman [77]. As can be seen, there is a very sharp peak in the final density of states at about 5 eV.

The 45° line in figure 18 indicates a transition from initial states at a fixed energy E_i since $E = E_i + h\nu$.

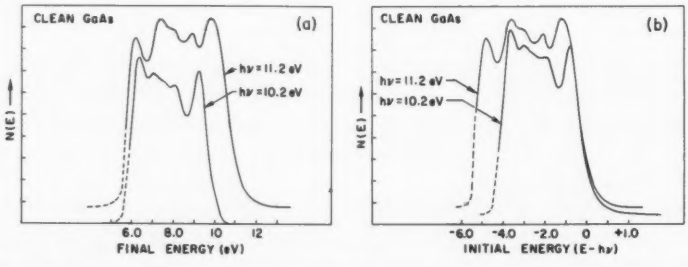

FIGURE 17. (a) *EDCs from GaAs for photon energies of 10.2 and 11.2 eV plotted as a function of final state energy.* (b) *EDCs for GaAs plotted vs* E − hν *to refer the energy distributions to the initial states. Note that the structure in the EDCs does not coincide on either a final energy plot (fig. 17a) or an initial energy plot as in this figure. This gives clear evidence that the transitions are direct.*

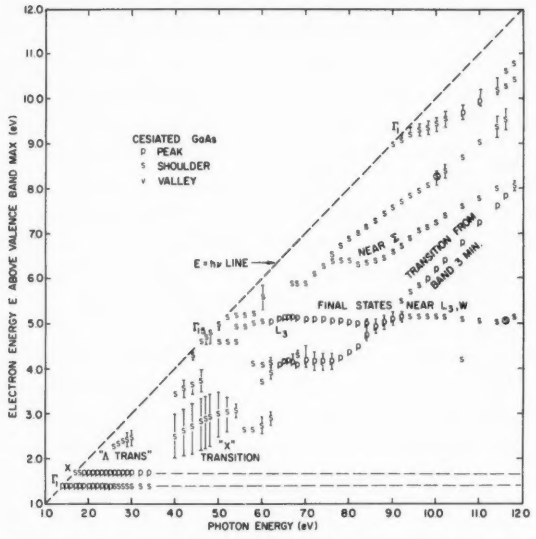

FIGURE 18. *A structure plot for the photoemission from cesiated GaAs. In such a plot the final energy of structure in the EDCs is plotted vs the photon energy. Such plots can be compared to predictions from band theories. They also provide at a glance certain information on the nature of the source of the structure in the EDCs, i.e., a horizontal line indicates transitions from flat portion of the valence band.*

Since the 45° line is located about 3.7 eV behind the $E = h\nu$ line, the initial states must be located this distance below the top of the valence band. As can be seen in the density of states plot of figure 19, there is a sharp density of states peak at just about this energy. Thus the two density of states peaks which are perhaps strongest and sharpest can be identified directly from the photoemission data; however, other strong structure which is not so narrow was not immediately detected from the photoemission data. This was because the curvatures were not sufficiently small so that a clear distinction could be made between the effects of initial and final density of states.

As is reported in a paper by Buss and Shirf [78] at this meeting, work by Spicer and Lapeyre [37] on PbTe seemed to have been successful in determining peaks in the density of states which correlate well with their band calculations. This occurred despite the fact that direct transitions are clearly important in these materials.

8. Comparison of Density of States Determinations Using Various Experimental Methods

In addition to uv photoemission spectroscopy, three other experimental techniques exist which can give direct information on the density of states of solids. In this section we will compare the density of states obtained by these methods for Cu with that obtained from our measurements.

8.1. Comparison with Results of Ion Neutralization Spectroscopy

In figure 20 the ODS for Cu is compared to the density of states obtained by Hagstrum [79] from Cu via the ion neutralization spectroscopy (INS) technique which he has developed. The peak between −2 and −4 eV is associated with the *d* states. As can be seen, the width of this peak is considerably greater than the *d* width indicated by the ODS or calculated band structure. In addition, there is no detailed structure in the ion neutralization results even though the instrumental resolution is sufficient to resolve structure such as that seen in the ODS or calculated density of states. Hagstrum has noted [80] that since his technique depends on electrons tunneling from the surface of the metal, it is sensitive to the electronic structure just at the surface and that for *d* electrons this structure may be different from that in the bulk of the material.

If it is suggested that a change of the electronic structure can take place at the surface, one must ask whether this can also affect photoemission studies. In principle, the photoemission is a bulk effect and thus would not be changed by variations in the electronic structure associated with the last atomic layer or so of the solid. However, the fast electron-energy dependency of the electron-electron scattering length (see fig. 3) and the low scattering length at high energies (as low as 10 Å in some materials) must be taken into account. Thus, as photon energy is increased up to 12 eV, the escaping electrons will come from regions closer and closer to the surface and it is possible that measurable changes in the EDCs might be due to changes in the electron structure at the surface. Comparison of the EDCs from cesiated [34] and uncesiated [4] Cu show that changes occur on cesiation in the relative strengths of the two leading *d* band peaks in Cu. Similar results are found in the Ni-Cu alloys [21]. These results are not understood, but are mentioned to indicate that the *d* band transitions appear to be sensitive to changes in the details of the conduction band electrons. If this is the case, changes of spatial distribution of conduction electrons at the surface might affect transitions from the *d* states. This could for example, contribute to the broadening of the first *d* peak from clean Cu which occurs as photon energy is increased (see fig. 4). The purpose of this discussion was to point out effects which might be important in photoemission but which have

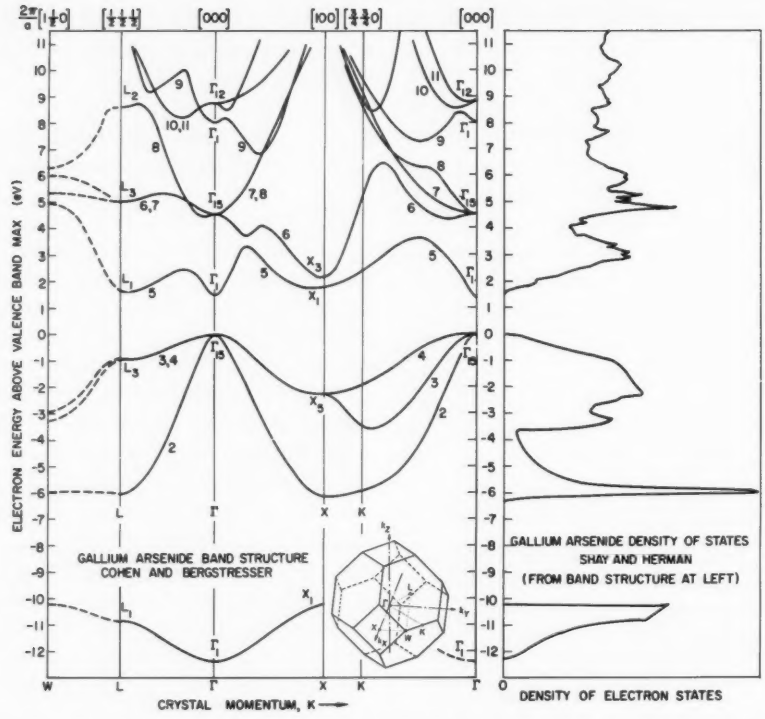
ELECTRON ENERGY ABOVE VALENCE BAND MAX (eV)
GALLIUM ARSENIDE BAND STRUCTURE
COHEN AND BERGSTRESSER
GALLIUM ARSENIDE DENSITY OF STATES
SHAY AND HERMAN
(FROM BAND STRUCTURE AT LEFT)
CRYSTAL MOMENTUM, K
DENSITY OF ELECTRON STATES

FIGURE 19. *The band structure of GaAs calculated by Cohen and Bergstresser* [76] *and the density of states calculated by Shay and Herman* [77].

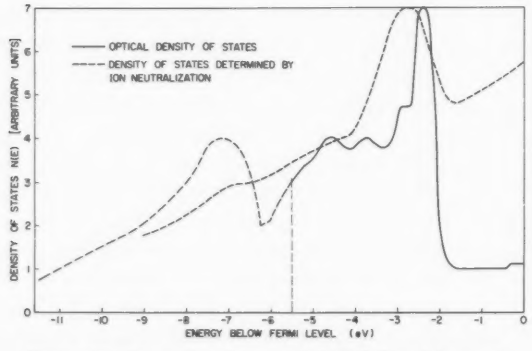
OPTICAL DENSITY OF STATES
DENSITY OF STATES DETERMINED BY ION NEUTRALIZATION
DENSITY OF STATES N(E) (ARBITRARY UNITS)
ENERGY BELOW FERMI LEVEL (eV)

FIGURE 20. *Comparison between the ODS* [4] *and the results obtained by Hagstrum* [79] *through ion neutralization studies for Cu.*

not been established. If they do exist, it would appear that these effects are much smaller than the perturbation of the electron structure as seen at the surface in the INS experiments.

8.2. Comparison with Results of X-Ray Photoemission Spectroscopy

Let us next compare the ultraviolet photoemission work with the x-ray photoemission data. The ODS for Cu is compared in figure 21 with the results obtained by Fadley and Shirley [81] using the technique of x-ray photoemission spectroscopy (XPS). The XPS result is characterized by a single, almost symmetric, peak with a width at half maximum of about 3 eV. Since the total instrumental line width was about 1.0 eV, this width and lack of detailed structure does not appear to be instrumental. If we make the reasonable assumption that the broad peak is due to *d* electrons, it is also signifi-

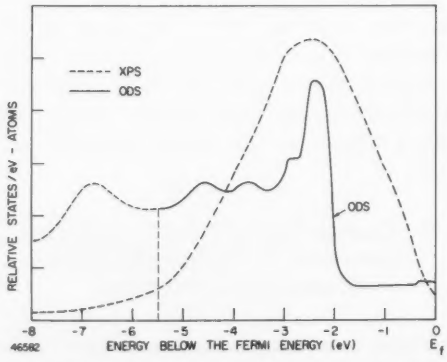

FIGURE 21. *Comparison between ODS* [4] *and results of the x-ray photoemission experiment of Fadley and Shirley* [81] *for Cu.*

cant that there is little evidence for the *s*- and *p*-derived states lying within 2 eV of the Fermi surface (see figure 5a and b). This effect can also be seen in the Au XPS data presented in figure 16. The *s*- and *p*-derived states can be clearly seen in the photoemission and INS work. The lack of any detailed structure in the excitation from the *d* states would also seem to be significant since such detailed structure does appear in the ODS as well as in the calculated band structure. However, it should be noted that substructure has been obtained in XPS results from Pt [81], Ag and Au [72] (see fig. 16) and that the position in energy of this structure is in reasonable agreement with structure in the ultraviolet photoemission work.

The reason for the lack of structure in the XPS for Cu is not clear at this time; however, it is interesting to note, as will be shown in the next section, that almost the same symmetric curve is obtained in soft x-ray emission spectroscopy as in the XPS results.

8.3. Comparison with Results of Soft X-Ray Emission Spectroscopy

A fourth experimental method used to investigate the filled states solids is that of soft x-ray emission spectroscopy (SXS). The results of such investigations [82,83] for Cu are compared in figure 22 with the ODS. As mentioned in the last section, the SXS curve is very similar to the XPS curve in that it contains a single almost symmetric peak and shows no evidence of the *s*- and *p*-derived states lying between the Fermi level and the top of the *d* band.

Cuthill, McAlister, Williams, and Watson [85] have reported structure in the SXS from Ni. However, it is not nearly as pronounced as that seen in the ODS of Eastman. There are some similarities between the ODS and the SXS results for Ni; however, the correlations do not seem to be strong.

Cu-Ni alloys have been studied both by SXS [86] and ultraviolet photoemission [21,23]. It is interesting to note that in the photoemission and optical work it has been possible to clearly identify a Ni virtual-bound state in the Cu-rich alloy and that these virtual-bound states are much different than Ni states in pure Ni. For example, their width at half maximum appears to be less than half of that of pure Ni for Ni concentrations up to about 25 atomic percent in Cu.

In contrast, in the x-ray work the spectrum obtained for Ni in Cu down to 10 percent concentrations was indistinguishable from that of pure Ni [86]. These results suggest that interactions with the deep hole override valence band structure in determining the SXS from

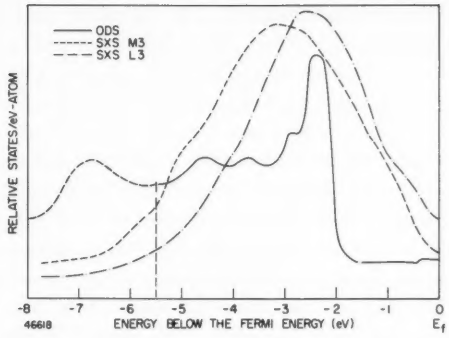

FIGURE 22. *Comparison between the ODS and results obtained from soft x-ray emission spectroscopy. The curve labeled* M3 *was obtained using* M_3 *radiation* [83] *and that labeled* L3 *using* L_3 *radiation* [84].

Ni; if this is so, the SXS would yield more information on the interaction between the deep hole and the valence electrons than on the valence band density of states.

9. Conclusions

The ultraviolet photoemission work done to date shows that density of states data can be obtained from such measurements. Because of the high resolution available in such measurements (0.05 to 0.3 eV), more detailed information can presently be obtained than by any other experimental method used to determine experimentally the density of states. In materials such as Cu where the most extensive work has been done, both experimentally and in theoretical calculations of the density of states, relatively good agreement is obtained between the position in energy of structure in the density of states. No other experimental method has given such clear-cut results or impressive agreement; however, good agreement is not obtained in the relative strengths of structure in the experimental and theoretical density of states. There are still fundamental questions which must be answered both with regard to the photoemission experiment and its interpretation and with regard to the band calculations and their relation to optical excitation spectra.

The photoemission data as well as calculations on Cu are probably the most complete available for any metal. The work of Smith [34] on Cu shows clear evidence of direct transitions from the regions of the *d* bands having large curvature. The calculations of Smith [34] and Smith and Spicer [33] show strong similarities between measurements and calculations based on direct transitions; however, the direct calculations predict much stronger modulation of the intensities of peaks than is seen experimentally. It should also be

noted that a broadening of 0.3 to 0.4 eV is used in the calculations to bring them into closer agreement with experiment. It is suggested that the experimental data is consistent with a model (suggested by Doniach's [46] theoretical work) which assumes that the delta function **k** selection rule be replaced by a selection distribution of **k**'s, with the width of the distribution increasing as the curvature of the bands decrease (*i.e.*, as the group velocity decreases). Thus, one would move in a continuous fashion from a completely direct transition model for a material with sufficiently wide bands to a non-direct-type of model for sufficiently narrow bands. The band widths at which such transitions take place would depend on the detailed characteristics of individual materials.

It appears that some density of states information can be obtained from photoemission data even when the transitions are completely direct. This can occur because peaks in the valence band density of states may produce EDC peaks which move with photon energy over a limited range of $h\nu$. Likewise, density of states peaks in the final states may produce peaks which fall at a constant energy over a limited range of $h\nu$. All of this is just a consequence of the fact that a large volume in **k** space must lie near a single energy to give a peak in the density of states. Such behavior has been pointed out at this meeting in, for example, GaAs and PbTe where the density of states peaks so identified have been found to correlate well with density of states peaks in the calculated band structure. However, other peaks in the density of states in GaAs were not identified. This may have been due to the fact that the $h\nu$ range used was not sufficiently large or that too crude a method is being used to identify density of states structure.

In a different type of approach, photoemission studies can also be used in direct collaboration with band calculations by providing empirical data on the band structure. This data can then be used to refine the band structure and the density of states can be calculated from the refined band structure.

10. Acknowledgment

It is a pleasure to acknowledge stimulating and fruitful conversations with Seth Doniach, Dean Eastman, Walter Harrison, Frank Herman, David Seib, Neville Smith and Leon Sutton as well as my other colleagues at Stanford University. I am particularly indebted to Seth Doniach, Dean Eastman, and Neville Smith for access to their work prior to publication.

11. References

[1] Koopmans' theorem states that the one-electron energy eigenvalue ϵ_j in the Foch equation for a solid is the negative of the energy to remove the electron in state ϕ_j from the solid. The proof of Koopmans' theorem depends on the spatial part of the wave function being of the Bloch type and on all other wave functions being unchanged when one electron is removed. If Koopmans' theorem holds, it follows that the photon energy necessary to excite an electron from state ϕ_j to state ϕ_k is just the difference between the one-electron energies of the two states. However, if the eigenfunctions of other states are modified in the excitation, Koopmans' theorem will not hold, and many-body effects must be taken into account. See also: F. Seitz, Modern Theory of Solids (McGraw-Hill Book Company, Inc., New York, 1940), p. 313; J. Callaway, Energy Band Theory (Academic Press, Inc., New York, 1964), p. 117; J. C. Phillips, Phys. Rev. **123,** 420 (1961); L. G. Parratt, Rev. Mod. Phys. **31,** 616 (1959).

[2] See, for example, refs. 3, 4, and 5.

[3] Berglund, C. N., and Spicer, W. E., Phys. Rev. **136,** A1030; **136,** A1044 (1964).

[4] Krolikowski, W. F., and Spicer, W. E., Phys. Rev., in press.

[5] Krolikowski, W. F., and Spicer, W. E., Phys. Rev., in press.

[6] Eastman, D. E., J. Appl. Phys. **40,** 1387 (1969).

[7] Beaglehole, D., Proc. Phys. Soc. (London) **85,** 1007 (1965).

[8] Ehrenreich, H., and Philipp, H. R., Phys. Rev. **128,** 1622 (1962).

[9] Mueller, F. M., and Phillips, J. C., Phys. Rev. **157,** 600 (1969).

[10] Gerhardt, U., Phys. Rev. **172,** 651 (1968).

[11] Spicer, W. E., and Berglund, C. N., Rev. Sci. Instr. **35,** 1665 (1964).

[12] Eden, R. C., Rev. Sci. Instr., in press.

[13] James, L. W., Moll, J. L., Spicer, W. E., and Eden, R. C., Phys. Rev. **174,** 909 (1968).

[14] James, L. W., Ph. D. Thesis, Stanford University (unpublished), 1969.

[15] Allen, F. G., and Gobeli, G. W., Phys. Rev. **144,** 558 (1966).

[16] Vehse, R. C., and Arakawa, E. T., Phys. Rev. **180,** 695 (1969).

[17] DiStefano, T. H., and Pierce, D. T., Rev. Sci. Instr., to be published.

[18] Koyama, R. Y., Ph. D. Thesis, Stanford University (unpublished), 1969.

[19] Spicer, W. E., Optical Properties and Electronic Structure of Metals and Alloys, F. Abelés, Editor (North-Holland Publishing Co., Amsterdam, 1965), p. 296.

[20] Eastman, D. E., and Krolikowski, W. F., Phys. Rev. Letters **21,** 623 (1968).

[21] Seib, D. H., and Spicer, W. E., Phys. Rev., to be published. (Cu-rich alloys)

[22] Calcott, T. A., and MacRae, A. U., Phys. Rev. **178,** 966 (1969).

[23] Seib, D. H., and Spicer, W. E., Phys. Rev., to be published. (Ni-rich alloys)

[24] Kane, E. O., Proc. Intern. Conf. Phys. Semiconductors, Kyoto, Japan, 1966, p. 37; Phys. Rev. **159,** 624 (1967).

[25] Eastman, D. E., private communication.

[26] Crowell, C. R., and Sze, S. M., Physics of Thin Films, G. Hass and R. E. Thun, Editors (Academic Press, 1967), Vol. 4.

[27] Kanter, H., to be published.

[28] Sze, S. M., Moll, J. L., and Sugano, T., Solid-State Elec. **7,** 509 (1964).

[29] Eastman, D. E., to be published.
[30] James, L. W., and Moll, J. L., Phys. Rev. **183,** 740 (1969).
[31] DiStefano, T. H., and Spicer, W. E., Bull. Amer. Phys. Soc. **13,** 403 (1968).
[32] Spicer, W. E., Phys. Rev. **154,** 385 (1967).
[33] Smith, N. V., and Spicer, W. E., Optics Comm., in press.
[34] Smith, N. V., Proc. of Electronic Density of States Symposium, Washington, D.C., November 3-6, 1969.
[35] Janak, J. F., Eastman, D. E., and Williams, A. R., Proc. of Electronic Density of States Symposium, Washington, D.C., November 3-6, 1969.
[36] Spicer, W. E., and Eden, R. C., Proc. of 9th Intern. Conf. on the Phys. of Semiconductors (Moscow, USSR), Vol. 2, p. 65 (1968).
[37] Spicer, W. E., and Lapeyre, J., Phys. Rev. **139,** A565 (1965).
[38] Shay, J. L., Proc. II-VI Conf., D. G. Thomas, Editor (Benjamin, Inc., New York, 1967), p. 651: Shay, J. L., Herman, F., and Spicer, W. E., Phys. Rev. Letters **18,** 649 (1967); Shay, J. L., and Spicer, W. E., Phys. Rev. **161,** 799 (1967); Shay, J. L., and Spicer, W. E., Phys. Rev. **169,** 650 (1968); and Phys. Rev. **175,** 741 (1968).
[39] Brust, D., to be published.
[40] Koyama, R. Y., and Spicer, W. E., Proc. of Electronic Density of States Symposium, Washington, D.C., November 3-6, 1969.
[41] Janak, J. F., Williams, A. R., and Eastman, D. E., to be published; Eastman, D. E., Janak, J. F., and Williams, A. R., to be published.
[42] Eastman, D. E., private communication.
[43] Smith, N. V., private communication.
[44] Snow, F. C., Phys. Rev. **171,** 785 (1968).
[45] Cohen, M. H., and Mueller, F. M., Atomic and Electric Structure of Metals (American Society of Metals, Metals Park, Ohio, 1967), p. 75.
[46] Doniach, S., private communication.
[47] Koyama, R. Y., Spicer, W. E., Ashcroft, N. W., and Lawrence, W. E., Phys. Rev. Letters **19,** 1284 (1967).
[48] Ashcroft, N. W., and Lawrence, W. E., Phys. Rev. **175,** 938 (1968).
[49] Shaw, R., and Smith, N., Phys. Rev. **178,** 985 (1969).
[50] Mosteller, L. P., Huen, T., and Wooten, F., Phys. Rev. **184,** 364 (1969).
[51] Blodgett, A., Spicer, W., and Yu, A., Optical Prop. and Electronic Structure of Metals and Alloys, F. Abelés, Editor (North-Holland Publishing Co., Amsterdam, 1965), p. 246.
[52] Lapeyre, G. J., and Kress, K. A., Phys. Rev. **166,** 589 (1968).
[53] Phillips, J. C., Solid-State Physics, F. Seitz and D. Turnbull, Editors (Academic Press, New York, 1966), Vol. 18, p. 55; Herman, F., Kortum, R. L., Kuglin, D. D., VanDyke, J. P., and Skillman, S., Methods of Computational Physics, B. Adler, S. Fernbach, and M. Rotenberg, Editors (Academic Press, New York, 1968), Vol. 8, p. 193.
[54] Donovan, T. M., Spicer, W. E., J. of Non-Crystalline Solids, in press.
[55] Donovan, T. M., Spicer, W. E., and Bennett, J., in preparation.
[56] Donovan, T., and Spicer, W. E., Phys. Rev. Letters **21,** 1572 (1968).
[57] Donovan, T., Ph. D. Thesis, Stanford University (unpublished), (1970).
[58] Herman, F., Kortum, R. L., Kuglin, C. D., and Shay, J. L., Proc. Intern. Conf. on II-VI Semiconductor Comp. (W. A. Benjamin, Inc., New York, 1967), p. 271.
[59] Brust, D., private communication.
[60] Seib, D. H., and Spicer, W. E., Phys. Rev. Letters **20,** 1441 (1968).
[61] Norris, C., and Nilsson, P. O., Solid State Comm. **6,** 649 (1968).
[62] Walldén, L., Solid State Comm., **1,** 593 (1969).
[63] Walldén, L., Seib, D., and Spicer, W., J. Appl. Phys. **40,** 1281 (1969).
[64] Smith, N. V., private communication.
[65] Herman, F., Kortum, R. L., Kuglin, C. D., and Short, R. A., Proc. Intern. Conf. Phys. Semiconductors, (Kyoto, Japan, 1966), p. 7.
[66] Herman, F., Intern. J. of Quantum Chem. **S,** in press.
[67] Gehardt, U., private communication.
[68] Eastman, D. E., Solid State Comm., in press.
[69] Loucks, T. L., Phys. Rev. **144,** 504 (1964); **159,** 544 (1967); Keeton, S. C., and Loucks, T. L., Phys. Rev. **168,** 672 (1968); Fleming, G. S., and Loucks, T. L., Phys. Rev. **173,** 685 (1968); Asono, S., and Yamashita, J., Phys. Soc. Japan **23,** 714 (1967).
[70] Snow, F. C., private communication.
[71] Yu, A., Blodgett, A., and Spicer, W. E., Proc. Intern. Colloquium Optical Properties and Electronic Structure of Metals and Alloys, F. Abelés, Editor (North-Holland Publishing Co., Amsterdam, 1966), p. 246.
[72] Siegbahn, K., Norling, C., Fahlman, A., Nordberg, R., Hamrin, K., Hedman, J., Johansson, G., Bergmark, T., Karlsson, S., Lindgren, I., Lindberg, B., ESCA Atomic, Molecular and Solid State Structure Studied by Means of Electron Spectroscopy (Almqvist and Wiksells Boktryckeri AB, Uppsala, 1967), Ser. IV, Vol. 20.
[73] Ballinger, R. A., and Marshall, C. A. W., to be published.
[74] Eden, R. C., Ph.D. Thesis, Stanford University (unpublished), (1968).
[75] Eden, R. C., Spicer, W. E., to be published.
[76] Cohen, M. L., and Bergstresser, T. K., Phys. Rev. **141,** 789 (1966).
[77] Shay, J. L., and Herman, F., private communication.
[78] Buss, D. D., and Shirf, V. E., Proc. of Electronic Density of States Symposium, Washington, D.C., November 3-6, 1969.
[79] Hagstrum, H. D., Phys. Rev. **150,** 495 (1966).
[80] Hagstrum, H. D., private communication.
[81] Fadley, C. S., and Shirley, D. A., Phys. Rev. Letters **21,** 980 (1968).
[82] Cauchois, Y., and Bonnelle, C., Proc. Intern. Colloquium Optical Properties and Electronic Structure of Metals and Alloys (North-Holland Publishing Co., Amsterdam, 1966), p. 83.
[83] Bedo, D. E., and Tomboulian, D. H., Phys. Rev. **113,** 464 (1959).
[84] Figure 40 has been taken from ref. 81.
[85] Cuthill, J. R., McAlister, A. J., Williams, M. L., and Watson, R. E., Phys. Rev. **164,** 1006 (1967).
[86] Clift, J., Curry, C., and Thompson, B. J., Phil. Mag. **8,** 593 (1963).

(Paper 74A3–607)

JOURNAL OF RESEARCH of the National Bureau of Standards—A. Physics and Chemistry
Vol. 74A, No. 3, May-June 1970

Beyond the One-Electron Approximation: Density of States for Interacting Electrons*

L. Hedin, B. I. Lundqvist, and S. Lundqvist

Chalmers University of Technology, Göteborg, Sweden

(October 10, 1969)

The concept "density of states" can be given many different meanings when we go beyond the one-electron approximation. In this survey we concentrate on the definition tied to excitation processes, where one electron is added or removed from the solid. We discuss the one-particle spectral function for conduction and core electrons in metals, how it can be approximately calculated, and how it can be related to different types of experiments like x-ray photoemission, x-ray emission and absorption, photoemission and optical absorption in the ultraviolet, and the Compton effect. We also discuss the form of the exchange-correlation potential for use in band structure calculations.

Key words: Density of states; interacting electrons; one-particle Green function; oscillator strengths; quasi particle density of states; x-ray emission and absorption.

1. Introduction

In the one-electron approximation the concept "electronic density of states" is unique and simple and is defined by the formula

$$N_1(\omega)=\sum_i \delta(\omega-\epsilon_i), \tag{1}$$

where ϵ_i denotes the single-particle energies. Similarly the optical density of states is given by the joint density of state for electrons and holes, thus

$$N_2(\omega)=\sum_i \delta(\omega-\epsilon_i^p+\epsilon_i^h). \tag{2}$$

These functions only describe the cruder aspects of experiments such as soft x-ray emission or optical absorption. They must be augmented with the proper *oscillator strengths*, which provide important selection rules and as well give rise to deviations from the density of state curves.

When one goes beyond the one-electron approximation and considers interactions not included in a self-consistent field theory the situation becomes non-trivial and one encounters a wide variety of density of states functions. The quantity which is most easy to define is the true density of states of the fully interacting systems

$$N(\omega)=\sum_n \delta(\omega-E_n), \tag{3}$$

where E_n are the energy levels of the system. Although being a key quantity in thermodynamics it is of no use for the description for *e.g.* optical, x-ray or energy loss spectra. We rather need the proper extensions of eqs (1) and (2) to describe one- and two-electron properties of the system. A particularly simple case is that of particles having a Lorentzian energy distribution

$$A_k(\omega)=\frac{1}{\pi}\frac{\Gamma_k}{(\omega-\epsilon_k)^2+\Gamma_k}\,. \tag{4}$$

The density of states is then given by

$$N_1(\omega)=\sum_k A_k(\omega). \tag{5}$$

In cases where the line width Γ_k is small compared with the width of the band, the formulas (5) and (1) obviously will give similar results.

The simple case just mentioned does not really carry us beyond the one-electron theory. We have in the general case to abandon a concept based on single-particle levels and instead use distribution functions or

* An invited paper presented at the 3d Materials Research Symposium, *Electronic Density of States*, November 3-6, 1969, Gaithersburg, Md.

spectral densities of which the function $A_k(\omega)$ given above is a simple and almost trivial case. Such distribution functions include the proper oscillator strengths, and they refer to formally exact many-electron states, properly weighted according to the physical process considered. They are closely related to correlation functions and Green functions. An example is the density-density correlation function $\langle \rho(\mathbf{r}t)\rho(\mathbf{r}'t')\rangle$, which correlates density fluctuations at different times and different positions. This function is of basic importance for describing optical experiments and energy loss spectra. Unfortunately it is very difficult to analyze its structure and we will here instead concentrate on a simpler entity, the one-particle Green function and its associated spectral function [1].

The one-particle spectral function is a generalization of the usual density of states $N_1(\omega)$. It gives an asymptotically exact description of x-ray photoemission, is connected with x-ray emission and absorption and also has some relevance for uv photoemission and absorption.

It is, however, not capable to describe edge effects in general, and does not at all account for final state or particle-hole interactions. Such effects, which in their simplest form are described by $N_2(\omega)$ or generalizations therefrom provide intricate problems upon which we shall only briefly touch here. These questions will be taken up in detail in the lecture by Mahan.

It has recently been noticed that the one-electron spectral function should exhibit some marked and strong structure. This structure is primarily associated with the interaction between the electron and plasmon excitations. It should be quite important in x-ray photoemission, influencing the line shape of the core electron peak and giving low energy satellites both to the core electron and conduction band structures. It is important in x-ray emission and absorption spectra showing up at the threshold, and giving rise to satellite structures. Its effect may also be noticeable in uv photoemission and optical absorption spectra.

We should also mention the structure in the one-electron spectrum caused by coupling to phonons. This structure is limited to a region of the order of the Debye energy around the Fermi level, but in that region it is quite pronounced, causing *e.g.* the well-known enhancement of the quasi particle density of states.

In the next section we will discuss the connections between the one-electron spectrum and x-ray photoemission, and with x-ray emission and absorption. In section 3 we discuss the spectrum of the conduction electrons from calculations to lowest order in the dynamic interaction between the electrons and between the electrons and phonons.

In section 4 we take up the core electron spectrum and discuss calculations to first order in the dynamic interaction with the valence electrons. We also survey the recent work by Langreth who obtained the exact solution to an important model problem. In section 5 we give a qualitative discussion of some experimental results for photon absorption and emission, photoemission and Compton scattering. In section 6 finally we give some concluding remarks.

2. The One-Electron Density of States in an Interacting System and its Connection with X-Ray Photoemission and with X-Ray Emission and Absorption

In this section we introduce some theoretical technicalities, which however seem unavoidable in order to establish a firm connection between theory and experiment.

The one-electron spectral weight function is defined as

$$A(\mathbf{x}, \mathbf{x}'; \omega) = \sum_s f_s(\mathbf{x}) f_s^*(\mathbf{x}') \delta(\omega - \epsilon_s). \qquad (6)$$

In the independent-particle approximation the quantities f_s and ϵ_s are the one-electron wave functions and energies. In an interacting system the oscillator strength function f_s is defined as

$$f_s(\mathbf{x}) = \langle N-1, s|\psi(\mathbf{x})|N\rangle, \qquad (7)$$

where $\psi(\mathbf{x})$ is the electron field operator. It gives the probability amplitude for reaching an excited state $|N-1,s\rangle$, when an electron is suddenly removed from the ground state $|N\rangle$. The quantity ϵ_s is the excitation energy

$$\epsilon_s = E(N) - E(N-1,s). \qquad (8)$$

These definitions apply for ω in eq (6) smaller than the chemical potential μ. For ω larger than μ, states with $N+1$ particles are involved.

In applications of the theory it is often practical to represent the spectral function as a matrix in a space spanned by some suitable complete orthonormal set of single-particle states $\mu_k(\mathbf{x})$, thus

$$A_{kk'}(\omega) = \int u_k^*(\mathbf{x}) A(\mathbf{x}, \mathbf{x}'; \omega) u_{k'}(\mathbf{x}') d\mathbf{x} d\mathbf{x}'$$
$$= \sum_s \langle N|a_k^+|N-1, s\rangle \langle N$$
$$-1, s|a_k|N\rangle \delta(\omega - \epsilon_s). \qquad (9)$$

The spectral weight function is the general distribution function describing one-electron properties, and is a generalization of the one-electron density matrix, which is obtained after an integration over the frequencies. Distributions with respect to a single variable are in the usual way obtained by summation over all other variables. Thus, the *one-electron density of states* is defined as

$$N(\omega) = \mathrm{Tr}\, A(\omega) = \int A(\mathbf{x}, \mathbf{x}; \omega) d\mathbf{x} = \sum_k A_{kk}(\omega). \quad (10)$$

As indicated, the definition is independent of the choice of matrix basis.

The spectral weight function is a key quantity in the Green function formulation of the many-electron problem. A more detailed account is given in many texts, *e.g.* in sections 9 and 10 of ref. [1].

We next discuss the particular cases of x-ray photoemission and soft x-ray emission, where approximate reductions to the one-electron spectrum can be made.

In the x-ray photoemission experiment (XPS), an energetic photon of energy ω is absorbed, exciting a photoelectron which leaves the system. If the electron has a large enough energy we can write the final state as

$$|\Psi_f\rangle = a_\kappa^+ |N-1, s\rangle, \quad (11)$$

where $\boldsymbol{\kappa}$ refers to a Bloch wave function of energy $\epsilon_\kappa \approx \hbar^2\mathbf{k}^2/(2m)$, describing the photoelectron. The probability of this event is, by the Golden rule,

$$W \sim \sum_f |\langle \Psi_f | \mathbf{P} | \Psi_i \rangle|^2 \delta(\omega - E_f + E_i)$$

$$= \sum_{\kappa, s} |\langle N-1, s | a_\kappa \sum_{k,k'} p_{k'k} \alpha_{k'}^+ a_k | N \rangle|^2 \delta(\omega - \epsilon_\kappa + \epsilon_s), \quad (12)$$

where $\mathbf{P}$ is the total momentum and $p_{kk'}$ the momentum matrix element. For a fast electron, which is outside the region of ground state fluctuations, $a_\kappa|N\rangle = 0$, and the expression for W reduces to

$$W \sim \sum_{\kappa, s} |\langle N-1, s | \sum_k p_{\kappa k}\, a_k | N \rangle|^2 \delta(\omega - \epsilon_\kappa + \epsilon_s)$$

$$= \sum_\kappa \sum_{k,k'} A_{kk'}(\epsilon_\kappa - \omega) p_{\kappa k}^*\, p_{\kappa k'}, \quad (13)$$

The energy distribution of photoelectrons is hence given by

$$I(\epsilon) \sim \sqrt{\epsilon} \sum_{k,k'} A_{kk'}(\epsilon - \omega) p_{\kappa k}^*\, p_{\kappa k'}, \quad (14)$$

taking $\epsilon_\kappa = \epsilon$. Using an average momentum matrix element and neglecting nondiagonal terms in A we obtain the simple result

$$I(\epsilon) \sim \sqrt{\epsilon}\, p_{\mathrm{eff}}^2 N(\epsilon - \omega). \quad (15)$$

The neglect of nondiagonal terms should be a good approximation if the one-electron functions are carefully chosen Bloch functions and core-electron functions. We note that if the electron is ejected from a core level and if we neglect excitations of the core electron system, the operator a_k in eq (13) must destroy a core electron ($a_k = a_c$), giving

$$W \sim \sum_{\kappa, s} |\langle N_v^*, s | N_v \rangle p_{\kappa c}\ |^2 \delta(\omega - \epsilon_\kappa + \epsilon_s). \quad (16)$$

Here $|N_v\rangle$ denotes the ground state of the valence electron system, and $|N_v^*, s\rangle$ are excited states in the presence of the core hole. We recognize eq (16) as the result in the sudden approximation.

We next turn to soft x-ray emission. In this case we may write the initial state as [2]

$$|\Psi_i\rangle = a_c |N^*\rangle \quad (17)$$

where the star on N indicates that the valence electron system is relaxed towards the core hole. Applying the Golden rule again we have for the x-ray intensity

$$I(\omega) \sim \omega \sum_f |\langle \Psi_f | \sum_{kk'} p_{k'k} a_{k'}^+ a_k a_c | N^* \rangle|^2 \cdot \delta(\omega - E_i + E_f)$$

$$= \omega \sum_s |\langle N_v - 1, s | \sum_k p_{ck} a_k | N_v^* \rangle|^2 \delta(\omega + \epsilon_c - \epsilon_s). \quad (18)$$

If we could neglect the relaxation effects in the initial state and replace $|N_v^*\rangle$ by $|N_v\rangle$, we would again have the spectral function A involved. The relaxation effects can be accounted for in an approximate way by only considering particle-hole excitations, thus

$$|N_v^*\rangle = (\alpha + \sum_{h,p} \alpha_h^p a_p^+ a_h) |N_v\rangle. \quad (19)$$

Insertion of this expression in eq (18) leads after some further approximations to a very simple expression

$$I(\omega) \sim \omega \sum_k |p_{ck}^{\mathrm{eff}}|^2 A_{kk}(\omega + \epsilon_c), \quad (20)$$

where p^{eff} involves the coefficients α and is ω-dependent. Such an approximation is however invalid at the Fermi edge, where, as Anderson [3] has pointed out, we need an infinite number of particle-hole pairs to represent $|N_v^*\rangle$.

The edge problem has recently been treated by several people [4–6]. We choose here to give a brief account of Langreth's version [6] of Nozieres; and de Dominicis' (ND) treatment of the problem in order to show how the one-electron spectrum enters the problem. The basic quantity needed for the evaluation of eq (18) is the correlation function

$$F_{kk'}(t) = \langle\, N^*|T(a_k(t)a_{k'}^+ a_c(t)a_c^+)|N^*\,\rangle. \quad (21)$$

To evaluate that function ND study the multiple time function

$$F_{kk'}(\tau, \tau'; t, t') = \langle\, N^*|T(a_k(\tau)a_{k'}^+(\tau')a_c(t)a_c^+(t')|N^*\,\rangle. \quad (22)$$

The simple way, in which the core state operator enters their model Hamiltonian, causes the equation of motion for F to close onto itself and allows a solution as a product,

$$F_{kk'}(\tau,\tau';t,t') = \phi_{kk'}(\tau,\tau';t,t')\, G_c(t,t') \quad (23)$$

where G_c is the core electron Green function,

$$G_c(t, t') = \langle\, N^*|T(a_c(t)a_c^+(t'))|N^*\,\rangle \quad (24)$$

and ϕ a valence electron Green function which obeys an equation with a transient potential from the core hole. The x-ray spectrum is given by a convolution of the core and valence electron spectra. Both spectra are singular at the edge as a power law and so is also the resulting convolution.

The point in keeping the operator a_c in eq (22) is that the time dependence of $a_k(t)$ then can be given by the same Hamiltonian as that used for $|N^*\rangle$, while when studying $\langle N_c^*|T(a_k(t)a_{k'}^+)|N_c^*\rangle$, the time evolution of $a_k(t)$ is given by a Hamiltonian that does not include the potential from the core hole, and thus the usual many-body techniques do not apply. X-ray absorption can be described in an analogous manner by the function F, only replacing $|N^*\rangle$ by $|N\rangle$.

It should be mentioned that the ND treatment is based on a model Hamiltonian that does not include interactions between the conduction electrons. This is quite appropriate for their purposes of treating the edge problem but is not sufficient for the spectrum far away from the edge. It is not clear if their treatment can be extended to the more general case. We then have to resort to other methods, such as the approximation in eq (19) or to a frontal attack on the dielectric function itself [7].

We have in this section given a definition of the one-electron density of states and have indicated its relation to some measurable quantities. We conclude from this that a theoretical investigation of this kind of experiments can not avoid the calculation of the one-electron density of states of interacting electrons, but at the same time due to a variety of effects there may be essential modifications of the density of states as it appears in the actual experiment. Explicit results from approximate calculations of the spectral function A and the density of states $N(\omega)$ are discussed in sections 3 and 4, and the actual comparison with experiment is made in section 5.

3. One-Electron Spectrum of Conduction Electrons

The common picture of the one-electron spectra of solids is obtained from energy band calculations, in which the Schrödinger equation of independent electrons in a periodic potential is solved. For the different bands one obtains the electron energy as a function of wave-vector, $\epsilon(\mathbf{k})$. The main contribution to the potential seen by an electron is the average electrostatic field or the Hartree field. When going beyond the one-electron approximation the next step would be to include dynamical effects of the interaction as well as exchange effects. Such effects can not be described by an ordinary local potential. A generalized "potential," non-local in space and time, must be introduced.

Let us for simplicity study the case, where specific effects of the periodicity are of minor importance, and assume the distribution of conduction electrons to be uniform. Due to the non-locality of the generalized "potential," its Fourier transform to momentum-energy space will show a dependence on both wave-vector $\mathbf{k}$ and energy ϵ, $\Sigma(\mathbf{k}, \epsilon)$. The quantity Σ is called the *self-energy* of the electron.

Adding the self-energy to the average potential, we have to solve the equation

$$\epsilon = \epsilon(\mathbf{k}) + \Sigma(\mathbf{k},\epsilon). \quad (25)$$

The self-energy includes all the interactions between the electron state considered and the system. This necessarily includes dissipative effects, which lead to the decay of the state. Consequently the self-energy must be a complex quantity, thus

$$\Sigma(\mathbf{k},\epsilon) = \Sigma_R(\mathbf{k},\epsilon) + i\Sigma_I(\mathbf{k},\epsilon). \quad (26)$$

The spectral weight function defined in section 2 is related to the self-energy according to the formula 1, sec-

tion 1

$$A(\mathbf{k},\epsilon)=\frac{1}{\pi}\frac{\left|\sum_I(\mathbf{k},\epsilon)\right|}{(\epsilon-\epsilon(\mathbf{k})-\sum_R(\mathbf{k},\epsilon))^2+\left(\sum_I(\mathbf{k},\epsilon)\right)^2}. \tag{27}$$

In the simple case that the self-energy Σ is independent of energy, the spectral function for fixed k will have a Lorentzian shape and Σ_I determines the width of the line. When Σ depends on energy there are no a priori restrictions on the shape of the spectrum.

Most of our present knowledge about the self-energy has been based on calculations, where vertex corrections have been neglected, *i.e.* using the formulae [9–13]

$$\sum(\mathbf{k},\omega)=\frac{i}{(2\pi)^4}\int e^{i\omega\delta}v(\mathbf{k}')\,\epsilon^{-1}(\mathbf{k}',\omega')G_0(\mathbf{k}+\mathbf{k}',\omega+\omega')d\mathbf{k}'d\omega', \tag{28}$$

where

$$G_o(\mathbf{k},\omega)=(\omega-\epsilon(\mathbf{k})+i\delta\ \text{sign}\ (k-k_p))^{-1} \tag{29}$$

is the propagator for a non-interacting electron, and

$$v(\mathbf{k})=4\pi e^2/\mathbf{k}^2 \tag{30}$$

is the bare Coulomb potential. The constant k_F means the Fermi momentum, and δ is a positive infinitesimal.

To make connection with another approximation, we note that the Hartree-Fock approximation corresponds to the choice $\epsilon=1$ in eq (28). As it stands, eq (28) expresses the lowest order coupling to the density fluctuations of the conduction electrons, described by the wave-vector- and frequency-dependent *dielectric function* $\epsilon(\mathbf{k},\omega)$. This function contains information about the static screening, given by $\epsilon(\mathbf{k},0)$, but also important effects of the dynamic behavior of the density fluctuations. The typical small-k-behavior of the spectral function for this kind of excitations, $-\text{Im}\ \epsilon^{-1}(\mathbf{k},\omega)$, is indicated in figure 1. The clearcut classification of the excitations into electron-hole pairs and plasmons is characteristic for the Linearized Time dependent Hartree (LTH) or Random Phase Approximation [14]. For small wave-lengths the electron-hole pair excitations become of increasing importance, while in the $k\to 0$-limit the plasmon exhausts completely the sum rule for Im ϵ^{-1}, *i.e.* it is the only excitation. The latter property follows from general arguments about charge conservation and translation invariance [8, p. 288], and should be valid for any useful approximation for $\epsilon(\mathbf{k},\omega)$. In the

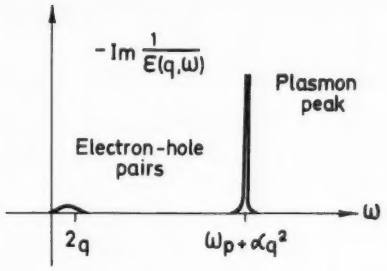

FIGURE 1. *Qualitative behavior of Im* $\epsilon^{-1}(q,\omega)$ *for small* q.

LTH approximation the plasmon is undamped for wave-numbers smaller than a critical value k_c, which at metallic densities is of the same order of magnitude as k_F.

A great part of the literature about the electron gas is devoted to the search for an improved dielectric function [15–20], particularly because of the failure of the LTH formula to describe interaction effects at short distances. The last word remains to be said in this question, but it is interesting to note the relative insensibility of the self-energy to the choice of dielectric function [11,12,21]. An approximation, which has proved to be most useful, is to take a plasmon-like sharp absorption for all $\mathbf{k}$ according to the formula

$$\epsilon^{-1}(\mathbf{k},\omega)=1.+\frac{\omega_p^2}{\omega^2-\omega^2(\mathbf{k})} \tag{31}$$

where ω_p is the classical plasma frequency and $\omega(\mathbf{k})$ the resonance frequency at wave number $\mathbf{k}$. The frequency $\omega(\mathbf{k})$ reduces to ω_p when $|\mathbf{k}|\to 0$ and is proportional to $|\mathbf{k}|^2$ for large $|\mathbf{k}|$. This formula correctly represents the small and large ω-limits and gives a quite reasonable interpolation for intermediate ω values [1, 1]. With this choice one can perform the frequency integration in eq (28) and obtain

$$\sum(\mathbf{k},\omega)=-\frac{1}{(2\pi)^3}\int d^3q\frac{v(q)n_0(\mathbf{k}+\mathbf{q})}{\epsilon(\mathbf{q},\epsilon(\mathbf{u}+q)-\omega)}+\frac{\omega p^2}{(2\pi)^3}\int d^3q\frac{v(\mathbf{q})}{2\omega(\mathbf{q})}\frac{1}{\omega-\epsilon(\mathbf{h}+\mathbf{q})-\omega(\mathbf{q})} \tag{32}$$

The first term in eq (32) is a *screened exchange potential*, $n_o(\mathbf{k})$ being the momentum distribution for independent electrons, and the second term describes the *correlation hole* around the electron [12,22].

Because of the plasma resonance in the dielectric function there will be a rapid variation in the real part

378-324 O - 70 - 8

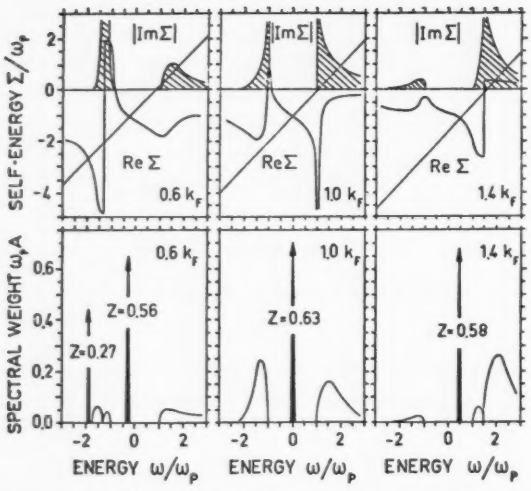

FIGURE 2. *The self-energy* Σ *and the corresponding spectral function* A *for* $r_s = 5$ [21]. The crossings between the Re Σ *curves and the straight lines give the solutions to the Dyson equation. The numbers at the peaks indicate the strengths of the lines.*

of Σ at the frequency $\omega = \epsilon(\mathbf{k}) + \omega_p$ for electrons and at $\omega = \epsilon(\mathbf{k}) - \omega_p$ for holes. This behavior of the electron gas seems to have been first noticed and discussed by Hedin *et al.* [23] and has been studied in great detail by Lundqvist [13,21]. Typical curves for Σ obtained with this dielectric function are shown in the upper half of figure 2. In the lower part of figure 2 we have given the results for $A(\mathbf{k},\omega)$ calculated from eq (27).

For $k = k_F$ there is only one strong peak in the spectral function, corresponding to the usual quasi particle. For the other k-values in the figure, we find three solutions of the Dyson equation

$$\omega = \epsilon(\mathbf{k}) + \Sigma_R(\mathbf{k},\omega). \tag{33}$$

One of them, however, falls at $\omega = \epsilon(\mathbf{k}) \pm \omega_p$, where the damping is very strong, and therefore this solution is effectively suppressed. Of the two remaining solutions, one corresponds to the usual quasi particle, *i.e.* a bare electron surrounded by a cloud of virtual plasmons and electron-hole excitations. For hole states, *i.e.* for $k < k_F$, a new state appears which has an energy lower than that corresponding to a hole plus a plasmon, *i.e.* $\epsilon(\mathbf{k}) - \omega_p$. This result from a low order treatment corresponds to a coherent state of hole-plasmon pairs, and may be thought of as holes coupled to *real* plasmons. This coupled state, which has been called a *plasmaron*, has a large oscillator strength, and thus gives an essential contribution to the sum rule for the one-electron spectrum. For electron states, $k > k_F$, there is no sharp state but a broad resonance with a sharp onset at $\omega = \epsilon(\mathbf{k}) + \omega_p$.

Figure 3 illustrates how the parabolic quasi particle dispersion law is accompanied by a second branch of the spectrum, the plasmaron. In figure 4 the momentum distribution function for the interacting electrons is given.

The characteristic structure due to plasmon effects will modify the density of states. This is demonstrated schematically in figure 5. The conduction band will retain approximately its parabolic shape. At an energy ω_p below the Fermi edge there is the onset of the second band due to the plasmaron states. This band is terminated at low energies with a rather distinct edge. For unoccupied states there is an extra contribution to the density of states starting at an energy ω_p above the Fermi level. Figure 6 gives a survey of the density of state curves at four different values of the electron gas parameter r_s ($r_s = 2$ corresponding roughly to the electron density of Al, and $r_s = 4$ to that of Na).

So far we have discussed the gross effects due to the coupling between electrons and plasmons. These are quite well represented by the plasmon-pole approximation for the dielectric function in eq (31). Electron-hole pair excitations are however not included, to represent

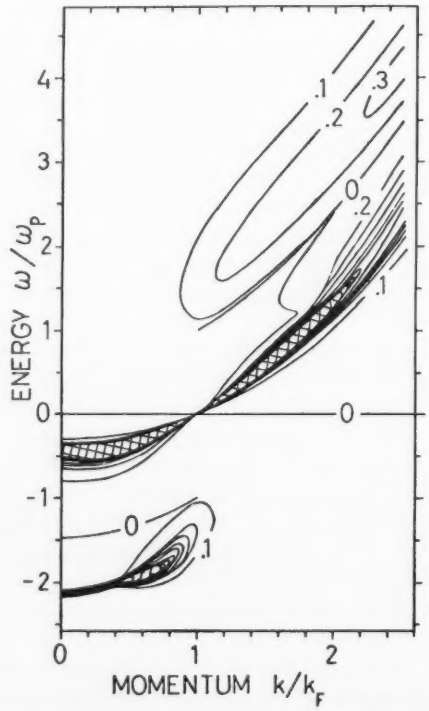

FIGURE 3. *The spectral weight function* A(k,ω) *given by level curves indicating the value of* $\hbar\omega_p$A, *at* $r_s = 4$ ($\hbar\omega_p = 0.435$ *Ry*) [13].

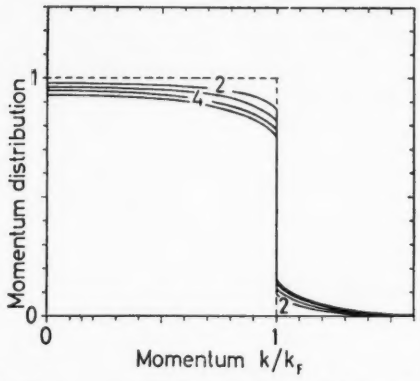

FIGURE 4. *The momentum distribution function* n(k) *at* $r_s = 2, 3, 4$ *and* 5 [13].

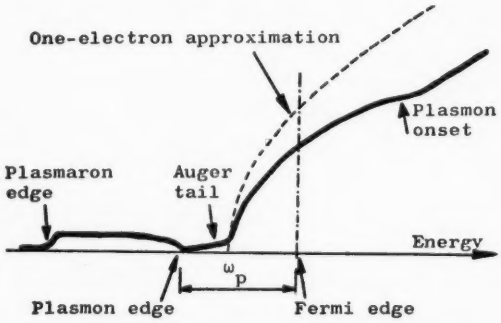

FIGURE 5. *Density of states for conduction electrons.*

them we must turn to the LTH dielectric function or higher approximations. These excitations are responsible for the broadening of the quasi particle peak and the Auger tail at the bottom of the main band in figures 5 and 6 as well as the broad spectral weight contours in figure 3.

Figure 7 shows $\Sigma_I(\mathbf{k},\epsilon(\mathbf{k}))$ calculated from eq (28) and is an indication of the high damping rate for quasi particles with k greater than $k_F + k_c$, *i.e.*, in the region where they can decay into plasmons [10,24]. However, as illustrated by the typical spectral forms for the quasi particle peak in figure 8, the quasi particle peak is always distinguishable from the spectral background, its width $\Gamma(\mathbf{k})$ is smaller than its excitation energy $E(\mathbf{k}) - \mu$.

From eq (28) one can also draw information about the exchange and correlation "potential" for the quasi particles. The inadequacy of the Hartree-Fock approximation in a metal is well-known, and in band calculations the effects of exchange and correlation are commonly simulated by using a local potential, such as the Slater [25] or the Gáspár [26,27] expressions. After solving the Dyson equation one can write the resulting quasi-particle energy in the form

$$E(\mathbf{k}) = \epsilon(\mathbf{k}) + V(\mathbf{k}), \tag{34}$$

where $V(\mathbf{k})$ can be interpreted as an effective exchange and correlation potential. In figure 9 such a potential is shown. It has a remarkably weak k-dependence for moderate wave vectors, its value lying roughly halfway between the Slater [25] and "2/3 Slater" values [26,27].

One of the shortcomings of the Hartree-Fock approximation is its prediction of a large bandwidth. The width of the occupied part of the main band deduced from eq (28) is practically the same as the Hartree value $\epsilon(k_F)$, a result which is in accord with the experimental findings.

For large momenta ($k \gtrsim k_F + k_c$) there is a characteristic k-dependence of $V(\mathbf{k})$, which might influence properties of electrons involved in photoemission and

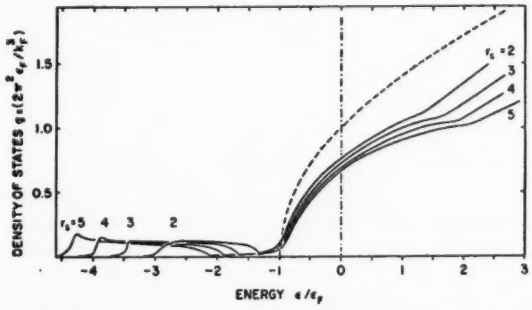

FIGURE 6. *The density of states for the values of the electron gas parameter* $r_s = 2, 3, 4, 5$. *The dashed curve is the result of the one-electron theory, and the vertical broken line indicates the Fermi level* [13].

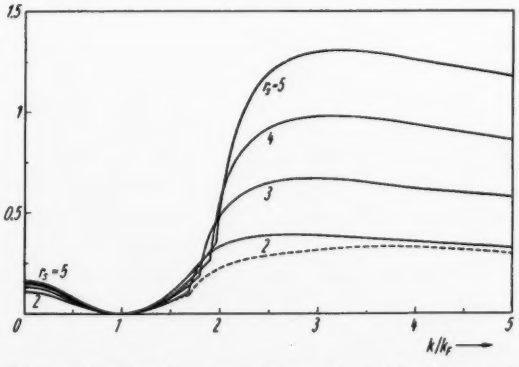

FIGURE 7. *The imaginary part of the quasi-particle self-energy Im* $\Sigma(\mathbf{k},\epsilon(\mathbf{k}))/E_F$ *as a function of the momentum* k *of the electron at different metallic densities* ($E_F = 0.921, 0.409, 0.230$, *and* 0.147 *Ry at* $r_s = 2, 3, 4$ *and* 5, *respectively*). *The dashed curve is Quinn's result at* $r_s = 2$ [10,13].

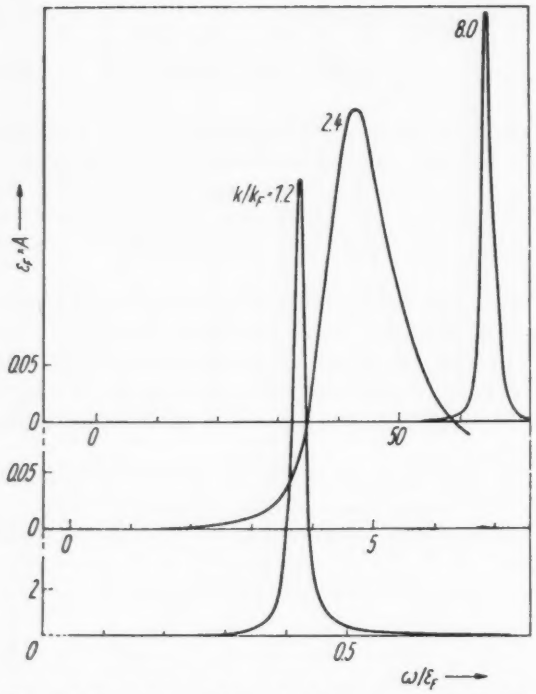

FIGURE 8. *Typical spectral forms for the quasi-particle peak of the spectral weight function in different momentum regions. The scales are different for the three curves, the energy ω is measured from the Fermi level μ, and the curves are drawn for* $r_s = 4$ [24].

LEED experiments. It is not clear, however, how much of this structure that may be observed due to the short-lifetime of the electrons at these energies.

We want to stress again that the discussion we have given of the one-electron spectrum is based on the assumption that vertex corrections are small. As discussed in the next section recent work by Langreth [29] shows that vertex corrections in the core electron problem can have a quite large effect on the form of satellite structures, while their effect on the quasi particle properties seems to be small. Preliminary investigations by one of us (L.H.) show similar strong vertex effects on the conduction band satellite. The details of the plasmaron structure should thus not be taken very seriously.

The quasi particle states close to the Fermi surface are of particular interest due to their importance for thermal and transport properties [30]. To study these problems the quasi particle density of states or density of levels rather than the one-electron density of states is of importance. Because of interactions the quasi-particle dispersion law is distorted, corresponding to the well-known mass enhancement at the Fermi surface. The corrections to the free-electron mass m due to the electron-electron interaction, as derived from eq (28), are small [11,12], *e.g.* $\delta m_e/m \approx -.01$ for Al and $\delta m_e/m \approx .06$ for Na, and the properties of the quasi particles close to the Fermi surface are dominated by the electron-phonon interaction.

The effects of the electron-phonon interaction on the quasi-particle dispersion law follow in a straightforward way using perturbation theory in the Brillouin-Wigner form, thus

$$E(\mathbf{k}) = \epsilon(\mathbf{k}) + \sum_{\mathbf{p}} |g_{\mathbf{k}-\mathbf{p}}|^2 \left[\frac{1 - f_{\mathbf{p}}}{E(\mathbf{k}) - \epsilon(\mathbf{p}) - \omega(\mathbf{k}-\mathbf{p})} + \frac{f_{\mathbf{p}}}{E(\mathbf{k}) - \epsilon(\mathbf{p}) + \omega(\mathbf{k}-\mathbf{p})} \right]. \qquad (35)$$

In this equation g_{k-p} is the matrix element for the electron-phonon coupling and $\omega(\mathbf{k}-\mathbf{p})$ the phonon frequency.

The qualitative effect of the phonons is to flatten out the dispersion curve in the immediate neighborhood of the Fermi surface, and this gives rise to the enhancement of the density of states (fig. 10), or, equivalently, of the *thermal effective mass* and one obtains from eq (35)

$$m_{ph} = m\ (1+\lambda) = N_0(E_F) \int \frac{d\Omega_{\mathbf{p}-\mathbf{k}}}{4\pi} \frac{|g_{\mathbf{p}-\mathbf{k}}|^2}{\omega(\mathbf{p}-\mathbf{k})}, \qquad (36)$$

where $N_0(E_F)$ is the density of states without electron-phonon interaction, $|\mathbf{p}| = |\mathbf{k}| = k_F$ and the integration extends over the full solid angle.

Ashcroft and Wilkins [32] first calculated the corrections for Na, Al and Pb using eq (36), and several similar calculations have been published over the last

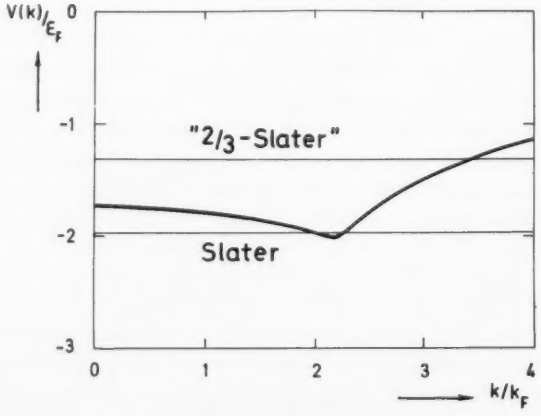

FIGURE 9. *Exchange-correlation potential for an electron gas at* $r_s = 4$ *compared with the Slater and the Gáspár (2/3 Slater) approximations* [28].

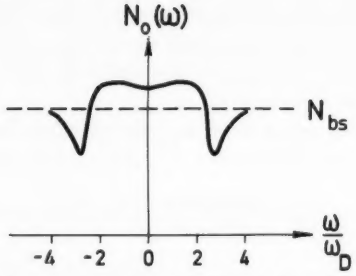

FIGURE 10. *Density of quasi-particle levels for Na at* T = 0°K [31].

few years. The most accurate values of λ are those deduced from tunneling data by McMillan and Rowell [33]. For example, the two methods give the values λ = 0.49 and 0.38, respectively, for Al; λ = 1.05 and 1.3, respectively, for Pb.

It is obvious that the enhancement varies with temperature and that no enhancement is left at high temperatures, where the phonon system behaves like a fluctuating classical medium.

Similarly to the case of electron-electron interaction the electron-phonon interaction gives a characteristic structure to the spectral function. Engelsberg and Schrieffer [34] pointed out that in the neighborhood of the Fermi surface the quasi particle picture will no longer apply. They calculated the spectral function for an Einstein model and for a Debye spectrum and obtained a spectral function with a very complex structure in the region close to the Fermi surface. For sodium no dramatic effects occur because of the rather weak electron-phonon interaction [31].

We conclude this section by noting that inclusion of dynamical and exchange effects, in particular consideration of the electron-electron interaction tells us why the one-electron theory works so well in explaining many gross features of metals and what limitations it has. However, at least in a low-order treatment there are also new structures introduced by the interaction, schematically characterized as due to the resonant coupling between electrons and plasmons. In section 5 we will discuss possibilities to observe this structure.

4. One-Electron Spectrum of Core Electrons

The preceding discussion has emphasized the strong effects of the electron-plasmon coupling on the spectrum of conduction electrons. Similar strong effects occur in the spectra of core electrons. For simplicity we limit the discussion to simple metals with small cores, so that the core electrons can be physically distinguished from the valence electrons and be well localized to a particular ion. The wave function of a core electron depends only weakly on the state of the outer electrons. The energy levels on the other hand are shifted by an appreciable amount compared to the corresponding atomic levels, typically of the order of 5 to 10 eV, which is large on the scale of valence electron energies but is a small *relative* change in the energy of a core electron. The core shifts can be measured accurately by the method of x-ray photoemission spectroscopy as well as by x-ray absorption and inelastic scattering of fast electrons.

The shift of the quasi particle energy of a core electron comes partly from changes in the average Coulomb field, partly from polarization effects. The *Coulomb shift* is due to the different valence charge distribution relative to that in a free atom. It generally results in a decrease of the binding energy. The *polarization shift* comes from the relaxation of the valence charge distribution around the hole created when we remove the electron. The valence electrons are drawn in towards the positive hole in the ion. This effect decreases the binding energy by half of the change in the Coulomb potential calculated at the core site, *i.e.* precisely the amount obtained if we calculate the self-energy of the hole using electrostatics. The shift in the core energy thus contains information about the valence electron distribution and polarizability, measured with the core electron as a probe. Theoretical calculations for simple metals (Li, Na, K, Al) are in very good agreement with the experimentally observed peaks in the XPS spectra [35].

In analogy with the strong effects of the interaction between particles and plasmons previously discussed, there is a corresponding coupling between a hole in the core and the density fluctuations of the conduction electrons. This leads to a strong structure in the core electron spectrum [36].

We assume for simplicity that we can neglect the spatial extension of the core electron wave function. Calculation of the self-energy to lowest order in the screened interaction gives the formula

$$\sum(\epsilon) = -\frac{i}{(2\pi)^4}\int d^3q\,d\omega\,v(q)\,[\epsilon^{-1}(q,\omega)-1]\,\frac{1}{\omega-\epsilon+\epsilon_n+i\delta}, \qquad (37)$$

where ϵ_n is the core quasi-particle energy. Remembering that $\epsilon^{-1}(q,\omega)$ has a strong resonance in the plasmon regime, we see that after integration over the frequency, the self-energy will show a resonance behavior in the energy region $\epsilon \simeq \epsilon_n - \omega_p$. This rapid variation will give rise to two solutions of the Dyson equation. The

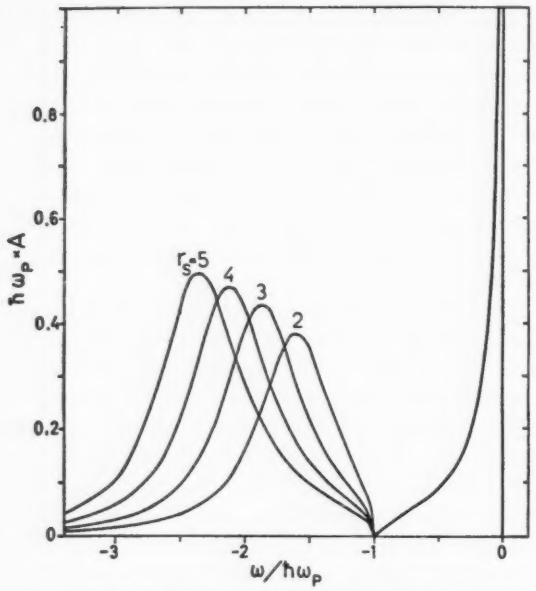

FIGURE 11. *Quasi-particle peak in the spectral function for a core electron and the associate plasmon satellite structure for different densities of the conduction electrons, measured by the electron gas parameter* r_s [36].

second solution, however, gives a quite broad peak in the spectral function. The results for different densities of the electron gas are illustrated in figure 11. The spectrum is measured from the shifted quasi particle energy, *i.e.* the zero of energy corresponds to complete relaxation of the electrons around the hole.

We summarize the characteristic features of the core spectrum

a. A large polarization shift of the core quasi particle level.
b. The shape of the spectrum is independent of the core level considered. This results from neglecting the actual size of the core wave function.
c. A pronounced satellite structure, which starts at $\omega = -\omega_p$ and has a broad peak.
d. An extended tail on the low energy side of the quasi-particle peak. This tail is due to the coupling between the hole and screened electron-hole pair excitations, and corresponds to states of the whole system involving two holes, one in the core and one in the conduction band plus one excited electron above the Fermi sea.
e. There is an appreciable reduction of the spectral strength of the quasi particle. Approximately half of the spectral strength corresponds to excitations close to the quasi particle state and approximately the same strength corresponds to high excitations of the conduction electrons as described by the broad satellite structure.

As discussed in section 2 the spectral function has the form (cf. eq (16))

$$A_c(\omega) = \sum_s |\langle N_v^*, s|N_v\rangle|^2 \delta(\omega - \epsilon_s) \qquad (38)$$

and shows a powerlaw singularity at the Fermi edge. The first order theory correctly predicts a singularity but of a somewhat different form, namely $(\omega \ln^2 \omega)^{-1}$.

The core electron spectrum can be obtained exactly if we use a simple model Hamiltonian

$$H = \epsilon a^+ a + a a^+ \sum_q g_q (b_q + b_{-q}^+) + \sum_q \omega_q b_q^+ b_q, \qquad (39)$$

Here a^+ is the creation operator for a core electron of energy ϵ and b_q^+ the creation operator for a plasmon of energy ω_q. The exact solution of this problem has been given by Langreth [29], and we now give a brief account of his work, which also shows the close resemblance of the problem to the Mössbauer or the impurity-phonon problem.

The self-energy Σ in this model is given by the sum of all diagrams where the core electron is dressed with plasmons (fig. 12). For the true Hamiltonian including all electron-electron interactions we have the same set of diagrams, where the plasmon propagator is replaced by a screened interaction $v(q)\,\epsilon^{-1}\,(q,\omega)$. Except for the first diagram the bare Coulomb potential gives no contribution (the hole propagates in only one direction) and we can thus replace ϵ^{-1} by $(\epsilon^{-1} - 1)$. By choosing the dielectric function in eq (31) and the coupling

$$g_q^2 = v(q)\omega_p^2/(2\omega_q), \qquad (40)$$

the plasmon diagrams and the screened interaction diagrams become the same. The core Green function

$$G_c(t) = -i\langle T(a(t)a^+(0))\rangle \qquad (41)$$

can be written as (cf. eq (38))

$$G_c(t) = i\langle 0|e^{i\tilde{H}t}|0\rangle e^{-i\epsilon t}\theta(-t) \qquad (42)$$

where $|0\rangle$ is the plasmon vacuum state and $\tilde{H}$ is the Hamiltonian for the plasmon in the presence of the core

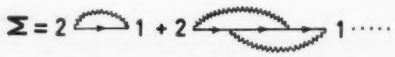

FIGURE 12. *Diagrams for the core electron self-energy.*

hole,

$$\tilde{H}=\sum_q g_q(b_q+b_{-q}^+)+\sum_q \omega_q b_q^+ b_q \qquad (43)$$

A canonical transformation shifts the zero point of the plasmon vibrations, thus

$$e^A \tilde{H} e^{-A}=H_0-\Delta\epsilon, \qquad (44)$$

where

$$A=\sum_q f_q(b_q^+-b_q);\ f_q=g_q/\omega_q;\ H_0=\sum_q \omega_q b_q^+ b_q;$$

$$\Delta\epsilon=\sum_q \omega_q f_q^2. \qquad (45)$$

We may hence write

$$\langle 0|e^{iHt}|0\rangle=\langle 0|e^{-A}e^{iH_0t}e^{A}|0\rangle e^{-i\Delta\epsilon t}$$
$$=\langle 0|e^{-A(0)}e^{A(t)}|0\rangle e^{-i\Delta\epsilon t}, \qquad (46)$$

where

$$A(t)=e^{iH_0t}Ae^{-iH_0t}=\sum_q f_q(b_q^+e^{i\omega}q^t-b_qe^{-i\omega}q^t). \qquad (47)$$

By applying the well-known formula

$$e^{A+B}=e^A\,e^B\,e^{-1/2[A,B]} \qquad (48)$$

repeated times the exact solution follows,

$$\langle 0|e^{iHt}|0\rangle=\exp(-\Delta\epsilon t)\exp\left(-\sum_q f_q^2\right)\exp\left(\sum_q f_q^2 e^{i\omega}q^t\right).$$

This gives for the spectral function (49)

$$A_c(\omega)=\frac{1}{\pi}\,\mathrm{Im}\,G_c(\omega)=\frac{1}{2\pi}\int_{-\infty}^{\infty}e^{i(\omega-\epsilon)t}\langle 0|e^{iHt}|0\rangle dt$$
$$=e^{-\sum_q f_q^2}\left\{\delta(\omega-\epsilon-\Delta\epsilon)+\sum_q f_q^2\delta(\omega-\epsilon-\Delta\epsilon+\omega_q)\right.$$
$$\left.+\frac{1}{2?}\sum_{qq'}f_q^2f_{q'}^2\delta(\omega-\epsilon-\Delta\epsilon+\omega_q+\omega_{q'})+\ldots\right\} \qquad (50)$$

To compare the first order results (the first diagram in fig. 12) with the exact solution we have used the simple dispersion law $\omega_q=\omega_p+q^2$ (in units of the Fermi energy and the Fermi momentum), which allows an analytic solution. The result for the electron density of sodium metal ($r_s=4$) is given in figure 13.

Since the dielectric function in eq (31) contains no particle-hole pairs, the quasi particle peak is a δ-function. A more realistic shape of the peak is indicated in the figure. The exact solution has structure also at $-3\omega_p$, $-4\omega_p$, *etc.*, which is not shown in the figure. This structure, however, has weak edges and carries only a few percent of the oscillator strength.

Comparing the results of the first order calculation and the exact solution we note:

1. The energy shift $\Delta\epsilon$ is exactly the same.

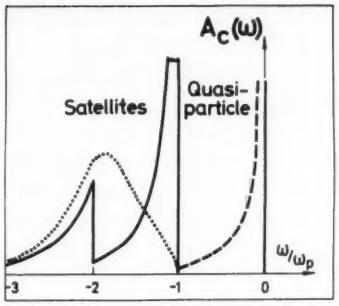

FIGURE 13. *Comparison of the first order (dotted line) and the exact result (full curve) for the core spectral function from the model Hamiltonian in eq (39). In this model the quasi-particle peak is a δ-function. The dashed curve indicates a more realistic form of that peak. The results are for* $r_s=4$.

2. The oscillator strengths in the satellites are closely the same.
3. In the exact solution the satellite has two marked peaks instead of one, and the peaks are sharper.

The large difference between the first order result and the exact solution for this model case should be a warning against taking the details of a low order calculation too seriously. Knowing the importance of the higher order diagrams in this case one may ask if not other higher order diagrams, like those of the paramagnon problem, may play a role also for the core spectrum. Finally, it should be stressed that while the satellite structure may be poorly accounted for in the first order theory, the position and singular nature of the quasi particle are quite well represented.

5. Qualitative Discussion of Some Experiments

We shall discuss some different types of experiments utilizing the connections with the one-electron spectrum discussed in section 2 and the results from the approximate calculations reported in sections 3 and 4. We can really not put forward much more than guesses about where many-body effects may possibly occur. The difficulty is that the predictions by the one-electron approximation have seldom been worked out in enough detail to give reliable level densities and matrix elements, and this knowledge is required both to evaluate the many-body effects per se as well as to find out how much of the experimental structure that is accounted for by the one-electron approximation. Also the experimental data are sometimes not as accurate and reliable as one would need. Thus surface conditions are often not under good enough control, background effects are

poorly known and disturbing secondary effects are not carefully analyzed and subtracted.

The discussion will neglect the effects of final state interactions between the electron and hole. This means that the treatment is a simple extension of the usual theory for interband transitions in which the density of states for electrons and holes in band theory is replaced by the corresponding quantities including many-electron interactions as illustrated in figures 6, 11, and 13. Although certainly of restricted validity it seems that the predictions of such an approach are worthwhile to summarize.

5.1. X-Ray Photoemission (XPS)

This experiment has a fairly clearcut relation to the one-electron spectrum. Ideally the energy distribution of photoelectrons will be given by eq (15). However, this equation is valid only if the photoelectrons leave the solid without being scattered. Structure due to satellites in the density of states will thus be mixed with structure due to energy losses.

The losses to volume excitations are proportional to the sample thickness, while the intensity of the satellite structure in the one-electron spectrum has a definite relation to the intensity of the quasi particle peak. Thus by varying the sample thickness one should be able to separate the two kinds of processes.

Theory predicts an asymmetric form of the core-quasi particle peak [4,5,6,29,36,37] and satellite structure starting at ω_p below the main peak. According to the Langreth model solution there should be two satellites also with an asymmetric line shape (cf. fig. 13), while the first order theory predicts the satellite in figure 11. There should be a satellite structure in the conduction band, as well. Even if the exact shape of this structure might differ from the results of the low-order theory discussed in section 3, the total intensity of the satellite band should be appreciable.

An experimental verification of the many-body structure would be of great aid for the further development of the theory. As regards the position of the core levels there seems to be a good agreement between theory and experiments but further experimental and theoretical work on this problem would help to clarify how point defects polarize and distort their surroundings.

5.2. Soft X-Ray Emission

We consider only the simplest possible case where we can assume complete relaxation of the Fermi gas around the hole before the emission takes place. This limits the approximate validity to the light metallic elements such as Li, Be, Na, Mg, Al and K and excludes *e.g.* all transition metals.

Through the recent work by Nozières and de Dominicis and others [4-6] the possibility of a singular structure at the Fermi edge seems to be well established. The magnitude of this Fermi edge peak and the influence of this effect on the intensity at energies outside the immediate vicinity of the edge is however so far unsettled, although important progress has been made [38]. As regards the main band it is clear that the presence of the core hole will give an enhancement of the intensity [1]. The actual magnitude of this enhancement factor and its variation over the main band is so far not well-known. To obtain the one-electron density of states in the main band from experiments seems to require both careful calculations of dipole matrix elements and better estimates of the enhancement factor.

Below the main band the edge for plasmon production is well established experimentally [1,39]. The intensity of the satellite structure is strongly affected by intricate cancellation mechanisms due to the presence of the core hole and the theoretical predictions are uncertain. The plasmaron edge (cf. figs. 5 and 6) has been searched for in Al, but the experiment was not conclusive [40]. As discussed in section 3, it is not clear whether this edge is a feature of an exact solution of the problem or just a result of the low order treatment. A clear experimental confirmation or dismissal would be of great aid for the further study of these many-body effects.

5.3. X-Ray Absorption

Consideration of these experiments requires a treatment of final state interactions but in the absence of a detailed theory for these we shall here take a simple point of view and treat the structure in the one-electron spectra as additional levels or groups of levels in a one-electron scheme. A similar discussion of plasmon effects in x-ray absorption in metals was given by Ferrell [41]. Due to the presence of satellite structure in both core and conduction band spectra there should be a characteristic structure above the threshold [36].

Accurate x-ray absorption spectra for simple metals have recently [42] been obtained, which show an edge anomaly very similar to what one may expect from the Mahan exciton effect [4-6]. The fine structure of the absorption coefficient for the $L_{II,III}$ transition in magnesium is shown in figure 14 [43]. Immediately above the edge there is more detailed structure which

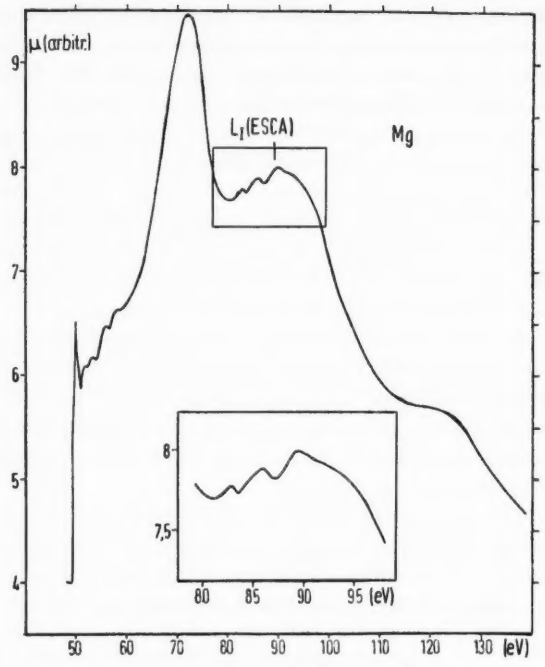

FIGURE 14. *The fine structure of the absorption coefficient for the* $L_{II,III}$ *transition in magnesium* [43].

possibly could be due to ordinary band structure effects in the final state.

At still higher energies comes a strong peak [43-45]. We will argue that this peak may be a many-body effect. In table 1 we give results for the positions of the peaks measured from the threshold [43], and compare with the position of the core plasmaron peak discussed in section 3 (cf. fig. 11). There is good agreement for aluminum but not for the other metals.

The important point, however, is that ϵ_{peak}/ω_p is a very smooth function of the electron density. Actually its value is closely 0.8 r_s in all cases. This indicates that the peak is associated with properties of the electron gas rather than being due to oscillator strength effects. The latter would be connected with the properties of the ion core and there is then no obvious reason to expect a regular variation with the conduction electron density. The position of the plasmaron peak should be given better at higher densities and the discrepancy with experiment at lower densities is in no way alarming. More serious is the fact that Langreth's calculation has shown the higher order effects to be strong. The strong peak could of course also be due to many-body effects involving final-state interactions.

TABLE 1. *Position of the strong peak in soft x-ray absorption and comparison with the location of the satellite peak* (ϵ_{pm}) *in figure 11.*

Element	r_s	ϵ_{peak}, eV	ϵ_{peak}/ω_p	ϵ_{pm}/ω_p
Al.....	2.07	24	1.6	1.7
Mg.....	2.66	22	2.1	1.8
Na.....	4.00	18	3.2	2.1

5.4. Photoemission in the Ultraviolet

The basic mechanisms of the photoemission process are still not well understood. It may be regarded in one extreme as a pure surface effect and in another as a pure volume effect. In the latter case we have to account for the very important inelastic scattering effects of the outgoing photoelectrons. If the surface effects are not too strong, and if we can sort out the inelastically scattered electrons, the photoemission results in the ultraviolet should reflect structure due to the satellite band of the conduction electrons. There is some hint of such a structure in the recent results for cesium [46] (fig. 15) at an energy of about 4 eV below the Fermi edge. However, the structure could also be due to a loss of two surface plasmons [46].

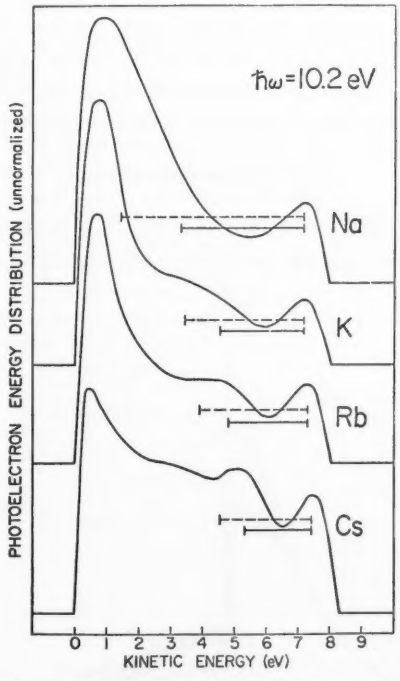

FIGURE 15. *Photoelectron energy distribution curves at* $\hbar\omega = 10.2$ *eV for Na, K, Rb and Cs* [46]. The horizontal bars indicate the values of the surface (full curve) and volume (dashed) plasmons.

5.5. Optical Absorption in the Ultraviolet

The description of optical properties of metals in terms of Drude (see *e.g.* refs 47,48) and interband contributions is often in qualitative agreement with experiment. To go beyond that description we need to know the dielectric function including final state interactions. The many-body effects may show up as changes in intensity and as new structures. Attempts to account for the former have been made *e.g.* by Mahan [49], who considered the contributions from virtually exchanged plasmons. Absorption caused by electron gas effects has been considered by Hopfield [50]. He observed that while the electron gas by itself cannot absorb radiation the effect of a weak perturbing potential from phonons or disorder is enough to provide the necessary momentum conservation for the absorption process and thus allow the plasmon resonances of the electron gas to show up.

A straightforward way to extend the one-electron joint density of states expression is to make a convolution of the spectral weights of occupied and unoccupied states. This has been done for semiconductors by Bardasis and Hone [51] who in addition considered vertex corrections. They obtained improved agreement with experiment. Calculations for metals by the convolution approximation indicate the existence of a plasmon-induced structure at photon energies above $E_g + \omega_p$ [52], where E_g is the interband threshold energy. There are some experimental indications of structure beyond the ordinary interband absorption in this energy region.

5.6. The Compton Effect

X-ray scattering from an electron gas in the regime of large momentum transfer is a direct measure of the one-dimensional momentum distribution [53]. From recent measurements of the Compton profiles of Li, Na and Al the linear momentum distribution has been derived [54]. The result for Li is shown in figure 16.

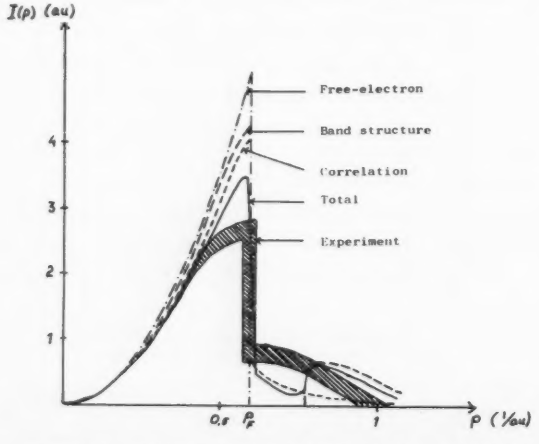

FIGURE 16. *The linear momentum distribution for Li* [54,55].

In section 3 approximate values of the momentum distribution for an electron gas have been shown (fig. 4). The corresponding linear momentum distribution shows a too small reduction compared to the free-electron case to reproduce the experimental results for Li (fig. 16) and Al, while for Na the electron gas curve falls almost entirely within the experimental region.

As band structure effects could be expected to be more important in Li and Al than in Na, this kind of correction has also been calculated using the OPW method [55]. As shown in figure 16 these effects reduce the discrepancy, even if a quantitative agreement has not been obtained.

This kind of experiment provides a way of illuminating another aspect of the distribution of electrons in metals and provides a useful way of checking theoretical models including many-body interactions.

6. Concluding Remarks

This paper has presented a discussion of the possible nature of many-electron effects on the density of states. It is based on a study of the one-electron spectrum including interactions and points out the existence of characteristic satellite structure in the density of states of electrons and holes in simple metals. Considering the joint density of states of electrons and holes as in the theory of interband transitions certain predictions about possible effects in x-ray and optical spectra can be made. All this material is however only qualitative and tentative. The structure in the one-particle spectrum has been calculated in low order and considerable changes may result by including higher-order effects. Further, the convolution of the electron and hole spectrum implies neglecting the final state interaction between the electron and the hole. The final state interactions may partly cancel out the structure in the electron and hole spectrum, and it leads to characteristic new effects such as edge singularities, and of course also gives an overall distortion of the spectrum. With all these reservations, however, the discussion points out the existence of a number of possible interesting effects which offer a challenge for further study. In assessing the possibility of pursuing this approach to obtain quantitative theoretical results one has to consider critically the present state of the art with regard to ordinary band theory. Indeed, rather little has yet been done in a quantitative way to calculate spectra

especially with regard to oscillator strengths. Such more detailed knowledge from energy band calculations also forms a necessary prerequisite for making quantitative statements about many-electron effects.

7. References

[1] For a general review, see L. Hedin and S. Lundqvist, Solid State Physics **23,** (F. Seitz, D. Turnbull and H. Ehrenreich, Editors (Academic Press, New York, 1969).

[2] Hedin, L., in "Soft X-Ray Spectra and the Electronic Structure of Metals and Materials," D. Fabian, Editor (Academic Press, New York, 1968).

[3] Anderson, P. W., Phys. Rev. Letters **18,** 1049 (1967).

[4] *e.g.*, Mahan, G. D., Phys. Rev. **163,** 612 (1967); Bergersen, B., and Brouers, F., J. Phys. Chem. **2,** 651 (1969); Mizuno, Y., and Ishikawa, K., J. Phys. Soc. Japan **25,** 627 (1968).

[5] Nozières, P., and de Dominicis, C. J., Phys. Rev. **178,** 1097 (1969).

[6] Langreth, D. C., Phys. Rev. **182,** 973 (1969).

[7] Longe, P., and Glick, A. J., Phys. Rev. **177,** 526 (1969).

[8] Nozières, P., Theory of Interacting Fermi Systems (W. A. Benjamin, Inc., New York, 1964).

[9] Quinn, J. J., and Ferrell, R. A., Phys. Rev. **112,** 812 (1958).

[10] Quinn, J. J., Phys. Rev. **126,** 1453 (1962).

[11] Rice, T. M., Ann. Phys. (N.Y.) **31,** 100 (1965).

[12] Hedin, L., Phys. Rev. **139,** A796 (1965).

[13] Lundqvist, B. I., Phys. Kondens. Materie **7,** 117 (1968).

[14] Lindhard, J., Dan. Math. Phys. Medd. **28,** No. 8 (1954).

[15] Hubbard, J., Proc. Roy. Soc. **A243,** 336 (1957).

[16] Glick, A. J., Phys. Rev. **129,** 1399 (1963).

[17] Geldart, D. J. W., and Vasko, S. H., Can. J. Phys. **44,** 2137 (1966).

[18] Singwi, K. S., Tosi, M. P., Land, R. H., and Sjölander, A., Phys. Rev. **176,** 589 (1968).

[19] Kleinman, L., Phys. Rev. **172,** 383 (1968).

[20] Langreth, D. C., Phys. Rev. **181,** 753 (1969).

[21] Lundqvist, B. I., Phys. Kondens. Materie **6,** 193 (1967); **6,** 206 (1967).

[22] Hedin, L., Lundqvist, B. I., and Lundqvist, S., Intern. J. Quantum Chem. **IS** (1967) 791.

[23] Hedin, L., Lundqvist, B. I., and Lundqvist, S., Solid State Comm. **5,** 237 (1967).

[24] Lundqvist, B. I., Phys. Stat. Sol. **32,** 273 (1969).

[25] Slater, J. C., Phys. Rev. **81,** 385 (1951).

[26] Gáspár, R., Acta Phys. Hung. **3,** 263 (1954).

[27] Kohn, W., and Sham, L. J., Phys. Rev. **140,** A1133 (1965).

[28] Hedin, L., Lundqvist, B. I., and Lundqvist, S. (to be published).

[29] Langreth, D. C. (to be published).

[30] *e.g.*, Pines, D., and Nozières, P., "The Theory of Quantum Liquids," **Vol. I,** (Benjamin, New York, 1966).

[31] Grimvall, G., J. Phys. Chem. Solids **29,** 1221 (1968); Phys. Kondens. Materie **6,** 15 (1967).

[32] Ashcroft, N. W., and Wilkins, J. W., Phys. Letters **14,** 285 (1965).

[33] McMillan, W. L., and Rowell, J. M., in "Superconductivity," R. D. Parks, Editor (Dekker, Inc., New York, 1969).

[34] Engelsberg, S., and Schrieffer, J. R., Phys. Rev. **131,** 993 (1963).

[35] Hedin, L., Ark. Fys. **30,** 231 (1965).

[36] Lundqvist, B. I., Phys. Kondens. Materie **9,** 236 (1969).

[37] Doniach, S., and Sunjić, M. (to be published).

[38] Ausman, G. A., Jr., and Glick, A. (to be published).

[39] Rooke, G. A., Phys. Letters **3,** 234 (1963).

[40] Cuthill, J. R., Dobbyn, R. C., McAlister, A. J., and Williams, M. L., Phys. Rev. **174,** 515 (1968).

[41] Ferrell, R. A., Rev. Mod. Phys. **28,** 308 (1956).

[42] Haensel, R., Keitel, G., Schreiber, P., Sonntag, B., and Kunz, C. (to be published).

[43] Haensel, R., and Kunz, C. (private communication).

[44] Fomichev, V. A., and Lukirskii, A. P., Soviet Physics—Solid State **8,** 1674 (1967); Sagawa, T., Iguchi, Y., Sasanuma, M., Ejiri, A., Fujiwara, S., Yokota, M., Yamaguchi, S., Nakamura, M., Sasaki, T., and Oshio, T., J. Phys. Soc. Japan **21,** 2602 (1966); Codling, K., and Madden, R. P., Phys. Rev. **167,** 587 (1968).

[45] Watanabe, H., J. Appl. Phys. **3,** 804 (1964); Swanson, N., and Powell, C. J., Phys. Rev. **167,** 592 (1968).

[46] Smith, N. V., and Spicer, W. E., Phys. Rev. Letters **23,** 769 (1969).

[47] Nettel, S. J., Phys. Rev. **150,** 421 (1966); Miskovsky, N. M., and Cutler, P. H., Solid State Comm. 7, 253 (1969).

[48] Haga, E., and Aisaka, T., J. Phys. Soc. Japan **22,** 987 (1967).

[49] Mahan, G. D., Phys. Letters **24A,** 708 (1967).

[50] Hopfield, J. J., Phys. Rev. **139,** A419 (1965).

[51] Bardasis, A., and Hone, D., Phys. Rev. **153,** 849 (1967); see also Brust, D., and Kane, E. O., Phys. Rev. **176,** 894 (1968).

[52] Lundqvist, B. I., and Lydén, C. (to be published).

[53] Platzman, P. M., and Tzoar, N., Phys. Rev. **139,** A410 (1965).

[54] Phillips, W. C., and Weiss, R. J., Phys. Rev. **171,** 790 (1968).

[55] Lundqvist, B. I., and Lydén, C. (to be published).

(Paper 74A3—608)

JOURNAL OF RESEARCH of the National Bureau of Standards—A. Physics and Chemistry
Vol. 74A, No. 3, May-June 1970

Ion-Neutralization Spectroscopy*

Homer D. Hagstrum

Bell Telephone Laboratories, Murray Hill, New Jersey 07974

(October 10, 1969)

The ion-neutralization spectroscopy (INS) is discussed in comparison with other spectroscopies of solids. It is shown that INS probes the local density of states of the solid at or just outside the solid surface. It is believed that this accounts for the clear-cut differences between INS results and those of other spectroscopies. Because of its unique specificity to the surface region INS is particularly useful in studying the surface electronic structures of atomically clean surfaces and of surfaces having ordered arrays of known atoms adsorbed upon them. In the latter case INS determines a portion of the molecular orbital spectrum of surface molecules formed from the adsorbed foreign atom and surface atoms of the bulk crystal. Such spectra provide information on local bonding symmetry and structure and electrical charging within the surface molecule which is as yet unavailable by any other method. INS is the first attempt to base a spectroscopy of electronic states on a two-electron process. More recent work on experimental and mathematical problems which such a spectroscopy entails are also briefly mentioned in this paper.

Key words: Auger processes; autoionization; density of states; ion-neutralization; transition probability.

1. Introduction

In general, spectroscopies of electronic states have been based on the absorption or emission of electromagnetic radiation when the system under observation is excited or de-excited. In absorption spectroscopies one can observe the absorption of the photon or observe the electrons emitted when the photon is absorbed as in photoelectron spectroscopy. All of these spectroscopies are based on one-electron transition processes. The ion-neutralization spectroscopy (INS), on the other hand, is the first, but not the only spectroscopy, to be based on a two-electron process in which a band transition density function is obtained. It is like the photoelectron spectroscopies in that the spectroscopic information is obtained by measurement of the kinetic energy distribution of electrons ejected in the process. However, because INS employs a two-electron process, the kinetic energy distribution contains the "spectroscopic function" in folded or convolved form, making data reduction somewhat more involved than for a spectroscopy based on a one-electron process.

INS is a relatively new spectroscopy of solids having its own unique set of characteristics, advantages, and limitations. It is the purpose of this paper to review these properties in comparison with other spectroscopies. We discuss the method and what it measures, its resolving power and operational limitations, and its unique contributions to our knowledge of electronic state densities.

2. The Nature and Method of INS

When an excited and/or ionized atom is projected at a solid surface, an excited solid-atom system is formed. The ion-neutralization process upon which INS is based is one of the processes of auto-ionization by which such an excited solid-atom system de-excites itself. Not all such processes are appropriate to INS, however. The autoionization processes can be divided into two principal classes depending upon whether unfilled electronic levels in the atom do or do not lie opposite filled electronic levels in the solid. These are in-

* An invited paper presented at the 3d Materials Research Symposium, *Electronic Density of States*, November 3-6, 1969, Gaithersburg, Md.

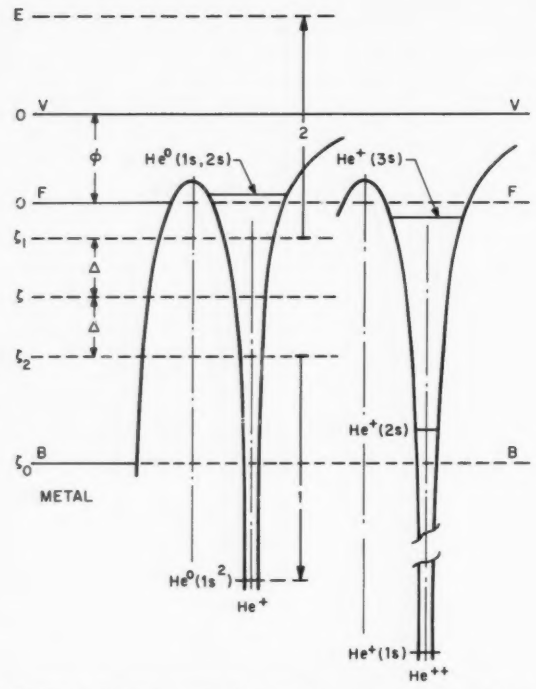

FIGURE 1. *Electron energy diagram showing metal at left and two atomic wells for He^+ and He^{++} cores.* V *is the vacuum level,* F *the Fermi level and* B *the bottom of the filled band. Transitions 1 and 2 are those of the ion-neutralization process.*

dicated schematically in figure 1. Here we show the electronic energy level diagram of a metal to the left and two atomic wells outside. One atomic well is that of the $He^+(1s)$ core in which the levels are those of He^0. The second well is that of the He^{++} core in which the energy levels are appropriate to He^+. We see that the two wells differ in that one (He^{++}) has two states [$He^+(2s)$ and $He^+(3s)$] lying in the energy range of the filled band of the metal, whereas the other (He^+) has no states in this energy range.

We expect that atomic levels lying in the range of allowed levels of the solid will become resonances or virtual bound states and that of these allowed levels, those lying in the range of the filled band will fill. Thus the atomic levels should control the autoionization process in some energy ranges when they can fill by tunneling. Preliminary experiments with doubly-charged He^{++} ions and with metastably-excited $He^+(2s)$ ions appear to bear this out. Thus if we want the autoionization process to be dominated by initial state electrons whose state density is determined by the solid or its surface there should be no atomic levels lying in the energy range of the filled band as is the case in figure 1 for He^+. This is a fundamental restriction on the ion-solid systems to which INS can be applied. For He^+ ions the solid band should lie within the energy range from ~4.5 eV to ~22.5 eV below the vacuum level. Earlier work has shown that the effective ionization energy of He is about two eV less than its 24.5 eV free-space value [1].

The transitions (1 and 2) of the two-electron, Auger-type, ion-neutralization process are also shown in figure 1. Since ζ_1 and ζ_2 may vary over the entire filled band we expect the ejected electrons to have energies lying in a broad band. Experimentally the kinetic energy distributions are measured by regarding potential means using apparatus we shall not describe here [2,3]. Examples of recorder plots of several kinetic energy distributions, $X(E)$, are shown in figure 2. It is clear that the X distribution is sensitive to the nature of the solid and the preparation of its surface. The spectroscopic information obtained by INS resides in these distributions. In order to extract it we must understand the structure of these distributions in detail.

The distribution functions which we need to understand the ion-neutralization process are shown for an atomically clean copper face in figure 3. Suppose we start with the simplification of constant transition probability independent of the initial energy ζ. Then it

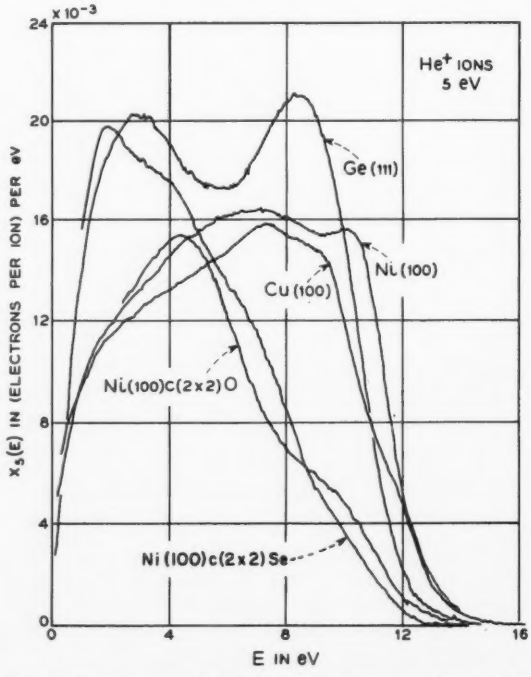

FIGURE 2. *Kinetic energy distribution of electrons ejected by 5 eV He^+ ions from atomically clean surfaces of Ge(100), Ni(100), and Cu(100) and from Ni(100) surfaces having ordered c(2×2)O and c(2×2)Se structures upon them.*

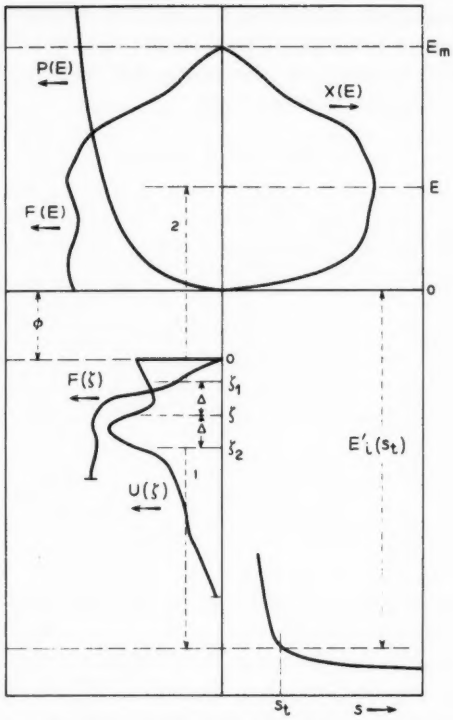

FIGURE 3. *Electron energy diagram showing distribution functions appropriate to copper. The arrows under the functional labels indicate the direction in which the function is plotted. Shown also is the variation of ground state position* $E_i'(s)$ *in the lower right-hand quadrant of the figure.*

is clear that the probability of the elemental process involving valence band electrons initially at ζ_1 and ζ_2 is $N(\zeta_1)N(\zeta_2)$ where $N(\zeta)$ is the appropriate state density of the combined metal-atom system. If we ask the relative probability of producing excited electrons in dE at E we see that all elemental processes contribute in which the electrons are symmetrically disposed on either side of the level ζ which lies halfway between the level E and the ground level of the atom at $-E_i'(s_t)$. Thus we must integrate over Δ obtaining the restricted pair distribution function $F_c(\zeta)$ appropriate to the assumption of constant transition probability:

$$F_c(\zeta) = \int_{-\zeta}^{\zeta} N(\zeta-\Delta)N(\zeta+\Delta)d\Delta. \qquad (1)$$

Relaxation of the restriction on transition probability to obtain a general $F(\zeta)$ function requires introduction into eq (1) of a factor proportional to the square of the matrix element. Thus:

$$F(\zeta) \propto \int_{-\zeta}^{\zeta} |H_{fi}|^2 N(\zeta-\Delta)N(\zeta+\Delta)d\Delta. \qquad (2)$$

We shall sidestep questions of antisymmetrization of wave functions discussed elsewhere [4] and discuss only the one elemental matrix element:

$$H' = \int\int u_g^*(1)u_v'(1)(e^2/r_{12})u_e^*(2)u_v''(2)d\tau_1 d\tau_2 \qquad (3)$$

in which u_v' and u_v'' are initial state functions in the band, u_g is the atomic ground state function, and u_e is the function for the excited electron. In eq (3) terms have been rearranged so that functions of the variables of the same electron are brought together.

We see that the matrix element may be viewed as a Coulomb interaction integral between two electron clouds of spatial extent $u_g u_v'$ and $u_e u_v''$. Since u_g is limited to the general vicinity of the atom the term $u_g u_v'$ varies in magnitude with u_v'. Thus the "down" electron makes a contribution to H' which varies with energy as $[u_v'(\zeta-\Delta)]_A$, the u_v' function evaluated near the atom position. If the "up" electron were also restricted to the vicinity of the atom we could make a similar argument relating to the energy variation of the contribution of the up election to H' to the magnitude of $[u_v''(\zeta+\Delta)]_A$. This requires in addition that u_e' vary little and smoothly with energy as appears reasonable.

Several reasons can be adduced for believing that the up electron is excited near the atom position. These are listed here without really adequate discussion:

(1) Experimentally the prominence of the molecular orbital peaks in the results for surface molecules indicates that the wave function magnitudes in the surface region are controlling.

(2) Dominance of atomic level resonances in the results for ions in which atomic levels fill also points to the dominance of wave function magnitude at the atom in governing the autoionization process.

(3) The difference between INS and photoelectric results for atomically clean surfaces can be understood only if INS is surface dominated.

(4) Energy broadening in the $X(E)$ distribution is reduced by a factor 10 when an ordered monolayer of O, S, or Se is formed on the surface of Ni(100). This must be the result of reduction of the density of states just above the Fermi level. Since this reduction can occur only in and outside the monolayer we have evidence in this result that the INS process occurs predominantly in this region.

(5) There appear to be many fewer inelastically scattered electrons in INS than for equivalent photon energy in photoelectric emission, again

suggesting a surface source of excited electrons.

(6) Theoretical considerations by Heine [5] and Wenaas and Howsmon [6] lead to the conclusion that the up electron is excited predominantly outside and in the first layer of the solid.

(7) Large momentum transfer between the two participating electrons means a close collision near the atom where we know the down electron is concentrated. Also viewing the Auger process as photoemission by the down electron followed by photoabsorption by the up electron points to the conclusion that the up electron is most likely excited in the rapidly-decaying near field of the dipole of the down electron transition.

(8) If the up and down electrons made very different contributions to H_{fi} we could not conclude that F is the convolution square U^*U but must be the convolution product V^*W of two dissimilar factors. When V^*W is inverted as though it were a convolution square it can be shown that spurious features will be introduced into $U(\zeta)$ unless $V \cong W$. These are not found.

We are thus led to the general conclusion that:

$$H_{fi} \approx [u_v'(\zeta-\Delta)]_A[u_v''(\zeta+\Delta)]_A, \tag{4}$$

from which eq (2) becomes:

$$F(\zeta) \propto \int_{-\zeta}^{\zeta} [u_v'(\zeta-\Delta)]_A^2 N(\zeta-\Delta)\,[u_v''(\zeta+\Delta)]_A^2 N(\zeta+\Delta)d\Delta. \tag{5}$$

eq (5) may be written as:

$$F(\zeta) = \int_{-\zeta}^{\zeta} U(\zeta-\Delta)U(\zeta+\Delta)d\Delta = U*U, \tag{6}$$

defining the transition density function $U(\zeta)$ which thus includes both state density and transition probability factors. We see also from eqs (5) and (6) that $U(\zeta)$ is essentially the so-called local density of states in the vicinity of the atom, *i.e.*, the actual state density weighted by the local wave function magnitude at the atom position. This wave function magnitude must, of course, include the effect of the presence of the atom itself in this vicinity.

The pair distribution function $F(\zeta)$ of eq (6) becomes the distribution in energy of excited electrons, $F(E)$, when band variable ζ is replaced by the outside energy variable E according to the relation:

$$E = E_i'(s_t) - 2(\zeta+\varphi). \tag{7}$$

This equation is obtained by equating magnitudes of the energy transitions 1 and 2 in figures 1 or 3. The externally observed electron energy distribution $X(E)$ is related to $F(E)$ by the equation:

$$X(E) = F(E)P(E), \tag{8}$$

where $P(E)$ is the probability of escape over the surface barrier and includes any other dependences on E such as variation in density of final states.

The method of INS consists in reversing the above development to obtain $U(\zeta)$ from measured $X(E)$. It proceeds in the following steps:

(1) Experimental determination of two $X_K(E)$ at ion energies $K = K_1$ and K_2. Usually $K_1 = 5$ eV and $K_2 = 10$ eV.

(2) Linear extrapolation of X_{K_1} and X_{K_2} to X_0 to reduce the natural broadenings present in the X_K distributions. This is done by use of the relation:

$$X_0(E) = X_{K_1}(E) + R[X_{K_1}(E) - X_{K_2}(E)]. \tag{9}$$

Since it has been shown that broadening varies with ion velocity, it is possible to write $R_{K_1K_2}$ as

$$R_{K_1K_2} = (K_2/K_1)^{1/2} - 1. \tag{10}$$

(3) Division of $X_0(E)$ by a $P(E)$ function, reversing eq (8), to obtain $F(E)$. This step is really not necessary since replacement of $P(E)$ by a constant merely changes the intensity level of $U(\zeta)$ progressively as ζ increases without disturbing the structure. However, we have usually divided by a parametric $P(E)$ whose parameters are chosen so that the pieces of $F(\zeta)$ obtained by He^+, Ne^+, and Ar^+ ions are essentially coincident.

(4) After change of variable, $F(\zeta)$ is inverted by a sequential deconvolution procedure. The formulas used are:

$$U_0 = (F_1/2\Delta\zeta)^{1/2},$$

$$U_2 = (1/U_0)\,(F_2/2\Delta\zeta),$$

$$U_{2n-2} = (1/2U_0)[(F_n/2\Delta\zeta) - \sum_{p=1,\,n-2} U_{2n-2p-2}U_{2p}],\ n \geq 2, \tag{11}$$

in which F and U are digitalized as $F_n = F(n\Delta\zeta)$, $n = 1,m$; $U_{2n-2} = U[(2n\text{-}2)\Delta\zeta]$, $n = 1,m$.

(5) Tests of the mathematical uniqueness of $U(\zeta)$ by variation of its origin and by comparison with $F'(\zeta)$, the derivative of the fold function. These steps cannot be discussed in this paper

but will be discussed extensively in a forthcoming publication [7]. Suffice it to say that, although deconvolution is in general a difficult procedure, the sequential unfold works extremely well for the general class of $F(\zeta)$ functions we have for which $F(0)=0$, $F'(0)=k$, and $F(\zeta)$ does not depart drastically from $F(\zeta)=k\zeta$.

The procedure we now use is essentially that given when the INS method was first discussed [4]. However, in the interim we have learned a good deal about the mathematical side of the data reduction, particularly the unfolding procedure. We have derived all possible digital sequential unfold formulations which invert directly or with the independent calculation of no more than the first data point U_0. We have also studied the noise characteristics and shown that the step-midpoint formulation given above in eq (11) not only is the only one which inverts directly without independent calculation of the first point but also has by far the best stability characteristics with respect to noise in the data. We have also faced up to the problems involved in the possibility that we are inverting as a convolution square *(U*U)* a function which is in reality a convolution product *(V*W)* and have devised tests to determine if any spurious structure could possibly be introduced in this way. The data reduction procedures, although more complicated than for a one-electron spectroscopy, proceed smoothly on the digital computer and produce unique and correct answers. We shall discuss further some of the properties and limitations of INS in section 4.

3. Examples of INS Results

We turn now to the presentation of INS results. These are in two categories: (1) results for atomically clean surfaces of the transition metals Cu and Ni [8], and (2) results for the Ni(100) surface with ordered monolayers of O, S, and Se adsorbed upon it [9]. Some unpublished results for Si and Ge will be mentioned in the discussion of item (1).

In figure 4 we reproduce figure 6 of reference 8 showing $F(\zeta)$ and $U(\zeta)$ for Cu(111). Also shown in the correct relative position is the $P(E)$ function used, indicating how flat it is over the energy range of the data. The average $U(\zeta)$ function for (100), (110), and (111) faces of Cu (fig. 15 of ref. 8) is compared in figure 5 here with the optical density of states curve (ODS) of Krolikowski and Spicer [10]. In figure 6 the $U(\zeta)$ curve for atomically clean Ni(100) from INS is shown and compared with Eastman's ODS curve for a nickel film obtained by photoemission [11].

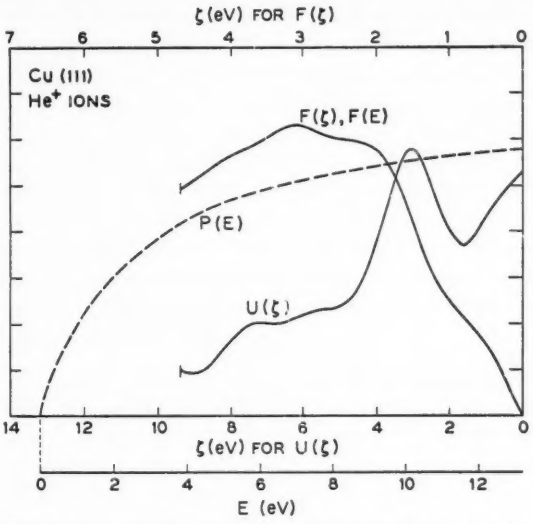

FIGURE 4. *F and U functions for atomically clean Cu(111) and He+ ions [fig. 6 of ref. 8]. The probability of electron escape used in the data processing is also shown.*

First, it is evident that the INS results show a peak in the general vicinity of the bulk *d*-band in both Cu and Ni. However, it is equally evident that this peak does not have the shape or width to be expected from band theory or measured by ultraviolet photoelectron spectroscopy (UPS). A strong case can be made that the differences evident in figures 5 and 6 are due to the fact that the two spectroscopic methods are sensitive to different things. Although the energy resolving power of INS is somewhat poorer than that of UPS, one cannot by any stretch of the imagination consider the INS $U(\zeta)$ curve as a smeared out version of the ODS curves. In reducing the Ni data of figure 6 very little digital

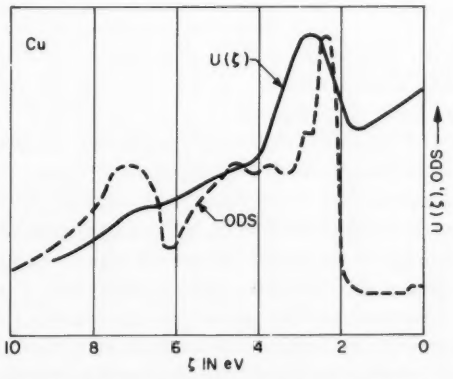

FIGURE 5. *Comparison of the average U(ζ) function for (100), (110), and (111) faces of Cu [fig. 15 of ref. 8] compared with the optical density of states curve (ODS) of Krolikowski and Spicer (ref. 10) obtained by photoelectron spectroscopy.*

378-324 O - 70 - 9

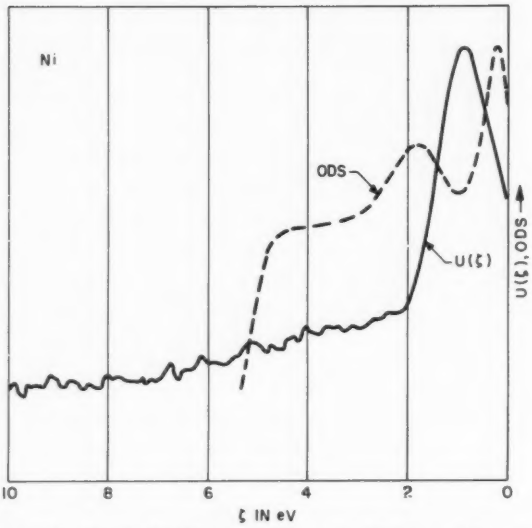

FIGURE 6. *U(ζ) for Ni(100) compared with the ODS curve of Eastman (ref. 11) also obtained by photoelectron spectroscopy. The amount of smoothing used in the INS data reduction was deliberately reduced to the point of leaving in the data the noise seen in an attempt to demonstrate the best resolving power of the INS method.*

smoothing of the data was used in an attempt to increase the resolving power at the expense of letting through low-frequency noise. Some increase in resolving power (about 20%) is evident when comparison with similar curves in reference 9 are made. The sharpness of the peak in $U(\zeta)$ at $\zeta = 1$ eV is an indication of the INS resolving power. In view of the characteristics of INS discussed above it is believed that the $U(\zeta)$ curve is in fact the local density of states at or just outside the surface whereas the UPS results are characteristic of the bulk.

Why the local density of states for *d* bands of transition metals outside the surface differs from the bulk band is an interesting question in surface physics. The reduction in number of nearest neighbors as well as a probable small dilatation of the lattice at the surface could narrow the tight-binding *d* band and make it more like an atomic level. Tight-binding bands are particularly vulnerable to such modification in the surface region. Unpublished work on Si and Ge appears to indicate that the INS results will much more closely mirror what is expected from bulk theory [12]. This is probably attributed to the fact that the *s* and *p* wave functions of the semiconductor valence bands overlap more strongly at the surface even though the surface atoms may be displaced from their "bulk positions" by larger amounts than are surface atoms of the transition metals. Another interesting suggestion to account for the INS results in Cu and Ni arises in the work of Pendry and Forstmann [13] who predict that on some faces of transition metal crystals a new type of surface state appears which should clearly modify the surface local density of states from the bulk density.

The second category of INS experimental result to be mentioned in this paper is found for metal surfaces upon which ordered monolayers of adsorbed atoms are present. In figure 7 is reproduced the $U(\zeta)$ functions from reference 9. Here in curve 1 is repeated the transition density for atomically clean Ni(100). Curves 2, 3, 4 are for $c(2\times2)$ structures of O, S, Se, respectively, and curves 2′, 3′, and 4′ are for $p(2\times2)$ structures involving these same adsorbed atoms, respectively. We note a very interesting increase in complexity of the *U* functions for the covered surfaces. These appear now

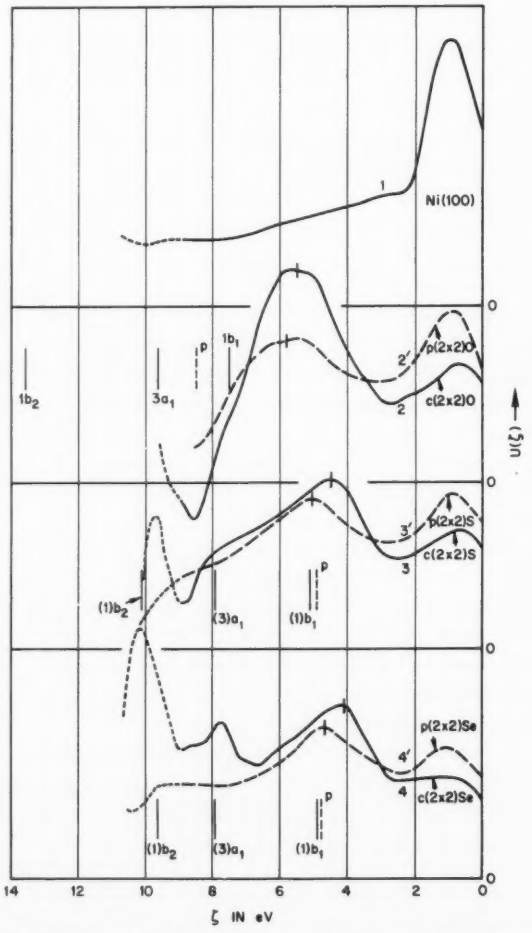

FIGURE 7. *Transition density functions, U(ζ) for atomically clean Ni(100) (curve 1) and for the surface with c(2×2) structures of O, S, Se (curves 2, 3, 4, respectively) and with p(2×2) structures of O, S, Se (curves 2′, 3′, 4′, respectively). Energies labelled* p, $1b_1$, $3a_1$, *and* $1b_2$ *are identified in the text.*

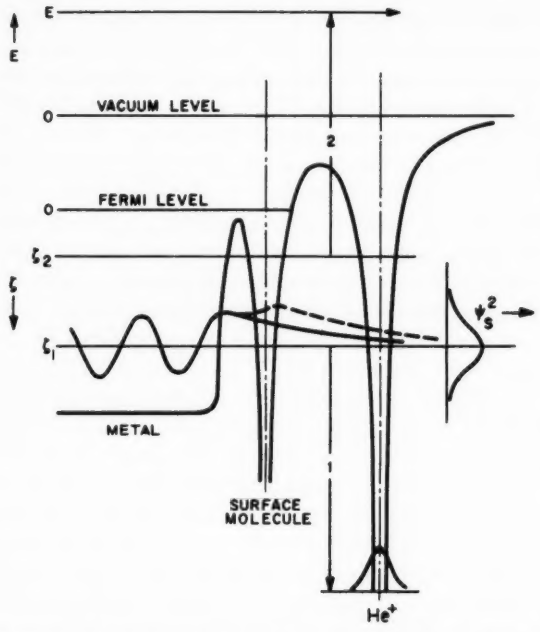

FIGURE 8. *Electron energy diagram illustrating the effect on INS of a resonance or virtual bound state of a surface molecule formed on a metal surface. The bond resonance in the surface molecule is assumed to lie at ζ_1 (which is also the initial energy of the down electron) and to increase the magnitude of the surface wave function ψ_s over a broadened energy range as indicated on the right-hand side of the diagram. The increase in wave function outside the solid in this energy region is indicated by the dashed-line modification of the electronic wave function at ζ_1.*

to indicate the energy spectra of electronic orbitals of electrons in the bonds of so-called "surface molecules" formed from the adsorbed atom and atoms of the substrate.

The electronic states to be associated with bond orbitals in surface molecules form resonances or virtual bound states. These will evidence themselves in the transition density for reasons we attempt to make clear by figure 8. The presence of the electronic orbital at the surface will increase the wave-function magnitude in the vicinity of the surface molecule as indicated by ψ_s^2 in the figure. This will in turn increase the tunneling probability for band electrons into the He^+ well. The dashed line indicates how a band wave function in the absence of the surface molecule (full line) is increased in the presence of the surface molecule (dashed line). These wave function increases in the He^+ well will result in peaks in the local density of states and hence the $U(\zeta)$ transition density function observed by INS.

This paper is not the place to discuss the results in figure 7 in any great detail. A preliminary discussion is to be found in the original publication [9] and an extensive paper is in preparation [7]. However, it is essential to an understanding of the scope of INS as a spectroscopy of electronic states to mention briefly the principal results for these cases of chemisorption. Several energies are indicated in figure 7. These are the levels of the atomic p orbitals in free O, S, and Se, labelled p in the figure. In the figure the second, third, and fourth panels from the top refer to adsorbates O, S, and Se respectively. The lines labelled $1b_1$, $3a_1$, and $1b_2$ are molecular orbital energies in the free molecules H_2X where X is O, S, or Se in the second, third, or fourth panels of the figure, respectively.

Three types of molecular orbital spectrum are to be found among the six curves for adsorbed species in figure 7. Curves 3 and 4 are the most complex spectra having peaks near the orbitals indicated for the free H_2X molecule. These have been attributed to the bridge-type bonding illustrated in figure 9(a) and (b). Relatively small negative charging of the $X = S,Se$ end of the surface molecule is indicated by the fact that the lone-pair orbital peak near $(1)b_1$ also lies near the atomic p orbital energy as for free H_2X.

When the structure is changed from the $c(2\times2)$ [fig. 9(b) to the $p(2\times2)$ [fig. 9(d)] by removal of half of the adsorbate we see that the molecular orbital spectra change completely to those of curves 3 and 4 in which there is a single peak below the Ni d-band peak indicating a change in the local bonding structure. The only other reasonable alternative is the π-type symmetrical bonding as shown in figure 9(c) and (d) for which we expect a nonbonding orbital in this energy range. Removal of the "center atom" in the $c(2\times2)$ structure removes the agent which distorts the square of Ni atoms of C_{4v} symmetry below each X atom into a rhombus of C_{2v} symmetry. C_{2v} symmetry is essential if the molecular structure is to resemble H_2X. Reversion to C_{4v} symmetry when the center atom is removed demands change of the molecular structure and spectrum as is indeed found.

Finally, both $c(2\times2)O$ (curve 2) and $p(2\times2)O$ (curve 2′) show a single peak shifted by a much larger amount toward the Fermi level from the atomic p level than is the case for either S or Se. This orbital spectrum (single peak in the available energy range) and larger negative charge (orbital energy shift) together with small work function change on adsorption can be shown to be consistent with a reconstructed surface in which the adsorbed atom is incorporated into the top layer of substrate atoms where relatively large charge will not result in large work function change. Although the above account of the data in figure 7 is admittedly

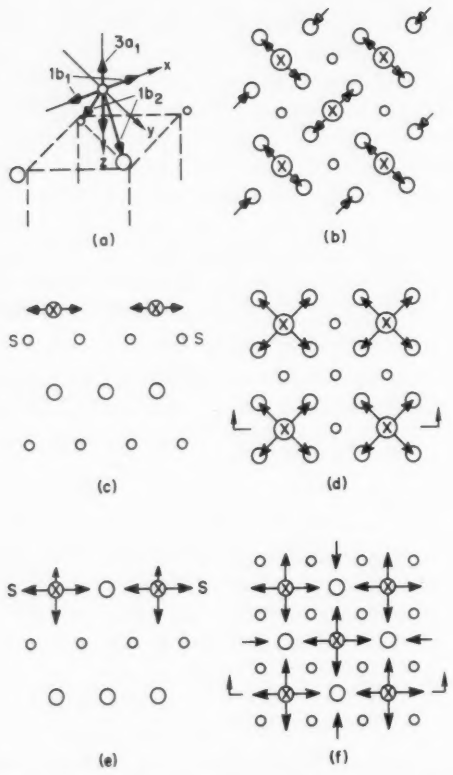

FIGURE 9. *Surface structures suggested (ref. 9) to account for the molecular orbital spectra of figure 7. (a) and (b) are for a bridge-type Ni_2X-type structure repeating over the surface in a c(2×2) pattern to account for curves 3 and 4 of figure 7. (c) and (d) illustrate a p(2×2) structure adequate to account for curves 3' and 4' of figure 7. (e) and (f) illustrate a reconstructed c(2×2) structure to account for curve 2 of figure 7. Simple removal of the "center atom" in (f) without other change produces the p(2×2) reconstructed surface thought to account for curve 2' of figure 7. In these figures bond orbitals are indicated by the heavy arrows with conical arrowheads.*

sketchy, it does indicate how INS determines a portion of the molecular orbital spectrum of a surface molecule and the power such information has in elucidating symmetry and bonding character.

4. Comparative Critique of INS

A comparative critique of INS is perhaps best carried out by listing its characteristics and attempting to assess them as advantages or disadvantages in comparison with other spectroscopies of solids. The other spectroscopies are the two forms of photoelectron spectroscopy, ultraviolet photoelectron spectroscopy UPS [10,11] and x-ray photoelectron spectroscopy XPS [14]; soft x-ray spectroscopy SXS [15], and the surface Auger spectroscopy SAS [16].

In the first place INS is a two-electron spectroscopy as is SAS whereas UPS, XPS, and SXS are one-electron spectroscopies. SAS is based on a two-electron Auger process similar to that underlying INS except that the vacant ground level in the excited system is an inner level of a surface atom rather than the ground level of the parent atom of an incoming atomic ion. The SAS process has been used extensively in the identification of surface impurities but Amelio and Scheibner [16] were the first to attempt to separate the Auger distribution from the large background of secondary electrons and to unfold it to obtain spectroscopic information as has been done in INS.

The fact that INS, like SAS, is a two-electron spectroscopy must in itself be considered a drawback since it necessitates unfolding of the data. However, in INS the data are of such quality that unfolding now offers no significant problem. We have learned much about unfolding methods and possible errors since the last discussion of these matters in the literature [4].

A second characteristic of INS is its surface specificity and hence surface sensitivity. This means, as we have seen, that INS results can be compared with the results of bulk spectroscopies only in special cases. However, INS gives us a tool to study variation of electronic band structure from bulk to surface, to study surface states on both metals and semiconductors, and, perhaps most importantly, to measure molecular orbital spectra of surface molecules formed in chemisorption. Some recent UPS work [17] with 21.2 eV radiation and grazing incidence has shown the possibility of detection of large molecules adsorbed on surfaces. Whether surface molecules of the type discussed here can be observed in this manner has yet to be demonstrated.

The transition probability factors of INS arise from its surface specificity and the tunneling character of the electronic transitions. Four types can be listed: (1) a tunneling factor which decreases with depth in the band, (2) a symmetry factor arising from extent of the surface wave function which decreases as the character proceeds from *s* to *p* to *d*, *etc.*, (3) a second tunneling factor which favors bulk states whose k vector is normal to the crystal face used, and (4) the enhancement in certain energy ranges caused by the surface resonances of adsorbed atoms. Although they are distinctive, there appears to be no particular disadvantage associated with these transition probability factors. It is the last one which makes possible the study of surface molecules and this must be listed as an advantage.

The energy range which can be explored in the solid is $E_i' - 2\varphi$ where E_i' is the effective neutralization ener-

gy of the incident ion near the surface (effective ionization energy of the parent atom) and φ is the work function of the solid. This means that INS is the equivalent of a photoelectric process for which $h\nu = E_i' - \varphi$. For He, $E_i' \sim 22.5$ eV and for a representative solid $\varphi \sim 4.5$ eV. Thus $E_i - \varphi \sim 18$ eV. To equal this range with UPS one must use the 21.2 eV He resonance radiation. XPS, SXS, and SAS, on the other hand, have essentially no energy range limitation with respect to the valence bands of solids. Like UPS, INS is limited by vacuum level cutoff making it difficult to extract data near the vacuum level because of the rapid variation of escape probability there.

Energy resolving power of INS is undoubtedly somewhat less than that of UPS but as figure 6 indicates not greatly less. It is in all probability better than that of SXS, XPS, or SAS since each of these involve the relatively broad inner level of an atom at one point or other.

Finally, we shall mention a series of side effects which must be considered in evaluating any spectroscopy. There appear to be fewer inelastically scattered electrons to contend with in INS than in UPS at higher energies. SAS has a serious background problem unknown to INS. Plasma losses, which can be a complicating interpretive factor, apparently play no role in INS results. SXS has a serious spectral superposition problem unknown to INS. The signal intensity in INS is adequate which sometimes cannot be said for SXS or SAS. INS has the possibility of variation of natural broadenings by variation of a controllable experimental parameter, namely incident ion velocity, making it possible to extrapolate out broadenings admittedly greater than those of UPS.

In conclusion it is possible to state that ion-neutralization spectroscopy is a viable spectroscopy of solids having its own peculiar set of characteristics. It appears that its most important area of application at present is to the study of the molecular orbital spectra of surface molecules formed in chemisorption. Here it holds promise of extending our knowledge of surface structure beyond what low-energy electron diffraction (LEED) now can do. LEED tells us how a given adsorption or bonding structure repeats itself over the surface. INS yields information about bonding symmetry, orbital energy-levels, and electric charging within the surface molecular structure, which in many cases, using LEED and work function data, will permit the specification of bonding structure. Surface state and surface modifications of band structure also promise to be interesting fields in which INS can make a contribution.

5. References

[1] Hagstrum, H. D., Phys. Rev. **96,** 336 (1954).
[2] Hagstrum, H. D., Rev. Sci. Instr. **24,** 1122 (1953).
[3] Hagstrum, H. D., Pretzer, D. D., and Takeishi, Y., Rev. Sci. Instr. **36,** 1183 (1965).
[4] Hagstrum, H. D., Phys. Rev. **150,** 495 (1966).
[5] Heine, V., Phys. Rev. **151,** 561 (1966).
[6] Wenaas, E. P., and Howsmon, A., private communication and Proc. 4th Int'l Materials Symp. on the Structure & Chemistry of Solid Surfaces, 6/19-21/68, Univ. of California, Berkeley.
[7] Hagstrum, H. D., and Becker, G. E., to be published.
[8] Hagstrum, H. D., and Becker, G. E., Phys. Rev. **159,** 572 (1967).
[9] Hagstrum, H. D., and Becker, G. E., Phys. Rev. Letters **22,** 1054 (1969).
[10] Krolikowski, W. F., and Spicer, W. E., Phys. Rev., to be published.
[11] Eastman, D. E., and Krolikowski, W. F., Phys. Rev. Letters **21,** 623 (1968); Eastman, D. E., J. Appl. Phys. **40,** 1387 (1969).
[12] Hagstrum, H. D., and Becker, G. E., to be published.
[13] Pendry, J., and Forstmann, F., private communication.
[14] Fadley, C. S., and Shirley, D. A., Phys. Rev. Letters **21,** 980 (1968).
[15] Cuthill, J. R., McAlister, A. J., Williams, M. L., and Watson, R. E., Phys. Rev. **164,** 1006 (1967).
[16] Amelio, G. F., and Scheibner, E. J., Surface Science **11,** 242 (1968). Other forthcoming papers by these authors will give results for Si and discuss the experimental and mathematical methods in greater detail.
[17] Bordass, W. T., and Linnett, J. W., Nature **220,** 660 (1969).

(Paper 74A3–609)

JOURNAL OF RESEARCH of the National Bureau of Standards—A. Physics and Chemistry
Vol. 74A, No. 3, May-June 1970

Local Theory of Disordered Systems*[1]

W. H. Butler[2] and W. Kohn

Department of Physics, University of California, San Diego, La Jolla, California

(October 10, 1969)

The most striking characteristic of crystalline solids is their periodicity. As a result of this feature, theoretical descriptions of physical phenomena in such systems are usually given in wave number or *momentum* space. The reciprocal lattice of a crystal and the Fermi surface of a metal are examples. In a disordered system, on the other hand, there is no such periodicity and momentum space descriptions are much less natural. However, in such systems, physical conditions near a point $\mathbf{r}$, in *coordinate* space, become independent of the conditions at a distant point $\mathbf{r}'$, provided that $|\mathbf{r}'-\mathbf{r}|$ is large compared to either a characteristic mean free path or some other appropriate length. This suggests that one can analyze a macroscopic disordered system by averaging over the properties of microscopic neighborhoods.

In the present paper we report some details of such a program. Although the point of view is of quite general applicability we have, for the sake of definiteness, studied so far only one type of system: Noninteracting electrons moving in the field of interacting, disordered scattering centers. We have focused especially on the electronic density of states. The macroscopic system is represented by an average over small neighborhoods. If one did not take special precautions, one would encounter one class of errors of the order of d/L where L is a characteristic dimension of the neighborhood, and d is a characteristic atomic dimension; and another class of errors of the order of $1/N$ where N is the number of ions. Both are too large to be tolerable for practical purposes. However, by an appropriate treatment of the statistical mechanics of the scatterers and by periodic repetition of the small neighborhoods, these errors can be avoided. The remaining errors are exponentially small in the ratio $\gamma(L/R)$ where γ is of order unity and R is the smaller of the electronic mean free path or the deBroglie wavelength of the electrons. This exponential convergence of the small neighborhood theory promises to make it a useful practical method for the study of disordered systems, especially very highly disordered ones.

Numerical examples are presented and discussed.

Key words: Binary alloys; density of states; disordered systems; periodically continued neighborhood.

1. Introduction

The physical properties of strongly interacting disordered systems are in general difficult to calculate since simplifying symmetries, present in crystalline materials, are not present. In this paper we present and develop to some small extent a viewpoint which appears to provide a useful line of attack on the theory of disordered systems.

We shall demonstrate and utilize the rather plausible fact that in a disordered system the physical characteristics at a point $\mathbf{r}$ depend significantly only on conditions inside a rather small neighborhood $|\mathbf{r}'-\mathbf{r}|<R$, where R is of the order of a mean free path l or a characteristic thermal deBroglie wavelength, Λ_t. The effects of the more distant environment fall off exponentially with distance. This suggests that the properties of an infinite disordered system could be accurately calculated by suitable averaging over an ensemble of small neighborhoods. This scheme, furthermore, should be most successful for strongly disordered systems in which the mean free path is short.

In the following sections we sketch an application of these ideas to the much-studied problem of the density

* An invited paper presented at the 3d Materials Research Symposium, *Electronic Density of States*, November 3-6, 1969, Gaithersburg, Md.

[1] Supported in part by the Office of Naval Research and the National Science Foundation.

[2] Present address: Department of Physics, Auburn University, Auburn, Alabama.

of states of noninteracting electrons moving in the static potential of disordered scattering centers.[3]

2. Demonstration of the Locality Principle

In this section we shall sketch the demonstration that the physical properties near a point $\mathbf{r}$ of a system of noninteracting electrons moving in a disordered external potential are nearly independent of the circumstances outside a characteristic range R. More specifically, the effect of a perturbation at a distant point $\mathbf{r}'$ on physical properties at $\mathbf{r}$ falls off exponentially, on a scale given by a range of influence, R, which is of the order of either the mean free path or, at high temperatures, the thermal wavelength of the electrons, whichever is the smaller.

We consider a very large system of volume Ω described by the Hamiltonian

$$H = H_0 + V + v; \tag{2.1}$$

here H_0 is a periodic Hamiltonian, which for simplicity we take to be the kinetic energy

$$H_0 = \mathbf{p}^2; \tag{2.2}$$

V is a potential produced by disordered scattering centers, located at the points $\mathbf{r}_\alpha$,

$$V = \sum_\alpha V_\alpha(\mathbf{r} - \mathbf{r}_\alpha); \tag{2.3}$$

and v is an additional small perturbation localized at a point $\mathbf{r}'$. We shall study the effect of v on physical conditions at the point $\mathbf{r}$.

First, we shall consider the one particle Green's function

$$G(\mathbf{r}, \mathbf{r}'; E) = \left(\mathbf{r} \left| \frac{1}{E - H} \right| \mathbf{r}' \right). \tag{2.4}$$

In terms of the eigenfunctions ψ_n of H, and the eigenvalues E_n,

$$G(\mathbf{r}, \mathbf{r}'; E) = \sum_n \frac{\psi_n^*(\mathbf{r})\psi_n(\mathbf{r}')}{E - E_n}. \tag{2.5}$$

Of special interest is the contracted function $G(\mathbf{r}, \mathbf{r}; E)$ which determines the density of states by means of the following relation,

$$n(E) = -\frac{1}{\pi} \operatorname{Im} \int d\mathbf{r} G(\mathbf{r}, \mathbf{r}; E + i0). \tag{2.6}$$

We see that we may regard the unintegrated quantity

$$n(\mathbf{r}, E) \equiv -\frac{1}{\pi} \operatorname{Im} G(\mathbf{r}, \mathbf{r}; E + i0) \tag{2.7}$$

as the local density of states density.

We would like to estimate the effect of introducing the weak additional potential v, at the point $\mathbf{r}'$, on $n(\mathbf{r}, E)$ at the point $\mathbf{r}$. The quantity of physical interest is then

$$\left\langle \frac{\delta}{\delta v(\mathbf{r}')} G(\mathbf{r}, \mathbf{r}; E + i0) \right\rangle = \langle G(\mathbf{r}, \mathbf{r}'; E + i0) G(\mathbf{r}', \mathbf{r}; E + i0) \rangle_{v=0} \tag{2.8}$$

where the brackets $\langle\rangle$ denote configuration average. The equation (2.9) follows directly from the equation of motion of G.

Now it is well known that, for weak random potentials V_α,

$$\langle G(\mathbf{r}, \mathbf{r}'; E + i0) \rangle \approx \frac{1}{4\pi|\mathbf{r} - \mathbf{r}'|} e^{i\sqrt{E}|r - r'|} e^{-|\mathbf{r} - \mathbf{r}'|/2l(E)}, \tag{2.9}$$

where $l(E)$ is the mean free path of an electron of energy E. Similarly, one can show from (2.8) that for large $|\mathbf{r}\text{-}\mathbf{r}'|$

$$\left| \left\langle \frac{\delta}{\delta v(\mathbf{r}')} G(\mathbf{r}, \mathbf{r}; E + i0) \right\rangle \right| \sim e^{-|\mathbf{r} - \mathbf{r}'|/l(E)} \tag{2.10}$$

Thus we see that when $|\mathbf{r}'\text{-}\mathbf{r}| \gg l(E)$, a change of potential at $\mathbf{r}'$ has a negligible effect on the quantity $n(\mathbf{r}, E)$.

Next we show a similar locality effect, this time not due to a finite mean free path but due to elevated temperature. We consider a system of independent electrons and use Boltzmann statistics for simplicity. We take as Hamiltonian

$$H = H_0 + v, \tag{2.11}$$

where, in comparison with (2.1), we have eliminated the disordered scattering potentials. We write the partition function as

$$Z = \int d\mathbf{r}\, Z(\mathbf{r}), \tag{2.12}$$

where

$$Z(\mathbf{r}) \equiv (\mathbf{r}|e^{-\beta H}|\mathbf{r}). \tag{2.13}$$

Our interest now is in the influence of a small perturbation v at $\mathbf{r}'$ on $Z(\mathbf{r})$. By standard perturbation theory one can show that, for large $|r' - r|$,

$$\frac{\delta Z(\mathbf{r})}{\delta v(r')} \sim -\frac{\pi^{5/2}}{16\beta^{3/2}|\mathbf{r} - \mathbf{r}'|} e^{-|\mathbf{r} - \mathbf{r}'|^2/\Lambda_T^2}, \tag{2.14}$$

[3] Among fairly recent papers we mention the following: H. Schmidt, *Phys. Rev.* **105**, 425 (1957); S. F. Edwards, *Phil. Mag.* **3**, 1020 (1958); ibid. **6**, 617 (1961); *Proc. Roy. Soc.* **A267**, 518 (1962); J. L. Beeby, *Proc. Roy. Soc.*, **A279**, 82 (1964); *Phys. Rev.* **135A**, 130 (1966); P. Soven, *Phys. Rev.* **151**, 539 (1966); ibid., **156**, 809 (1967).

where Λ_t is the thermal wavelength

$$\Lambda_t \equiv \beta^{1/2}(=\hbar/(2mkT)^{1/2}). \tag{2.15}$$

Of course at high temperature *and* with disorder, the characteristic "range of influence" R will be either a representative mean free path $\bar{l}$, or Λ_t, whichever is the smaller.

3. The Periodically Continued Neighborhood

We shall now develop a concrete method of calculation, based on the locality principle of the previous section. We shall concentrate on the density of states $n(E)$.

The most straightforward way would be as follows. We imagine the large disordered system as given. We choose at random a large number of points $\mathbf{R}_l$ and surround them by spheres of radius ρ considerably larger than the "range of influence" R, but not too large. Each sphere is surrounded by an infinite wall (see fig. 1). The electronic Hamiltonian for each sphere is given by

$$H = H_0 + V \tag{3.1}$$

where

$$V = \begin{cases} \Sigma V_\alpha(\mathbf{r}-\mathbf{r}_\alpha) & |\mathbf{r}-\mathbf{R}_l| \leq \rho \\ +\infty & r > \rho \end{cases} \tag{3.2}$$

We then calculate for each sphere the density of states density at its center, $n(\mathbf{R}_l,E)$. Because of the relatively small size of the neighborhood this is a much more manageable problem than $n(E)$ for the macroscopic disordered system. In view of the locality principle, $n(\mathbf{R}_l,E)$ is only insignificantly affected by the presence of the infinite wall. Hence, the density of states for the macroscopic system is given by

$$n(E) \approx \Omega \overline{n(\mathbf{R}_l,E)}, \tag{3.3}$$

where the bar denotes an average over many $\mathbf{R}_l$.[4]

The practical drawbacks, for finite ρ/R_0, are two: (1) The replacement, in the outside region, of the actual potential, ΣV_α, by an infinite repulsive barrier is a quite drastic change and unless ρ/R is very large, will cause sizeable errors. (2) This method does of course not lead to the exact results in the special case of a vanishing or periodic potential.

These drawbacks can be largely overcome by using, instead of a finite and bounded neighborhood, as in figure 1, a periodically continued finite neighborhood as indicated in figure 2. We choose a fundamental cell, say the cube, of volume $\Omega_L \equiv L^3$,

$$|x|,\ |y|,\ |z| \leq \frac{L}{2}$$

$$L \gg 2R \tag{3.4}$$

and construct the space-lattice generated by it. Let us call $\boldsymbol{\tau}^{(\nu)}$ the lattice translation vectors. Then we place any number of scatterers in some definite configuration c in the fundamental cell and populate the other cells in the identical way (see fig. 2). The electrons now move in a periodic cubic lattice. Their energy eigenvalues

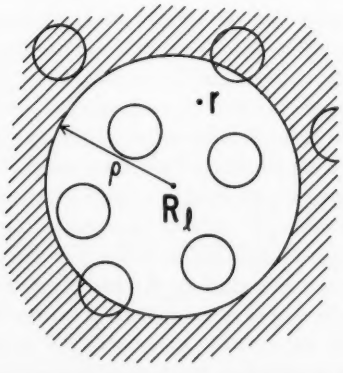

FIGURE 1. *Spherical neighborhood centered at* $\mathbf{R}_l$.

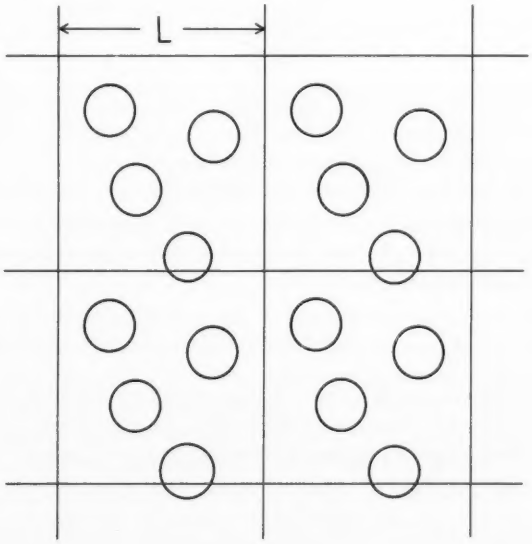

FIGURE 2. *Periodically continued neighborhood.*

[4] If we would use the total densities of states of the spherical neighborhoods, rather than the quantities $n(\mathbf{R}_l,E)$ computed at their centers, we would incur large errors behaving as L^{-1}, due to the presence of the infinite wall boundaries.

are, because of the relatively small size of the unit cell, much more amenable to calculation than the eigenvalues of the macroscopic disordered system. Let us call the density of states, corresponding to the configuration c and total volume Ω, $n_c(E)$. Then our approximation for the density of states of the actual macroscopic system will be

$$n(E) \approx \sum_c w_c n_c(E). \tag{3.5}$$

where w_c are weights, which we shall presently discuss, and the approximate equality, $\approx$, will signify accuracy to within terms exponentially small in $L/2R$.[5]

We shall now describe a suitable choice of w_c and later demonstrate that it leads to the claimed accuracy. Let us suppose that in the actual, macroscopic system under consideration there are given two-body forces between the scatterers,

$$\varphi_{\alpha\beta} = \varphi_{\alpha\beta}(\mathbf{r}_\alpha - \mathbf{r}_\beta), \tag{3.6}$$

which vanish beyond a range a which is much smaller than L. Let us suppose further than the scatterers obey classical statistics. Thus, in the macroscopic system the probability of a given configuration $c = (\mathbf{r}_1, \mathbf{r}_2, \ldots)$ is given by the grand canonical weight function,

$$w_c^{(\infty)} = A^{(\infty)} \exp\left\{-\beta\left[\frac{1}{2}\sum_{\alpha\neq\beta}\varphi_{\alpha\beta} - \sum_j \mu_j N_j\right.\right. \tag{3.7}$$

where $A^{(\infty)}$ is the normalization constant, μ_j is the chemical potential of scatterer of type j, and N_j is the total number of scatterers of this type.[6]

A suitable choice of w_c, for the periodically continued neighborhood, is obtained as follows. We take the unit cell and associate with each original position vector $\mathbf{r}$, the infinite set of vectors

$$\mathbf{r}^{(\nu)} \equiv \mathbf{r} + \boldsymbol{\tau}^{(\nu)} \tag{3.8}$$

This corresponds to the topology of a three dimensional torus and is illustrated in figure 3 in one dimension.

The weight w_c is then determined by the equation

$$w_c = A \exp\left\{-\beta\left[\frac{1}{2}\sum_{\alpha\beta}\varphi_{\alpha\beta}(\bar{\mathbf{r}}_{\alpha\beta}) - \sum \mu_j N_j\right]\right\} \tag{3.9}$$

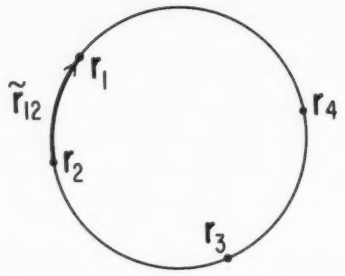

FIGURE 3. *Schematic representation of the toroidal topology. The circumference is* L.

where $\mathbf{r}_{\alpha\beta}$ is the shortest vector contained in the set $\mathbf{r}_\alpha^{(\mu)} - \mathbf{r}_\beta^{(\mu)}$. For example, $\mathbf{r}_{12}$ is shown schematically in figure 3. The normalization constant A is chosen so that

$$\sum_c w_c = 1, \tag{3.10}$$

where the sum goes over all configurations, including all possible numbers of the scatterers.

It can be shown that, with the choice (3.10), the correlation functions, $n_s(\mathbf{r}_1 \ldots \mathbf{r}_s | L)$, in the finite toroidal system, differ negligibly from those of the infinite system, $n_s(\mathbf{r}_1, \ldots \mathbf{r}_s | \infty)$, for values of $|\mathbf{r}_\alpha - \mathbf{r}_\beta| \leq L/2$ and s up to $s \leq L/a$. The error of a given correlation function behaves as $\exp[-\alpha_s L/a]$, where α_s is of order unity. This fact assures that, if $L \gg a$, the statistical distributions of the ions in any neighborhood of size $< L/2$ are practically identical in the ensemble of periodically continued neighborhoods and in the macroscopic system. Hence, in view of the locality principle demonstrated in section 2, the density of states $n(E)$ of the infinite system may be determined, via eq (3.5), from the density of states in the periodically continued neighborhoods. The error will be exponentially small in the quantity L/R or L/a, whichever is the smaller. Typically both a and R are of the order of 1 Å, so that one must work with neighborhoods of dimensions of several in order to obtain quantitatively useful results.

It is evident that this method will give exact results for perfectly periodic systems. Since it is also very accurate for highly disordered systems (small R), it should give good answers for most intermediate situations.

The ensemble of systems defined by eq (3.9) is a grand canonical ensemble in which the volume $\Omega_L (= L^3)$ is fixed while the numbers of particles N_j assumes all possible values. For a single species of atoms it has been found practically preferable to work with a periodically continued isothermal-isobaric ensemble, in which N is fixed but the volume Ω_L is variable. Here

[5] Provided the forces between the scatterers are sufficiently short range.

[6] For the macroscopic system, one could of course equally well use a canonical distribution. However, in our local neighborhood theory, this would lead to unacceptable errors of order $1/N$, where N is a mean number of scatterers in Ω_L.

a unit cell of volume Ω_L, with the N atoms in a configuration c must be given the weight

$$w_{\Omega_L,c}=\frac{A}{\Omega_L}\exp\left\{-\beta\left[\frac{1}{2}\sum_{\alpha,\beta}\varphi_{\alpha\beta}(\bar{\mathbf{r}}_{\alpha\beta})-R\Omega_L\right]\right\} \quad (3.11)$$

where P is the pressure. The density of states of the actual macroscopic system is approximated by

$$n(E)\approx\int d\Omega_L\sum_c w_{\Omega_L,c}n(E;\Omega_L;c) \quad (3.12)$$

where $n(E;\Omega_L;c)$ is the density of states, per unit cell Ω_L, in the periodically continued neighborhoods. The normalization A of $w_{\Omega_L,c}$

$$\int d\Omega_L\sum_c w_{\Omega_L,c}=N_{\text{tot}}/N \quad (3.13)$$

where N_{tot} is the total number of scatterers in the macroscopic system. Again the convergence of (3.13) to the exact result is exponential, as for the case of the grand canonical ensemble.

4. Numerical Illustration

To illustrate the theory of the previous sections we have numerically studied the following model of a one-dimensional alloy:

$$H=-\frac{d^2}{dx^2}+\sum_\alpha \lambda_\alpha\delta(x-\alpha d) \quad (4.1)$$

where the distance between potentials, d, was taken as 1, and λ_α was taken, with equal probability, as -2 and -4. (This corresponds to a high temperature limit for the two different kinds of scatterers, an idealized model for crystalline Cu Au well above the ordering temperature.) Here the grand canonical method was appropriate. Two calculations were performed, with $L=6$ and $L=10$. Let us take the case $L=6$. A typical, periodically continued neighborhood is shown schematically in figure 4. Each configuration of potentials in the fundamental interval $0<x\leq 6$ has the same weight, 2^{-6}.

In this simple example all correlation functions are evidently exact, as long as the crystal sites considered are all contained in a single unit cell.

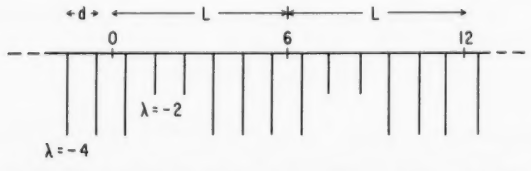

FIGURE 4. *A typical periodically continued neighborhood of the illustrative model.*

The density of states curves was calculated for each of the 2^6 configurations and then averaged. For $L=10$ a sampling procedure was used. The results are shown in figure 5, together with the exact result obtained for the infinite system using the Schmidt method.[3] Our approximation reproduces quite accurately all the details of the density of states structure, even for $L=6$. To obtain similar accuracy from a single randomly populated chain would require a length of the order of $L\approx 10^3$.

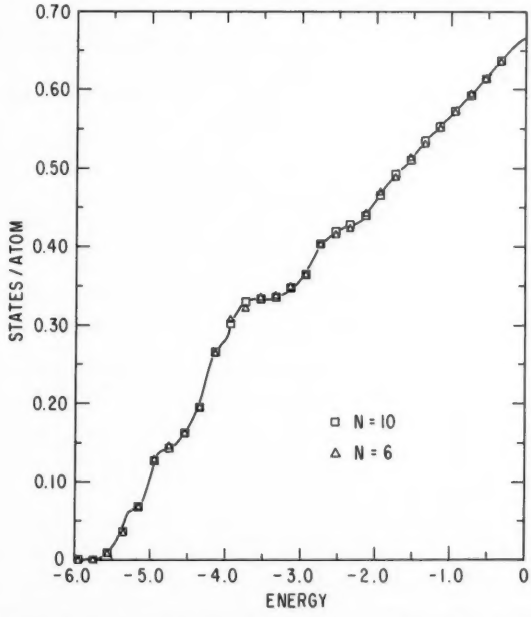

FIGURE 5. *Integrated density of states for binary alloy. The solid line is the exact result.*

5. Concluding Remarks

It is commonplace to emphasize the theoretical difficulties caused by disorder. In the present paper we draw attention to a favorable feature: For a highly disordered system the physical properties near a given point depend only on circumstances in a small neighborhood, whose dimension is of the order a mean free path. Consequently, a macro-system may be treated, so to speak, neighborhood by neighborhood and the macro-problem can be reduced to an ensemble of micro-problems. We have shown that the errors of such a procedure can be made to vanish exponentially with the size of the neighborhood. A numerical model calculation bears out these considerations.

A more complete account of this program will be published elsewhere.

(Paper 74A3–610)

JOURNAL OF RESEARCH of the National Bureau of Standards—A. Physics and Chemistry
Vol. 74A, No. 3, May-June 1970

Density of States Information from Low Temperature Specific Heat Measurements*

Paul A. Beck and Helmut Claus

University of Illinois, Urbana

(October 10, 1969)

The calculation of one-electron density of state values from the coefficient γ of the term of the low temperature specific heat linear in temperature is complicated by many-body effects. In particular, the electron-phonon interaction may enhance the measured γ as much as twofold. The enhancement factor can be evaluated in the case of superconducting metals and alloys. In the presence of magnetic moments, additional complications arise. A magnetic contribution to the measured γ was identified in the case of dilute alloys and also of concentrated alloys where parasitic antiferromagnetism is superimposed on an over-all ferromagnetic order. No method has as yet been devised to evaluate this magnetic part of γ. The separation of the temperature-linear term of the specific heat may itself be complicated by the appearance of a specific heat anomaly due to magnetic clusters in superparamagnetic or weakly ferromagnetic alloys.

Key words: Alloys; density of states; low temperature specific heat; magnetic specific heat; many-body effects; superconductivity.

1. Introduction

In the Sommerfeld-Bethe theory of metals the electronic specific heat at low temperatures is linear in temperature in first order approximation. The lattice specific heat in the low temperature approximation is proportional to T^3 so that, in the absence of other contributions, the total specific heat

$$C=\gamma T+\beta T^3 \tag{1}$$

If C is known as a function of T, the two terms can be separated by making use of the linear variation of C/T with T^2 and by extrapolating to $T=0$. The intercept of the extrapolated line with the ordinate axis gives the temperature coefficient of the electronic specific heat γ. In the simplest case, γ is proportional to the electronic density of states at the Fermi surface, $N(E_F)$:

$$\gamma=(1/3)\pi^2\alpha k^2N(E_F) \tag{2}$$

where k is the Boltzman constant and α is a numerical factor determined by the units used for γ, $N(E_F)$ and k.

Unfortunately, in a very large majority of cases, the simple procedure just described cannot be used, or at least it does not give reliable results. Many-body effects and, in some alloys, magnetic effects may make the determination of $N(E_F)$ from low temperature specific heat data more complicated than implied by eqs (1) and (2), or even impossible at the present state of the art.

2. Many-body Effects

In recent years it has become known that many-body effects, in particular the electron-phonon interaction, require renormalization of the effective mass of the electrons at the Fermi surface. This increases the measured electronic specific heat coefficient over the one-electron "band structure" value by the enhancement factor $(1+\lambda)$. For Na, Al and Pb, it was possible to determine the value of this factor [1], by comparing the "band structure electronic specific heat," calculated from the known band structure and the topography of the Fermi surface, with the measured electronic specific heat. These values: 1.25, 1.45 and 2.00, respectively, were found to agree quite well with the enhance-

*An invited paper presented at the 3rd Materials Research Symposium, *Electronic Density of States*, November 3-6, 1969, Gaithersburg, Md.

ment factors calculated from band structure, Fermi surface topography and phonon dispersion curves, on the basis of the electron-phonon interaction [1]. Unfortunately, for most other metals calculations of this sort cannot be made at present since at least some of the required data are not yet available. For superconducting metals the electron-phonon coupling constant λ has been recently calculated by McMillan [2], using the following equation which he derived from the strong coupling theory:

$$T_C = \frac{\theta}{1.45} \exp - \left[\frac{1.04(1+\lambda)}{\lambda - \mu^*(1+0.62\lambda)} \right], \qquad (3)$$

where T_C is the superconducting transition temperature and θ is the Debye temperature. The electron-electron interaction constant μ^* was assumed to have a value of 0.13 for all transition metals. The values of λ calculated by McMillan [2] for superconducting metals are given in table I.

TABLE I. *The Electron-Phonon Interaction Coefficient* λ *and "Band Structure" Density of States* $N(E_F)$ *for Superconducting Metals.*[2]

Element	T_c °K	Θ °K	λ	$N(E_F)$ $eV^{-1}atom^{-1}$
Be	.026	1390	.23	.032
Al	1.16	428	.38	.208
Zn	.85	309	.38	.098
Ga	1.08	325	.40	.091
Cd	.52	209	.38	.106
In	3.40	112	.69	.212
Sn	3.72	200	.60	.238
Hg	4.16	72	1.00	.146
Tl	2.38	79	.71	.182
Pb	7.19	105	1.12	.276
Ti	.39	425	.38	.51
V	5.30	399	.60	1.31
Zr	.55	290	.41	.42
Nb	9.22	277	.82	.91
Mo	.92	460	.41	.28
Ru	.49	550	.38	.46
Hf	.09	252	.34	.34
Ta	4.48	258	.65	.77
W	.012	390.	.28	.15
Re	1.69	415	.46	.33
Os	.65	500	.39	.35
Ir	.14	420	.34	.51

It is now clear that the enhancement factor $(1+\lambda)$ of the electronic specific heat due to the electron-phonon interaction can be as high as 2, or more. This interaction affects only the electrons whose kinetic energy is close to the Fermi energy. The density of states at lower levels, that is for most of the electrons in the metallic band, may be assumed to correspond to the one-electron "band structure" situation. Hence, the lower, "band structure density of states" values must be used in determining the band width, for instance, rather than the density of states enhanced by electron-phonon interaction, as obtained from low temperature specific heat measurements. Using the electron-phonon coupling constant λ, for instance the values given in table I, the "band structure density of states" at the Fermi level $N(E_F)$ can be calculated from the experimentally determined value of the low temperature specific heat coefficient γ' as follows:

$$N(E_F) = \frac{3}{\pi^2 k^2 \alpha (1+\lambda)} \gamma' \qquad (4)$$

For most of the nonsuperconducting metals and alloys the value of λ is at present unknown and, as a result, the "band structure density of states" cannot be calculated from the low temperature specific heat.

As seen in figure 1, the experimental electronic specific heat coefficient γ' for the b.c.c. 3*d*-transition metals and their alloys as a function of electron concentration [3] shows prominent maxima and minima in the range of *e/a* from 4 to 9. Since in the region of the minima and of the second maximum the alloys are not superconducting, the "band structure density of states" cannot be calculated at present. Thus, the interesting question whether the prominent features of these curves are due to changes in the electron-phonon enhancement factor upon alloying, or indeed these features are characteristic of the electronic band structure of the transition metals concerned, cannot be answered

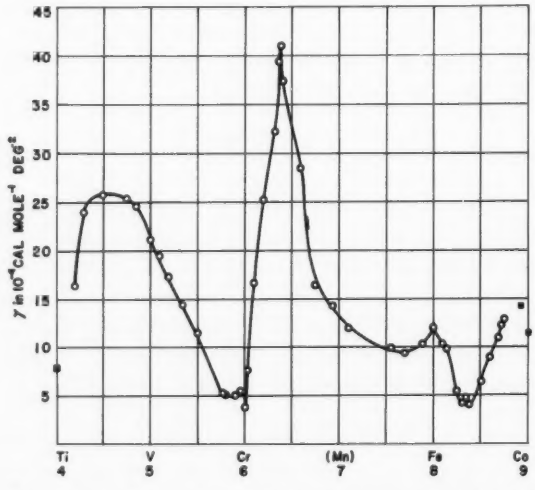

FIGURE 1. *Coefficient* γ' *or* γ'' *of the low temperature specific heat term linear in temperature vs electron concentration e/a for b.c.c. alloys of* 3d *transition metals* [3]. *Points marked by filled squares represent data for close-packed structures.*

with certainty. However, the work of McMillan [2] allows the conclusion that the electron-phonon coupling constant (and, thus, the enhancement factor) depends primarily on the phonon frequencies, rather than on the electronic properties. Since the elastic constants and, therefore, the phonon frequencies are not known to undergo drastic changes with the composition in such solid solution alloys composed of metals near one another in the same row of the periodic table, it may be concluded with a reasonable degree of probability that the prominent features mentioned of the γ' versus e/a curve of figure 1 are in fact resulting from corresponding variations in the "band structure density of states," even though the relative magnitude of the various minima and maxima may be appreciably altered by the gradual changes in the coupling constant with composition.

3. Magnetic Effects

Considerable difficulties are often encountered in determining the value of γ' for solid solution alloys of ferromagnetic with antiferromagnetic or nonmagnetic metals. For instance, it was found [4] for the random solid solution alloys Mn-Ni that, in addition to the electronic specific heat coefficient γ', the measured coefficient γ'' of the term of the low temperature specific heat linear in temperature includes also a magnetic contribution γ_m:

$$\gamma'' = \gamma' + \gamma_m. \tag{5}$$

The alloy $MnNi_3$ can be ordered by thermal treatment and, in the well-ordered condition, the coefficient of the linear term of the low temperature specific heat is approximately half that for the disordered alloy of the same composition. This lower value is substantially free of the magnetic contribution γ_m and it may be considered as approximately equal to the real experimental electronic specific heat γ' of the alloy. On the other hand, the larger γ'' value for the disordered alloy includes γ_m. Similar magnetic contributions to γ'' were identified in a number of other f.c.c. solid solution alloy systems [4] and in b.c.c. Fe-Al alloys [5]. It is significant that in the same alloy systems, and at similar compositions, magnetic measurements by Kouvel [6,7] detected the appearance of an asymmetrical hysteresis loop after cooling in a magnetic field through the Curie temperature ("exchange anisotropy"). In addition to this effect of field cooling on the magnetic properties, in several instances an effect of field cooling on γ_m was also detected [4,8], figure 2.

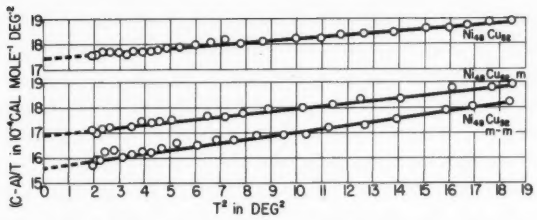

FIGURE 2. (C-A)/T *vs* T^2 *(where* C-A *is low temperature specific heat less magnetic cluster contribution, see eq (5)) for alloy* $Ni_{0.48}$ $Cu_{0.52}$ *cooled without a magnetic field (top graph), cooled in 14 kOe field from 300 to 4.2 K with the field turned off during the measurements (graph* m*) and field-cooled with the field on during measurements (graph* m − m*)* [8].

The occurrence in the same alloys of "exchange anisotropy" and of a magnetic contribution to the low temperature specific heat term linear in temperature suggests that these two phenomena may be associated with the same structural condition. This expectation is further supported by the fact that γ_m is normally also affected by field cooling. According to Kouvel's highly successful model [7], the structural condition responsible for "exchange anisotropy" is a spatially inhomogeneous magnetic state, *e.g.*, the superposition of local "parasitic antiferromagnetism" on net overall ferromagnetism. Overhauser [9] and Marshall [10] connected the magnetic contribution to the linear term of the low temperature specific heat with the location of a sufficient number of spins in a near-zero field. In Overhauser's theory this condition arises at the nodes of the static spin density waves of an antiferromagnet. Marshall pointed out that the required condition may arise in dilute spin systems, where the average distance between neighboring spins is sufficiently large, so as to make the interactions weak, as in dilute Cu-Mn alloys. The alloys considered above are neither antiferromagnetic nor dilute. However, because of the peculiar, complicated spin arrangement, resulting from the superposition of local parasitic antiferromagnetism on net overall ferromagnetism, it may be expected that many spins are located in small regions where ferromagnetic and antiferromagnetic exchange interactions nearly cancel each other locally, so that the average field in such regions is near zero [4]. In accordance with this "local field-cancellation" model, the effect of field cooling on γ_m may come about if the application of an external magnetic field during cooling through the Curie temperature increases or decreases the number of spins located in near-zero field. Both increase and decrease [($MnNi_3$ [4], $Ni_{0.48}Cu_{0.52}$ [8])] were in fact observed. It is easy to visualize that the change in γ_m as a result of field cooling may also happen to be negligibly

small, even though the value of the magnetic contribution γ_m itself is large. Thus, while the occurrence of a measurable effect of field cooling on the temperature-linear term of the low temperature specific heat may be considered as a proof for the existence of a magnetic contribution to this term, the absence of such an effect does *not* prove that γ_m is zero, or that it arises through a mechanism different from the "local field cancellation."

If the experimentally determined coefficient of the temperature-linear term of the low temperature specific heat includes a magnetic contribution, it is at present not possible to derive from such a γ'' value the "experimental electronic specific heat coefficient" γ', which is free from γ_m. This is well illustrated by the Ni-Cu alloys, for which the coefficient of the linear term has a maximum around the composition $Ni_{0.48}Cu_{0.52}$ [8]. A detailed study of the properties of these f.c.c. solid solutions at compositions in the vicinity of the maximum [11] shows that the experimental values of the coefficient do in fact include a magnetic contribution. It is, therefore, not possible to tell whether the maximum is entirely due to γ_m, or whether γ' itself has a maximum, which is merely increased by the addition of γ_m. A maximum in γ' has been expected on theoretical grounds [12] because of enhancement due to the electron-paramagnon interaction [13,14]. The theory

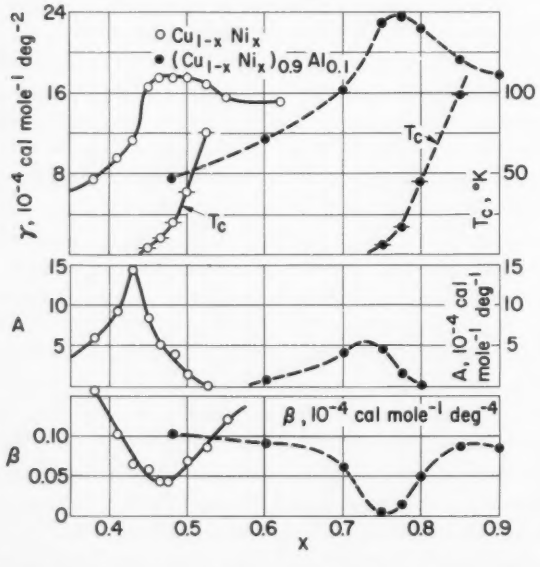

FIGURE 3. *Coefficient γ'' of the temperature-linear low temperature specific heat term, Curie temperature T_C, temperature independent specific heat term A and coefficient β of the T^3 term, obtained by least squares fitting to eq (5), for $Cu_{1-x}Ni_x$ (solid lines) and for $(Cu_{1-x}Ni_x)_{0.9}Al_{0.1}$ (dashed lines) alloys vs x [11,22,24].*

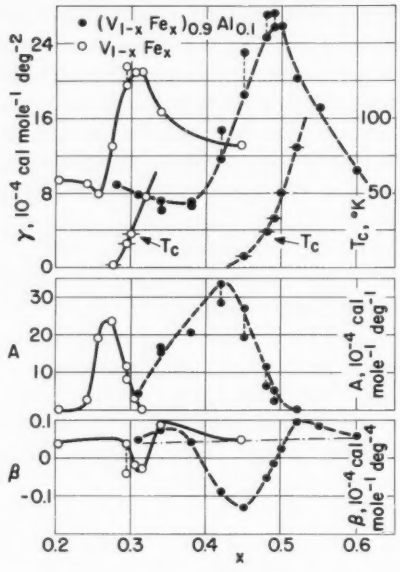

FIGURE 4. *Low temperature specific heat and Curie temperature data, as in figure 3, for $V_{1-x}Fe_x$ (solid lines) and $(V_{1-x}Fe_x)_{0.9}Al_{0.1}$ (dashed lines), alloys [3,23,24].*

would require the maximum of γ' to occur at the critical composition, where ferromagnetism just begins to set in at 0 K. Detailed study of the magnetic properties showed [11] that the critical composition is at approximately 57 percent Cu, where γ'' already decreased to a value far below its maximum. Figure 3 gives γ'' for the Ni-Cu solid solutions, together with Curie temperature data, which define the critical composition. One may conclude that the maximum in γ'' is largely, or entirely, due to γ_m, rather than to γ'. That the maximum in γ_m should occur in the weakly ferromagnetic region is entirely consistent with the "local field cancellation" model discussed above. It is quite likely that the maximum in the coefficient of the linear term for the f.c.c. Rh-Ni solid solutions, which apparently also occurs off the critical composition on the ferromagnetic side [15,16], is also due to a magnetic contribution γ_m. In fact, several solid solution alloy systems are now known to exhibit similar conditions. Figure 3 shows this for a series of Ni-Cu-Al ternary alloys with a constant Al-content of 10 percent. It is seen that the Al addition shifts the critical composition to a higher Ni/Cu ratio, that the maximum in γ'' (which is here even higher than for the binary alloys) is also shifted, and that it again appears away from the critical composition, on the ferromagnetic side. Further examples are given in figure 4, which shows similar data for b.c.c. V-Fe binary and V-Fe-Al ternary solid solutions with a constant Al-content of 10 percent.

As yet there appears to be no experimental evidence for the theoretically predicted [14] peak in γ' in alloys at the critical composition, resulting from the electron-paramagnon interaction.

Figures 3 and 4 illustrate also a complication, which arises quite frequently in extracting the coefficient of the temperature-linear term from low temperature specific heat data for weakly ferromagnetic and almost ferromagnetic alloys. In many alloy systems in a certain region around the critical composition an anomaly in the measured low temperature specific heat is observed, so that C is no longer given by eq (1). This anomaly is conspicuously evident in the usual C/T versus T^2 graph. Instead of being a straight line, this graph becomes a curve, extending upward at low temperatures. It was shown by Schroeder [16] that, in such cases, eq (1) can be usually replaced by

$$C = A + \gamma T + \beta T^3. \tag{6}$$

Schroeder found that the addition of a temperature-independent term A to the low temperature specific heat results from the thermal excitation of magnetic clusters present in many nearly ferromagnetic and weakly ferromagnetic alloys. The presence of magnetic clusters in Ni-Cu alloys in the composition range 50-56 percent Cu has been recently beautifully documented by Hicks, Rainford, Kouvel, Low and Comley [17] by means of neutron magnetic diffuse scattering. In Schroeder's theory the magnetic clusters, which interact with a weak crystal field, are thermally excited and they contribute an Einstein specific heat, which is temperature-independent above the Einstein temperature. The temperature range of 1.4 to 4.2 K, frequently used in low temperature specific heat measurements, appears to be above the Einstein temperature in most such systems. Investigations by Scurlock [18] show a decrease at lower temperatures of the anomalous specific heat from its constant value above 1.4 K, suggesting that the Einstein temperature is near 1.4 K. Since A includes an equal contribution of k for each cluster, regardless of the cluster moment [16], the low temperature specific heat data, from which the value of A can be extracted by least squares fitting to eq (6), give reliable information as to the number of thermally excited magnetic clusters. The correlation of the number of clusters for Ni-Cu alloys by specific heat measurements [11] with the number of clusters derived from neutron scattering [17] is given in figure 5. It is seen that the low temperature specific heat data for the superparamagnetic alloys (Cu-content larger than 57%) are quite consistent with the neutron scattering data. For the weakly ferromagnetic alloys the number of thermally excitable clusters rapidly decreases with increasing Curie temperature (decreasing Cu-content). In this composition range most of the magnetic clusters interact with one another and become part of the ferromagnetic system. As seen in figures 3 and 4 the maximum of A corresponds well with the critical composition for all four alloy systems considered. Figures 3 and 4 also show the anomalous behavior of the parameter β, obtained by least squares fitting to eq (6). The anomalous variation of β with composition occurs in all four alloy systems in the vicinity of the critical composition, and it is clearly magnetic in origin [5].

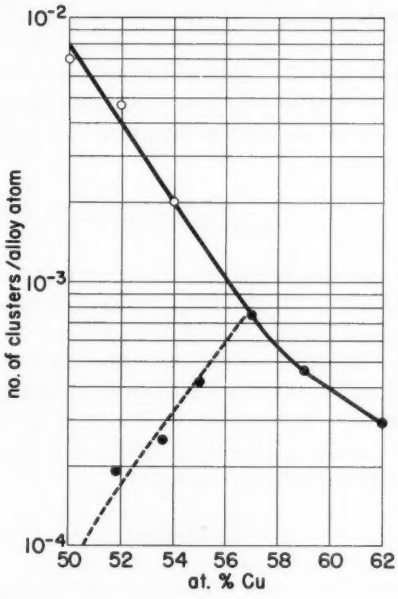

FIGURE 5. *Concentration of magnetic clusters in Ni-Cu alloys vs composition* [22]. *Filled circles represent cluster concentrations calculated from specific heat data. Empty circles give magnetic cluster concentrations derived from neutron magnetic diffuse scattering* [17].

4. Nuclear Specific Heat Effects

It was shown by Marshall [19] that the hyperfine interaction between the dipole moments associated with certain nuclides and the effective field H_{eff} at these nuclei, resulting from electronic spin moments, gives rise to a contribution to the low temperature specific heat. This contribution decreases rapidly with increasing temperature; in the 1.4 to 4.2 K range it is proportional to T^{-2} ("high temperature" approximation). Consequently, the nuclear magnetic specific heat term can

378-324 O - 70 - 10

be separated easily from the electronic specific heat term γT in that temperature range. The nuclear quadrupole specific heat recently reported by Phillips [20] and by Martin [21] is also proportional to T^{-2} and, thus, poses no problem in determining the electronic specific heat.

5. Acknowledgments

This work was supported in part by grants from the United States Army Research Office, Durham, and by the National Science Foundation. Most of the heretofore unpublished low temperature specific heat data for Ni-Cu-Al alloys were measured by C. G. Robbins. One of the alloys in this series was measured by R. Viswanathan. T. J. Rowland's help in reviewing the manuscript is much appreciated.

6. References

[1] Ashcroft, N. W., and Wilkins, J. W., Phys. Letters **14,** 285 (1965).
[2] McMillan, W. L., Phys. Rev. **167,** 331 (1968).
[3] Cheng, C. H., Wei, C. T., and Beck, P. A., Phys. Rev. **120,** 426 (1960); and Cheng, C. H., Gupta, K. P., Van Reuth, E. C., and Beck, P. A., Phys. Rev. **126,** 2030 (1962).
[4] Gupta, K. P., Cheng, C. H., and Beck, P. A., J. Phys. Chem. Solids **25,** 73 (1964).
[5] Cheng, C. H., Gupta, K. P., Wei, C. T., and Beck, P. A., J. Phys. Chem. Solids **25,** 759 (1964).
[6] Kouvel, J. S., and Graham, C. D., J. Phys. Chem. Solids **11,** 220 (1959).
[7] Kouvel, J. S., J. Appl. Phys. **30,** 313S (1959) and **31,** 142S (1960).
[8] Gupta, K. P., Cheng, C. H., and Beck, P. A., Phys. Rev. **133,** A203 (1964).
[9] Overhauser, A. W., J. Phys. Chem. Solids **13,** 71 (1960).
[10] Marshall, W., Phys. Rev. **118,** 1519 (1960).
[11] Robbins, C. G., Claus, H., and Beck, P. A., J. Appl. Phys. **40,** 2269 (1969).
[12] Bennemann, K. H., Phys. Rev. **167,** 564 (1968).
[13] Berk, N. F., and Schrieffer, J. R., Phys. Rev. Letters **17,** 433 (1966).
[14] Doniach, S., and Engelsberg, S., Phys. Rev. Letters **17,** 750 (1966).
[15] This is suggested by the data in the following papers, although their authors did not reach this conclusion: Bucher, E., Brinkman, W. F., Maita, J. P., and Williams, H. J., Phys. Rev. Letters **18,** 1125 (1967); and Brinkman, W. F., Bucher, E., Williams, H. J., and Maita, J. P., J. Appl. Phys. **39,** 547 (1968).
[16] Schroder, K., J. Appl. Phys. **32,** 880 (1961).
[17] Hicks, T. J., Rainford, B., Kouvel, J. S., Low, G. G., and Comly, J. B., J. Appl. Phys. **40,** 1107 (1969).
[18] Scurlock, R. G., and Wray, E. M., Phys. Letters **6,** 28 (1963); and Proctor, W., and Scurlock, R. G., Proc. 11th Conf. Low Temp. Phys. (St. Andrews, 1969), p. 1320.
[19] Marshall, W., Phys. Rev. **110,** 1280 (1958).
[20] Phillips, N. E., Phys. Rev. **118,** 644 (1960).
[21] Martin, D. L., Phys. Rev. Letters **18,** 839 (1967).
[22] Robbins, C. G., University of Illinois Thesis, (1969).
[23] Pessall, N., Gupta, K. P., Cheng, C. H., and Beck, P. A., J. Phys. Chem. Solids **25,** 993 (1964).
[24] New measurements by H. Claus, to be reported in detail elsewhere.

(Paper 74A3–611)

JOURNAL OF RESEARCH of the National Bureau of Standards—A. Physics and Chemistry
Vol. 74A, No. 3, May–June 1970

Publications of the National Bureau of Standards*

Selected Abstracts

Brown, J. E., Tryon, M., Horowitz, E., **Thermal decomposition of Cu(II)-*bis*(8-hydroxy-5-quinolyl) methane coordination polymer,** *J. Appl. Poly. Sci.* **13,** *1937–1947 (1969).*

Key words: *Bis*(8-hydroxy-5-quinolyl) methane; coordination; copper; decomposition; 8-hydroxyquinoline; infrar-red spectrophotometry; ligand; mass spectrometry; polymer; thermal.

The volatile products formed when the coordination polymer of copper(II) and *bis*(8-hydroxy-5-quinolyl) methane was heated in vacuum at elevated preselected temperatures were examined. The amount of weight loss at each temperature was determined with a recording thermal balance. Infrar-red spectrophotometry was used to aid in the identification of the major volatile component. A sample was pyrolyzed directly into the mass spectrometer. The results show that the volatile product is for the most part the organic ligand, *bis*(8-hydroxy-5-quinolyl) methane and not derivatives of the copper complex or fragments of the ligand. The mechanism for the decomposition reaction previously proposed is supported.

Burke, P. G., Cooper, J. W., Ormonde, S., **Low energy scattering of electrons by helium,** *Phys. Rev.* **183,** *No. 1, 245–264 (July 5, 1969).*

Key words: Close coupling; eigenphase; electron helium scattering; excitation; polarization; resonance.

The close coupling equations for electron-helium scattering have been solved in the energy range near the $n=2$ thresholds. Cross sections for elastic scattering from both ground and excited states, for excitation of the ground state to the $n=2$ states (2^3S, 2^1S, 2^3P and 2^1P) and for excitation and de-excitation processes involving only the $n=2$ levels are presented and compared with experimental evidence on total metastable production, on angular distributions of excitation cross sections to the $n=2$ levels and on processes involving only the $n=2$ states. The percentage polarization of light emitted by electron impact excitation to the 2^3P and 2^1P states is computed and compared with experiment. The calculations indicate the importance of resonances in near threshold excitation and de-excitation processes in He. An attempt has been made to understand the resonant structure by considering both the energy dependence of the eigenphases of the many-channel S matrix produced by solving the close coupling equations and the energy dependence of eigenvalues of the related time delay matrix.

Carpenter, B. S., Cheek, C. H., **Trace determination of uranium in biological material by fission track counting,** *Anal. Chem.* **42,** *No. 1, 121–123 (Jan. 1970).*

Key words: Activation analysis; biological material; fission track; microanalysis; nuclear track; uranium.

The nuclear track technique for determining micro quantities of uranium in material, which consists of counting fission tracks produced in solid-state detectors as a result of neutron irradiation, is employed to determine trace quantities of uranium in such biological materials as mammalian blood and plasma and oak leaves. Dry-ashed samples of the material are dissolved in dilute acid and make up to standard volumes. Aliquots to these solutions are placed on Lexan polycarbonate detectors, evaporated to dryness, and enclosed in a polyethylene bag. After irradiation in a thermal neutron flux, the bag is removed and the Lexan detectors are etched in a sodium hydroxide solution. The amount of uranium present in the biological matrices is determined by counting the etched fission tracts with an optical microscope and comparing the results with those obtained for simultaneously irradiated reference standards containing known amounts of uranium. Average results obtained from thermal neutron irradiations for the blood plasma samples were 86.1 ppb and 60.5 ppb, respectively, while the values for oak leaves ranged from 1.62 to 15.2 ppm.

Colwell, J. H., **Molecular reorientation and nuclear spin conversion in the solid deuteromethanes at low temperature,** *J. Chem. Phys.* **51,** *No. 9, 3820–3832 (Nov. 1, 1969).*

Key words: CD_4; CHD_3; CH_3D; CH_2D_2; heat capacity; heat capacity anomaly; residual entropy; Zero-point entropy.

The heat capacities of the solid deuteromethanes have been measured down to 0.3 K, tracing out the low temperature heat capacity anomalies which had been detected in the earlier work of Colwell, Gill, and Morrison. The anomalies in CH_3D and CHD_3 have maxima at 0.43 and 0.48 K respectively, but the CH_2D_2 heat capacity is still increasing with decreasing temperature at 0.3 K. A small anomaly was found in CD_4 but this is ascribed to chemical and isotopic impurities present in the sample.
The observed anomalies are attributed to the removal of the orientational degeneracies of the molecules on the lattice sites which give rise to the well known residual entropies of R ln 4 in CH_3D and CHD_3 and R ln 6 in CH_2D_2. Nuclear spin conversion also occurs in CH_3D. This is substantiated by the measured entropy change of $\Delta S = 1.614R$ over the range 0.3 to 4 K which exceeds the maximum value of R ln 4 ($1.386R$) for molecular reorientation occurring separately. The occurrence of conversion was also indicated by a slow process characterized by a relaxation time ranging from 75 to 35 seconds in going from 0.3 to 4 K. There was no indication of conversion occurring in either CH_2D_2 or CHD_3.
The heat capacity anomalies are of the Schottky form and the results have been analysed on the basis that the energy levels available to the molecules are independent of the extent of order in the system. Precise values of the energy level splittings are obtained for CH_3D and CHD_3, but there is some ambiguity as to which symmetry species the rotational states in CH_3D belong. Poor agreement between the calculated heat capacity and the observed anomaly in CH_2D_2 is taken as an indication that there may be cooperative effects occurring in this transition.

Darwent, B. deB., **Bond dissociation energies in simple molecules,** *Nat. Bur. Stand. (U.S.), Nat. Stand. Ref. Data Ser. 31, 52 pages (Jan. 1970), 55 cents, SD Catalog No. C13.48:31.*

Key words: Bond dissociation energy; gaseous state; inorganic simple compounds; recommended value; zero vibrational state of the ground electronic state.

Bond dissociation energy values (kcal/mol) and (kJ/mol) of simple compounds are tabulated from a literature review covering the years 1962–1966 inclusively. Some selected values which appeared in the years 1956–1962 are also included. Organic compounds are excluded except those containing one carbon atom. The groups > CO and —CN are not considered to be organic.

The values are quoted usually at 0 K or 298 K and refer to the gaseous state. They represent the energy required to break a bond at the specified temperature with all substances in the zero vibrational state of the ground electronic state. The experimental method for the energy value listed is given and referenced in the table. A value recommended by the author is listed as the final value for each reaction.

Davis, J. C., **Radiation errors in air ducts under nonisothermal conditions using thermocouples, thermistors, and a resistance thermometer,** *Nat. Bur. Stand. (U.S.), Bldg. Sci. Ser. 26, 14 pages (November 1969), 25 cents, SD Catalog No. C13.29/2:26.*

Key words: Conduction error; radiation error; resistance thermometer; temperature measurement; thermistor; thermocouple.

Studies were made to determine the radiation error in temperature measurements made with thermocouples, thermistors, and a resistance thermometer in moving air at velocities ranging from 300 to 1300 fpm when the temperature of the duct wall surrounding the air stream was from 0 to 50 deg F higher than that of the air in the center of the duct. To eliminate all but the variable under study, conduction errors were minimized to a point where they were almost nonexistent by using Chromel P–constantan thermocouple wire and by employing other techniques. Radiation effects were studied when the probe housing the three types of temperature sensors was unshielded and again when it was shielded. The studies showed that when the sensors were unshielded and the temperature difference between the duct wall and the air was 50 deg F (28 K, approximately), the error in the sensors was about 3.8 deg F (2.1 K) for an air velocity of 300 fpm (1.5 m/s) and 1.0 deg F (0.6 K) for an air velocity of 1300 fpm (6.6 m/s). When the sensors were shielded, the error was about 0.2 deg F (0.1 K) for 300 and 500 fpm velocities and the same duct wall air-temperature difference. Tests were not performed at 1300 fpm with the sensors shielded because theory indicated that radiation error would be negligible at this velocity. Under the test conditions that prevail in the testing of air conditioners and heat pumps in laboratories, it should be possible to reduce the error in temperature measurement of the moving air to about 0.2 deg F (0.1 K) by a suitable combination of air mixers, duct insulation, radiation shields, and calibration techniques.

DeVoe, J. R., Editor, **Radiochemical Analysis Section: Mössbauer spectroscopy, nuclear chemistry, nuclear instrumentation, radioisotope techniques.** *Summary of activities, July 1968 to June 1969, Nat. Bur. Stand. (U.S.), Tech. Note 501, 149 pages (Feb. 1970), $1.25, SD Catalog No. C13.46:501.*

Key words: Calculations; conversion electrons; counting statistics; cross sections; cryostats; electric field gradient tensor; electronics; gas analysis; heterogeneity; iron; interferometric; internal magnetic field; molybdenum; Mössbauer spectrometer; Mössbauer spectrometry; nickel–61; proportional detector; radiochemistry; radioisotope dilution; rutile; self-consistent crystal field; Standard Reference Materials; structure analysis.

This is the sixth summary of progress of the Radiochemical Analysis Section of the Analytical Chemistry Division at the National Bureau of Standards.
The section's effort comprises five major areas: Mössbauer spectroscopy, nuclear chemistry, nuclear instrumentation, radioisotope tracer techniques and the application of statistics in nuclear and analytical chemistry.
Low temperature devices for Mössbauer spectroscopy are a subject of continuing interest, and this year's effort is centered around the design of variable temperature devices. A high temperature device is also described.
Preliminary data on the detection of conversion electrons show the potential for Mössbauer spectroscopy in the field of chemical bonding in surfaces.
Further exploration of the potential of Mössbauer spectroscopy for the measure of structural parameters of nickel compounds have been made.
Preliminary data are presented on the structure of iron doped rutile (TiO_2) which is of significance to the determination of mineral structures found on the moon. Theoretical predictions of Mössbauer spectra resulting from electric field gradients due to crystal field interactions are presented. Evaluation of the basic integrals using the self-consistent Hartree-Fock method is given for ions of the first row of transition elements.
Precautions to be taken in the analysis of gamma-ray spectra are presented when model errors exist and when a gain shift is detected.
A system for gas analysis which utilizes gas chromatography is described. Its application to nuclear cross-section studies is also presented. A method for setting limits on sample heterogeneity using a specific analysis method provides a useful indicator for evaluation of the adequacy of standard reference materials.
An interesting presentation of detection and measurement in the femtogram region is given.
The complete circuitry for the optical interferometric Mössbauer spectrometer is presented in this report.
Quantitative analysis for molybdenum and iron using radioisotope dilution to a precision that rivals most other techniques is described.

Durst, R. A., Editor, **Ion-selective electrodes.** *Proceedings of a symposium held at the National Bureau of Standards, Gaithersburg, Maryland, January 30–31, 1969, Nat. Bur. Stand. (U.S.), Spec. Publ. 314, 474 pages (November 1969), $3.50, SD Catalog No. C13.10:314.*

Key words: Ion-selective electrodes; review of ion-selective electrodes; specific-ion electrodes; symposium proceedings.

This volume contains a review of ion-selective electrodes, emphasizing the non-glass types, and provides a thorough and critical evaluation of the subject. It consists of eleven invited review papers and selected discussions from the Symposium on Ion-Selective Electrodes held at NBS on January 30–31, 1969. This publication provides a comprehensive survey of the field and should prove very valuable in advancing the state of the art. The chapters include discussions on the theory, characteristics, and methodology of all types of ion-selective electrodes; their use in thermodynamic, kinetic, and complex-ion studies; standards; pure and applied research in various biomedical areas of interest; industrial analysis and control systems; and applications to diverse analytical problems. Both the present status and future potential of these sensors are discussed in a wide range of scientific disciplines, from the physical sciences to biomedicine. Extensive bibliographies provide an excellent survey of the literature for anyone using or anticipating the use of these electrodes.

Eisele, J. W., **Technical Standard Coordinator, Uncored slab urethane foam for bedding and furniture cushioning,** *Nat. Bur. Stand. (U.S.), Prod. Stand. 13–69, 6 pages (Dec. 1969), 10 cents, SD Catalog No. C13.20/2:13–69.*

Key words: Cellular; flexible; slab; uncored; urethane foam.

The foam covered by this Product Standard is intended for uses such as inserts for mattresses and cushions for indoor and outdoor furniture. This Standard provides material and dimensional requirements for uncorded slab urethane foam and requirements and methods of test for the specific properties of load bearing capacity, permanent set, moisture resistance, fatigue resistance, and resiliency. The fatigue requirements will be revised to incorporate dynamic fatigue specifications when adequate data are available. Methods for marking and labeling to indicate compliance with this Standard are also provided.

Fatiadi, A. J., **Novel iodination of the γ-methylene group in 1,3-diphenylpropane-1,3-dione and related β-diketones with periodic acid,** *Chem. Commun., p. 11 (1970).*

Key words: Acyclic, β-diketones; iodic acid; iodo derivatives; periodic acid.

On treatment with iodic acid, 1,3-diphenyl-1,3-propanedione is converted into the 2-iodo derivative in about 50% yield. When periodic acid is used the diketone can be converted either into the 2-iodo or the 2,2-diiodo derivative. Formation of 2-iodo derivatives has been observed for other acyclic β-diketones.

Furukawa, G. T., **Automation problems in thermometry and calorimetry** *(Proc. 2nd & 3rd Japanese Calorimetry Conf., Osaka,*

Japan, Nov. 27–28, 1967), Chapter 1 in Calorimetry, Thermometry, and Calorimetry, Y. Otsubo, H. Kanbe, and S. Seki, ed., 2, 1–35 (Kagaku Gijitsu-Sha, Tokyo, Japan, 1969).

Key words: Automatic calorimetry; calorimetry; heat capacity; Mueller bridge; thermometry.

For high-precision low-temperature calorimetry, the techniques used in measurement periods of temperature and of power are discussed separately. The application of electronic preset counters to automatic control of the calorimetric process is proposed. The thermometer resistances are measured by means of an automated Mueller bridge and the measurements are analyzed on a high-speed digital computer to obtain temperature-time observations. The electrical power introduced is automatically determined using a commercially available integrating digital voltmeter (IDVM) to measure a small fraction of the total calorimeter heater voltage biased by a stable reference voltage. A modification of the IDVM to integrate over the heating interval to obtain the total electrical energy input is described.

Hummer, D. G., **Non-coherent scattering—VI. Solutions of the transfer problem with a frequency-dependent source function,** *Mon. Not. R. astr. Soc.* **145,** *95–120 (1969).*

Key words: Doppler broadening; noncoherent scattering; radiation scattering; spectral line.

A generalized discrete-ordinate method is used to obtain accurate numerical solutions of the line transfer problem in what the scattering is described by a redistribution function. Extensive results are obtained and discussed for the cases of pure Doppler broadening and of Doppler and natural broadening combined. It is shown that, in the latter case, the intensity of radiation emerging from a semi-infinite isothermal atmosphere approaches that for coherent scattering in the line wings instead of approaching the value of the Planck function.

Jacox, M. E., Milligan, D. E., **Matrix-isolation study of the infrared and ultraviolet spectra of several first-series transition-metal dichlorides,** *J. Chem. Phys.* **51,** *No. 9, 4143–4155 (Nov. 1, 1969).*

Key words: Cl_2 reactions; $CoCl_2$; $CrCl_2$; emission spectrum; $FeCl_2$; infrared spectrum; matrix isolation; $MnCl_2$; molecular orbitals; $NiCl_2$; transition-metal reactions; ultraviolet spectrum.

Individual molecules of $CrCl_2$, $MnCl_2$, $FeCl_2$, $CoCl_2$, and $NiCl_2$ have been isolated in an argon matrix at 14 K in sufficient concentration for infrared and ultraviolet spectroscopic study not only by using the conventional effusion cell as a source of the MCl_2 species, but also by trapping the products of the reaction of chlorine with the hot transition-metal surface. Studies of the infrared spectra of all of these species in the 250–4000-cm^{-1} spectral range are consistent with a linear structure. Ultraviolet absorptions in the 2000–5500-Å spectral range are in good agreement with the previously reported gas-phase absorptions. However, the absorption observed for matrix-isolated $NiCl_2$ between 4400 and 5000 Å must be attributed to three different electronic transitions, one of which exhibits extensive band structure. A molecular-orbital treatment involving participation of the 3d nickel electrons in the bonding of the molecule predicts the occurrence of several transitions in this energy range and provides a framework for understanding the appearance of extensive vibrational structure in several of the electronic transitions of $NiCl_2$.

Jefferson, C. F., Baker, C. K., **Mechanism of electrical conductivity in nickel-iron ferrite,** *IEEE Trans. Magnetics* **MAG-4,** *No. 3, 460–464 (Sept. 1968).*

Key words: Conductivity; ferrites; Hall mobility; thermal emf; transition metal oxides.

Measurements of the frequency dependence of the dielectric conductivity, Hall mobility and thermal emf as a function of temperature on polycrystalline $Ni_{0.6}Fe_{0.4}Fe_2O_4$ indicate that this data can be interpreted in terms of the band model. Previous analyses of the semiconductor properties of ferrites according to the hopping model assume that the number of carriers, n, is identical with the concentration of divalent iron ions. Hall measurements indicate that this is not the case here and that n is best described by the equation

$$n^2 = (N_D - n)N_0 \frac{m^*}{m}^{\frac{3}{2}} g^{-1} \exp -\frac{E_D}{kT}$$

Assigning a value of 2 to g, $\frac{m^*}{m}$ is 9.3 and E_D is 0.034 eV.

The temperature depencence of the dc conductivity is considerable different from that of the ac conductivity. This difference is found for polycrystalline $Ni_{0.6}Fe_{0.4}Fe_2O_4$ and $LiFe_5O_8$ as well as for single crystal $LiFe_5O_8$. A Wagner type relaxation associated with interfacial polarization is present in all materials, indicating that precautions must be taken in the interpretation of dc conductivity data even when single crystals are used.
The thermal emf, calculated from Hall data, shows that the measured value is considerably larger than the calculated value. This implies that the measured values might contain a contribution from the phonon drag effect.

Knoeck, J., Taylor, J. K., **Aqueous boric acid-borate-mannitol equilibria,** *Anal. Chem.* **41,** *No. 13, 1730–1734 (Nov. 1969).*

Key words: Borate; boric acid; combining ratio; complex; formation constant; mannitol.

Despite recent reports to the contrary, the stoichiometry of the aqueous boric acid-borate-mannitol system has been shown to involve both a 1:1 and 2:1 mannitol-borate complex. Reliable values of the formation constants of these complexes have been determined from electrometric pH measurements. Widely divergent results obtained by previous workers in this area have been shown to be largely the result of misinterpretation of experimental data rather than anomalous behavior of the system. Reliable data taken from previous work has been shown to give the same results as data obtained in this laboratory thus providing a consistent model for boric acid-borate-mannitol equilibria.

Koeser, R. L., Report Editor, **Report of the 54th national conference on weights and measures 1969,** *Nat. Bur. Stand. (U.S.), Spec. Publ. 318, 270 pages (Nov. 1969), $1.50, SD Catalog No. C13.6/3:318.*

Key words: Conference; weights and measures; weights and measures—history; weights and measures—laws; weights and measures—regulations; weights and measures—technical requirements.

This is a report of the proceedings (edited) of the Fifty-fourth National Conference on Weights and Measures, sponsored by the National Bureau of Standards, held in Washington, D.C., June 9–13, 1969 and attended by State, county, and city weights and measures officials and representatives of the Federal Government, business, industry, railroads, and associations.

Kuriyama, M., **X-ray diffraction from a crystal containing isolated imperfections,** *Acta Cryst.* **A,** *No. 25, 682–693 (Nov. 1969).*

Key words: Anomalous absorption; contrast; diffuse scattering; dynamical diffraction; extinction; imperfect crystal; kinematical diffraction; topography.

The X-ray scattering amplitude from a crystal containing isolated imperfections is expressed in terms of the Fourier transform of the atomic displacement vectors. The amplitude contains only the local properties of the imperfections which are "seen" by the incident beam of a finite size. The disruption of the Borrmann transmitted (or diffracted) beam, the narrowing of the dynamical diffraction range and the "diffuse" scattering caused by dynamically diffracted X-rays are some of the results obtained from the scattering amplitude. The formations of black, white and black-white images in topographs are explained by the present theory. Image contrast is also discussed in terms of the thickness of the crystal.

Lutz, G. J., LaFleur, P. D., **Determination of yttrium in rare earths by photon activation analysis,** *Talanta* **16,** *1457–1460 (1969).*

Key words: Coincidence spectrometry; photon activiation analysis; rare earths; yttrium.

The determination of yttrium in the presence of large amounts of the rare earths by the thermal neutron reaction $^{89}Y(n, \gamma)^{90}Y$ is complicated because of frequent problems of sample self shielding from major constituents of the sample and the difficulty of separating ^{90}Y, a pure beta emitter, from other elements which are very similar chemically.
A non-destructive photon activation analysis method has been developed for this determination. Bremsstrahlung from a 35-μA beam of 35-MeV electrons induces the photonuclear reaction $^{89}Y(\gamma, n)^{88}Y$. Optimum sensitivity is obtained by coincidence counting of the 0.90 and 1.83 MeV gamma rays associated with the decay of ^{88}Y. The detection limit is less than one microgram of yttrium.

Margoshes, M., Rasberry, S. D., **Application of digital computers in spectrochemical analysis—computational methods in photographic microphotometry,** *Spectrochim. Act.* **24B,** *497–513 (Jan. 14, 1969).*

Key words: Computers; micro photometry; photographic emulsion; photographic photometry; programs; spectrochemical analysis.

A new method is described for calibration of photographic emulsions and conversion of microphotometer readings to relative intensities on a digital computer with special application to spectrochemical analysis. The method for emulsion calibration replaces graphical procedures by a numerical method which is well suited for digital computations. The method of computation and its underlying assumptions are described, and results are given of tests of the procedure. It is recognized that the entire experimental arrangement is being calibrated, not merely the photographic emulsion, and it is shown how malfunctions of the microphotometer which affect the calibration can be recognized from the output of the computer. The program for conversion of microphotometer readings to relative intensities provides for several alternate calculations, including selection of the proper calibration parameters according to the wavelength of the line when these data are supplied for more than one wavelength region, as well as correction for step and background where required. The program is written to provide for automatic selection of the required alternative calculation, based on preliminary analysis of the input data.

Milligan, D. E., Jacox, M. E., **Studies of the photoproduction of electrons in inert solid matrices. The electronic spectrum of the species C_2^-,** *J. Chem. Phys.* **51,** *No. 5, 1952–1955 (Sept. 1, 1969).*

Key words: Acetylene; C_2; C_2^- ion; cesium; electron affinity; matrix isolation; photoionization; Swan bands; ultraviolet; spectrum; vacuum-ultraviolet photolysis.

The vacuum-ultraviolet photolysis of acetylene isolated in an argon matrix at 14 K in the presence of a small concentration of a photoelectron source leads to a marked enhancement in the intensity of the 5206–A band system previously assigned to the Swan transition of C_2. Cesium atoms have been found to provide an especially abundant electron source for these studies. The vibrational band spacings observed for the 5206–A band system agree much more closely with those recently reported by Herzberg and Lagerqvist for the 5416–A band system of a species tentatively identified as C_2^- produced upon flash discharge through methane than with the band spacings observed in the gas phase for the Swan transition of C_2. Accordingly, it is suggested that the 5416–A band system of the gas-phase studies and the 5206–A band system of the argon matrix experiments correspond to the same transition. The enhancement of this band system in the presence of a photo-electron source supports the hypothesis that the species which contributes it is negatively charged.

Motz, J. W., Olsen, H. A., Koch, H. W., **Pair production by photons,** *Rev. Mod. Phys.* **41,** *No. 4, Part I, 581–639 (Oct. 1969).*

Key words: Electrons; pair production; photon polarization; photons; positrons; triplet production.

The present report reviews, analyzes, and integrates the various quantitative results that have been obtained for the process of pair production by photons. This summary includes a detailed review of total and differential pair cross sections with a critical evaluation of the conditions of validity and the accuracy of the results. In addition, a summary is given of the important kinematic relations and the polarization effects that occur in pair production.

O'Connell, J. S., Prats, F., **Isospin sum rules and the photodisintegration of the $A=3$ nuclei,** *Phys. Rev.* **184,** *No. 4, 1007–1012 (Aug. 20, 1969).*

Key words: Helium-3; isospin; photonuclear; radii; sum rule; tritium.

Three sum rules for the electric dipole photodisintegration cross section of the $A=3$ nuclei are split into their final state isospin components. The isospin doublet contribution to the three-nucleon breakup mode is found to be of the order of 10–20% and to originate primarily in the high energy region.

Qureshi, I. H., McClendon, L. T., LaFleur, P. D., **Extraction studies of the group IIIB–VIIB elements and the lanthanides utilizing bis(2-ethyl-hexyl) orthophosphoric acid,** *Radiochim. Acta* **12,** *No. 2, 107–111 (Aug. 1969).*

Key words: Group IIIB–VIIB elements; HDEHP; hydrochloric acid; lanthanides; nitric acid; perchloric acid; solvent extraction.

The extraction behavior of the group IIIB–VIIB elements and the lanthanides from 1–11*M* hydrochloric, perchloric and nitric acid solutions into 0.75*M bis*(2-ethyl-hexyl) phosphoric acid solution has been studied. The group IVB elements and scandium exhibit high extraction which is independent of hydrogen ion concentration; the group VIIB elements are essentially unextracted. The extraction of some elements of group VB and VIB and of the lanthanides reaches a minimum and than increases with increasing acidity. This behavior is attributed to a change in extraction mechanism.

Snyder, N. S., **Thermal conductance at the interface of a solid and helium II (Kapitza conductance),** *Nat. Bur. Stand. (U.S.), Tech. Note 385, 90 pages (Dec. 1969), $1.00, SD Catalog No. C13.46:385.*

Key words: Heat transfer; helium II; Kapitza conductance.

A review is presented of the experimental and theoretical work on Kapitza conductance, including a compilation of the available data on conductance to helium II. A short derivation of the phonon radiation limit indicates the reason for the approximate T^3 temperature dependence and the small size of the Kapitza conductance for most solids. Considerable qualitative and quantitative correspondence of the data with this limit is found. From the limited evidence available, the role of surface conditions, and of bulk parameters such as the Debye temperature in determining the conductance are considered empirically. Theoretical knowledge of the Kapitza conductance is seen to give an inadequate explanation of the data. In addition, the phenomena which occur when the heat flux is high enough that properties of the bulk liquid are also involved in the measured conductance are described briefly.

Stern, K. H., Weise, E. L., **High temperature properties and decomposition of inorganic salts. Part 2. Carbonates,** *Nat. Bur. Stand. (U.S.), Nat. Stand. Ref. Data Ser. 30, 32 pages (Nov. 1969), 45 cents, SD Catalog No. C13.48:30.*

Key words: Carbonates; thermal decomposition; thermodynamic functions.

The literature dealing with the high-temperature behavior of inorganic carbonates has been critically reviewed. Free energy functions, of reactants and products of the decomposition reactions were calculated and have been tabulated from 298 K up to as high a temperature as possible. Free energy functions and equilibrium constants of reactions were tabulated. Auxiliary data on phase transitions, densities, and kinetics of thermal decomposition have also been included. The literature of the endothermic decomposition kinetics of solids, as it applies to carbonates, has been reviewed.

Thompson, B. A., Lafleur, P. D., **Activation analysis for molybdenum in samples containing large amounts of tungsten,** *Anal. Chem.* **41,** *No. 13, 1888–1889 (Nov. 1969).*

Key words: Activation analysis; molybdenum; radiochemistry; solvent extraction; technetium; tungsten.

Molybdenum has been determined by neutron activation analysis in the presence of large amounts of tungsten using a double extraction with *bis*(2-ethylhexyl) orthophosphoric acid (HDEHP). In the first extraction W and Mo are separated from the matrix elements. In the second extraction, made after equilibration of ^{99m}Tc with ^{99}Mo, the ^{99m}Tc daughter of ^{99}Mo is separated from W and Mo and used as a measure of the Mo present. The method is very rapid and has good precision and accuracy.

Toots, J., Marton, L., **Optical properties of antimony and bismuth in the far ultraviolet,** *J. Opt. Soc. Am.* **59,** *No. 10, 1305–1308 (Oct. 1969).*

Key words: Antimony; bismuth; collective oscillations; dielectric constant electron-energy-losses; free-electron gas optical properties; plasma resonance; reflectance.

We have measured the multi-angle reflectance of Sb and Bi films in the region of collective oscillation resonance, for photon energies between 10 and 26 eV. Reflectances have been used to calculate the optical constants n and k, which in turn yield ϵ_1 and ϵ_2 as well as the real and imaginary parts of ϵ^{-1}. F or Sb the ϵ^{-1} function can be closely fitted with the inverted Drude-Sellmeier resonance formula. The center of the resonance is at 16.0 eV, with a half-width of 5.2 eV corresponding to a decay time of 1.2×10^{-16} s. The Bi data can not be fitted with a simple Drude-Sellmeier model, but it is in good qualitative agreement with the known electron energy absorption properties.

Waclawski, B. J., Hughey, L. R., **Effect of heating on the photoelectron yield of polycrystalline tungsten in the vacuum ultraviolet,** *J. Opt. Soc. Am.* **59,** *1494 (Nov. 1969).*

Key words: Heating effects; photoelectron yield; spectral response; tungsten; ultra-high vacuum; vacuum ultraviolet.

The effect of heating on the spectral response of a previously atmosphere-exposed, polycrystalline tungsten photocathode was investigated for photon energies of 7.7, 10.2, 11.8, 16.9, and 21.2 eV. Use of ultra-high vacua $< 2 \times 10^{-9}$ torr precluded significant contamination of the sample after heating. The vacuum system bakeout at 630 K, as well as flashing the sample to 2200 K produced appreciable changes in the photoelectron yield (electrons per incident photon). The spectral response was modified by heating such that, compared to atmosphere-exposed tungsten, the yield decreased for photon energies greater than about 8 eV, but increased for lower photon energies.

Wiese, W. L., Bridges, J. M., Kornblith, R. L., Kelleher, D. E., **Transition probabilities for prominent Ar I lines in the near infrared,** *J. Opt. Soc. Am.* **59,** *No. 9, 1206–1212 (Sept. 1969).*

Keywords: Atomic; infrared lines; neutral argon; transition probabilities; wall-stabilized arc.

Relative transition probabilities of 81 infrared Ar I lines in the wavelength range from 9000–24000 Å have been measured with a wall-stabilized arc operating in argon at atmospheric pressure. The large majority of the lines from the $4p–5s$ and $4p–3d$ transition arrays has been observed and the measurements are consistent with the J-file sum rule. The data have been normalized to an absolute scale by utilizing other recent arc and lifetime values.

Other NBS Publications

J. Res. Nat Bur. Stand. (U.S.), 74B (Math. Sci.), No. 1 (Jan.–Mar. 1970), SD Catalog No. C13.22/sec. B:74/1.

Partitions—a survey. H. Gupta.
A relation between the coefficients and roots of two equations and its application to diophantine problems. T. N. Sinha.
An enumeration problem for a congruence equation. R. A. Brualdi and M. Newman.
Orthogonal decompositions of tensor spaces. S. Pierce.
Partitioned hermitian matrices. R. Merris.
Bounds on a polynomial. T. J. Rivlin.
Entire functions of exponential type. F. Gross.

Armstrong, G. T., Hydrogen fluoride and the thermochemistry of fluorine, Proc. Conf. Interagency Chemical Rocket Propulsion Group, Thermochemistry Working Group. Cleveland, Ohio, Apr. 9–11, 1969, 7th Meeting Bulletin 1, 119–135 (Chemical Propulsion Information Agency, Johns Hopkins University, Applied Physics Laboratory, Silver Spring, Maryland, Aug. 1969).

Armstrong, G. T., King, R. C., The heats of formation of some fluorine-containing oxidizers, Proc. Conf. Interagency Chemical Rocket Propulsion Group, Thermochemistry Working Group, Cleveland, Ohio, Apr. 9–11, 1969, 7th Meeting Bulletin 1, 19–40, (Chemical Propulsion Information Agency, Johns Hopkins University, Applied Physics Laboratory, Silver Spring, Maryland, Aug. 1969).

Bates, R. G., Measurement of pH, Handbook of Biochemistry, H. A. Sober, Ed., pp. J190–J194 (Chemical Rubber Company, Cleveland, Ohio, 1967).

Bullis, W. M., Measurement methods for the semiconductor device industry—a summary of NBS activity, Nat. Bur. Stand. (U.S.), Tech. Note 511, 24 pages (Dec. 1969), 30 cents, SD Catalog No. C13.46:511.

Hall, L. A., A bibliography of thermophysical properties of air from 0 to 300 K, Nat. Bur. Stand. (U.S.), Tech. Note 383, 121 pages (Oct. 1969), $1.25, SD Catalog No. C13.46:383.

Heaton, H. T., II, Use of an on-line computer in neutron time-of-flight measurements, Nat. Bur. Stand. (U.S.), Tech. Note 515, 31 pages (Jan. 1970), 35 cents, SD Catalog No. C13.46:515.

Knoeck, J., Vibrational spectrometric and electrochemical evidence for lanthanum(III)-nitrate complexes aqueous solution, Anal. Chem. **41,** No. 14, 2069–2071 (Dec. 1969).

Kushner, L. M., The NBS contribution to technological measurements and standards, Mater. Res. Std. **9,** No. 10, 8–10 (Oct. 1969).

Lehner, J., Lectures on modular forms, Nat. Bur. Stand. (U.S.), Appl. Math. Ser. 61, 77 pages (Dec. 1969), 70 cents, SD Catalog No. C13.32:61.

Marron, B. A., Tauber, S. J., Evolution of a general computer-based information system from pharmacological requirements, Proc. Conf. 32nd Annual Meeting of the American Society for Information Science, San Francisco, California, Oct. 1–4, 1969, 6, 223–230 (Greenwood Publ. Corp., Westport, Conn., 1969).

Post, M. A., Determination of styrene-butadiene and styrene-acrylate resins in solvent type paint, J. Paint Technol. **41,** No. 537, 567–580 (Oct. 1969).

Roberts, D. E., Recrystallization and melting of partially melted stark rubber, Rubber Chem. Technol. **42,** 540–546 (Mar. 1969).

Scribner, B. F., Editor, Activities of the NBS Spectrochemical Analysis Section, July 1968 to June 1969, Nat. Bur. Stand. (U.S.), Tech. Note 502, 108 pages (Dec. 1969), $1.00, SD Catalog No. C13.46:502.

Simson, B. G., Radlinski, R. W., The accuracy of air tower pressure gages in suburban Washington, D.C., Nat. Bur. Stand. (U.S.), Tech. Note 512, 10 pages (Dec. 1969), 25 cents, SD Catalog No. C13.46:512.

Sparks, L. L., Powell, R. L., Progress on cryogenic thermocouples, (Proc. 1968 Cryogenic Engineering Conf., Cleveland, Ohio, Aug. 19–21, 1968), Chapter in Advances in Cryogenic Engineering 14, 316–321 (Plenum Press, Inc., New York, N.Y., 1969).

White, H. S., Jr., Editor, Congressional districts of the United States. Federal general data standard representations and codes, Nat. Bur. Stand. (U.S.), Fed. Info. Process. Stand. Publ. (FIPS Pub.) 9, 4 pages (Nov. 14, 1969), 10 cents, SD Catalog No. C13.52:9.

**Publications for which a price is indicated are available by purchase from the Superintendent of Documents, U.S. Government Printing Office, Washington, D.C. 20402 (foreign postage, one-fourth additional). The NBS non-periodical series are also available from the Clearinghouse for Federal Scientific and Technical Information, Springfield, Va. 22151. Reprints from outside journals and the NBS Journal of Research may often be obtained directly from the authors.*

U.S. GOVERNMENT PRINTING OFFICE : 1970 OL—378-324

NBSA OCT 46129
UNIVERSITY MICROFILMS INC
ATTN SERIALS SECTION
300 NORTH ZEEB RD
ANN ARBOR MICH 48106

UNITED STATES
GOVERNMENT PRINTING OFFICE
DIVISION OF PUBLIC DOCUMENTS
WASHINGTON, D.C. 20402

OFFICIAL BUSINESS

POSTAGE AND FEES PAID
U.S. GOVERNMENT PRINTING OFFICE

JOURNAL OF RESEARCH of the National Bureau of Standards
A. Physics and Chemistry

Vol. 74A, No. 3 May–June 1970

Contents

Page

The crystal structure of hydrazinium trinitromethide $(N_2H_5^+[C(NO_2)_3]^-$ at ~ -160 °C. Brian Dickens. 309

A refinement of the crystal structure of $Na_2CO_3 \cdot H_2O$. B. Dickens, F. A. Mauer, and W. E. Brown. 319

Anisotropic reaction kinetics of oxygen with pyrolytic graphite. William S. Horton. 325

The viscosity and thermal conductivity of dilute gaseous hydrogen from 15 to 5000 K. H. J. M. Hanley, R. D. McCarty, and H. Intemann. 331

Temperature classification of the spectra of dysprosium (Dy , Dy). Arthur S. King, John G. Conway, Earl F. Worden, and Charlotte E. Moore. 355

Papers presented at the Conference, Electronic Density of States, National Bureau of Standards, Gaithersburg, Maryland November 3–6, 1969

Optical density of states ultraviolet photoelectric spectroscopy. W. E. Spicer. 397

Beyond the one-electron approximation: Density of states for interacting electrons. Lars Hedin, Bengt Lundqvist, and Stig Lundqvist. 417

Ion-neutralization spectroscopy. Homer D. Hagstrom. 433

Local theory of disordered systems. W. H. Butler and W. Kohn. 443

Density of states information from low temperature specific heat measurements. Paul A. Beck and Helmut Claus. 449

Publications of the National Bureau of Standards. 455

Library of Congress Catalog Card Number: 62–37059

For sale by the Superintendent of Documents, U.S. Government Printing Office, Washington, D.C. 20402. (Order by SD Catalog No. C 13.22/sec.A:74/3). Single copy price varies. This issue $1.75. Subscription price $9.50 a year; $2.25 additional for foreign mailing.

UNITED STATES GOVERNMENT PRINTING OFFICE, WASHINGTON : 1970

XU

KUM